



Asphalt Research Consortium

Quarterly Technical Progress Report January 1 – March 31, 2009

April 2009

Prepared for
Federal Highway Administration
Contract No. DTFH61-07-H-00009

By
Western Research Institute
Texas A&M University
University of Wisconsin-Madison
University of Nevada-Reno
Advanced Asphalt Technologies

www.westernresearch.org
www.ARC.unr.edu

TABLE OF CONTENTS

INTRODUCTION	1
GENERAL CONSORTIUM ACTIVITIES	3
PROGRAM AREA: MOISTURE DAMAGE.....	5
Category M1: Adhesion.....	5
Category M2: Cohesion	17
Category M3: Aggregate Surface	49
Category M4: Modeling.....	58
Category M5: Moisture Damage Prediction System	67
PROGRAM AREA: FATIGUE.....	71
Category F1: Material and Mixture Properties	71
Category F2: Test Method Development.....	101
Category F3: Modeling	116
PROGRAM AREA: ENGINEERED MATERIALS.....	133
Category E1: Modeling.....	133
Category E2: Design Guidance.....	164
PROGRAM AREA: VEHICLE-PAVEMENT INTERACTION.....	183
Category VP1: Workshop	183
Category VP2: Design Guidance	183
Category VP3: Modeling	189
PROGRAM AREA: VALIDATION.....	193
Category V1: Field Validation.....	193
Category V2: Accelerated Pavement Testing	194
Category V3: R&D Validation	195
PROGRAM AREA: TECHNOLOGY DEVELOPMENT.....	207
PROGRAM AREA: TECHNOLOGY TRANSFER.....	211
Category TT1: Outreach and Databases	211

INTRODUCTION

This document is the Quarterly Report for the period of January 1 to March 31, 2009 for the Federal Highway Administration (FHWA) Contract DTFH61-07-H-00009, the Asphalt Research Consortium (ARC). The Consortium is coordinated by Western Research Institute with partners Texas A&M University, the University of Wisconsin-Madison, the University of Nevada Reno, and Advanced Asphalt Technologies.

The Quarterly Report is grouped into seven areas, Moisture Damage, Fatigue, Engineered Paving Materials, Vehicle-Pavement Interaction, Validation, Technology Development, and Technology Transfer. The format of the report is based upon the Research Work Plan that is grouped by Work Element and Subtask.

This Quarterly Report summarizes the work accomplishments, data, and analysis for the various Work Elements and Subtasks. This report is being presented in a summary. The Quarter of January 1 to March 31, 2009 is fourth quarter of the Year 2 contract year. Reviewers may want to reference the Revised Year 2 Work Plan in order to obtain background information on specific areas of research. The more detailed information about the research such as approaches to test method development, data collection, and analysis will be reported in research publications as part of the deliverables. The Revised Year 2 Work Plan is posted on the ARC website, www.ARC.unr.edu. Reviewers may also want to reference the Year 3 Work Plan as some plans have been modified based on research findings to date.

The previous quarterly reports, Year 1, Revised Year 2, and Year 3 Work Plans, and other related documents and information about the Asphalt Research Consortium can be found at the ARC website, www.ARC.unr.edu.

SUPPORT OF FHWA AND DOT STRATEGIC GOALS

The Asphalt Research Consortium research is responsive to the needs of asphalt engineers and technologists, state DOT's, and supports the FHWA Strategic Goals and the Asphalt Pavement Road Map. More specifically, the research reported here supports the Strategic Goals of safety, mobility, and environmental stewardship. By addressing the causes of pavement failure and thus determining methods to improve asphalt pavement durability and longevity, this research will provide the motoring public with increased safety and mobility. The research directed at improved use of recycled asphalt pavement (RAP), warm mix asphalt, and cold mix asphalt supports the Strategic Goal of environmental stewardship.

GENERAL CONSORTIUM ACTIVITIES

PROGRESS THIS QUARTER

All Consortium partners and many of their staff attended the 88th Annual Meeting of TRB where several members/staff made presentations, and/or participated as members of TRB committees. During the week of TRB, a Consortium Advisory Board meeting was conducted to discuss the progress on the preparation of the Year 3 Work Plan and other business.

All Consortium members and staff completed the preparation and delivery of the Annual Work Plan for Year 3 to FHWA in January 2009. In addition, a Quarterly Report on the Consortium activities for the period October 1, 2008 to December 31, 2008 was prepared and delivered.

Consortium members attended the February 2009 Binder, Mix and Construction, and Fundamental Properties and Advanced Models ETG meetings in Irvine, California. Essentially the entire agenda and program of the Fundamental Properties and Advanced Models ETG meeting focused on the modeling activities and deliverables of the Asphalt Research Consortium. Presentations, in the form of updates on specific activities, were made at the Binder, and the Mix and Construction ETG meetings.

Several Consortium partners and staff attended the annual Association of Asphalt Paving Technologists (AAPT) meeting in Minneapolis, Minnesota in March.

WORK PLANNED FOR NEXT QUARTER

ARC members, Dr. Hussain Bahia, Dr. Elie Hajj, and Michael Harnsberger, are planning on attending the RAP Expert Task Group meeting in Manchester, New Hampshire on April 22 & 23, 2009 that is being hosted by New Hampshire DOT and the University of New Hampshire. Dr. Hussain Bahia of the University of Wisconsin Madison and Dr. Elie Hajj of the University of Nevada Reno are planning on presenting an update on the RAP research being conducted by the ARC.

Dr. Peter Sebaaly is planning on attending the 7th International RILEM Symposium on Advanced Testing and Characterization of Bituminous Materials (ACTBM09) May 27-29, 2009 in Rhodes, Greece to present an update on the research of the effect of non-standard heavy load vehicles and the Warm-Mix Asphalt & Recycling Symposium, June 8-10, 2009 in Sacramento, CA.

PROGRAM AREA: MOISTURE DAMAGE

CATEGORY M1: ADHESION

Work Element M1a: Affinity of Asphalt to Aggregate (UWM)

Work Done This Quarter

Tests were conducted to correlate Dynamic Shear Rheometer (DSR)-modified tack test results to Pneumatic Adhesion Tensile Testing Instrument (PATTI) results. The original tack test procedure uses two steel plates. The research team evaluated the tack test using plate-and-rock to correlate results to PATTI test as discussed in last quarter. Materials used to fit the testing matrix in this quarter are as follows:

- CRM, a PG 58-28 neat binder with a low content of asphaltenes (9.06% as determined per ASTM D4124-01).
- Flint Hills (FH), a PG 64-22 neat binder with a high content of asphaltenes (16.25% as determined per ASTM D4124-01).
- FH + 2% wt Sasobit, a PG 64-22 modified binder.
- FH + 3% wt linear styrene-butadiene-styrene (LSBS), a PG 70-22 modified binder.

For the tack test, 25 mm granite plates were prepared. For the PATTI test, large granite plates were also prepared. Moisture damage tests were performed based on the approved testing matrix. The main focus this quarter was on evaluating the testing conditions that affect the PATTI test results and comparing results from the tack test on rock-plate with results from the PATTI test.

Significant Results

To compare results from the tack test to the PATTI test, both procedures need to have the same testing matrix. The tack test allows better control of temperature, film thickness and rate of deformation. With the PATTI test, controlling temperature and rate of deformation is challenging, which could lead to less repeatable data. Film thickness in the PATTI test is controlled by resting the stubs on spacers for a film thickness of 0.4 mm. Trimmed 8 mm mold binder samples are used to ensure that the same amount of binder is used for every sample. Effects of film thickness, loading rate, and temperature were evaluated.

Preparation protocol and control of film thickness

PATTI tests were run to compare pullout strength when using the trimmed molds and when pouring binder directly on granite plates. Examples of the results are shown in figure M1a.1. The complete set of data is shown in table M1a.1.

As table M1a.1 shows, the results from using the trimmed mold are better than the results from pouring, as they tend to result in smaller coefficients of variation for the pullout rate. The team

recommends using trimmed molds for PATTI tests to ensure uniform film thicknesses and rates of deformation.

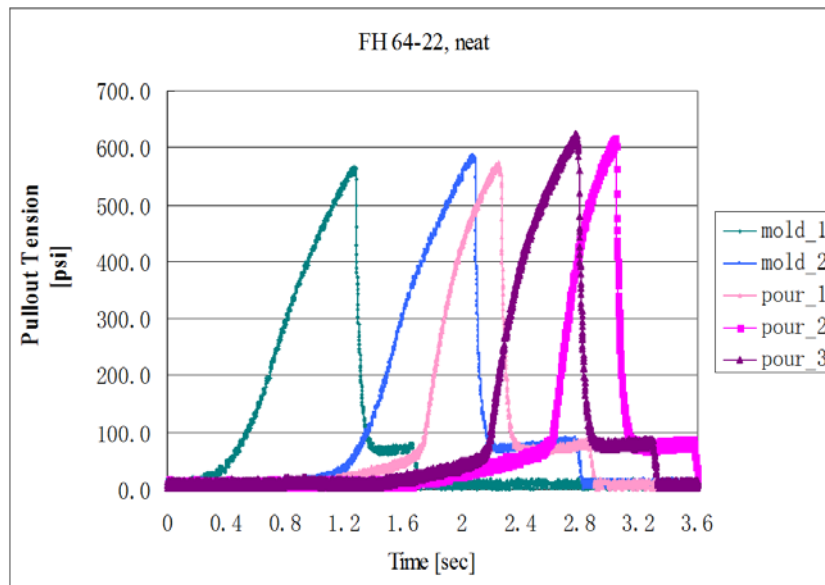


Figure M1a.1. Graph. PATTI test results at 25 °C from the FH neat binder in dry conditions using trimmed mold or pouring directly on granite plate.

Table M1a.1. Pullout rate of PATTI results using a trimmed mold or pouring binder directly on granite plates in dry conditions.

	Run		Pullout Rate (psi/s)	Run		Pullout Rate (psi/s)
FH 64-22, neat	Poured	1	1325.97	Molded	1	783.907
		2	1747.91		2	830.673
		3	1259.09			
		Average	1444.32		Average	807.29
		St. Dev.	265.03		St. Dev.	33.07
		Coeff. of Var.	18.35%		Coeff. of Var.	4.10%
FH 70-22 + 3% LSBS	Pour_7	1	832.447	Mold_7	1	852.123
		2	764.228		2	672.151
		3	1269.14			
		Average	955.27		Average	762.14
		St. Dev.	273.95		St. Dev.	127.26
		Coeff. of Var.	28.68%		Coeff. of Var.	16.70%

Rate of deformation

Rate of deformation is an important parameter that affects results in both tests. To compare the PATTI test results to the tack test results, similar rates of deformation should be used for every type of binder in the PATTI test. The rate used in the tack test is 0.01 mm/s. One parameter affecting rate of deformation is flow control. Figure M1a.2 shows an example of the effects of flow control. In the figure, runs 1, 2 and 3 were tested using the same flow control without venting the system between runs; runs 4 and 5 were tested with system venting between runs. Run 5 has a constant rate until failure. It matches the condition in tack test and is the desired PATTI testing rate. Table M1a.2 includes the results measured using 3 settings of the flow rate (6, 7 and 8). As can be seen, the rate of deformation and amount of flow setting are not proportional. It is clear that a better flow control is needed for the test procedure.

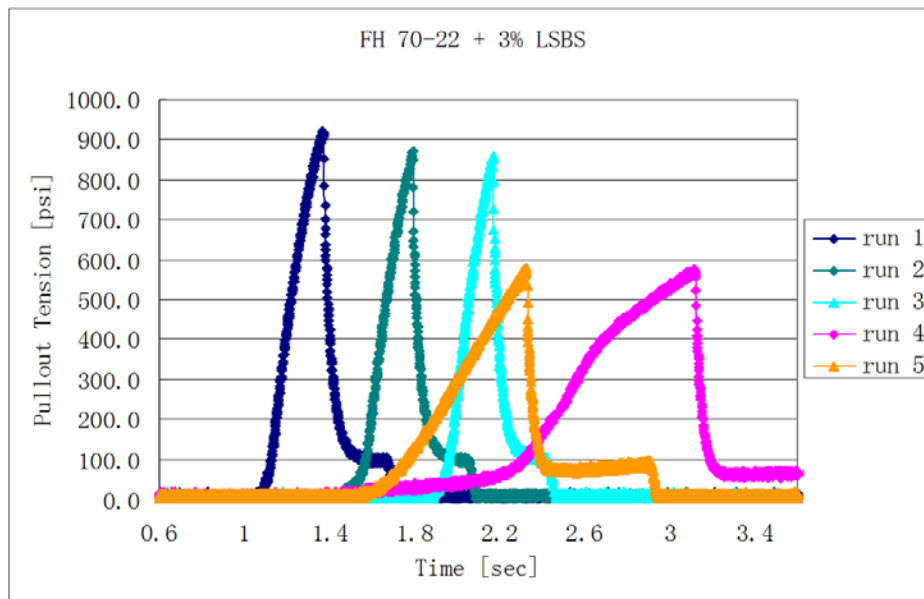


Figure M1a.2. Graph. PATTI test results at room temperature from the FH LSBS modified binder mold in dry conditions with different flow control settings.

Table M1a.2. Pullout rate of PATTI from CRM neat binder mold at room temperature in dry conditions with different flow control.

		Run	Pullout Rate (psi/s)			Run	Pullout Rate (psi/s)			Run	Pullout Rate (psi/s)
CRM 58-28, Neat	Mold, Flow control 5	1	1213.61	Mold, Flow control 7	1	1679.95	Mold, Flow control 8	1	1481.1		
		2	1360.04		2	1619.72		2	1551.96		
		3	1238.93		3	1677.9		3	1440.82		
		Average	1270.86		Average	1659.19		Average	1491.29		
		St. Dev.	78.26		St. Dev.	34.2		St. Dev.	56.27		
		Coeff. of Var.	6.16%		Coeff. of Var.	2.06%		Coeff. of Var.	3.77%		

Temperature

Temperature appears to be the most important factor in both tests because asphalt is a highly temperature-sensitive material. Table M1a.3 shows the effects of temperature are great on both binders. The PATTI device doesn't have a way to control temperature, but results can be compared by testing at similar temperatures.

Table M1a.3. Test results of PATTI from CRM neat binder mold, flow control 7, under dry and wet conditions at different testing temperatures.

	Run		Temp (°C)	Failure Type (a = adhesive, c = cohesive)	PATTI Factor (psi*s)	Max Pullout Tension (psi)	Pullout Rate (psi/s)	
FH 64-22, neat	Granite	Dry	1	24.9	100%c	194.2	556.894	1465.51
			2	24.5	100%c	252.9	587.701	824.843
			3	24.3	100%c	176.8	575.852	1952.04
		average			208	573.5	1414.1	
		St. Dev.			39.9	15.5	565.4	
		Coeff. of Var.			19.17%	2.71%	39.98%	
	Granite	Wet	1	20.7	40%a,60%c	471.5	708.559	836.058
			2	20	40%a,60%c	402.7	754.1	783.959
			3	18.8	20%a,80%c	390.5	690.1	874
		Average			421.6	717.6	831.3	
		St. Dev.			43.7	32.9	45.2	
		Coeff. of Var.			10.36%	4.59%	5.44%	
CRM 58-28, neat	Granite	Dry	1	24.4	100%c	91.3	374.7	704.595
			2	24.1	100%c	92	436.4	296.629
			3	23.7	100%c	143	341.5	236.696
		Average			108.8	384.2	412.6	
		St. Dev.			29.6	48.2	254.6	
		Coeff. of Var.			27.26%	12.53%	61.70%	
	Granite	Wet	1	20.2	30%a,70%c	127.6	486.2	686.996
			2	20	80%a,20%c	100.6	398.4	648.495
			3	19.9	60%a,40%c	94.4	388.9	690.701
		Average			107.5	424.5	675.4	
		St. Dev.			17.7	53.6	23.4	
		Coeff. of Var.			16.42%	12.64%	3.46%	

Effect of wet conditioning of samples

Based on the evaluation of critical testing factors, testing with the PATTI were conducting using trimmed molds, flow control setting of 7, testing temperature of 40 °C and waiting time of 6

hours in dry and wet condition . Table M1a.4 includes the results collected to date. They show that PATTI pullout tensions in wet conditions are smaller than in dry conditions for similar amounts of both binders. This means that the PATTI test can be effectively used to evaluate water effects in moisture damage tests.

Table M1a.4. Test results of PATTI from trimmed mold binder, flow control 7, under dry and wet conditions, with similar testing temperatures.

	Run		Temp (°C)	Failure Type (a = adhesive c = cohesive)	PATTI Factor (psi*s)	Max Pullout Tension (psi)	Pullout Rate (psi/s)	
FH 64-22, neat	Granite	Dry	1	24.2	100%c	365.4	673.012	806.003
			2	24.2	100%c	316.2	639.836	815.077
			3	24.2	100%c	301.7	623.247	966.275
			Average			327.8	645.4	862.5
			St. Dev.			33.4	25.3	90.0
			Coeff. of Var.			10.19%	3.93%	10.44%
	Granite	Wet	1	24	90%a, 10%c	207.7	528.457	788.742
			2	23.9	30%a,70%c	252.8	578.222	684.286
			3	23.9	80%a,20%c	263.7	587.701	765.743
			Average			241.4	564.8	746.3
			St. Dev.			29.7	31.8	54.9
			Coeff. of Var.			12.30%	5.63%	7.35%
CRM 58-28, neat	Granite	Dry	1	24.4	100%c	197.4	518.978	1199.95
			2	24.5	100%c	198.6	533.196	1152.86
			3	24.5	100%c	208.2	497.65	1031.4
			Average			201.4	516.6	1128.1
			St. Dev.			5.9	17.9	87.0
			Coeff. of Var.			2.94%	3.46%	7.71%
	Granite	Wet	1	24.3	100%c	143.8	476.322	1488.510
			2	24.2	100%c	150.2	478.692	1160.470
			3	24.2	100%c	154.4	464.473	1146.850
			Average			149.5	473.2	1265.3
			St. Dev.			5.3	7.6	193.4
			Coeff. of Var.			3.57%	1.61%	15.29%

Tack factor results from the DSR

Table M1a.5 includes the results collected using the DSR Tack Test before and after conditioning in water. The results listed show that the tack factor for water-conditioned binder is

much smaller than for dry-conditioned. Compared with PATTI test at 24 °C (table M1a.4), the tack test shows a larger water effect than PATTI test results on the same binder. Examples of the tack testing results in the dry and wet condition are shown in figure M1a.3.

Table M1a.5. Test results of tack test from FH neat binder at 24 °C on granite with 0.4 mm thickness and 0.01 mm/s rate of deformation under dry and wet conditions.

FH 64-22, Neat (Granite)	Wet	Run	Tack Factor (N*s)	Average	St. Dev.	Coeff. of Var.	Testing Temperature (°C)	Maximum Stress (psi)
		1	164.52	133.77	43.49	32.51%	24	23.08
2	103.02	24	14.4					
Dry	1	298.09	296.575	2.14	0.72%	24	31.7	
	2	295.06				24	37.5	
	3	328,28				24	43.3	

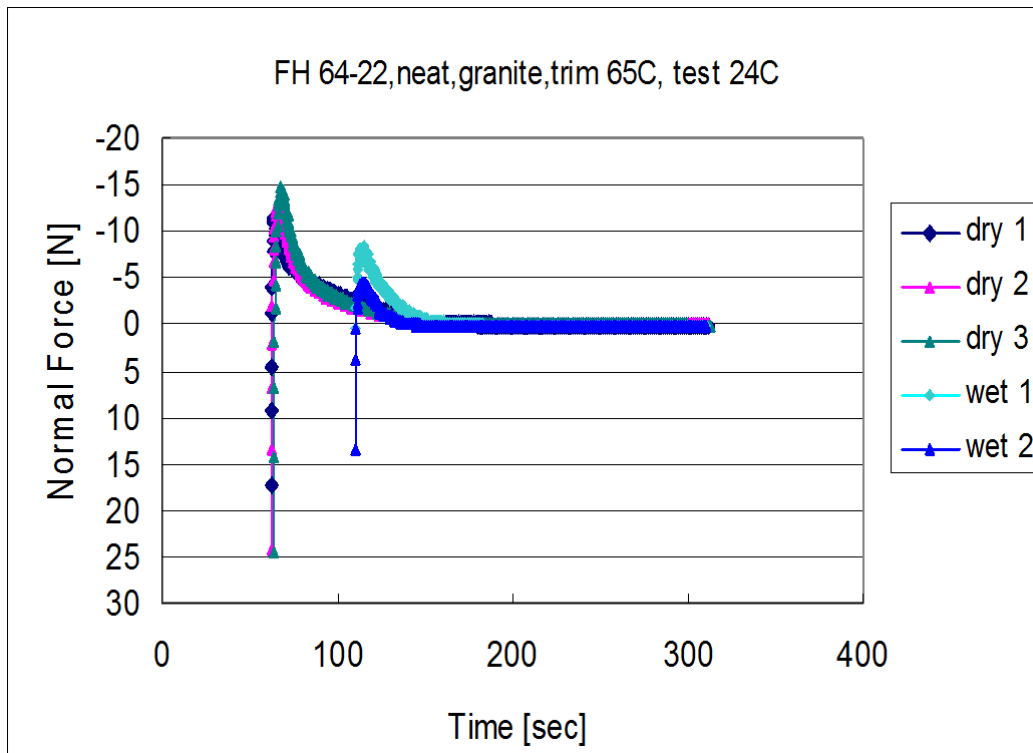


Figure M1a.3. Graph. Tack test on FH neat binder at 24 °C on granite with 0.4 mm thickness and 0.01 mm/s rate of deformation under dry and wet conditions.

The preliminary testing procedures are summarized in tables M1a.6 (PATTI test) and M1a.7 (tack test).

Table M1a.6. Preliminary testing procedures, PATTI test.

Film Thickness (mm), small stub	0.4
Tank Pressure (psi)	100
Glass and Stub Temp (°C)	65
Binder Temp (°C)	150
Testing Temp (°C)	24
Testing Conditions	Lab
Water/Dry Conditioning (°C)	40 for 6 h
Flow Control	Between yellow and green, 7

Table M1a.7. Preliminary testing procedures, Tack Test.

Film Thickness (mm)	0.4
Rate of Deformation (mm/s)	0.01
Trimming Temp (°C)	65
Binder Temp (°C)	150
Testing Temp (°C)	24
Testing Conditions	Lab
Water Conditioning (°C)	40 for 6 h

Significant Problems, Issues and Potential Impact on Progress

The rate of deformation remains difficult to control. In addition, the tack test conducted with the aggregate plate under water produces results that are not sufficiently repeatable. A new version of the PATTI test, called the Quantum Gold PATTI, has been purchased. The new device provides much better control of the flow rate and its computer software allows better recording and analysis of the data.

Work Planned Next Quarter

Next quarter, the research team will continue running underwater tack tests with different binder types to get more repeatable results. PATTI tests with 24-hour conditioning time will be conducted to achieve similar water effects compared to the tack tests.

Work Element M1b: Work of Adhesion Based on Surface Energy

Subtask M1b-1: Surface Free Energy and Micro-Calorimeter Based Measurements for Work of Adhesion (TAMU)

Work Done This Quarter

The method development phase for this subtask was completed in conjunction with another FHWA project and the findings were reported in the Year 3 work plan. The next goal of this subtask is to provide material property inputs required in other work elements as required. Any data obtained from this subtask will be included in the material properties database.

Work Planned Next Quarter

Work on this subtask will be conducted in conjunction with and as required by other work elements.

Subtask M1b-2: Work of Adhesion at Nano-Scale using AFM (WRI)

Work Done This Quarter

Adhesive and cohesive forces within the asphalt/filler/aggregate matrix are responsible for the strength, resilience, and durability of asphalt pavements. Adhesive forces can be understood in terms of interfacial thermodynamics where the free energy (G) is the sum of the enthalpy (H) and the entropy ($-TS$) for a given system at a specified temperature. In this subtask a range of scanning probe microscopy techniques will be used to investigate entropic properties at the adhesive interface to provide a better understanding of adhesion thermodynamics as it relates to the performance and/or failure of asphalt pavements.

Experimental work related to this subtask will involve the collection and interpretation of numerous pull-off-force measurements, hereinafter referred to as force distance curves (FDC). To collect a FDC, a spherical glass probe tip is brought into contact with an asphalt thin film sample at a specified rate, a controlled contact pressure is applied for a specified time, and then the probe is retracted from the surface at a specified rate. FDC's along with nano-scale surface images will be collected over a range of temperatures on films of different thicknesses. The resultant FDC's and images will be used to evaluate entropic contributions to surface energy for asphalts of various crude source types as a function of film thickness and temperature. To facilitate these measurements, work this quarter was mainly directed toward some hardware modifications that we believe will greatly improve the accuracy and efficiency of the process involved in FDC collection.

Our AFM was purchased with a research customization package (RCP) that provides monitor points for direct access to various processed and unprocessed signals within the microscope. This past quarter we interfaced the AFM, using RCP monitor points, to a separate laptop PC to collect FDC data. With this arrangement two (or more) channels of unprocessed voltage/time data can be collected simultaneously from the AFM. Unlike the microscope data files, data collected with

the PC is saved in a format that can be imported directly into an Excel[®] spreadsheet. This new data collection arrangement will allow for much greater efficiency in the subsequent analysis of FDC data.

With the appropriate calibration and an understanding of the contact area, force distance curves can provide a direct measure of adhesive strength as it is related to interfacial energies. A FDC is essentially the readout from a tiny spring-balance. To measure the force, the displacement of the spring is multiplied by the “spring constant” for the particular spring as used in the balance. The precision and accuracy of the measured force is directly dependent upon the precision and accuracy of the measured displacement and spring constant.

In a separate project WRI is working toward development of a method for measurement of rheological properties at nano-scale. During this past quarter the AFM was fitted with a new sample stage to facilitate this “nano-rheology” project. The new stage will provide accurate sample positioning that is completely independent of the AFM electronics.

A new cantilever calibration procedure has been established to help improve the accuracy of nano-rheological measurements. For these measurements, an accurate determination of cantilever spring constants is essential. In this procedure cantilever spring constants will be calculated by oscillating the probe tip in a Newtonian viscosity standard and measuring the phase difference between an applied force and the cantilever response.

For this subtask we plan to adapt the nano-rheology techniques and the cantilever spring constant calibration procedure developed in the above mentioned project. Using traceable viscosity standards will provide an alternate method with which to establish and/or verify spring constants for cantilevers that will be used to collect FDC data. Nano-rheology will be used to measure changes in asphalt stiffness related to film thickness. Nano-rheological measurements combined with FDC data will provide a quantitative measure of the relationship between physical properties (adhesive strength and mechanical stiffness) and film thickness for asphalt binders over a range of film thicknesses and temperatures typically encountered in asphalt pavements.

The experimental work related to this subtask involves the measurement of asphalt adhesive strength as a function of both temperature and film thickness. Rapid preparation of thin film samples of known and consistent thickness will be an important part of the experimental program. Toward this end our spin casting apparatus was fitted with a robotic arm in work conducted during the previous quarter.

In preliminary work conducted this quarter, testing of the robotic spin caster revealed a tendency for the sample droplet to climb up the syringe needle applicator unless the tip was in contact with the surface of the substrate. This problem was addressed by adjusting the geometry between the syringe needle and the substrate surface. We also found significant run-out (0.015-inch) in the spin caster’s platen surface causing the surface to oscillate up and down as the platen revolved. This problem was corrected by tapping the high side of the platen while monitoring run-out with a dial indicator. On this particular machine the interchangeable platens are fit into a resilient mounting, so this adjustment will probably only provide a temporary fix. We are currently

investigating more permanent solutions for the problem. However, a number of satisfactory thin-film test samples have been prepared with the robotic spin caster as currently adjusted.

To accommodate FDC measurements as a function of temperature a new micro-scale thermal stage has been designed for use in conjunction with the AFM system. The thermal stage designed for use in this subtask will provide the ability to subject thin-film samples to various thermal cycles and/or thermal gradients while simultaneously imaging changes in phase distribution at the sample surface.

AFM imaging of asphalt films has shown significant changes in the appearance of sample surfaces as a function of sample aging. For many materials (e.g. polymers and metals) thermal history can have a significant effect on the physical properties of the material. Different rates of cooling from the melted or heated state can result in large changes in the strength, ductility, hardness, etc. of otherwise identical materials. These changes are entropy related.

Asphalt pavements undergo a variety of annual and daily thermal cycles as well as reversals of thermal gradients particularly near the pavement surface. Thermal cycles may result in the formation of areas of concentrated stress within the pavement and thus contribute to fatigue failure. Using the new thermal stage we will investigate the effect of cooling rate and thermal cycling on the observable distribution of phases at the sample surface for a selected group of samples. FDC and nano-rheological measurements will be conducted to attempt to differentiate properties of the various phases and to determine if the phase properties change as a function of cooling rate.

Significant Results

None.

Significant Problems, Issues and Potential Impact on Progress

None.

Work Planned Next Quarter

For work planned next quarter, a set of samples will be prepared from one of the SHRP core asphalts at several thicknesses. FDC measurements will be conducted to provide information relevant to work of adhesion as a function of film thickness. Data collected from this first sample set will be evaluated to determine the efficacy of the experimental technique. Based upon this evaluation the technique will be modified as needed and preparation of the full suite of samples will begin. Also next quarter, work will continue toward the development of a method for making nanorheological measurements and application of the method to this subtask.

Subtask M1b-3: Identify Mechanisms of Competition Between Water and Organic Molecules for Aggregate Surface (TAMU)

Work Done This Quarter

This sub task is investigating the mechanisms responsible for adhesion and debonding of model organic compounds (representing functional groups in asphalt binder) to minerals and representative aggregates. We are measuring the heat of reactions of the chemical mechanisms using a dual-mode flow adsorption calorimeter. Differences in molar heats of reaction of different organics bonding to the same absorbent are indicative of differences in the bonding strength of each absorbate with the absorbent of interest.

Work during this quarter focused on continued development of the instrument. We are currently conducting studies to validate the ability of the instrument to differentiate between bonding characteristics of materials produced under different conditions. These materials are known to have variable surface properties depending on the temperature of formation and other environment conditions. Currently we are evaluating the instrument ability to accurately measured changes in surface characteristics as a function of the pH of the aqueous environment.

Significant Results

There are no significant results for this quarter as we focused on aggregate characterizations.

Significant Problems, Issues and Potential Impact on Progress

There are no significant issues.

Work Planned Next Quarter

We plan on initiating flow through experiments to measure the molar heat of reaction of the adhesion of model organic compounds that represent asphalt to minerals and aggregates, as well as the molar heats of reactions of water adsorption to organic-coated minerals and aggregates.

Adhesion will be modeled in the flow-through calorimeter by organic sorption from nonaqueous phase solvents. Experimental variables include the chemistry of the model organic, single versus mixtures of model organics, ionic salt content of the nonaqueous phase solvent, and the surface chemistry of the mineral or aggregate.

Competition of water and the model organics for the mineral or aggregate surfaces will be characterized through flow-through experiments that introduce small amounts of water to the systems created during the adhesion studies above.

Work Element M1c: Quantifying Moisture Damage Using DMA (TAMU)

Work Done This Quarter

The research team has obtained information on the performance of a number of treated/untreated full asphalt mixtures used in different states as presented in table M1c-1. These mixtures were produced using different aggregates and binders with and without treated agents. Researchers will select one of these mixtures to produce a Fine Aggregate Mixture (FAM) for the DMA test. The test protocol will include different modes; stress- controlled and strain-controlled at different conditions; dry and wet.

Table M1c-1. Performance results using AASHTO T 283 test.

State		Untreated	Liquid treated	Lime-treated
Alabama	Unconditioned Tensile Strength, psi	113	107	120
	Conditioned Tensile Strength, psi	92	90	109
	Tensile Strength Ratio, %	81	84	90
California	Unconditioned Tensile Strength, psi	214	180	164
	Conditioned Tensile Strength, psi	155	164	155
	Tensile Strength Ratio, %	72	91	95
Illinois	Unconditioned Tensile Strength, psi	138	135	149
	Conditioned Tensile Strength, psi	112	115	129
	Tensile Strength Ratio, %	82	85	87
South Carolina	Unconditioned Tensile Strength, psi	152	154	162
	Conditioned Tensile Strength, psi	92	125	141
	Tensile Strength Ratio, %	61	81	87
Texas	Unconditioned Tensile Strength, psi	159	112	155
	Conditioned Tensile Strength, psi	98	112	153
	Tensile Strength Ratio, %	61	100	98

Work Planned Next Quarter

The DMA tests will be completed.

CATEGORY M2: COHESION

Work Element M2a: Work of Cohesion Based on Surface Energy

Subtask M2a-1: Methods to Determine Surface Free Energy of Saturated Asphalt Binders (TAMU)

Work Done This Quarter

No activity was planned for this quarter.

Significant Results

None.

Significant Problems, Issues and Potential Impact on Progress

None.

Work Planned Next Quarter

Work on this task is anticipated to start in year 4 of the project.

Subtask M2a-2: Work of Cohesion Measured at Nano-Scale using AFM (WRI)

Work Done This Quarter

In work conducted this quarter it has been shown analytically that solubility parameters (or the square-root of cohesive energy density), the surface tension (or one half of the work of cohesion), and the activation energy of viscous flow of an asphalt determined in the linear viscoelastic region are all related based on thermodynamic arguments. It was shown that the activation energy of viscous flow, $E_a(\eta)$, measured for the SHRP asphalts correlates as a linear function with the phase transition temperature. With respect to fatigue fracture, it was shown that energy dissipation due to plastic deformation appears to correlate with the temperature dependent viscous flow of the “solvent phase” (SEC-II fraction) of the asphalt.

In brittle fracture (Roylance 2001) it is generally accepted that the strain energy released per unit thickness of a material specimen to form a crack of length a may be defined as

$$U = -\pi a^2 U^* = -\frac{\sigma^2 \pi a^2}{2E} \quad (\text{M2a-2.1})$$

where the strain energy per unit volume is expressed as

$$U^* = \int \sigma d\delta = \frac{E\delta^2}{2} = \frac{\sigma^2}{2E} \quad (\text{M2a-2.2})$$

given

$\sigma = f / A$: stress

$\delta = dx / L$: strain

$E = \sigma / \delta$: modulus

Furthermore, a surface energy contribution,

$$S = 2\gamma a \quad (\text{M2a-2.3})$$

is associated with the formation of the crack such that the total energy is given as

$$E = S + U = 2\gamma a - \frac{\sigma^2 \pi a^2}{2E} \quad (\text{M2a-2.4})$$

If the derivative of the total energy to form a crack is evaluated in terms of the crack length at zero (figure M2a-2.1),

$$\frac{\partial}{\partial a} E = 2\gamma - \frac{\sigma^2 \pi a}{E} = 0 \quad (\text{M2a-2.5})$$

a critical crack length is given as

$$a_c = \frac{2\gamma E}{\pi \sigma^2} \quad (\text{M2a-2.6})$$

and with simple re-arrangement of equation M2a-2.6, the stress to form the crack is then given as

$$\sigma = \sqrt{\frac{2\gamma E}{\pi a_c}} \quad (\text{M2a-2.7})$$

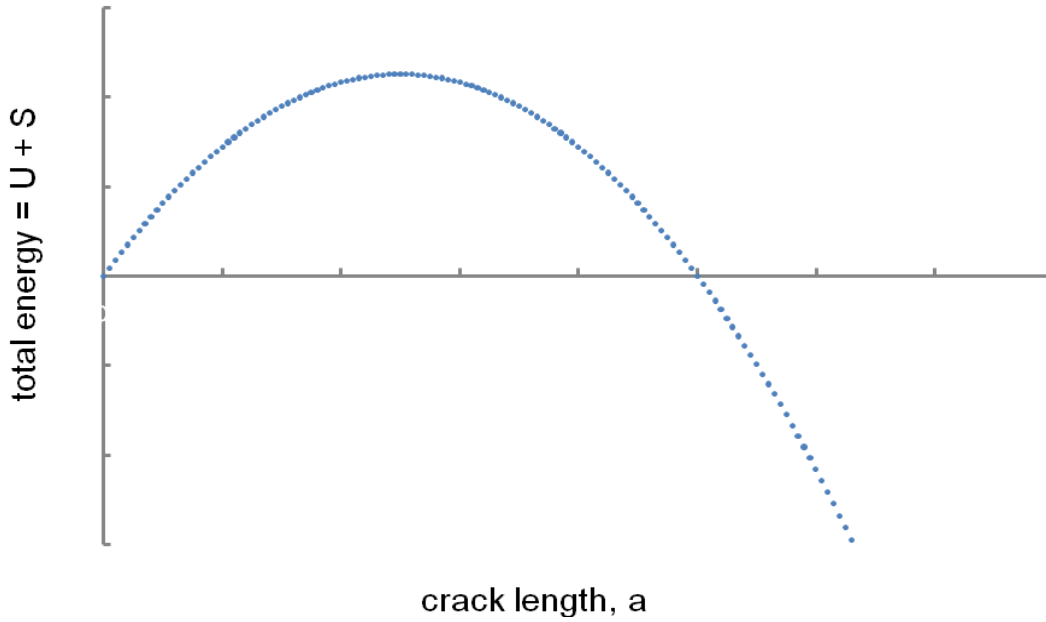


Figure M2a-2.1. Energy versus crack length function (based on equation 4).

If on the other hand it is assumed that plastic deformation occurs in the material, which would account for dissipation of energy at the crack tip, equation M2a-2.7 may be re-written as

$$\sigma = \sqrt{\frac{G_c E a}{\pi a}} \quad (\text{M2a-2.8})$$

where

$$G_c = W + G_p \quad (\text{M2a-2.9})$$

G_c is then referred to as the critical strain energy, which is now expressed as a sum of both a surface energy term, $W = 2\gamma$, (i.e., the work of cohesion), and a plastic deformation energy term G_p ,

In ductile materials, G_p may be observed to be several orders of magnitude greater than W .

Energy Balance Expressions in Polymer Fracture Mechanics

In polymer fracture mechanics (summarized from Williams [1984]), modeling of crack propagation in these materials is again based on energy balance expressions to describe the differential energy contributions of the system. In classical linear elasticity theory, the energy input to a system is balanced by the sum of the forces of recovery of the system. The energy balance equation may be written in terms of the following variational expression,

$$\frac{\delta U_{input}}{\delta u} - \frac{\delta U_{irr,dis}}{\delta u} = \frac{\delta U_{P.E.}}{\delta u} + \frac{\delta U_{K.E.}}{\delta u} \quad (M2a-2.10)$$

where

$$dU_{irr,dis} = \eta \left(\frac{\partial u}{\partial t} \right) du \quad (M2a-2.11)$$

is the irreversible dissipative energy term,

$$dU_{P.E.} = kudu \quad (M2a-2.12)$$

is the potential energy term, and

$$dU_{K.E.} = m \left(\frac{\partial^2 u}{\partial t^2} \right) du \quad (M2a-2.13)$$

is the kinetic energy term. In equations M2a-2.11 through M2a-2.13, u is a length of displacement, t is time, η is viscosity, and m is mass.

It may be shown, by combining equations M2a-2.10 through M2a-2.13, that the load force, P , is derived much like a mechanical oscillator, expressed as

$$P \equiv F_{load} = \frac{dU_{load}}{du} = m \left(\frac{\partial^2 u}{\partial t^2} \right) + \eta \left(\frac{\partial u}{\partial t} \right) + ku \quad (M2a-2.14)$$

For a crack of area, A , in a film of material of undefined thickness, the strain energy release rate, \mathbb{G} , which is the change in internal energy per change in area to form a crack face, is defined as

$$\mathbb{G} = \frac{dU_{load}}{dA} - ku = R + m \left(\frac{\partial^2 u}{\partial t^2} \right) \quad (M2a-2.15)$$

where it may be shown that the fracture resistance, R , is defined as

$$R = \eta \left(\frac{\partial u}{\partial t} \right) \quad (M2a-2.16)$$

In other words, the viscous dampening response in fracture, modeled as a mechanical oscillator, is one of the mechanisms by which the system tends to resist fracture.

Thermodynamic Model of Gas-to-Liquid Phase Transitions

If we now consider a molecular picture of the energetics to create new surface area, as in the case of a nucleation processes, for example, ΔG is said to be a measure of the free energy to transfer n molecules of A-type from the vapor phase to the liquid phase in the absence of surface energy (i.e., a vapor to liquid phase transition process), given the normal vapor pressure of a gas, P_0 , to begin forming a drop, given the pressure observed at the curved interface of the drop, P , the temperature, T , and Boltzmann constant, k_B (Adamson and Gast 1997). The surface free energy consumed or released in the forming of the drop is, much like the Griffith model, taken into account by both bulk and surface energy contributions, written as

$$\Delta G = -nk_B T \ln\left(\frac{P}{P_0}\right) + 4\pi r^2 \gamma \quad (\text{M2a-2.17})$$

given the radius of the drop, r , which defines the surface area $4\pi r^2$, and the work of cohesion, 2γ . Assuming further, based on symmetry considerations, as "spherically shaped" drops form, the Gibb's free energy of formation of such a liquid drop may be re-defined as

$$\Delta G = \left[4\pi r^2 \gamma - \frac{4}{3} \pi r^3 \frac{\rho}{M} RT \ln\left(\frac{P}{P_0}\right) \right] \quad (\text{M2a-2.18})$$

The critical radius to form a drop under a specific set of temperature and pressure conditions is then determined by evaluating the derivative of the free energy in terms of the radius of curvature of the drop interface (figure M2a-2.2)

$$0 = \left[\frac{\partial(\Delta G)}{\partial r} \right]_{r \rightarrow r_c} = -4\pi r_c^2 \frac{\rho}{M} RT \ln\left(\frac{P}{P_0}\right) + 8\pi r_c \gamma \quad (\text{M2a-2.19})$$

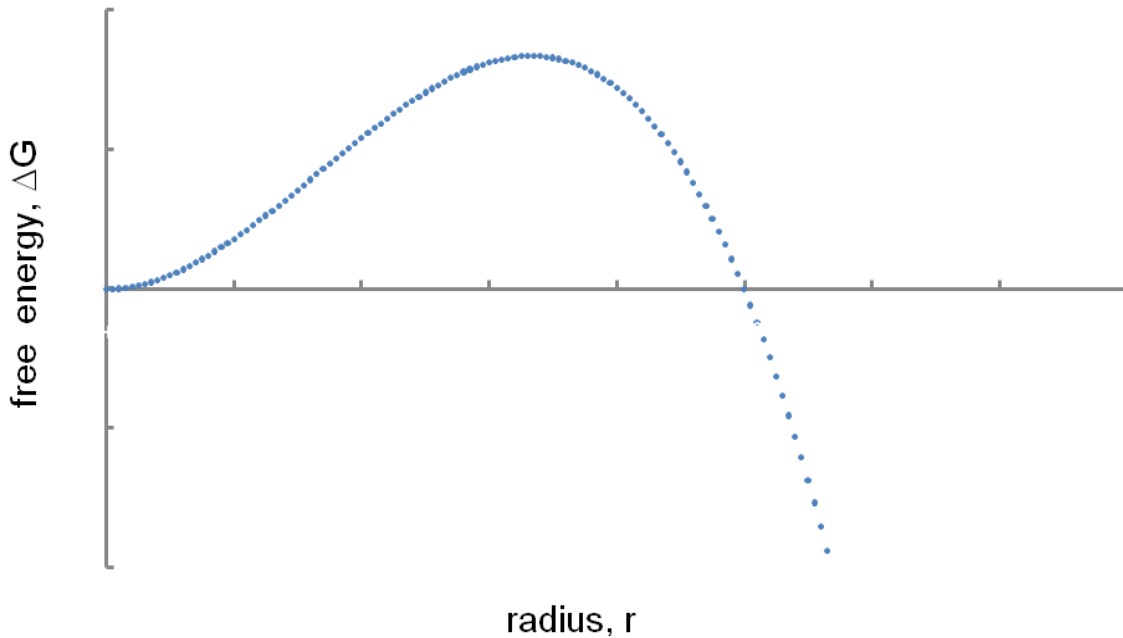


Figure M2a-2.2. Free Energy versus critical radius function (based on equation 18)

Assuming still further that not only pressure, but also temperature changes influence “nucleation” processes leading to the formation of drops of liquids, the Clausius-Clapeyron equation may be conveniently employed to express the thermodynamic relationship between T and P, which is written as

$$RT \ln\left(\frac{P}{P_0}\right) = \Delta H_{vap} \left(1 - \frac{T}{T_b}\right) \quad (\text{M2a-2.20})$$

given the change in the enthalpy of vaporization, ΔH_{vap} and molar mass per density as the molar volume, $M/\rho = \bar{V}$.

Thus, if equation M2a-2.20 is back substituted into equation M2a-2.18, with re-arranged, an expression may be derived which it is then virtually identical to the form of the expression given for equation M2a-2.4 of the Griffith model, given as

$$\frac{\Delta G}{2\pi r} = 2\gamma r - \left(\frac{\Delta T \Delta H_{vap} r^2}{3T_b \bar{V}}\right) \quad (\text{M2a-2.21})$$

This expression suggests that the condensation which occurs at the liquid-vapor interface is then modeled in terms of the temperature change across the interface of the drop by combining equations M2a-2.19 and M2a-2.20, where the critical radius of the drop is conveniently defined in terms of the temperature change, i.e.,

$$\Delta T = T_b - T = \frac{2\gamma M T_b}{r_c \Delta H_{vap} \rho} = \frac{2\gamma \bar{V} T_b}{\Delta H_{vap} r_c} \quad (\text{M2a-2.22})$$

Further rearrangement of equation M2a-2.22 then leads to an expression for the enthalpy of vaporization, described by the interfacial energy measured relative to the temperature change and the critical radius of the drop, written here as

$$\Delta H_{vap} = \frac{2\gamma M T_b}{\Delta T r_c \rho} = \frac{2\gamma \bar{V} T_b}{\Delta T r_c} \quad (\text{M2a-2.23})$$

Finally, recognizing that the enthalpy of vaporization is related to the solubility parameter, δ , of the fluid which comprises the liquid drop, written as

$$\Delta H_{vap} = \delta^2 \bar{V} + RT, \quad (\text{M2a-2.24})$$

upon substitution of equation M2a-2.24 into equation M2a-2.23, an expression may be derived directly relating the solubility parameter to the surface tension, which is written as

$$2\gamma = \frac{r_c \Delta T}{T_b} (\delta^2 + P) \quad (\text{M2a-2.25})$$

In equation M2a-2.25 the substitution $P = RT / \bar{V}$ has been made. Equation M2a-2.25 now constitutes a relationship between T, P, the surface tension, and the cohesive energy density (the solubility parameter squared), that describes the force balance condition at the liquid-vapor interface. Generally it is found that $\delta^2 \gg P$ so that

$$2\gamma \approx \frac{r_c \Delta T}{T_b} \delta^2 \quad (\text{M2a-2.26})$$

For many common organic liquids, the surface tensions, solubility parameters, and boiling point temperatures have been reported. These values, with the aid of equation M2a-2.26 may be used to calculate critical radii (see table M2a-2.1)

An interesting point to make in regard to equation M2a-2.26 is that it helps to rationalize the concept of interaction-types (e.g., dispersive forces-d, hydrogen bonding-h, polar interactions-p, etc. associated with both solubility parameters and surface free energies, this may be expressed in an equation as

$$\gamma_{dispersive} + \gamma_{h-bond} + \gamma_{polar} + \dots = \frac{r_c \Delta T}{T_b} (\delta_d^2 + \delta_h^2 + \delta_p^2 + \dots) \quad (\text{M2a-2.27})$$

Re-arrangement of equation M2a-2.26 leads to

$$\delta = \sqrt{\frac{2\gamma T_b}{r_c \Delta T}} \quad (\text{M2a-2.28})$$

Thus, equation M2a-2.28 may be interpreted as the cracking analog of the nucleation process given by equation M2a-27 from the Griffith model, i.e.,

$$\sigma = \sqrt{\frac{2\gamma E}{\pi a_c}} \quad (\text{M2a-2.7})$$

i.e., note the similarity between equations M2a-2.7 and M2a-2.28.

Table M2a-2.1. Physico-chemical properties applicable to equation M2a-2.26 list for several model organic liquids

Organic liquid	Surface tension @ 20°C (mJ/m ²)	Boiling Temperature (°C)	Solubility Parameter (J/m ³)	Critical radius (mm)	Density (g/mL)
pentane	16.00	36.1	14.69	2.85	0.626
hexane	18.40	69.0	15.24	1.11	0.655
heptane	20.00	98.4	15.26	0.81	0.684
octane	21.80	125.7	15.46	0.69	0.703
nonane	23.00	150.8	15.63	0.61	0.718
decane	23.90	174.0	15.79	0.56	0.730
undecane	24.70	194.5	15.95	0.52	0.741
dodecane	25.40	214.5	16.04	0.50	0.751
water	72.75	100.0	48.07	0.29	1.000
methanol	22.60	64.7	29.21	0.40	0.791
ethanol	22.27	78.4	24.48	0.45	0.788
propanol	23.80	97.2	21.12	0.51	0.804
toluene	28.43	110.6	18.28	0.72	0.867
benzene	28.90	80.1	18.72	0.97	0.879
cyclohexane	25.30	80.7	17.20	1.00	0.779

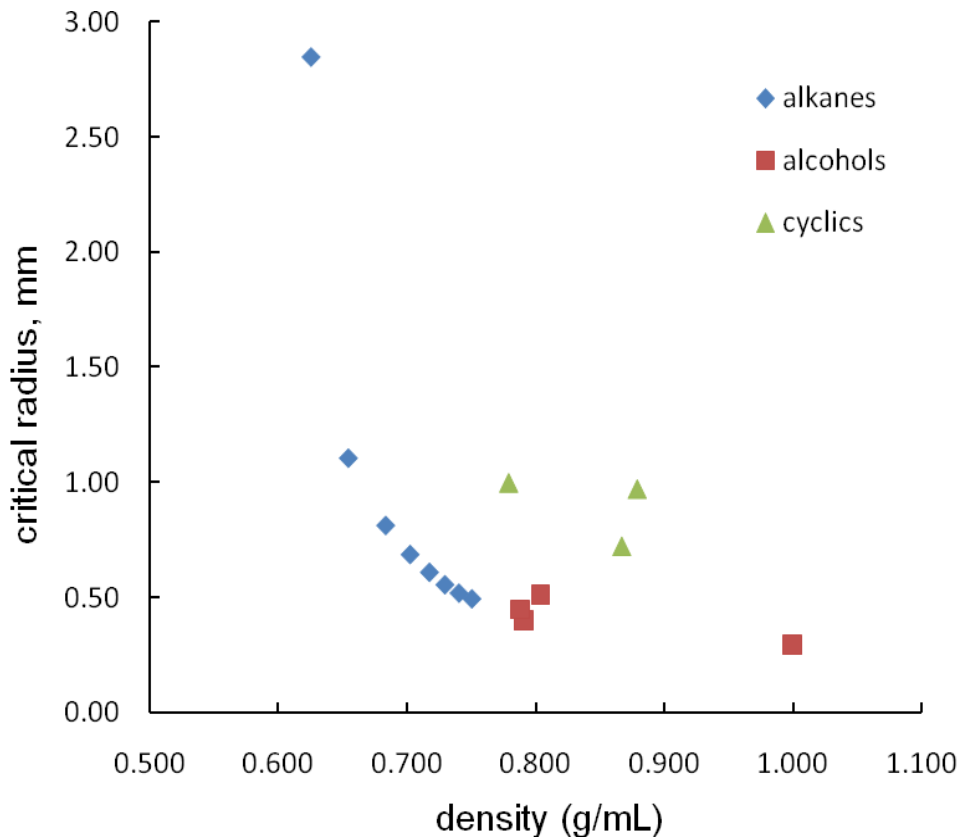


Figure M2a-2.3. Critical radius of condensing drop plotted versus liquid density.

Furthermore, equation M2a-2.27 may just as well be substituted into equation M2a-2.7 to give

$$\sigma = \sqrt{\frac{\left(r_c \delta^2 \frac{\Delta T}{T_b} \right) E}{\pi a_c}} \quad (\text{M2a-2.29})$$

Einstein's Theory of Phenomena of Capillarity Applied to Asphalt Flow

Experimental approaches were undertaken in previous work (Robertson 2005, 2006) to determine the surface free energy properties of hot liquid asphalts employing surface tension measurements, and room temperature asphalts employing contact mechanic approaches. In order to better interpret the results that were obtained, Einstein's model of capillary phenomena is considered. In this work, Einstein (Einstein 1906; Beck and Havas 1989) proposed that the amount of mechanical work supplied to a liquid, γ , to increase the surface free energy by one unit (not specified) is a cyclic process denoted as

$$\gamma_1(A_2 - A_1) = \gamma_2(A_2 - A_1) \quad (\text{M2a-2.30})$$

where $(A_2 - A_1)$ is the isothermal increase in the surface area, such that the total heat supplied to the system is equal to the total heat withdrawn. The enthalpy of this process may then be denoted as

$$dH = c^\sigma AdT + (\gamma + q^\sigma) dA \quad (\text{M2a-2.31})$$

where c^σ is the specific heat defined at the surface $^\sigma$, and q^σ is the heat necessary to form the surface of unit area. The Free energy of this process is then expressed as

$$dG \equiv \gamma dA = dH - q^\sigma dA - c^\sigma AdT \quad (\text{M2a-2.32})$$

where the entropy is given as

$$dS = \frac{c^\sigma AdT}{T} + \frac{q^\sigma}{T} dA \quad (\text{M2a-2.33})$$

or

$$-TdS = -c^\sigma AdT - q^\sigma dA \quad (\text{M2a-2.34})$$

The total differentials are then expressed as

$$\frac{\partial(c^\sigma A)}{\partial A} = \frac{\partial(\gamma + q^\sigma)}{\partial T} \quad (\text{M2a-2.35})$$

and

$$\frac{\partial}{\partial A} \left(\frac{c^\sigma A}{T} \right) = \frac{\partial}{\partial T} \left(\frac{q^\sigma}{T} \right) \quad (\text{M2a-2.36})$$

Einstein then suggested that no heat should be ascribed to the surface, but rather, that the energy of the surface was potential by nature, (i.e., by definition $c^\sigma = 0$). It then follows from solving the differentials given by equations M2a-2.35 and M2a-2.36, assuming $c^\sigma = 0$ that

$$(\gamma + q^\sigma) dA = dH - c^\sigma AdT \quad (\text{M2a-2.37})$$

Thus, the total energy necessary to form a unit of surface is expressed as

$$\gamma + q^\sigma = \gamma - T \frac{\partial \gamma}{\partial T} \quad (\text{M2a-2.38})$$

By taking the derivative of this expression in terms of T ,

$$\frac{\partial}{\partial T}(\gamma + q^\sigma) = \frac{\partial}{\partial T}\left(\gamma - T \frac{\partial \gamma}{\partial T}\right) \quad (\text{M2a-2.39})$$

the interfacial heat capacity may be derived as

$$c^\sigma = \frac{\partial \gamma}{\partial T} + \frac{\partial q^\sigma}{\partial T} = -T \frac{\partial^2 \gamma}{\partial T^2} = 0 \quad (\text{M2a-2.40})$$

This then lead Einstein to consider the attractive forces between molecules at a surface, separated by a distance, r , where the difference in the relative potential, $\Delta\Phi$, between two molecules could then be expressed as

$$\Delta\Phi \equiv \Phi - \Phi_\infty = -\xi_1 \xi_2 \varphi(r) \quad (\text{M2a-2.41})$$

where $\xi_1, \xi_\alpha, \xi_\beta, \dots$ are constants characteristic of the molecules, and $\varphi(r)$ is the intermolecular potential function. Thus, for n molecules at the surface,

$$n = \frac{1}{2} \xi_\alpha \xi_\beta \sum_{\alpha=1}^n \sum_{\beta=1}^n \varphi(r_{\alpha\beta}) \quad (\text{M2a-2.42})$$

which may be written

$$n = \frac{1}{2} \xi_\alpha^2 \sum_{\alpha=1}^n \sum_{\alpha=1}^n \varphi(r_{\alpha\alpha}) \quad (\text{M2a-2.43})$$

for a surface comprised of identical molecules.

If it is then assumed that the magnitude in the potential due to the molecular forces is representative of a homogeneous distribution of particles in the material (i.e., a spherical drop of water floating in zero gravity for example) the change in the relative potential of the system may be expressed as

$$\Delta\Phi = -\frac{\left(\sum \xi_\alpha\right)^2}{2\bar{V}} \iint \varphi(r) dA \quad (\text{M2a-2.44})$$

where \bar{V} is the molecular volume. If it is finally assumed that the density of the liquid is constant in this volume up to the surface, then the potential energy per unit volume within the liquid may be defined as

$$\Delta\Phi = -E \frac{\left(\sum \xi_\alpha\right)^2}{\bar{V}} \quad (\text{M2a-2.45})$$

where $E = \frac{1}{2} \iiint_{\pm\infty} \varphi(r) d\tau$, $r = \sqrt{x^2 + y^2 + z^2}$ and $d\tau = dx dy dz$. If the surface is then taken into account

$$\Delta\Phi = -\frac{\left(\sum \xi_{\alpha}\right)^2}{\bar{V}}(EV + E'A) \quad (\text{M2a-2.46})$$

where $E' = \int_{x'=0}^1 \int_{y'=0}^1 \int_{z'=-\infty}^{\infty} \int_{x=-\infty}^{\infty} \int_{y=-\infty}^{\infty} \int_{z=0}^{\infty} \varphi\left(\sqrt{(x-x')^2 + (y-y')^2 + (z-z')^2}\right) d\tau d\tau'$,

the potential of the surface of the liquid drop, Φ , is finally expressed as

$$\Phi = E' \frac{\left(\sum \xi_{\alpha}\right)^2}{\bar{V}} = \gamma - T \frac{d\gamma}{dT} \quad (\text{M2a-2.47})$$

Adamson (Adamson and Gast 1997), later showed that Φ was simply the total surface energy, E^S , which may be approximated as the surface enthalpy, H^S .

Asphalt surface tensions measured as a function of temperature employing duNOÛY ring tensiometry (Robertson et al. 2001) were combined with asphalt surface free energies determined by contact mechanics techniques (i.e., AFM pull-off force work of adhesion measurements [Robertson et al. 2005]). Figure M2a-2.4 depicts a plot of surface tension versus temperature, $T^{\circ}\text{C}$, measured for SHRP core asphalt AAB-1.

It is observed by inspection of figure M2a-2.4, where asphalts were measured throughout the temperature range from ambient, 25°C to $\sim 130^{\circ}\text{C}$, exhibit a non-linear behavior in terms of surface tension measured as a function of temperature. Curve fit analysis of surface tension versus temperature data suggests that a third-order polynomial function approximates the trend in the data. Table M2a-2.2 lists regression parameters and phase transition temperatures calculated for seven of the eight SHRP core asphalts, based on a non-linear fit of $\gamma(T^{\circ}\text{C})$ vs. $T^{\circ}\text{C}$ data points to a third order polynomial expression of the form

$$\gamma(T^{\circ}\text{C}) \approx g_0 + g_1T + g_2T^2 + g_3T^3 \quad (\text{M2a-2.48})$$

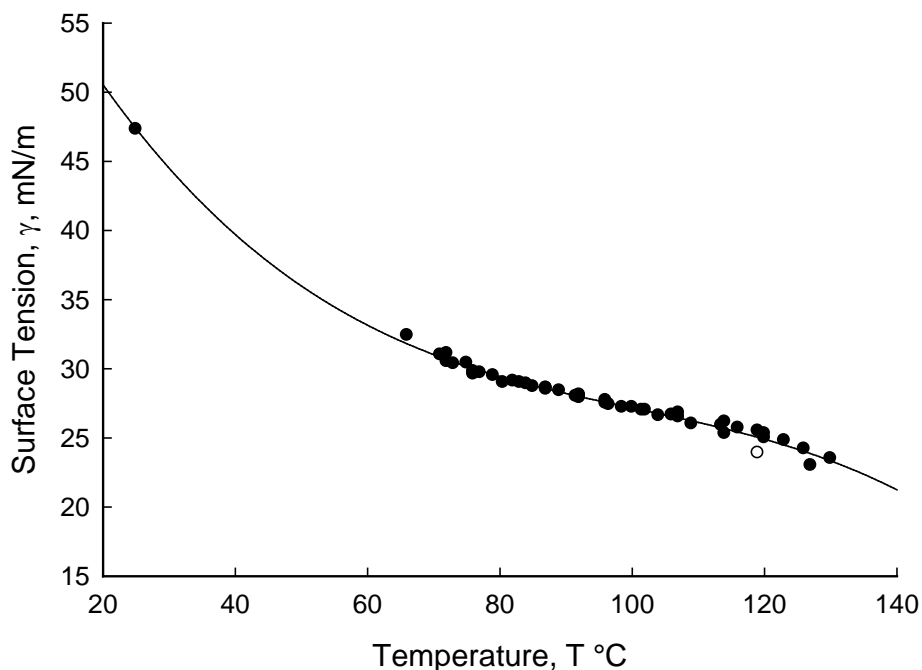


Figure M2a-2.4. SHRP asphalt AAB-1; temperature, T °C, plotted versus surface tension, γ (mN/m).

Table M2a-2.2. Regression coefficients and phase transition temperatures, T^* °C, calculated and/or estimated for seven of the eight SHRP core asphalts, and asphalt flow activation energies.

Asphalt	g_0	g_1	g_2	g_3	T^* °C	$E_a(\eta)$, kcal/mol
AAA-1	175.40	-4.7421	5.2300E-02	-2.00E-04	87.17	33
AAB-1	67.07	-0.9920	8.9000E-03	-2.95E-05	100.44	37
AAC-1	59.09	-0.7488	6.3000E-03	-2.07E-05	101.58	38
AAD-1	50.36	-0.5001	4.0000E-03	-1.43E-05	93.24	34
AAF-1	63.72	-0.7345	5.1000E-03	-1.47E-05	115.42	42
AAG-1	81.87	-1.3827	1.2300E-02	-3.91E-05	104.87	39
^{est} AAK-1	-0-	-0-	-0-	-0-	95	36
AAM-1	67.39	-0.9045	7.3000E-03	-2.23E-05	108.93	41

Phase-transition temperatures, T^* °C, listed in table M2a-2.2 were derived for the eight SHRP asphalts by taking the second derivative in the third order polynomial function in order to determine an inflection point, estimated as

$$T^* \text{ °C} = \frac{-g_2}{3g_3} \quad (\text{M2a-2.49})$$

this is rationalized when Einstein's concept of a surface heat capacity is applied to interpret the surface tension versus temperature data, where

$$\begin{aligned}
\frac{c^\sigma}{T} &= \frac{d^2}{dT^2} \gamma \\
&= \frac{d^2}{dT^2} (g_0 + g_1 T + g_2 T^2 + g_3 T^3) \\
&= 2g_2 + 6g_3 T \\
&= 0
\end{aligned}
\tag{M2a-2.50}$$

Phase transitions in asphalt surface tension, such as the type measured here may best be defined as a Newtonian liquid to viscoelastic liquid (semi-solid) phase change at a “softening” temperature, T^* . During these types of experiments it is often observed that above the phase transition temperature, the platinum ring cleanly snaps off of the surface of the “liquid” asphalt, but as the phase transition temperature is approached and passed through (below the “melting” temperature), the asphalt material begins to “neck” or “strand” up with the ring, constituting a ductile state of the material.

If Ewell’s and Eyring's (Ewell and Eyring 1937) equation, $\Delta U_{vap} = n_E E_{a,vis}$, relating the flow activation energy, $E_{a,vis}$, to the internal energy of vaporization, where n_E is referred to as the Eyring number and which varies between 3 to 4 depending on the shape of the molecules which a liquid of interest, is substituted into equation M2a-2.23, given the relationship between internal energy and enthalpy, $\Delta H_{vap} = \Delta U_{vap} + RT$, the following expression may be derived,

$$E_{a,i} = \left(\frac{2\gamma_i \bar{V}}{n_E r_c (\Delta T)^2} \right) T^* - \frac{RT}{n_E}
\tag{M2a-2.51}$$

In this expression i -subscripts denote a specific liquid, and T^* denote a melting or softening point phase transition temperature.

Figure M2a-2.5 depicts a plot of the activation energy of viscous flow, $E_a(\eta)$, reported for the eight SHRP core asphalts plotted as a function of the surface tension versus temperature based measurement of the phase transition temperatures, T^* ($^{\circ}C$), as reported in table M2a-2.2.

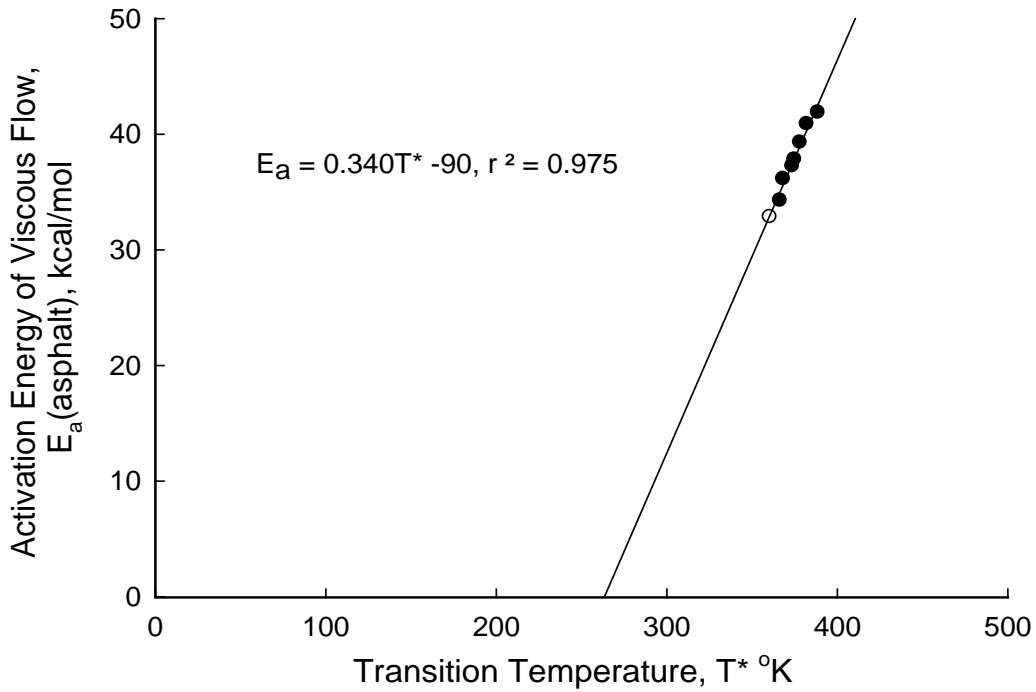


Figure M2a-2.5. Plot of the activation energy of viscous flow of the asphalt, $E_a(\eta)$, reported for the eight SHRP core asphalts plotted as a function of the phase transition temperatures, T^* ($^{\circ}\text{C}$).

This figure clearly shows that the activation energy of viscous flow, $E_a(\eta)$, measured for the SHRP asphalts correlates as a linear function with the phase transition temperature, T^* ($^{\circ}\text{C}$), in accordance with equation M2a-2.51,

$$E_{a,vis} = b_1 T^* - b_0 \quad (\text{M2a-2.52})$$

It directly follows from the two previous sections that solubility parameters (or the square-root of cohesive energy density), the surface tension (or one half of the work of cohesion), and the activation energy of viscous flow of an asphalt determined in the linear viscoelastic region are all related based on thermodynamic arguments. Thus, activation energies of viscous flow determined for neat asphalts, and asphalt fractions including n-heptane soluble maltenes and SEC-II materials were used to calculate the "effective work of cohesion" for the eight SHRP asphalts, i.e.,

$$\delta = \sqrt{\frac{\Delta U_{vap}}{\bar{V}}} = \sqrt{\frac{n_E E_{a,vis}}{\bar{V}}} = \sqrt{\frac{2\gamma T_c}{r_c \Delta T}} \quad (\text{M2a-2.28})$$

In order to carry out these calculations, values for average boiling temperature, molecular mass and radius of curvature had to be established for asphalt. The values that were ultimately used were $T_c = 300^{\circ}\text{C}$, $\bar{V} = M / \rho = (850\text{ g/mol}) / (1.0\text{ g/mL}) = 850\text{ mL/mol}$, and $r_c = 0.29\text{ mm}$. The

choice of using a critical radius equal to that of water is based on the trends in data depicted in figure M2a-2.3 (*Figure M2a-2.3. Critical radius of condensing drop plotted versus liquid density.*), given that asphalts are observed to have the same density as water.

Table 3 lists activation energies of viscous flow measured for the eight SHRP asphalts based on low shear viscosity versus temperature measurements in the 25°C to 60° temperature range, and the 25°C solubility parameter and surface tension determined based on equation M2a-2.28.

Table M2a-2.3, activation energies of viscous flow measured for the eight SHRP asphalts based on low shear viscosity versus temperature measurements in the 25°C to 60° temperature range, and 25°C solubility parameter and surface tension determined based on equation M2a-2.28.

Asphalt	E _a (kJ/mol)	solubility Parameter (J/m ³)	surface tensions (mJ/m ²)
AAA1	138	24	39
AAB1	156	25	45
AAC1	158	26	45
AAD1	144	24	41
AAF1	175	27	50
AAG1	165	26	47
AAK1	151	25	43
AAM1	171	27	49

The asphalt surface tensions calculated here are found to be very similar to asphalt surface tensions measured based on other methods (Miknis et al. 2004). In the following section viscous flow activation energies of asphalt and asphalt fraction materials will be shown to correlate with fatigue life.

Fatigue Testing (Fracture Excluding Healing)

As part of the SHRP program, Tayebali (Tayebali et al. 1994) determined the fatigue life, N_f , for asphalt mixtures where

$$N_f = a \left(\frac{1}{\dot{\epsilon}_0} \right)^b \left(\frac{1}{S_0} \right)^c \quad (\text{M2a-2.53})$$

given

$\dot{\epsilon}_0$: initial tensile strain

S_0 : initial stiffness of mixture

a , b , and c : fitting coefficients

In this work tests were carried out employing the Flexural Beam Fatigue Test to determine the number of load cycles to failure of test specimens prepared as asphalt-aggregate mixtures. Based on this approach the cumulative dissipated energy to failure, W_N may be related to the fatigue life as

$$W_N = A(N_f)^z \quad (M2a-2.54)$$

given A , z : fitting parameters. Figure M2a-2.6 depicts the relationship for W_N as a function of N_f for test data obtained for mixtures prepared from the eight SHRP core asphalts and two SHRP aggregates, RD and RH. This particular data represents the average in an 8 X 2 experimental matrix. With the exception of mixtures prepared with SHRP asphalt AAM-1 the remaining data fit the relationship expressed in equation M2a-2.54 where A and z are determined as 11.4 and 0.49, respectively.

Table M2a-2.4. Flexural stiffness, fatigue life, and cumulative dissipated energy (Tayebali et al. 1994), fracture temperature (Jung and Vinson 1993), and activation energy of viscous flow of SEC-II materials listed for the Eight SHRP core asphalts.

Asphalt Source	Flexural Stiffness (poise)	Fatigue Life	Cumulative dissipated energy (psi)	Fracture Temp (°C)	Ea(SEC-II) (kcal/mol)
AAA-1	295,400	99,300	3100	-30.50	20
AAB-1	409,900	70,300	2700	-25.00	23
AAC-1	552,700	41,200	2100	-23.00	33
AAD-1	386,200	74,400	2800	-26.00	17
AAF-1	1,033,000	25,100	1800	-17.00	39
AAG-1	1,172,700	7,200	600	-16.00	46
AAK-1	592,800	46,200	2400	-22.50	23
AAM-1	604,800	71,200	3400	-21.00	39

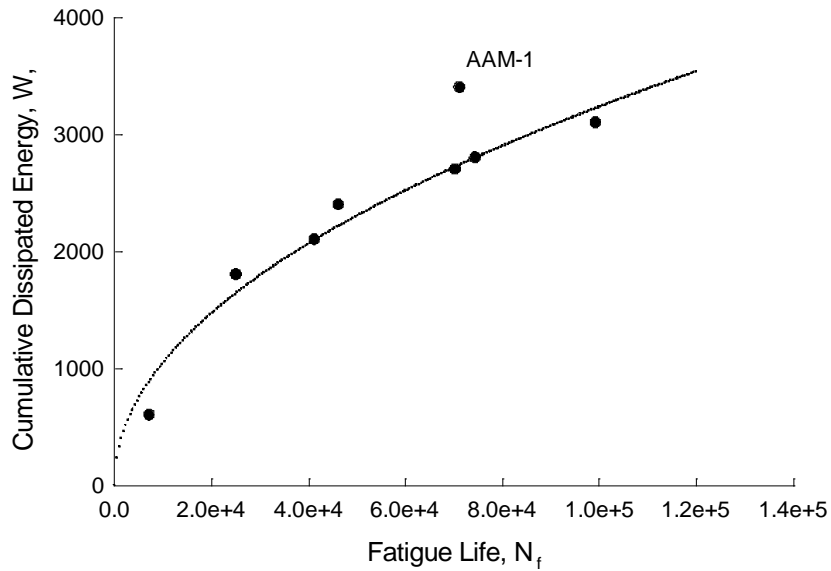


Figure M2a-2.6. Cumulative dissipated energy to failure, W_N (psi), determined based on the flexural beam fatigue test, plotted as a function of the fatigue life, N_f , reported as the number of cycles to failure.

If it is further assumed, based on discussions presented in the previous sections, the cumulative dissipated energy should correlate with an activation energy of viscous flow (refer to equations M2a-2.15, M2a-2.26 and M2a-2.28), thus, activation energies of viscous flow of neat asphalts, n-heptane maltenes and SEC-II fractions are each considered. Figure M2a-2.7 depicts the best correlation that was found. Furthermore, figure M2a-2.7 depicts the cumulative dissipated energy to failure, W_N (psi), determined based on the flexural beam fatigue test, plotted as a function of the viscous flow activation energy of SEC-II materials, $E_a(SECII)$, kcal/mol, determined for the eight SHRP core asphalts.

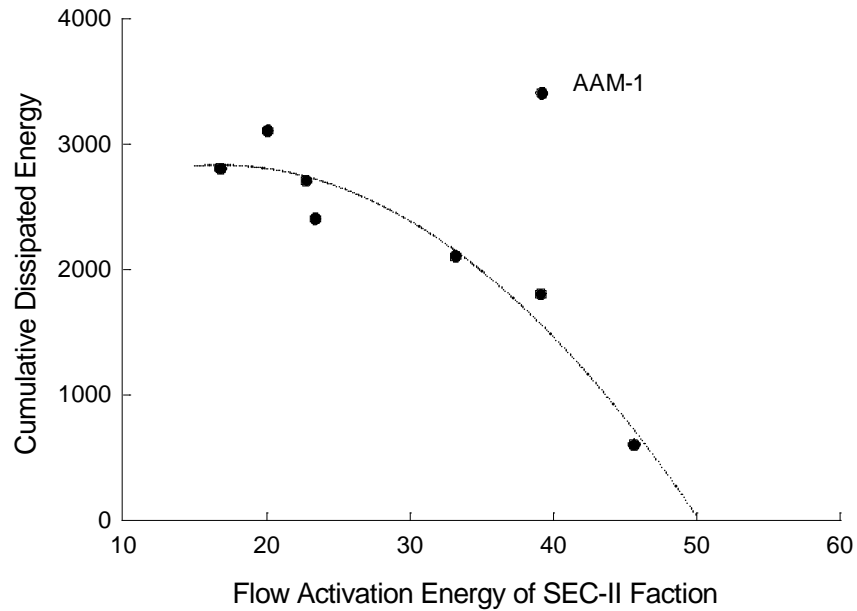


Figure M2a-2.7. Cumulative dissipated energy to failure, W_N (psi), determined based on the flexural beam fatigue test, plotted as a function of the viscous flow activation energy of SEC-II materials, $E_a(SECII)$, kcal / mol , determined for the eight SHRP core asphalts.

Furthermore, both fatigue life and flexural strength values could be correlated with the fracture temperature (Jung and Vinson 1993), (refer to figures M2a-2.8 and M2a-2.9).

The theories and correlations present in this and the previous sections strongly suggest that fatigue fracture may be closely related to brittle modes of fracture at lower temperatures. In other words, it is difficult to imagine asphalts fracturing at warm temperatures when in a fluid state. Furthermore, the mode of energy dissipation due to the plastic deformation appears to correlate with the temperature dependent viscous flow properties of the "solvent phase" of the asphalt, as measured by the activation energy of viscous flow of the SEC-II fraction. Unfortunately, this approach does not address the phenomena of healing, which effectively reverses some of the accumulated damage brought about due to fatigue fracture.

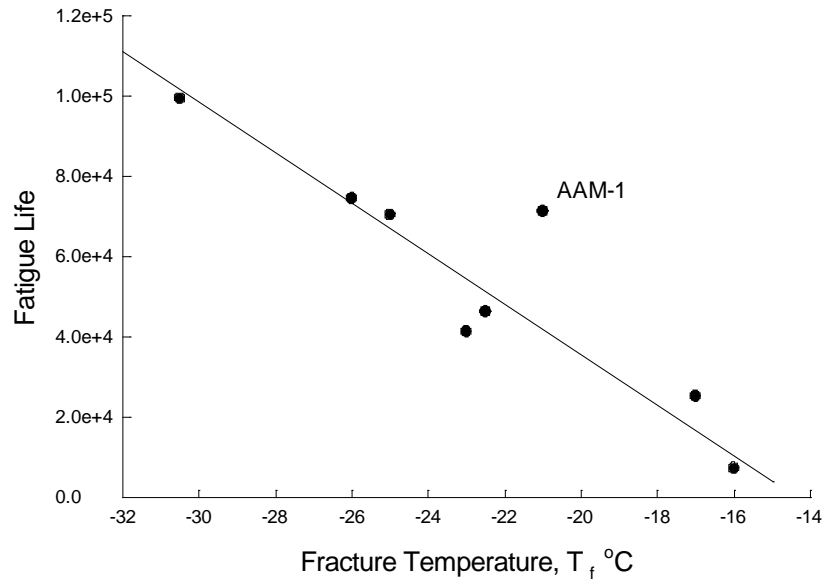


Figure M2a-2.8. Fatigue life, N_f , determined based on the flexural beam fatigue test, plotted as a function of the fracture temperature based on TSRST.

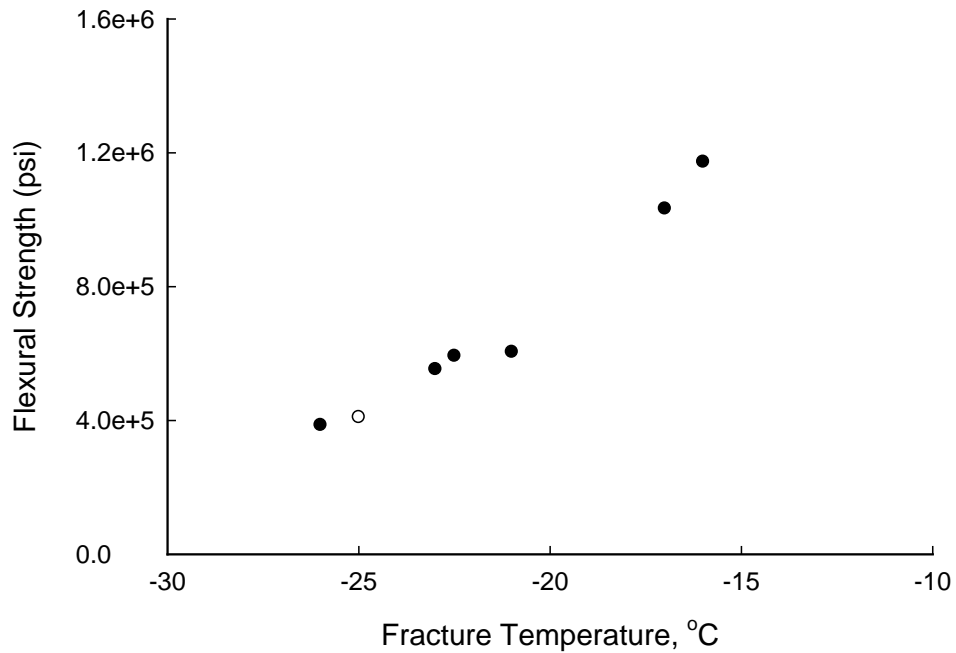


Figure M2a-2.9. Flexural Strength (psi), determined based on the flexural beam fatigue test, plotted as a function of the fracture temperature based on TSRST.

Healing Associated with Fatigue

Little et al., 2001, had the following to report in regard to fatigue and healing: "Surface energy density (SED) is explained by Schapery (1988) to be an integral part of the fracture and healing processes. Furthermore, Lytton et al. (1998) propose an allied theory of how the rate of fracture and the rate of healing (in asphalt mixtures) can be explained by the first principles of fracture originated by Schapery and considering the effects of SED. Since SED is a measurable parameter for both of the two major components of the asphalt mixture (bitumen and aggregate), and since it is related fundamentally to fracture and healing theory, the authors considered it wise to develop a theoretical understanding that links SED to the fatigue process and hopefully to explain differences in fatigue and healing among different bitumen and aggregates based on their different SED values (for both bitumen and aggregate). Furthermore, it should follow that SED values of the bitumen should relate to differences in the aromatic, amphoteric, and wax contents of these bitumen."

In this work (Lytton et al. 2001) showed how healing mechanisms could be explained in terms of surface energies, where the surface energy density, γ_f ,

$$2\gamma_f \equiv E_R D_f(t_d) J_v \quad (\text{M2a-2.55})$$

given E_R , the reference modulus, $D_f(t_d)$, the tensile creep compliance as the time required to propagate the crack length distance ahead of the crack within the process zone and J_v , the J-integral may be related to both short term, \dot{h}_1 , and long term, \dot{h}_2 , healing rates, expressed as

$$\frac{\partial h_1}{\partial t} \equiv \dot{h}_1 = \beta \cdot \left[\frac{k_{th} E_R D_{1c} H_v}{2\gamma_h} \right]^{1/m_c} \quad (\text{M2a-2.56})$$

and

$$\frac{\partial h_2}{\partial t} \equiv \dot{h}_2 = \beta \cdot \left[\frac{2\xi_m E_R^2 D_{1c} \gamma_h}{(1-\nu) C_m^{1/m_c} H_v} \right]^{1/m_c} \quad (\text{M2a-2.57})$$

given

β : size of crack healing zone

E_R : reference modulus

D_{1c} : compressive creep compliance constant

γ_h : wetting surface energy

ν : Poisson's ratio

k_{th} , ξ_m , C_m : fitting constants

H_v : healing integral

m_c : creep compliance slope

According to Lytton et al. 2001 *"In order to understand the healing mechanism of asphalt concrete, it is helpful to keep the healing models developed for polymers in mind. Petersen (1984) claims that the association force (secondary bond) is the main factor controlling the physical properties of asphalt. That is, the higher the polarity, the stronger the association force is, and the more viscous the fraction is, even if molecular weights are relatively low. Petersen also presented a vivid description of the effect of degree of peptization on the flow properties as follows: Consider what happens when a highly polar asphaltene fraction having a strong tendency to self-associate is added to a petrolene fraction having a relatively poor solvent power for the asphaltenes. Intermolecular agglomeration will result, producing large, interacting, viscosity-building networks. Conversely, when an asphaltene fraction is added to a petrolenes fraction having relatively high solvent power for the asphaltenes, molecular agglomerates are broken up or dispersed to form smaller associated species with less inter-association; thus, the viscosity-building effect of the asphaltenes is reduced. Traxler (Traxler 1960) also suggested that the degree of dispersion of the asphalt components is inversely related to the complex (non-Newtonian) flow properties of the asphalt."*

Based on the hypotheses proposed by Lytton (Lytton et al. 2001), correlations were sought which would relate colloidal dispersion properties of neat asphalts to the healing rates determined by Lytton. Figure M2a-2.10 depicts a correlation between the short term healing rate determined by DMA (Dynamic Mechanical Analysis) fatigue testing of asphalt mixtures plotted versus the reversible asphaltene peptizability "compatibility" parameter, determined based on ASTM D04 6703, Standard Method for Automated Heithaus Titrimetry. Furthermore, figure M2a-2.11 depicts a correlation relating the long term healing rate determined by DMA testing of asphalt mixtures to the activation energy of viscous flow of the SEC-II fraction solvent material of asphalt.

The correlation depicted in figure M2a-2.10 suggests that asphalts which are more compatible (i.e., more solvent-like in their colloidal composition, less asphaltenes, and more ductile), tend to heal at a faster rate compared to less compatible materials, (i.e., asphalts, which are more brittle and tend to have a higher asphaltene content). The correlation depicted in figure M2a-2.11, on the other hand, is counter intuitive, in that, asphalts which require more energy to move molecules (i.e., higher activation energy of viscous flow) correlate with a more rapid long term healing rate.

The results presented in this report constitute a starting point and direction for future studies. Some critical points that relate the present findings would be; 1. The most recent studies regarding asphalt composition suggest that the dispersive interactions may be more important to the colloidal stability and flow properties of asphalt than polar interactions, 2. Asphalt flow properties are readily modeled as a binary solute-solvent system, thus, a proof for the existence of colloidal assemblages is still forth coming, instead, asphalt appears to be a viscous solution which solidifies and becomes brittle on the basis of molecular motion and effective mass

arguments, and 3. Structuring phenomena in asphalt thin films appears to be more related to the presence of wax in asphalts.

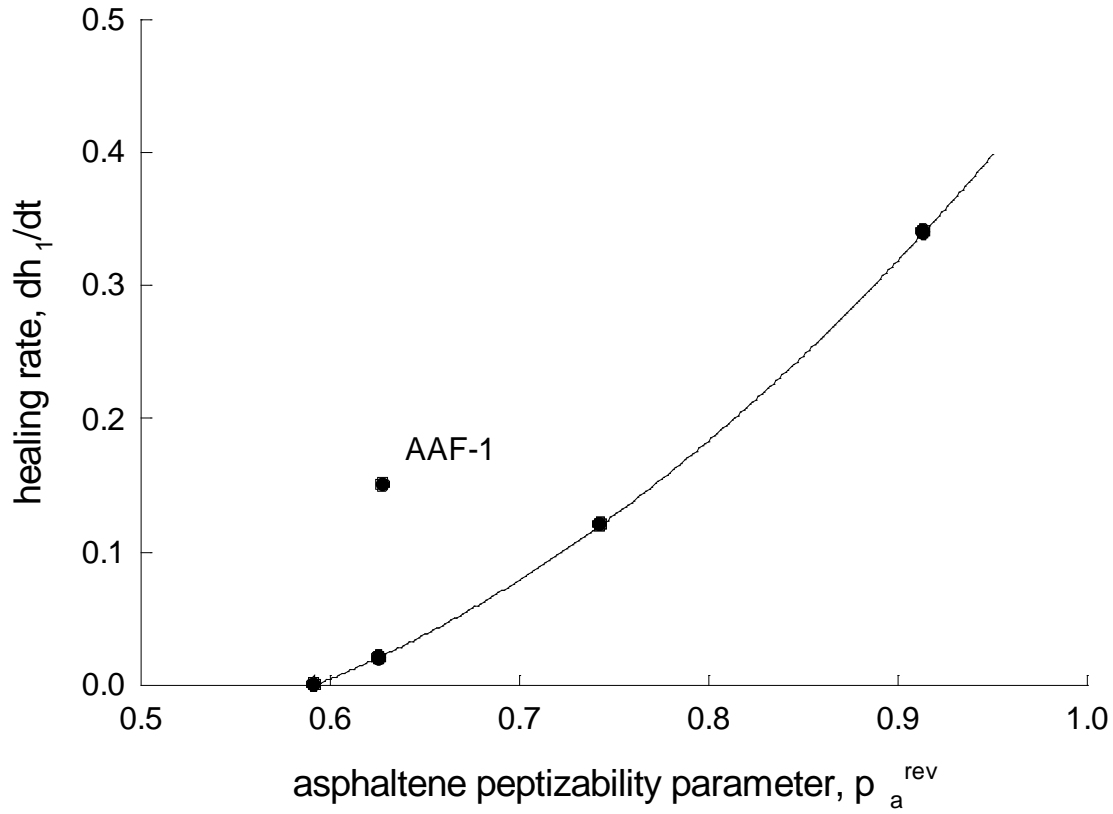


Figure M2a-2.10. Short term heating rate determined by DMA analysis of asphalt mixtures plotted versus the reversible asphaltene peptizability "compatibility" parameter, determined based on ASTM D04 6703, Standard Method for Automated Heithaus Titrimetry (ASTM 2008).

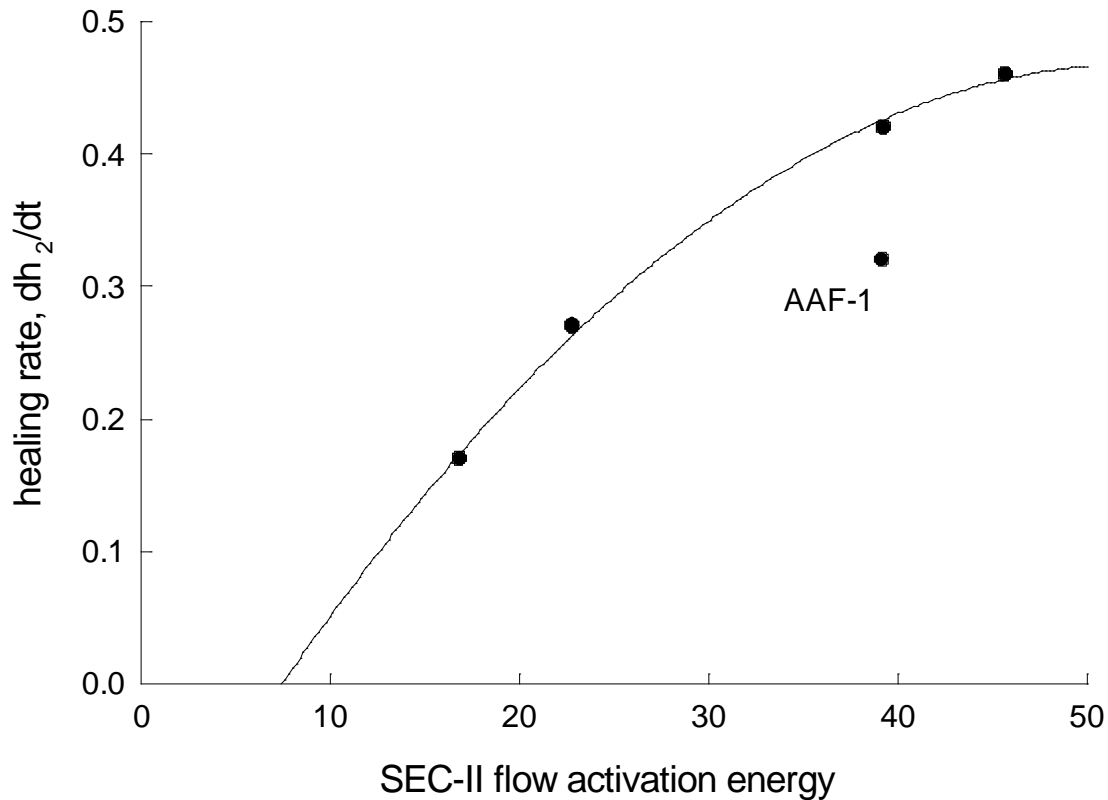


Figure M2a-2.11. Long term heating rate determined by DMA analysis of asphalt mixtures plotted versus the activation energy of viscous flow of the SEC-II fraction solvent material of asphalt.

Significant Results

In the work conducted this quarter it has been shown both analytically and computationally that the cohesive energy density, the work of cohesion and the activation energy of viscous flow of whole asphalt and asphalt fractions determined in the linear viscoelastic region are all related based on classical thermodynamic arguments. It was shown that functional relationships could be developed between the activation of viscous flow of an asphalt solvent phase material (e.g., SEC-II fraction material), as determined by size-exclusion chromatography, and a Newtonian liquid to viscoelastic semi-solid phase transition temperature based on temperature dependent surface tension measurements. With respect to fatigue cracking, the activation energy of viscous flow of the SEC-II material phase of asphalts could be further correlated with the cumulative dissipative energy determined based on flexural beam testing. These correlations strongly suggest that the mode of energy dissipation due to plastic flow in asphalt is somehow related to the viscoelastic properties of asphalt, specifically measured as the activation energy of viscous flow of the SEC-II material phase of asphalts. It was further shown that fatigue life, when healing is neglected, correlated with the fracture temperature. This finding may suggest that

fatigue cracking is closely related to embrittlement of the asphalt at low temperatures. Finally, correlations were developed relating the healing rates based on DMA testing to both asphalt compatibility and the flow property of the binder, again expressed as the activation energy of viscous flow of the SEC-II material phase of asphalts. These correlations suggested that the rate of short term healing could be related to the sol-gel nature of asphalt, where sol-type asphalts tend to heal at a faster rate than gel-type asphalts. By contrast, long term healing rates, which were found to correlate with the activation energy of viscous flow of the SEC-II material phase of asphalts, did so based on counterintuitive expectations. With this particular correlation, asphalts which had higher activation energies (i.e., higher energy barriers to overcome in order to begin to flow) were also observed to correlate with faster healing rates, thus futures work will focus on explaining these discrepancies.

Significant Problems, Issues and Potential Impact on Progress

None.

Work Planned Next Quarter

Work planned for next quarter, will be directed toward determining the effect of moisture with respect to flow properties of asphalt binders. Work will continue toward the development of a method for making nanorheological measurements and application of the method to this subtask specifically with respect to investigation of the plastic zone associated with energy dissipation as asphalt fatigues and ultimately fractures. An AFM scratch test protocol will be developed to begin to investigate flow phenomena associated with cracking and healing.

Cited References

Adamson, A. W., and A. P. Gast, 1997, *Physical Chemistry of Surfaces*, 6th Ed., A Wiley Interscience Publication, John Wiley & Sons, Inc., New York.

ASTM D6703-07, 2008 Standard Method for Automated Heithaus Titrimetry. *Annual Book of ASTM Standards, Road and Paving Materials; Vehicle-Pavement Systems*, Section 4, vol. 04.03. ASTM International, West Conshohocken, PA. 808-816.

Beck, A., and P. Havas, 1989, *The Collected Papers of Albert Einstein, Volume 2, The Swiss Years: Writings, 1900-1909*. Anna Beck, Translator. Peter Havas, Consultant. The Hebrew University of Jerusalem. Princeton University Press, Princeton, New Jersey.

Einstein, A., 1901, *Folgerungen aus den Capillaritätserscheinungen*. *Annalen der Physik*, 4, p 513.

Ewell, R. H., and H. Eyring, 1937, *Theory of the Viscosity of Liquids as a Function of Temperature and Pressure*. *Journal of Chemical Physics*, 5: 726-736.

Jung, D. and T. S. Vinson, 1993, *Thermal Stress Restrained Specimen Test to Evaluate Low-Temperature Cracking of Asphalt-Aggregate Mixtures*. *Transp. Res. Rec.* 1417, 12-20.

Little, D. N., R. L. Lytton, D. Williams and C. W. Chen, 2001, Microdamage Healing in Asphalt and Asphalt Concrete, Volume I: Microdamage and Microdamage Healing, Project Summary Report, FHWA-RD-98-141. Federal Highway Administration, U. S. Department of Transportation, McLean, VA.

Lytton, R. L., C. W. Chen and D. N. Little, 2001, Microdamage Healing in Asphalt and Asphalt Concrete, Volume III: A Micromechanics Fracture and Healing Model for Asphalt Concrete, FHWA-RD-98-143. Federal Highway Administration, U. S. Department of Transportation, McLean, VA.

Miknis, F. P., A. T. Pauli, A. Beemer, and B. Wilde, 2004, *Use of NMR Imaging to Measure Interfacial Properties of Asphalts*. *Fuel*, 84(9): 1041-1051.

Petersen, J. C., 1984, Chemical Composition of Asphalts Related to Asphalt Durability: State of the Art, Transportation Research Board, No. 999, pp. 13-30.

Robertson, R. E., K. P. Thomas, P. M. Harnsberger, F. P. Miknis, T. F. Turner, J. F. Branthaver, S-C. Huang, A. T. Pauli, D. A. Netzel, T. M. Bomstad, M. J. Farrar, D. Sanchez, J. F. McKay, and M. McCann. "Fundamental Properties of Asphalts and Modified Asphalts II, Final Report, Volume I: Interpretive Report," Federal Highway Administration, Contract No. DTFH61-99C-00022, Chapters 5-7 submitted for publication, March 2006.

Robertson, R. E., K. P. Thomas, P. M. Harnsberger, F. P. Miknis, T. F. Turner, J. F. Branthaver, S-C. Huang, A. T. Pauli, D. A. Netzel, T. M. Bomstad, M. J. Farrar, J. F. McKay, and M. McCann. "Fundamental Properties of Asphalts and Modified Asphalts II, Final Report, Volume I: Interpretive Report," Federal Highway Administration, Contract No. DTFH61-99C-00022, Chapters 1-4 submitted for publication, November 2005.

Roylance, E., 2001, Introduction to Fracture Mechanics.
<http://web.mit.edu/course/3/3.11/www/modules/frac.pdf>

Schapery, R.A., 1984, Correspondence Principles and a Generalized J-integral for Large Deformation and Fracture Analysis of Viscoelastic Media. *Int. J. Fract.*, 25, pp. 195-223.

Schapery, R.A., 1973, A Theory of Crack Growth in Visco.-Elastic Media. Report MM2764-73-1, Mechanics and Materials Research Center, Texas A&M University.

Schapery, R.A., 1988, Theory of Mechanical Behavior of Elastic Media with Growth Damage and Other Changes in Structure. Report No. MA4 5 762-88-1, Texas A& M University.

Schapery, R.A., 1989, On the Mechanics of Crack Closing and Bonding in Linear Viscoelastic Media. *Int. J. Fract.*, 25, pp. 163 - 189.

Tayebali, A. A., J. A. Deacon, J. S. Coplantz, F. N. Finn, and C. L. Monismith, 1994, SHRP-A-404, Fatigue Response of Asphalt-Aggregate Mixes, Part II. Extended Test Program. Strategic Highway Research Program, National Research Council, Washington, DC.

Traxler, R. N., 1960, Relation Between Hardening and Composition of Asphalt. *Preprints, Div. Petrol. Chem., Am. Chem. Soc.*, 5, pp. A71-A77.

Williams, J. C., 1984, *Fracture Mechanics of Polymers*, Ellis Horwood Limited, Chichester, England, division of John Wiley & Sons, Inc., New York, 9-187.

Work Element M2b: Impact of Moisture Diffusion in Asphalt Mixtures

Subtask M2b-1: Measurements of Diffusion in Asphalt Mixtures (TAMU)

Work Done This Quarter

The main effort on these past months was to establish the methodology to determine the influence of hysteresis in moisture gradient on the diffusivity through asphalt binder films. The procedure for sample preparation, and film thickness and refractive index measurement is the same as described in previous quarterly reports. However, for the hysteresis test, the asphalt sample is monitored under water for a fixed period of time before it reaches equilibrium necessarily. For the first series of tests, the duration for hydration for fixed at 15 days. During these 15 days, the diffusion of water through the film of the asphalt binder was monitored using the ATR-FTIR as before. After 15 days, water from the ATR chamber was removed using a syringe. The specimen was then monitored using the FTIR to determine the rate and amount of water that escaped from the binder. Typically, the water diffused out of the binder within less than a day. The spectra of the binder film dried in this manner were very similar to the spectra of the original binder film.

The researchers had hypothesized the process of water diffusing into and out of the binder film is likely to change the microstructure of the binder. Consequently, during the second hydration cycle water would diffuse at much faster rate through the film as compared to the rate of diffusion through the original binder for the first time.

The result of cycle is plotted (concentration versus time) to evaluate the difference in time to reach a common concentration (figure M2b-1.1). The figure clearly indicates that the time to reach 80% saturation in the second cycle, t_2 , was much smaller than the time to reach 80% saturation t_1 during the first cycle.

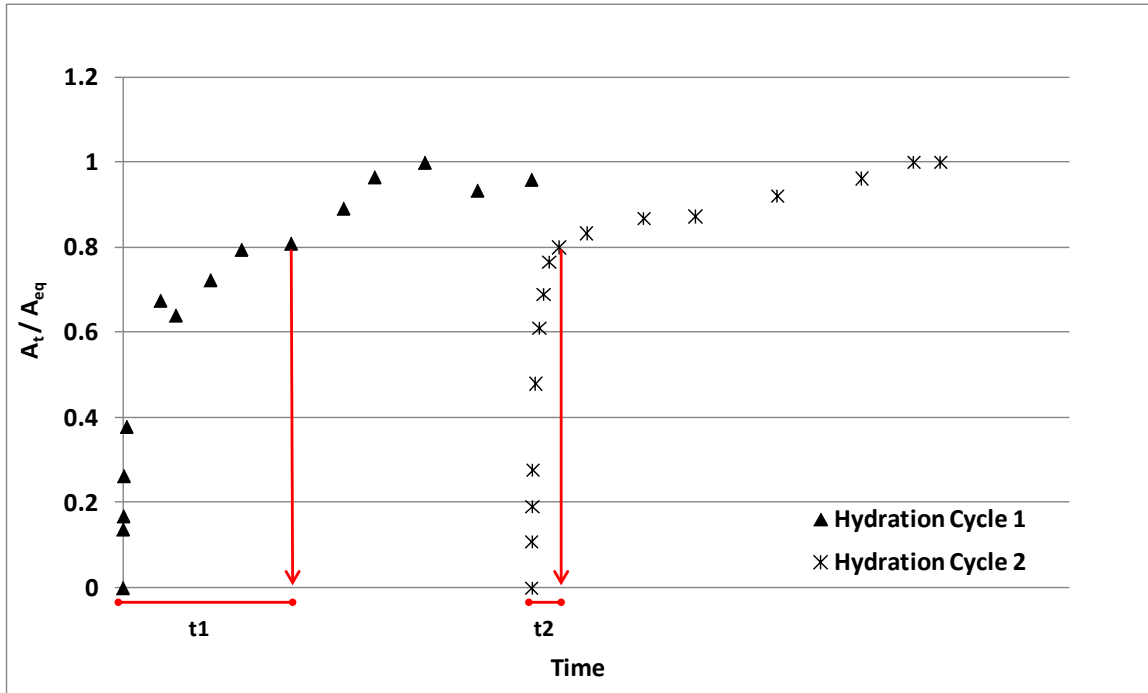


Figure M2b-1.1: Impact of hysteresis in rates of moisture diffusion for a film of binder subjected to cyclic wetting and drying ($t_2 =$ time to reach 80% saturation in second cycle $<$ $t_1 =$ time to reach 80% saturation in the first cycle).

Significant Results

Tests on moisture diffusion and hysteresis are proceeding as per the test plan. Significant results will be reported after the complete data set of results is available.

Significant Problems, Issues and Potential Impact on Progress

Some binders have demonstrated more variability in the results than others. The reasons for this are being investigated and further tests are being conducted.

Work Planned Next Quarter

The focus of work in the next quarter will be to evaluate the results from all the measurements that have been made thus far. The influence of repeated wet and dry cycles on moisture diffusion, especially in the initial level of saturation will be evaluated in terms of the mechanisms that cause this hysteretic behavior.

Subtask M2b-2: Kinetics of Debonding at the Binder-Aggregate Interface (TAMU)

Work Done This Quarter

Most of the work accomplished under subtask M2b-1 also directly relates to this subtask. The most significant difference in this subtask is that a portion of the binder-ATR window interface will be purposefully exposed to be in direct contact with the water. This will allow the water to diffuse through the film as well as propagate along the binder-ATR window interface.

Work Planned Next Quarter

Researchers plan to continue work with emphasis on M2b-1 before addressing the specifics of this subtask.

Work Element M2c: Measuring Thin Film Cohesion and Adhesion Using the PATTI Test and the DSR (UWM)

Work Done This Quarter

The research team continued to work with the Pneumatic Adhesion Tensile Testing Instrument (PATTI), developing test methods and procedures to produce repeatable data. It also investigated PATTI testing as a surrogate method for conducting the Dynamic Shear Rheometer (DSR) tack test. While the response variables differ for each method, results may be correlated using the tack factor. In January 2009 the team began a full experiment to evaluate four aggregate surfaces (diabase, granite and two kinds of limestone); curing conditions; environmental conditions; and water/no-water conditioning. Collaboration with the University of Stellenbosch, South Africa, continues on a cost-share basis, and a student there is conducting parallel testing and providing data to this research effort. Most of the work conducted for this task this quarter was in coordination with work element E1c-2, which is focused on testing emulsions. Although the data are being used in E1c-2 to evaluate emulsion behavior, they are being used in this task to evaluate the operational factors that could affect the quality of testing results.

Significant Results

The research team obtained two new PATTI Quantum Gold units. The new units will be phased into testing and shared with the University of Stellenbosch.

The research team also developed rock plate sample preparation and testing procedures that are applicable to hot binders as well as emulsions.

Examples of the results of PATTI testing of emulsions with limestone, granite and diabase are shown in figures M2c.1 through M2c.3. The results were collected after curing emulsions at different temperatures, humidity levels and curing times. Due to the finding that temperature is a very important testing factor, the samples for the PATTI tests were conditioned in a temperature- and humidity-controlled chamber. The results clearly show the PATTI procedure can detect the

effects of curing time, humidity and temperature. More importantly, the results shown in the figures M2c.1 through M2c.3 indicate that the repeatability of the test has greatly improved from previous measurements and is within acceptable levels.

The effect of surface roughness and moisture condition was also studied. As shown in the figures, the roughness was controlled by using two levels of smoothing powders (220 and 280) and the moisture conditions studied so far include air dry and saturated surface dry (SSD).

The issue of the pullout rate (pressure as a function of time) remains a concern, since it appears to be dependent on material stiffness. Figure M2c.4 shows a plot of pullout rate versus maximum tension for a large number of PATTI test runs measured at three curing times. There is a trend of increasing rate with curing, but there is no clear bias toward the longer curing time. Values of G^* for the materials included in the testing program will be studied to evaluate the relationship between rate and G^* of binders.

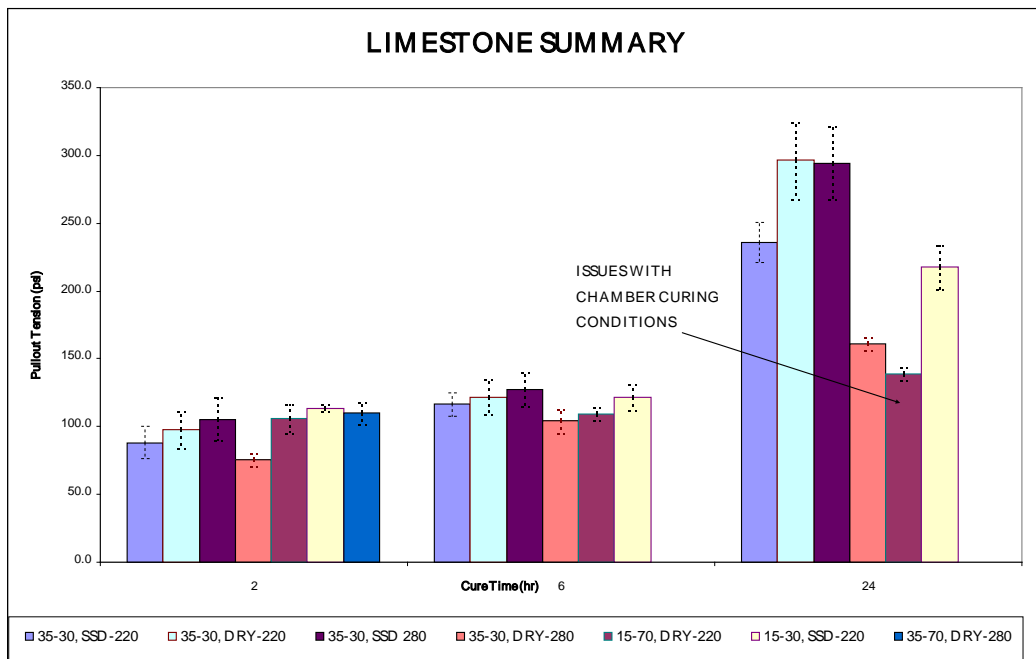


Figure M2c.1. Graph. PATTI testing results for limestone. (The legend indicates curing temperature ($^{\circ}\text{C}$), percent humidity, surface moisture condition, and roughness level.)

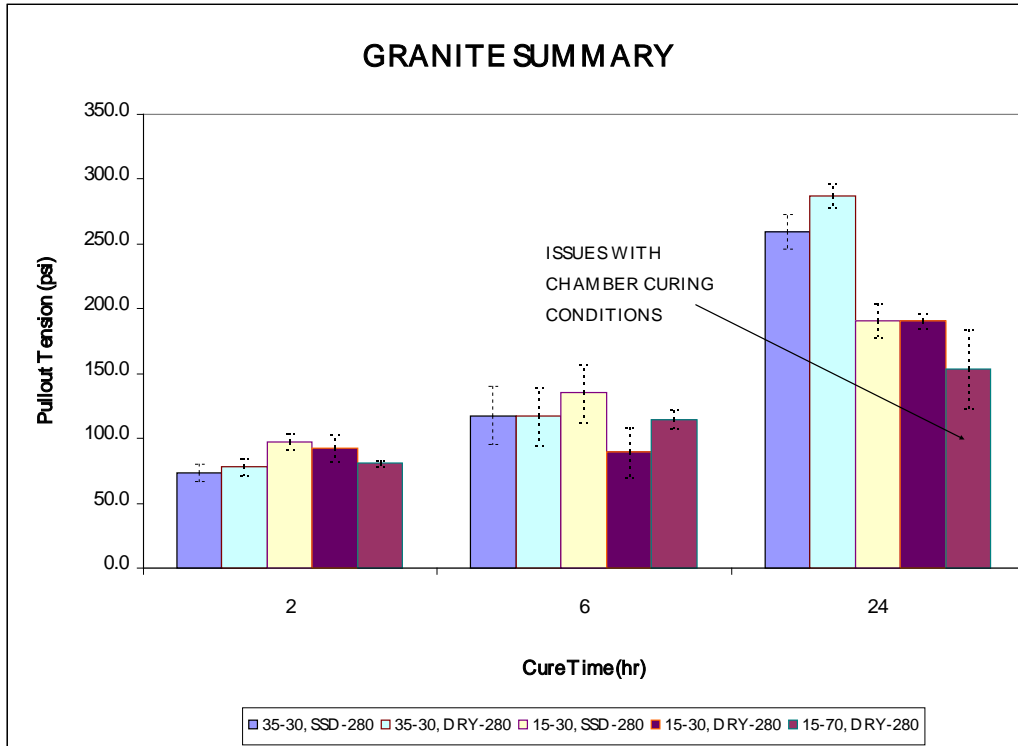


Figure M2c.2. Graph. PATTI testing results for granite. (The legend indicates curing temperature (°C), percent humidity, surface moisture condition, and roughness level.)

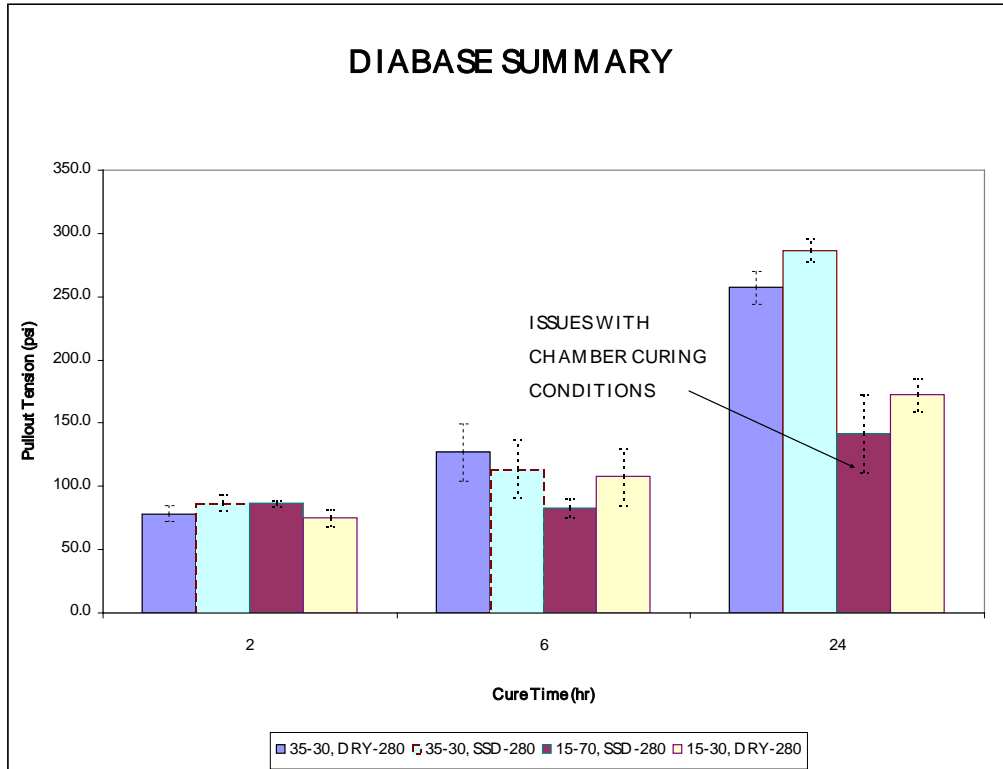


Figure M2c.3. Graph. PATTI testing results for diabase. (The legend indicates curing temperature (°C), percent humidity, surface moisture condition, and roughness level.)

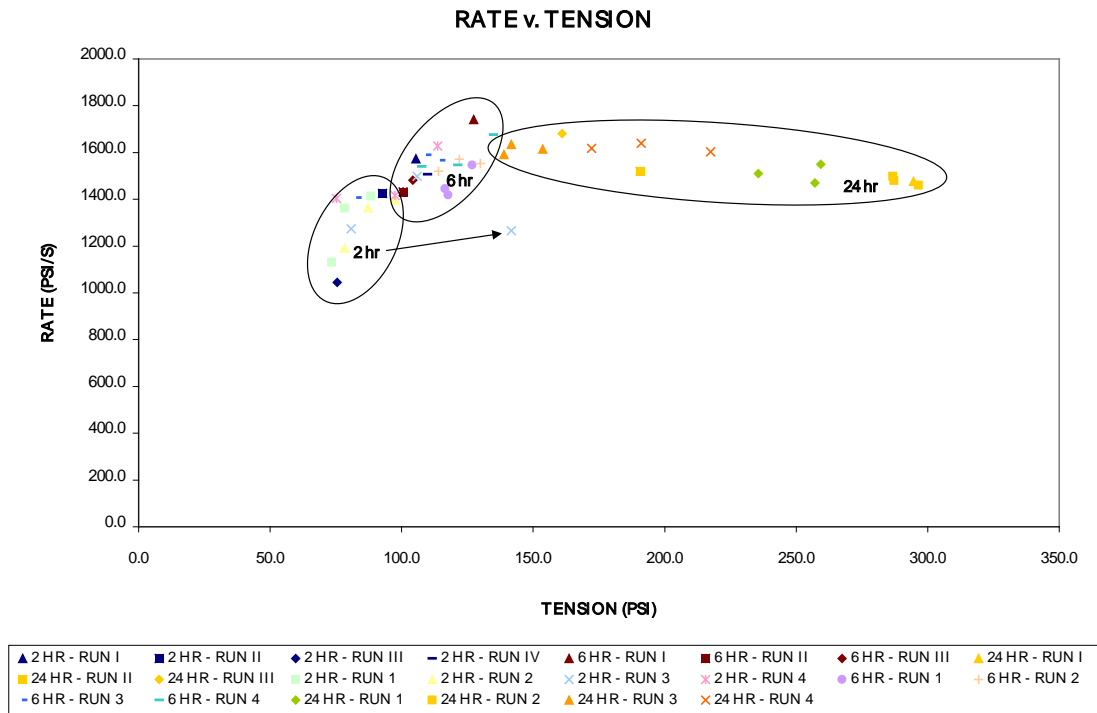


Figure M2c.4. Graph. Pullout rate versus tension for several PATTI test runs.

Significant Problems, Issues and Potential Impact on Progress

The control of the pullout rate is an important issue that is being addressed by using a new testing design. The new PATTI is expected to solve this issue and provide better control. No impact on progress is expected at this time.

Work Planned Next Quarter

Next quarter, the research team will phase the new PATTI Quantum Gold instrument into testing and evaluate its capabilities.

CATEGORY M3: AGGREGATE SURFACE

Work Element M3a: Aggregate Surface Characterization (TAMU))

Work Done This Quarter

Physical and chemical properties of aggregates at the macro and molecular scale influence the performance of asphalt mixes. These properties control the nature and durability of the bond between aggregates and asphalt in wet and dry conditions and its resistance to moisture induced

damage and fatigue cracking. Recent research by Little and colleagues have shown that surface energy of the aggregate-asphalt interface is a reliable predictor of engineering properties of the asphalt mixture. Current understanding of the aggregate and bitumen properties that control and shape surface energy is limited, limiting our ability to *a priori* predict surface energy of any given aggregate-asphalt combination.

Current tasks are organized around the (1) characterization of the chemical composition of the surfaces of reference minerals and aggregates through electron beam spectroscopies, including electron microprobe, backscatter electrons and electron-dispersive spectroscopy (EDS), (2) the characterization of the surface energies of reference minerals and aggregates through the universal sorption device and microcalorimetry, (3) quantification of surface (upper 14 nm) atomic species and chemical state with an x-ray photoelectron spectroscope (XPS), and (4) surface topography characterization with scanning electron microscopy (SEM). The results from these tasks will support the development of a predictive model of aggregate surface energies based upon the surface energies of the minerals that compose the aggregate.

Tasks completed this quarter include additional mineral chemistry analysis for the following aggregates: Lithonia granite (RA), basalt (RK), and Gulf Coast Gravel (RL) and mineralogical analysis for the MM sandstone. Mineral chemistry and mineralogical analysis were also carried out on five additional mineral reference samples. Specific accomplishments are highlighted in the tables below.

Surface energy measurements for quartz, microcline, labradorite, biotite, andesine, microcline, albite, augite, hornblende, hematite, siderite, dolomite, and calcite have been collected using the universal sorption device. The components of surface energy were calculated on replicates of the samples.

Sample preparation and aggregate surface characterization tasks completed this quarter are shown in the table below.

Table M3a.1. Status of tasks associated with mineralogical and chemical characterization of aggregates.

SHRP	Name	Yr.Qtr	Thin Section Prep Status	Microprobe Analysis Status
RA	Lithonia Granite	08.1	1 aggr sample prepared, 2 more in progress	1 set of X-ray maps, 1 set of BSE images, 1 preliminary set of WDS quant analyses
		08.2	2 more aggregate samples prepared	2 sets of X-ray maps, BSE images are not needed because of grain size
		09.1		WDS quant analyses of major minerals completed
RC	Limestone (higher absorption)	08.1	2 aggr samples prepared	1 set of X-ray maps, 1 set of BSE images, 1 preliminary set of WDS quant analyses
		08.2	-	No additional analyses
RD	Limestone (low absorp.)	08.1	4 aggr samples prepared,	4 sets of X-ray maps, 1 set of BSE images, 1 preliminary set of WDS quant analyses
		08.2	-	No additional analyses
RK	Basalt	08.1	2 aggr samples prepared, 1 more in progress	2 sets of X-ray maps, 1 set of BSE images, 1 preliminary set of WDS quant analyses
		08.2	1 sample in progress	3 additional sets of X-ray maps, 13 set of BSE images, 1 set of WDS quant analyses for pyroxene, olivine, amphibole
		09.1		WDS quant analyses of feldspar, pyroxene and clay completed.
RL	Gulf Coast Gravel	08.1	5 aggr samples prepared, 9 more in progress	4 sets of X-ray maps, 1 set of BSE images, 1 preliminary set of WDS quant analyses
		08.2	9 more in progress	9 sets of X-ray maps
		09.1		WDS quant analyses of mineral grains in 9 gravel particles completed.
MM	MM Sandstone	09.1	One 25mm aggr mount prepared with > 20 fragments	1 sets of X-ray maps acquired

Sample preparation and mineral surface characterization tasks completed this quarter are shown in the tables below.

Table M3a.2. Status of tasks associated with mineralogical and chemical characterization of mineral components of aggregates.

Mineral	Group	Yr.Qtr	(1) Acquisition Status (2) Microprobe Mount Status	Microprobe Analysis Status
Quartz	Silica Mineral	08.1	(1) > 200 grams acquired (Arkansas, RNG specimen) (2) Polished microprobe mount in preparation	In progress
		08.2	In progress	In progress
Microcline	Alkali Feldspar	08.1	(1) > 160 grams acquired (G&G collection, B0434) (2) Preliminary polished mount prepared	Preliminary homogeneity and quantitative chemical analysis acquired.
		08.2	In progress	In progress
Albite	Plagioclase Feldspar	08.1	(1) > 100 grams acquired (G&G collection, B0469) (2) Polished mount to be prepared	In progress
		08.2	In progress	In progress
Oligoclase	Plagioclase Feldspar	08.3	> 100 grams acquired (G&G collection, 008)	In progress
Andesine	Plagioclase Feldspar	08.1	(1) > 65 grams acquired (G&G collection, B0513) (2) Preliminary polished mount prepared	Preliminary homogeneity and quantitative chemical analysis acquired.
		08.2	In progress	In progress
Labradorite	Plagioclase Feldspar	08.1	(1) > 160 grams acquired (Naim, Labrador; RNG specimen) (2) Preliminary polished mount prepared	Preliminary homogeneity and quantitative chemical analysis acquired.
		08.2	In progress	In progress
Anorthite	Plagioclase Feldspar	08.1	Samples to be acquired	NA
		08.2	NA	NA

Table M3a.2. Status of tasks associated with mineralogical and chemical characterization of mineral components of aggregates (cont).

Mineral	Group	Yr.Qtr	(1) Acquisition Status (2) Microprobe Mount Status	Microprobe Analysis Status
Hornblende	Amphibole	08.1	(1) > 350 grams acquired (G&G collection, B0545) (2) Preliminary polished mount prepared	Preliminary homogeneity and quantitative chemical analysis acquired.
		08.2	In progress	In progress
Hornblende	Amphibole	08.1	(1) > 70 grams acquired (G&G collection, Room 008) (2) Polished mount to be prepared	In progress
		08.2	In progress	In progress
		09.1	(2) Polished mount prepared	X-ray map acquired; WDS quant analyses completed.
Augite	Pyroxene	08.1	(1) > 0 (?) grams acquired (G&G collection, B1007) (2) Preliminary polished mount prepared	Preliminary homogeneity and quantitative chemical analysis acquired.
		08.2	In progress	In progress
Augite	Pyroxene	08.1	(1) > 80 grams acquired (G&G collection, Room 008) (2) Polished mount to be prepared	In progress
		08.2	In progress	In progress
		09.2		WDS quant analyses completed.
Forsteritic Olivine	Olivine	08.1	(1) > 280 grams acquired (San Carlos, AZ) (2) Polished mount to be prepared	In progress
		08.2	In progress	In progress

Table M3a.2. Status of tasks associated with mineralogical and chemical characterization of mineral components of aggregates (cont).

Mineral	Group	Yr.Qtr	(1) Acquisition Status (2) Microprobe Mount Status	Microprobe Analysis Status
Muscovite	Mica	08.1	(1) > 65 grams acquired (G&G collection, Room 008) (2) Polished mount to be prepared	Preliminary quantitative chemical analysis acquired.
		08.2	In progress	In progress
		09.1	(2) Polished mount prepared	X-ray map acquired; WDS quant analyses completed.
Biotite	Mica	08.1	(1) > 175 grams acquired (G&G collection, B0857) (2) Polished mount to be prepared	In progress
		08.2	In progress	In progress
		09.1		WDS quant analyses completed.
Biotite	Mica	08.1	(1) > 150 grams acquired (G&G collection, Room 008) (2) Polished mount to be prepared	Preliminary quantitative chemical analysis acquired.
		08.2	In progress	In progress
Calcite	Carbonate	08.1	(1) > 100 grams acquired (Mexico; RNG specimen) (2) Polished mount to be prepared	In progress
		08.2	In progress	In progress
Dolomite	Carbonate	08.1	Samples to be acquired	NA
		08.2	NA	NA
		09.1	(2) Polished mount prepared	X-ray map acquired; WDS quant analyses completed.
Siderite	Carbonate	09.1		WDS quant analyses completed.

Table M3a.2. Status of tasks associated with mineralogical and chemical characterization of mineral components of aggregates (cont).

Mineral	Group	Yr.Qtr	(1) Acquisition Status (2) Microprobe Mount Status	Microprobe Analysis Status
Hematite	Iron Oxide	08.1	Samples to be acquired	NA
		08.2	NA	NA
		09.1	(2) Polished mount prepared	X-ray map acquired; WDS quant analyses completed.
Magnetite	Iron Oxide	08.1	Samples to be acquired	NA
		08.2	NA	NA
Ilmenite	Iron Titanium Oxide	08.3	> 100 g sample (Ontario; RNG specimen)	NA
		09.1	(2) Polished mount prepared	X-ray map acquired; WDS quant analyses completed.
Goethite	Iron Oxyhydroxide	08.1	Samples to be acquired	NA
		08.2	NA	NA
Kaolinite (KGA-1B)	Clay Mineral	08.3	Samples acquired	NA
		08.2	Samples acquired	In progress
Kaolinite	Clay Mineral	08.3	Samples acquired	NA
		08.2	Samples acquired	In progress
Montmorillonite (SAz-2)	Clay Mineral	08.3	Samples acquired	NA
		08.2	Samples acquired	In progress
Chlorite	Clay Mineral	08.3	Samples acquired; ~25 g Calumet and New Melones (RNG)	NA
		08.2	Samples acquired	In progress

Significant Results

Establishing a Surface Energy Predictive Model

One of the first goals will be to establish a model for predicting aggregate bulk surface energies based on mineralogical composition. Improved prediction of aggregate bulk properties pertinent to moisture damage susceptibility can lead to better methods to measure material properties and

moisture damage susceptibility of asphalt/aggregate mixes. Development of a simple visual field test of aggregate surface energy properties will aid in on-site evaluation of aggregate moisture damage susceptibility.

We expect the bulk/total surface energy of an aggregate to be a function of the component surface energies of its mineralogical constituents as:

$$Se_{aggregate} = \sum (Se_{Mineral} \cdot SA) + \sigma$$

where Se is surface energy, SA is surface area, and σ is the error term. A visual inspection of rock mineralogy based on percent of constituents can accurately predict total surface energy of the sample.

Methods –A Universal Sorption Device can be used to measure pure phase mineral surface energies by calculating the amount of a reference gas (water, hexane, and methylpropyl ketone in this case) sorbed to the mineral surface at various pressures. The adsorption isotherm for each reference gas is used to calculate equilibrium spreading pressure for each of the vapors along with the specific surface area (SSA) using the BET Equation. The equilibrium spreading pressure of each vapor is then used to calculate the three surface energy components using GvOC Equations. These values will then be used to establish an additive model of total surface energy for previously characterized rock samples based on percent of each constituent at the surface. The validity of the model will be tested by using the same Universal Sorption Device technique on the aggregate samples. A statistical analysis will be performed on the observed measurements versus predicted values.

Experiments – Although rock mineralogy has the capacity to be very complex it is dominated by a relatively small group of minerals of predictable variability in North America. The mineralogy of common aggregates used in hot asphalt mixes across America is outlined in the aggregate analysis data from the Strategic Highway Research Program's (SHRP) materials reference library. Pure phase minerals are being collected by Dr. Ray Guillemette based on the findings of the SHRP. These minerals are the dominant constituents in all major aggregates of the study. The chosen minerals are listed in table M3a.1.

The surface energies of these pure phase minerals will be calculated using a Universal Sorption Device using three reference gases to determine spreading pressures. Each mineral will be crushed and passed through a number 10 sieve. Minerals will be washed with distilled water and heated for 24 hours at 80° Celsius in a Fisher Isotemp® Oven. Each reference gas will be used on a separate sample of each pure phase mineral. After the test is run each sample will be washed with distilled water and reheated at 80° C for future analysis.

After each of the pure phase mineral surface energies have been quantified the SHRP aggregate samples themselves will be crushed and analyzed on the Universal Sorption Device to statistically determine the linear additive model's validity.

Data- The data gained from this experiment will be in $erg / (cm)^2$ for each pure phase mineral and SHRP aggregate. In order to calculate mineral surface energy the isotherm for each reference gas must be calculated. To obtain a full isotherm, the aggregate is exposed to ten equal increments of partial probe vapor pressure from vacuum to saturated vapor pressure. At each stage the adsorped mass is recorded after it reaches equilibrium. The adsorped mass of each stage is then used to plot the isotherm. The measured isotherm for hexane is then used to calculate the specific surface area (SSA) using the Branauer, Emmett, and Teller BET equation:

$$A = \left(\frac{N_m N_0}{M} \right) \alpha$$

where N_0 =Avogadro's number; M =molecular weight of the probe vapor; α = projected area of a single molecule; and N_m =monolayer capacity of the aggregate surface. The specific surface area and each adsorption isotherm are then used to calculate three surface energy components using the GvOC equation:

$$W = 2\sqrt{\gamma_s^{lw}\gamma_v^{lw}} + 2\sqrt{\gamma_s^+\gamma_v^-} + 2\sqrt{\gamma_s^-\gamma_v^+}$$

where g^{Total} = total surface energy of the material; g^{lw} = Lifhsitz-van der Waals or dispersive component; g^{AB} = acid-base component; g^+ = Lewis acid component, and g^- = Lewis base component.

Current Results

In order to use the Universal Sorbtion Device as an appropriate measuring device for surface energy the reproducibility must first be known. In order to test the reproducibility one of the SHRP aggregates was chosen at random and the surface energy was measured on the sorption device. The aggregate was RD-7, a shaly limestone composed primarily of calcite. Hexane and methylpropyl ketone were run in triplicate and water vapor was tested four times. The results indicated that there was a good deal of internal consistency between the test runs, and the overall surface energy calculation was within a 95 percent confidence interval to previous study of the aggregate over two years ago. In total 8 minerals are currently at various stages of testing. All minerals will be tested in quadruplicate for each vapor. The results to date are included in the following chart.

		Mineral Surface Energy					
Mineral	SSA	LW	e- Acceptor	e- Donor	Polar Component	Fractional Polarity	Total
Quartz	0.10	51.42	0.00	399.58	0.65	0.01	52.07
Microcline	0.10	44.00	0.46	202.79	19.35	0.31	63.35
Calcite		41.67	0.09	153.71	7.43	0.15	49.10
Biotite	0.06	52.51	0.07	809.97	14.90	0.22	67.41
Labradorite	0.23	39.72	0.03	1062.51	11.55	0.23	51.27
Andesine	0.10	40.64	0.40	4953.93	89.24	0.69	129.88
Albite	0.19	51.57	0.22	501.69	21.22	0.29	72.79
Augite	0.03	52.67	8.69	6981.14	492.71	0.90	545.38
Siderite	0.07	61.39	1.59	789.63	70.80	0.54	132.18
Hematite	0.05	48.99	2.85	558.07	79.82	0.62	128.81
Dolomite	0.08	60.29	0.18	564.05	20.28	0.25	80.57
Hornblende	0.09	51.92	0.91	1338.86	69.70	0.57	121.63

Significant Problems, Issues and Potential Impact on Progress

No significant problems at this time.

Work Planned Next Quarter

Work planned in the next quarter includes continued analysis of the aggregates and minerals, with specific reference to surface energies.

CATEGORY M4: MODELING

Work Element M4a: Micromechanics Model (TAMU)

Work Done This Quarter

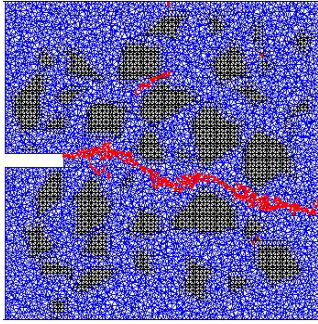
Lattice Micromechanical Model

Development of the basic lattice micromechanical models is the same as that for Subtask F3b-1. The progress this quarter under Subtask F3b-1 also benefits the objectives for this work element. Thus, this part of the report is shown in both areas.

The new lattice modeling engine of multi-scale virtual fabrication and lattice modeling (MS-VFLM) developed in the last quarter is finalized with significant increase in computational efficiency. It has all the functionality of the previous lattice modeling software except the viscoelastic deformation. A sample output from the new MS-LFVM run is shown in the figure, which contains scaling up of fracture energies, sample crack patterns and final load-deflection curve at scale 1. Comparison of efficiency indicates that both tension (TEN) test and single-edge notch (SEN) tests require less than 8 times the previous implementation. The practical

implication is that the result shown in the figure takes around 1.1 hours, as opposed to more than 9 hours it took with the previous implementation. This indicates that *virtual testing of laboratory scale specimen can now be done within a reasonable time*. Further reduction of computational cost is currently being investigated. In addition to the computational work, work has initiated on investigating the discrepancy in time-dependency between binder deformation and mastic deformation.

(a)



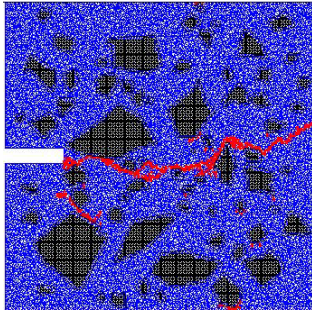
SEN Virtual Testing of RVEs at scale 3

(b)

Specimen No.	1	2	3	4	5
Mastic Cohesion of RVEs (N.mm/mm ²)	0.00150	0.00075	0.00102	0.00099	0.00121
Mastic and Aggregate Adhesion of RVEs (N.mm/mm ²)	0.00064	0.00026	0.00040	0.00038	0.00049



(a)



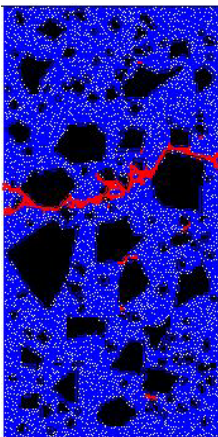
SEN Virtual Testing of RVEs at scale 3

(b)

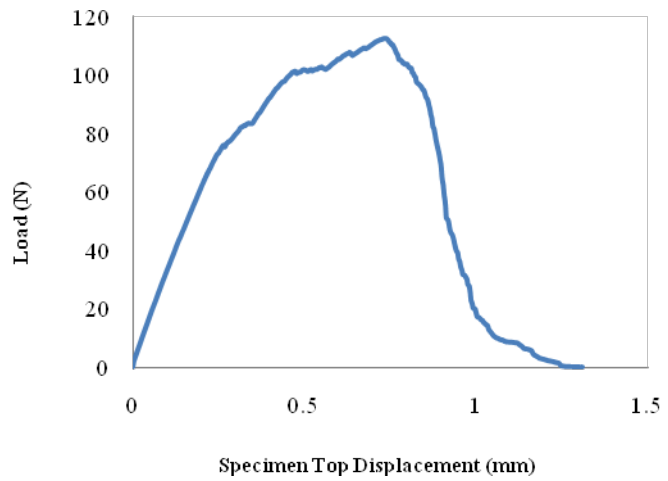
Specimen No.	1	2	3	4	5
Mastic Cohesion of RVEs (N.mm/mm ²)	0.04990	0.02207	0.03711	0.02375	0.02706
Mastic and Aggregate Adhesion of RVEs (N.mm/mm ²)	0.02483	0.01092	0.01844	0.01176	0.01342



(c)



Cracking Pattern (Scale 1)



Sample output from MS-VFLM (the new implementation takes around 1.1 hours)

Cohesive Zone Micromechanical Model

During this quarter the researchers at TAMU completed a comprehensive parametric analysis on the effect of material properties on the susceptibility of asphalt mixtures to moisture damage. The coupled micromechanical model of moisture damage has been explained with more detail in previous reports. In summary, the model is able to couple the effect of moisture diffusion into the mechanical performance of an asphalt mixture by: (1) reducing the linear viscoelastic relaxation modulus of the asphalt matrix as a function of the moisture content (i.e., cohesive deterioration); and (2) using the cohesive zone model (CZM) technique to simulate fracture at the aggregate-matrix interfaces (i.e., adhesive deterioration and fracture). In order to couple the adhesive response of the interfaces to the amount of moisture content reaching these zones, the adhesive properties were also made moisture-dependent. The model has been implemented in the commercial finite element software Abaqus[®] using a moisture-mechanical sequentially coupled scheme.

Figure M4a.1 presents the microstructure used for the parametric analysis and its implementation in finite elements. The mixture was composed by 33 aggregates embedded in a fine aggregate matrix (FAM) comprising the fine portion of the aggregates (i.e., passing 1.18mm) and the asphalt binder. A thin layer of 0.02 or 0.03 mm was added in the middle of the aggregates and the FAM to represent the interfaces between these materials. These interfaces, named *adhesive zones*, are modeled using the CZM technique, which makes possible the representation of adhesive cracks initiation and propagation.

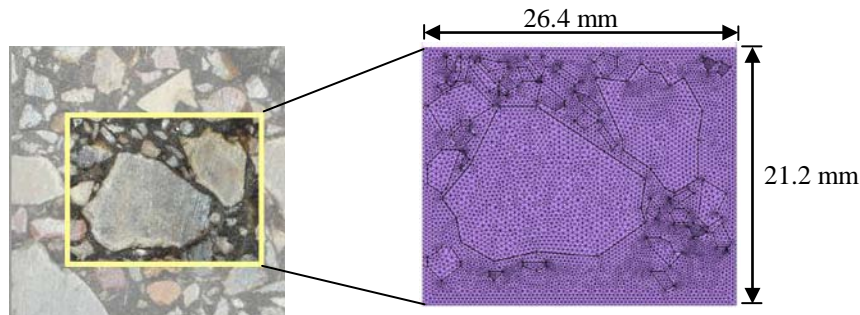


Figure M4a.1. Microstructure used in the parametric analysis and its corresponding finite element implementation.

Three different types of FAM and two types of aggregates, each one having different mechanical material properties, were considered in the study. Besides, any type of FAM or aggregate was allowed to have two different moisture diffusion coefficients ($D_{\text{FAM-A}}=2.78 \cdot 10^{-5} \text{ mm}^2/\text{s}$ or $D_{\text{FAM-B}}=5.56 \cdot 10^{-6} \text{ mm}^2/\text{s}$ for the FAMs, and $D_{\text{AgA}}=2.44 \cdot 10^{-4} \text{ mm}^2/\text{s}$ or $D_{\text{AgB}}=1.39 \cdot 10^{-6} \text{ mm}^2/\text{s}$ for the aggregates). The combination of these materials produced a total of 24 different asphalt mixtures. The properties of the aggregates-FAM interfaces (i.e., bond strength and fracture toughness of the adhesive zones), were made dependent on the type of aggregate and FAM present in the mixture. In other words, the model took into account the fact that the adhesive

properties of the interfaces are functions of the individual properties of the aggregates and the asphalt matrix.

Each one of the 24 mixtures was subjected to the same moisture diffusion and mechanical loading conditions (figure M4a.2). The mechanical test consisted in applying two loading-unloading cycles under a displacement-controlled scheme. The mechanical response of the mixtures under dry and moisture-conditioned cases was analyzed. The reduction of the maximum force supported by the mixture from the dry case to the moisture-conditioned case was used as an indicator of moisture susceptibility.

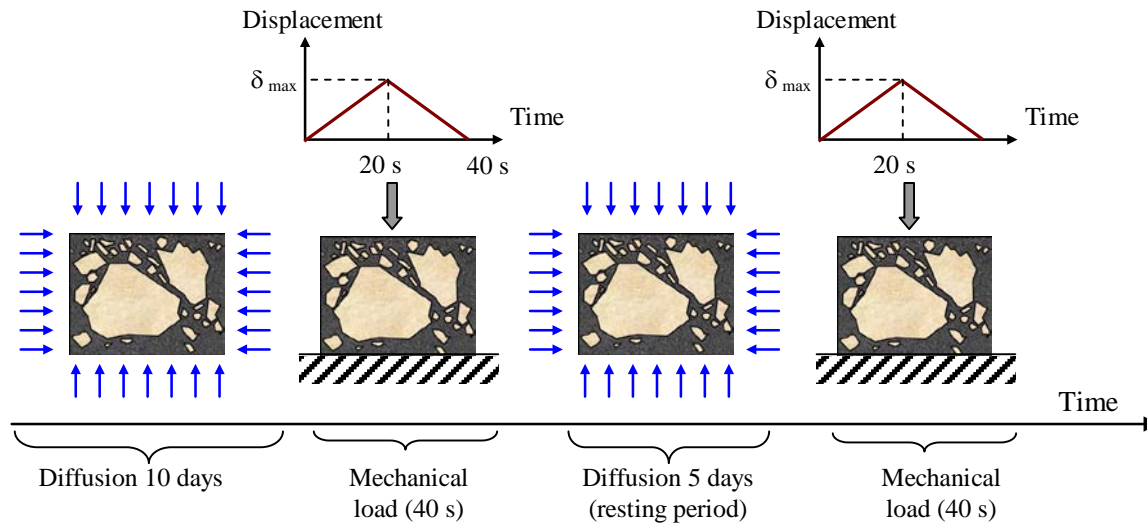


Figure M4a.2. Moisture and mechanical loading scheme used for the parametric study.

The results showed that, in general, all mixtures were highly susceptible to the combined deterioration caused by moisture and mechanical loading (i.e., 35.1% of reduction in the maximum force supported by the mixtures caused by the presence of moisture). However, the data suggest that the physical properties of the materials (i.e., the moisture diffusion coefficients) play the most significant role in the development of damage. It was demonstrated, with no exception, that samples subjected to more aggressive moisture profiles performed poorer and experience more damage. It was found that a difference of one order of magnitude in the diffusivity of the FAM reduced the maximum force experienced by the mixture at a given displacement by up to 3.7 times compared to a similar dry mix. In terms of the role of the moisture diffusivity of the aggregates, it was found that a difference of two orders of magnitude in this property reduced the maximum force of resistance of the mixtures from 1.2 to almost 2 times in comparison with similar dry mixes.

The results also showed that all mixtures containing aggregates associated with more resistant adhesive bonds were less susceptible to the deleterious effects of moisture. In fact, the average reduction of the maximum force due to the presence of moisture in mixtures containing aggregates associated with stronger adhesive bonds (aggregate-1) was 33%, in comparison to a

reduction of 36% for those mixtures containing aggregates related with weaker bonds (aggregate-2). This finding can be observed in figure M4a.3 that illustrates the differences in the mechanical responses obtained during the first loading cycle for a mixture containing one type of FAM and aggregate-1 (left), and the same type of FAM but aggregate-2 (right). This figure also shows that those mixtures containing materials with the largest moisture diffusivities (i.e., D_{FAM-A} for the FAM and D_{AgA} for the aggregates) are associated with poorer mechanical performances, proving the previously mentioned importance of the moisture diffusion coefficients in the development of damage.

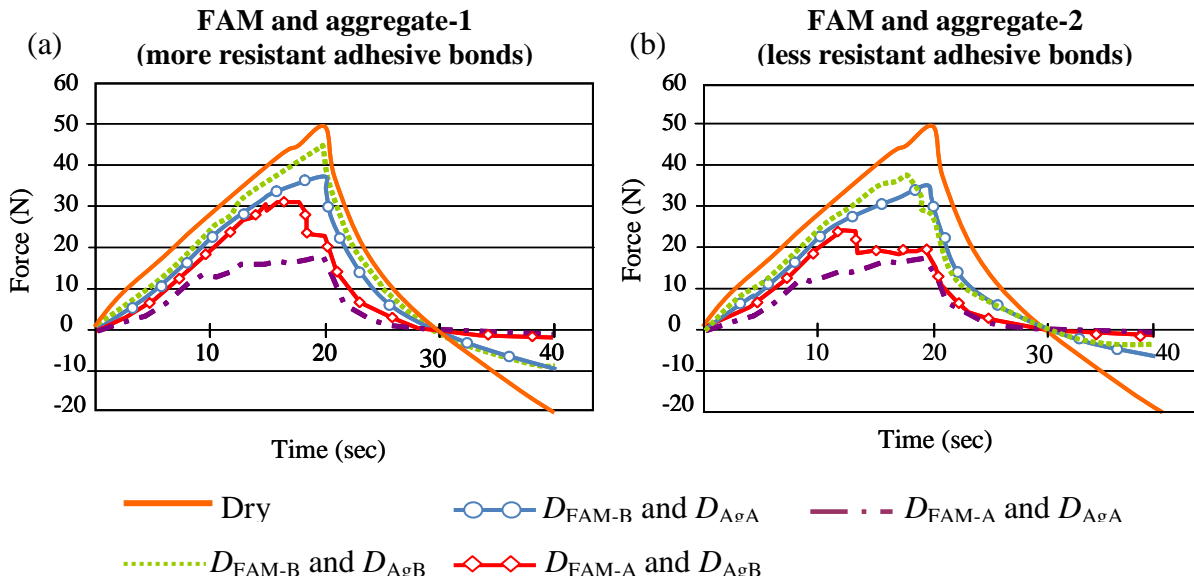


Figure M4a.3. Force vs. time curves obtained for a mixture comprising one of the three types of FAM and (a) aggregate-1 and (b) aggregate 2. The different curves represent different moisture profiles that result from combining the two possible moisture diffusion coefficients of the FAM (i.e., D_{FAM-A} and D_{FAM-B}) with the two possible moisture diffusion coefficients of the aggregates (D_{agA} and D_{agB}).

Significant Results

Lattice Micromechanical Model

MS-VFLM software is now completely integrated and is more than 8 times more efficient than the previous implementation. This should facilitate practical virtual testing once lattice modeling effort is complete.

Cohesive Zone Micromechanical Model

The coupled micromechanical model has been successfully applied to identify the role of different physical and mechanical material properties in the initiation and evolution of moisture damage. As a result of this study, a paper titled "Micromechanical Modeling of the Influence of

Material Properties on Moisture-Induced Damage in Asphalt Mixtures" was submitted for evaluation to the Journal of Construction and Building Materials (March, 2009). Besides, the paper titled "A Coupled Micromechanical Model of Moisture Damage in Asphalt Mixtures", that was submitted to the Journal of Materials in Civil Engineering (ASCE) during the previous quarter, was accepted for publication and is currently in press.

Significant Problems, Issues and Potential Impact on Progress

Lattice Micromechanical Model

None

Cohesive Zone Micromechanical Model

The results demonstrated the necessity of accounting for experimental data in obtaining the model's parameters to better represent the mechanical properties of the adhesive zones and FAM, as well as the deterioration of those properties caused by the presence of moisture. Current parallel tasks are focused in the experimental determination of these properties (subtask F1a.3.), and the results obtained from such task during this quarter will be incorporated in the modeling work planned for the following quarter.

Work Planned Next Quarter

Lattice Micromechanical Model

Work will continue on increasing computational efficiency and scaling up from binder deformation behavior to mastic deformation behavior. Modeling of viscoelastic deformation and fracture will also be initiated.

Cohesive Zone Micromechanical Model

The research will focus in studying the effect of the internal air void structure in the susceptibility of asphalt mixtures to moisture damage. A 5cm by 5cm microstructure model containing close to 250 aggregates is under implementation in finite elements. Based on a previously reported probabilistic distribution of air voids within an asphalt mixture (i.e., distribution of air void sizes by volume of mixture), models containing different amount of total air void contents are being randomly generated. It is expected that the application of the coupled micromechanical model to these different microstructures will provide information on the probabilistic role of air voids in the damage induced in asphalt mixtures by the presence of diffused moisture.

Work Element M4b: Analytical Fatigue Model for Mixture Design

The initial development of this work element is the same as Subtask F3c-1. The development of a method to separate the viscoelastic response from fatigue damage and the development of a model to analyze resistance to fatigue cracking under both dry and wet conditions is provided under subtask F1b-1. See the progress reported under Work Element F3c.

Work Element M4c: Unified Continuum Model

Work Done This Quarter

Work element F3c presents the development of the mechanical damage formulation as part of the TAMU continuum model. We have worked in the past quarter on the development of a coupled mechanical and moisture damage constitutive model and its numerical implementation in the finite element code Abaqus through the user material Fortran subroutine UMAT. Isotropic damage variable, ϕ^m (i.e. mechanical properties are degraded equally in different directions), is assumed as a start for simplicity. However, the mechanical damage model can distinguish between damage due to compression or extension. The damage model is coupled to the already formulated and implanted nonlinear viscoelastic and viscoplastic constitutive model. On the other hand, the degrading effect due to moisture manifests in two physical phenomena: (1) adhesive moisture damage, ϕ_a^M , which is the degradation of the bond strength between the aggregates and the asphalt mastic due to the existence and diffusion of moisture through the thin films surrounding the aggregate particles and along the aggregate-mastic interfaces; (2) cohesive moisture damage, ϕ_c^M , which is the degradation of the cohesive strength of the asphalt mastic itself. Both (1) and (2) may ultimately lead to erosion of the mastic film due to jetting water flow imposed by passing traffic. The work in this quarter focused on modeling these phenomena (i.e. mechanical damage, moisture adhesive damage, and moisture cohesive damage) independently, which allows one to introduce fundamental mechanical properties (e.g. bond strength and cohesive strength) and model the transition between adhesion and cohesion damage. We are currently preparing a journal paper that will document the modeling of the mechanical damage and moisture damage as part of the TAMU continuum model. Figure M4c.1 shows the predicted stress-strain behavior and damage evolution results for constant strain rate loadings with different moisture exposures. The normalized moisture content θ is held constant for 2000s and then the material is loaded at constant strain rate. Note the effect of moisture damage cause the material to become weaker and less stiff. Also, damage grows due to the presence of moisture and accelerates due to mechanical loading.

Figure M4c.2 shows the creep-recovery response for several moisture conditioning levels for a time period of 2000s and then loading under constant tensile stress for 50s followed by relaxation for another 50s. The figure shows that as the moisture level increases as the creep strain increases.

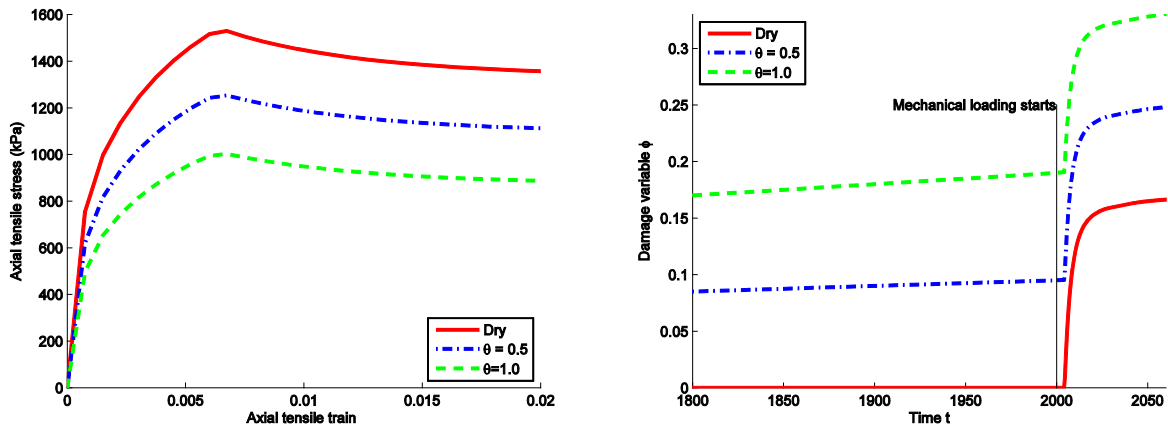


Figure M4c.1. Stress-strain and damage evolution plots for constant strain rate simulations for several moisture conditioning levels.

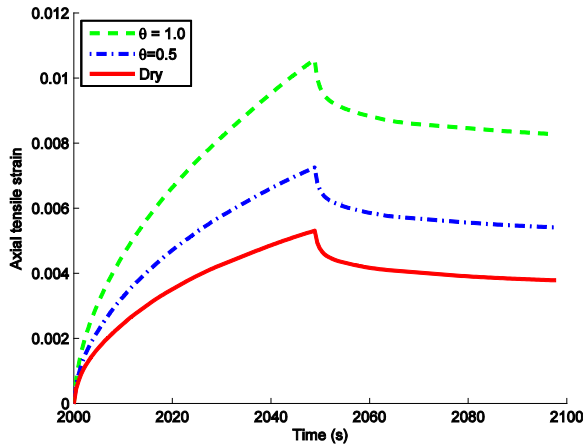


Figure M4c.2. Strain versus time response for tensile creep-recovery simulations for several moisture conditioning levels.

Work Planned Next Quarter

Fitting experimental data to the model is a nontrivial task, due to the large number of material parameters and their inter-coupling in tests. Work is currently underway at TAMU to develop a systematic way to fit all material parameters in the proposed model for a given asphalt concrete mix. Then the coupled nonlinear viscoelastic, viscoplastic, and damage model will be used to predict small-scale and large-scale wheel acceleration tests in order to determine the strengths and weaknesses of the model for further development.

The work will be on including the moisture damage formulation as part of the main formulation of TAMU continuum model. We will also conduct parametric analysis of the continuum model with different parameters in the moisture damage model. The parametric analysis results will be useful to verify that the model is capturing the main effects of moisture on the response of asphalt mixtures. We will compare the model results with limited data of the response of asphalt mixtures subjected to cyclic loading at different moisture conditions.

CATEGORY M5: MOISTURE DAMAGE PREDICTION SYSTEM




This area is planned to start later in the project.

Moisture Damage Year 2		Year 2 (4/08-3/09)											
		4	5	6	7	8	9	10	11	12	1	2	3
Adhesion													
M1a Affinity of Asphalt to Aggregate - Mechanical Tests													
M1a-1	Select Materials						DP						
M1a-2	Conduct modified DSR tests					P					P		
M1a-3	Evaluate the moisture damage of asphalt mixtures												DP
M1a-4	Correlate moisture damage between DSR and mix tests												
M1a-5	Propose a Novel Testing Protocol											P	
M1b Work of Adhesion													
M1b-1	Adhesion using Micro calorimeter and SFE												
M1b-2	Evaluating adhesion at nano scale using AFM												
M1b-3	Mechanisms of water-organic molecule competition												JP, D
M1c Quantifying Moisture Damage Using DMA													
Cohesion													
M2a Work of Cohesion Based on Surface Energy													
M2a-1	Methods to determine SFE of saturated binders												
M2a-2	Evaluating cohesion at nano scale using AFM												
M2b Impact of Moisture Diffusion in Asphalt													
M2b-1	Diffusion of moisture through asphalt/mastic films												
M2b-2	Kinetics of debonding at binder-agreagte interface												
M2c Thin Film Rheology and Cohesion													
M2c-1	Evaluate load and deflection measurements using the modified PATTI test		DP		JP						D		F
M2c-2	Evaluate effectiveness of the modified PATTI test for Detecting Modification										D	DP	F
M2c-3	Conduct Testing												
M2c-4	Analysis & Interpretation												
M2c-5	Standard Testing Procedure and Recommendation for Specifications												
Aggregate Surface													
M3a Impact of Surface Structure of Aggregate													
M3a-1	Aggregate surface characterization												
Models													
M4a Micromechanics model development													
M4b	Analytical fatigue model for use during mixture design											JP	
M4c	Unified Continuum model												
M5	Moisture Damage Prediction System												

LEGEND

Deliverable codes

- D: Draft Report
- F: Final Report
- M&A: Model and algorithm
- SW: Software
- JP: Journal paper
- P: Presentation
- DP: Decision Point
- [x]

-  Work planned
-  Work completed
-  Parallel topic

Deliverable Description

- Report delivered to FHWA for 3 week review period.
- Final report delivered in compliance with FHWA publication standards
- Mathematical model and sample code
- Executable software, code and user manual
- Paper submitted to conference or journal
- Presentation for symposium, conference or other
- Time to make a decision on two parallel paths as to which is most promising to follow through
- Indicates completion of deliverable x

Moisture Damage Year 2 - 5		Year 2 (4/08-3/09)				Year 3 (4/09-3/10)				Year 4 (04/10-03/11)				Year 5 (04/11-03/12)			
		Q1	Q2	Q3	Q4	Q1	Q2	Q3	Q4	Q1	Q2	Q3	Q4	Q1	Q2	Q3	Q4
Adhesion																	
M1a	Affinity of Asphalt to Aggregate - Mechanical Tests																
M1a-1	Select Materials		DP														
M1a-2	Conduct modified DSR tests		P		P												
M1a-3	Evaluate the moisture damage of asphalt mixtures				DP		P			P							
M1a-4	Correlate moisture damage between DSR and mix tests						P			P							
M1a-5	Propose a Novel Testing Protocol				P				P						JP, F		
M1b	Work of Adhesion																
M1b-1	Adhesion using Micro calorimeter and SFE						JP				JP, F						
M1b-2	Evaluating adhesion at nano scale using AFM							JP					JP				JP, F
M1b-3	Mechanisms of water-organic molecule competition				JP, D						JP	D	F				
M1c	Quantifying Moisture Damage Using DMA																
Cohesion																	
M2a	Work of Cohesion Based on Surface Energy																
M2a-1	Methods to determine SFE of saturated binders														JP		
M2a-2	Evaluating cohesion at nano scale using AFM							JP						JP			JP, F
M2b	Impact of Moisture Diffusion in Asphalt																
M2b-1	Diffusion of moisture through asphalt/mastic films						JP	D	F		JP	D	F				
M2b-2	Kinetics of debonding at binder-agreagte interface										JP	D	F				
M2c	Thin Film Rheology and Cohesion																
M2c-1	Evaluate load and deflection measurements using the modified PATTI test	DP	JP	D	F												
M2c-2	Evaluate effectiveness of the modified PATTI test for Detecting Modification				D	DP, F											
M2c-3	Conduct Testing						JP										
M2c-4	Analysis & Interpretation				P				D		D, JP		F				
M2c-5	Standard Testing Procedure and Recommendation for Specifications						D						D	P, F			
Aggregate Surface																	
M3a	Impact of Surface Structure of Aggregate																
M3a-1	Aggregate surface characterization																
Models																	
M4a	Micromechanics model development				JP				JP					M&A	D	DP	F, SW
M4b	Analytical fatigue model for use during mixture design																M&A, F
M4c	Unified Continuum model								JP					M&A	D	DP	F, SW
M5	Moisture Damage Prediction System																

LEGEND

Deliverable codes

- D: Draft Report
- F: Final Report
- M&A: Model and algorithm
- SW: Software
- JP: Journal paper
- P: Presentation
- DP: Decision Point

[x]

-  Work planned
-  Work completed
-  Parallel topic

Deliverable Description

- Report delivered to FHWA for 3 week review period.
- Final report delivered in compliance with FHWA publication standards
- Mathematical model and sample code
- Executable software, code and user manual
- Paper submitted to conference or journal
- Presentation for symposium, conference or other
- Time to make a decision on two parallel paths as to which is most promising to follow through
- Indicates completion of deliverable x

PROGRAM AREA: FATIGUE

CATEGORY F1: MATERIAL AND MIXTURE PROPERTIES

Work Element F1a: Cohesive and Adhesive Properties

Subtask F1a-1: Critical Review of Measurement and Application of Cohesive and Adhesive Bond Strengths (TAMU)

Work Done This Quarter

The work on improving the white paper relating the ideal work of fracture to the practical work of fracture was continued.

Work Planned Next Quarter

Improvements to this white paper will be made continually based on literature review. In addition, researchers plan to validate the findings from this paper in the context of bituminous materials by accomplishing the various subtasks in this work element.

Subtask F1a-2: Develop Experiment Design (TAMU)

Work Done This Quarter

The experiment design was completed and reported in the last quarterly report.

Work Planned Next Quarter

At this time, researchers do not anticipate any changes to this experiment design. However, as the work progresses in this subtask and in the area of modeling, some refinement to the proposed experiment design may be required in future.

Subtask F1a-3: Thermodynamic Work of Cohesion and Adhesion (Year 1 start)

Work Done This Quarter

The objective of this subtask is to provide the surface free energy of asphalt binders that will be used in other subtasks as a material property input or for the comparison with results from other test methods. Based on the requirements from other tasks, tests under this subtask will be ongoing through the remainder of this project.

Work Planned Next Quarter

Based on the requirements from other tasks, tests under this subtask will be ongoing through the remainder of this project.

Subtask F1a-4: Mechanical Work of Adhesion and Cohesion

Work Done This Quarter

The test protocols to evaluate the mechanical work of adhesion and cohesion were finalized during this quarter. In addition, samples were prepared and tested using the developed protocol. Both the force and displacement of the sample are measured during the test. Using this information, it is possible to calculate the energy required to fracture the sample as shown in the example in figure F1a-4.1. The fracture energy, also known as the practical work of fracture, is dependent on the experimental conditions of the test and the ideal work of fracture of the material. The ideal work of fracture based on surface free energy, is the work required to create two new unit areas of surface. The ideal work of fracture is much smaller than the practical work of fracture; however, it is related to and influences the practical work of fracture. In other words, materials with a higher ideal work of fracture will show a larger value of practical work of fracture during testing. An example of this relationship can be seen in figure F1a-4.2 below. Figure F1a-4.2 illustrates how the practical work of fracture between the asphalt and steel sample holder increases with an increase in the ideal work of fracture between the two materials. The results of AAB and AAD in comparison to ABD are more noticeable due to a larger difference in the surface free energy.

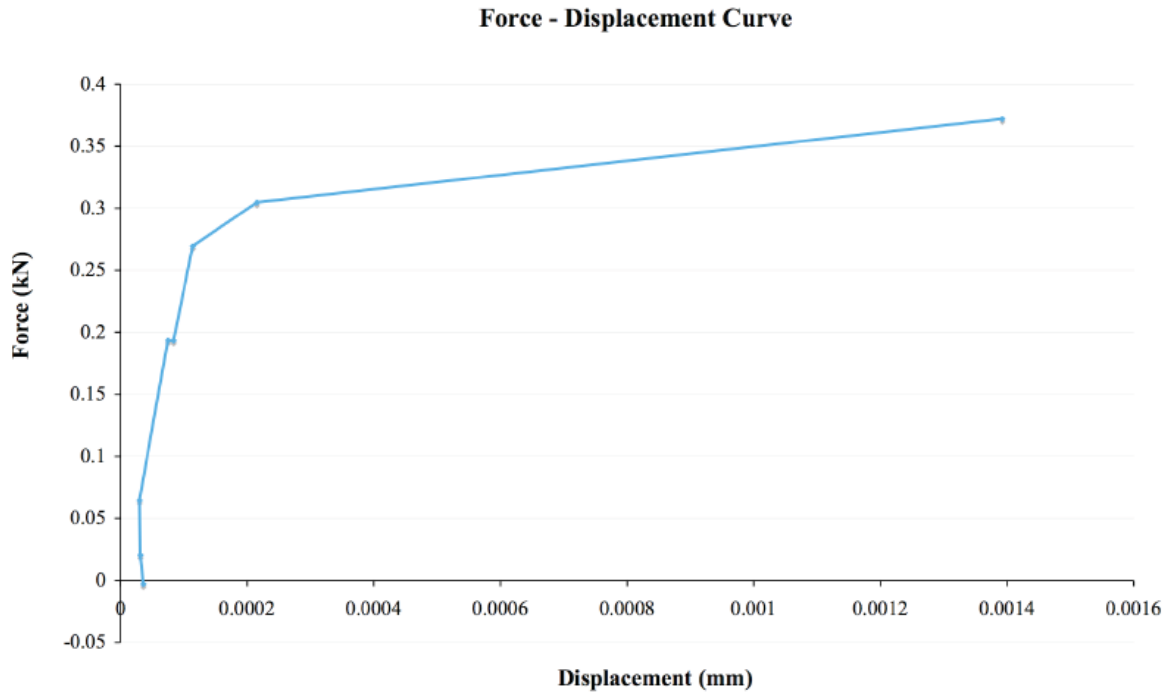


Figure F1a-4.1. Typical force displacement curve.

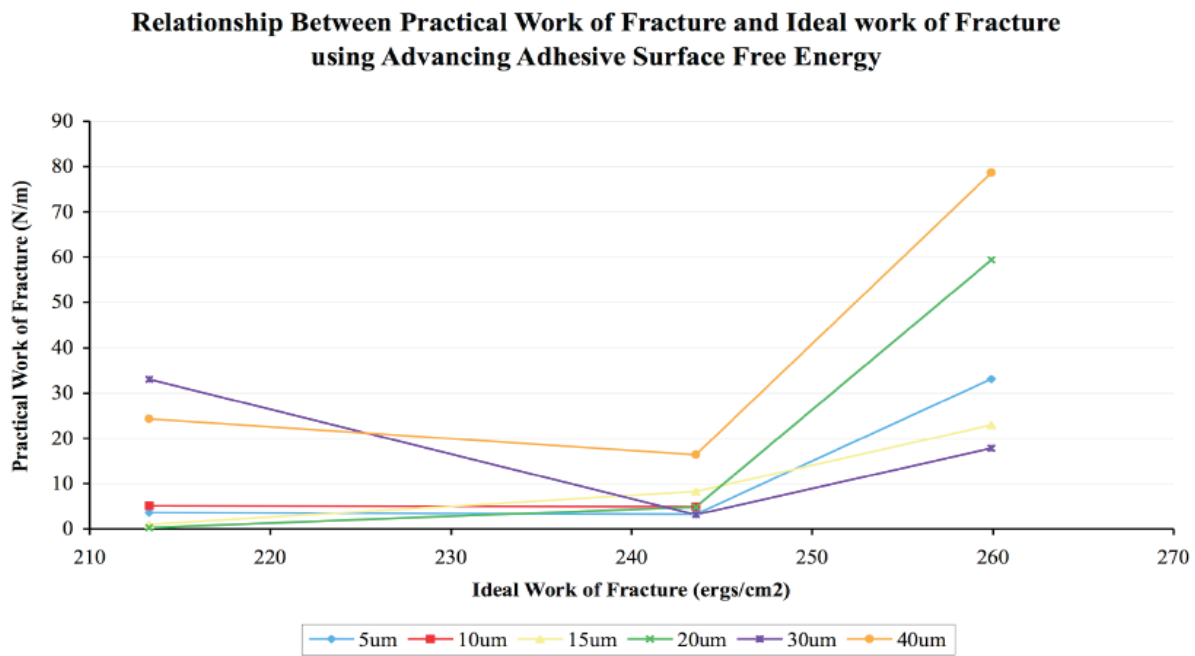


Figure F1a-4.2. Ideal vs. practical work of fracture.

Significant Results

The relationship between ideal and practical work of fracture using experimental measurements was demonstrated.

Significant Problems, Issues and Potential Impact on Progress

The main problems encountered this past quarter were alignment of the sample during preparation and testing. During preparation, researchers encountered problems orienting the sample faces precisely parallel to each other. Alignment problems during testing consisted of the top and bottom grips being slightly out of alignment. This occurred because the threaded attachment locations (base plate and bottom of load cell) were not perfectly aligned. The majority of the alignment problems have been solved, with work continuing to further eliminate afore mentioned problems.

Work Planned Next Quarter

Researchers plan to begin the next phase of testing using sample holders constructed of aggregate instead of stainless steel. Two aggregate types will be used, limestone and granite, in conjunction with the three original asphalts. This testing will evaluate the effects of moisture on the bond strength of the asphalt/aggregate interface and the effect of changes in loading rate.

Subtask F1a-5: Evaluate Acid-Base Scale for Surface Energy Calculations

Work Done This Quarter

No activity was planned for this quarter.

Work Planned Next Quarter

Work on this subtask is planned in year 4 of this project.

Work Element F1b: Viscoelastic Properties (Year 1 start)

Subtask F1b-1: Separation of Nonlinear Viscoelastic Deformation from Fracture Energy under Cyclic Loading (TAMU)

Work Done This Quarter

The main objective of this task was to develop an approach to determine the following three main aspects of material response during cyclic loading:

- i) identify the limiting stress or strain amplitude that results in a nonlinear viscoelastic response without causing damage,

- ii) model and monitor the change in the nonlinear viscoelastic parameters with increasing number of load cycles, and
- iii) model and monitor the change in the nonlinear viscoelastic parameters within each cycle.

Researchers have made significant progress to achieve the first two steps that were reported in the previous quarterly reports. The last step is important because the researchers hypothesized that during each load cycle only specific portions of the load cycle contribute to damage. Also, in order to obtain accurate estimate of the dissipated energy due to fatigue damage, the non-linear viscoelastic response and response due to damage must be accurately modeled and discounted for at each and every point within the load cycle.

For the last step, researchers are currently using typical data for non-linear viscoelastic materials to develop the model to capture the effect of non-linear viscoelastic response within each load cycle. As mentioned earlier, Schapery's nonlinear viscoelastic model was used to predict the material nonlinear viscoelastic response under dynamic loading. The four nonlinear parameters, g_0 , g_1 , g_2 , and a_σ were found as a function of stress and incorporated in the model. Researchers are trying to develop a simplified form of the analytical solution for resulting strain due to sinusoidal loading with all four parameters as a function of stress (which is in turn a function of time). In the meantime, in order to facilitate evaluating the model a combination of analytical and numerical solutions was used. Portions of the Boltzmann superposition integral with the four non-linear terms were solved analytically while the resulting strain from the integral itself was computed numerically.

Consequently, a numerical method was applied to find the material response under the cyclic loading of controlled stress test. To avoid any extrapolation for nonlinear parameters, the stress magnitude was kept in the range of stress that were used to determine nonlinear parameters. For the evaluation of this model, it was also assumed that material behaves similarly in both tension and compression. The model can easily be modified to accommodate different responses in tension and compression. Figure F1b-1.1 below illustrates that at high stress level the material response is nonlinear and consequently the hysteresis loop departs significantly from a standard ellipse that could be expected from a linear material. As expected, the manifestation of non-linearity is similar to damage, i.e., there is a reduction in modulus and increase in hysteresis area due to nonlinearity.

The area related to the linear hysteresis loop is dissipated energy due to delayed elasticity that has nothing to do with damage. The difference in area can be considered as dissipated energy due to nonlinearity (or damage that has a similar manifestation).

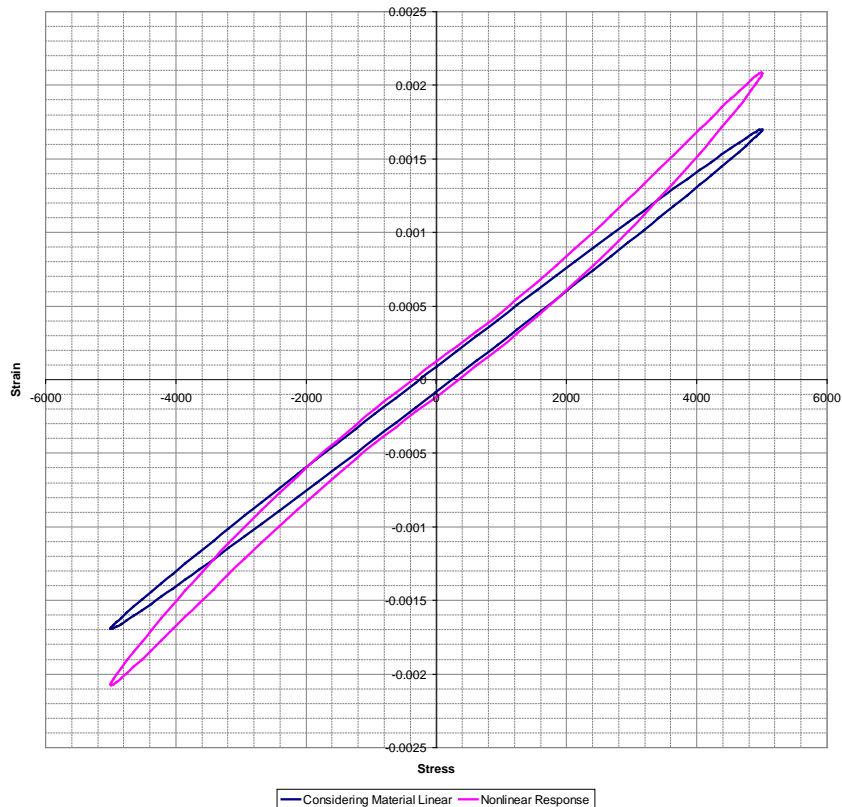


Figure F1b-1.1. Comparison of response of a non-linear material subjected to cyclic loading compared to a linear material.

Work Planned Next Quarter

In the next quarter, researchers will conduct tests on asphalt binders using the DSR to validate the applicability and limitations of this model. A series of creep-recovery tests will be conducted to obtain the four non-linear viscoelastic parameters. The parameters will then be used in the model and compared with the measured response from cyclic loading.

Subtask F1b-2: Separation of Nonlinear Viscoelastic Deformation from Fracture Energy under Repeated and Monotonic Loading

Work Done This Quarter

The revised CMSE* test protocol was used to characterize the fracture and permanent deformation damage of asphalt mixtures under the repeated direct tension (RDT) test. This test protocol was detailed in the quarterly reports for Work Element F2c and in a report, entitled *Aging Experiment Design Including Revised CMSE* Testing Protocols and Analysis to Characterize Mixture Fatigue Resistance*, which has been submitted to the Federal Highway Administration (FHWA).

In the test protocol, a controlled-strain RDT test was conducted on a lab-mixed-lab-compacted (LMLC) asphalt mixture specimen. The maximum strain level was approximately 300 $\mu\epsilon$ in order to

introduce damage to the specimen. The stress and strain waves are shown in figure F1b-2.1. When conducting a controlled-strain test, compressive stress must be applied to the asphalt mixture specimen at the end of each loading cycle. It was found that, when the stress was compressive, the measured properties of the specimen were different from the properties when the stress was tensile (Luo et al. 2009a). Specifically, when the applied stress was compressive, the measured magnitude and phase angle of the asphalt mixture specimen were different from those when the applied stress was tensile. Therefore, different models were used to simulate the stress and strain in different stress states. figure F1b-2.1 shows the measured and modeled stress and strain data, which indicates the good fit of the models used. In addition, a student's t-test was performed to prove that the two kinds of properties were indeed different from a statistical point view.

Based on the proper simulation of measured stress and strain data, the pseudo strain and dissipated pseudo strain energy (DPSE) were calculated for different stress states (Luo et al. 2009b). When calculating the DPSE, each loading cycle was divided into six bands since the measured properties were different in different stress states. As indicated in figure F1b-2.1, the loading cycle from 0 to 2π is divided into six bands, marked using 1 through 6. Therefore, the sections with compressive stress were separated from the sections with tensile stress. The DPSE was determined for each band first, and the total DPSE was calculated. The total DPSE was separated into two components: i) W_{R1} , the DPSE used to develop cracking, and ii) W_{R2} , the DPSE used to develop permanent deformation. Figure F1b-2.2 illustrates the dissipated energy components within a loading cycle, including: i) dissipated strain energy, which is the area within the dashed loop, ii) DPSE used to develop cracking, W_{R1} , and iii) DPSE used to develop permanent deformation, W_{R2} . The sum of W_{R1} and W_{R2} is the total DPSE used to develop the total damage including both fracture and permanent deformation damage within a single cycle.

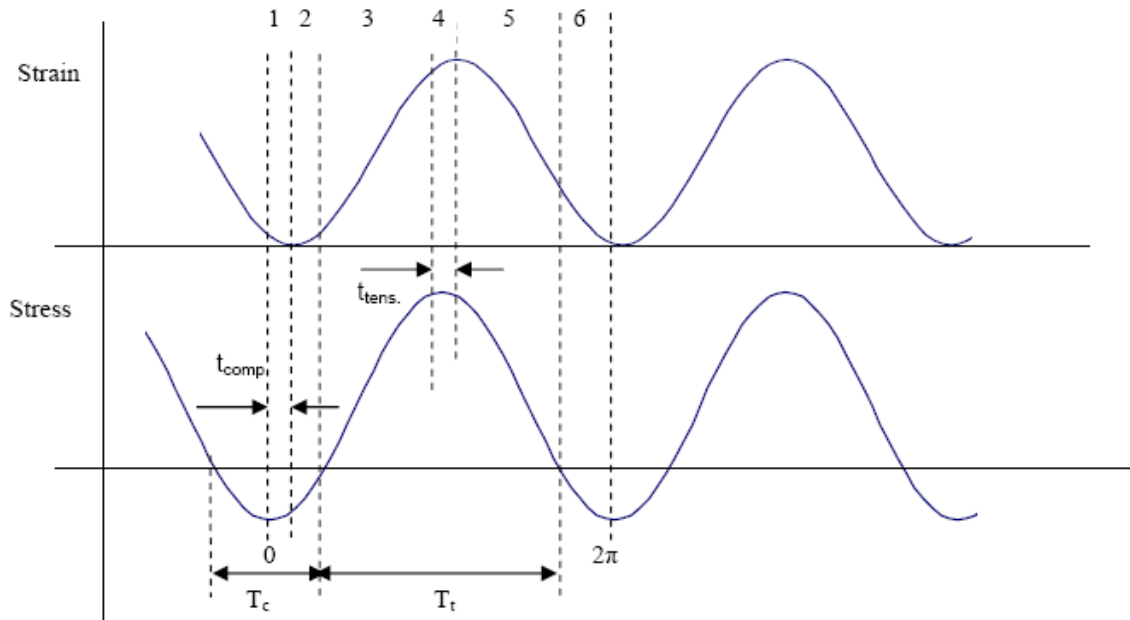


Figure F1b-2.1. Diagram of stress and strain waves in the revised CMSE* test.

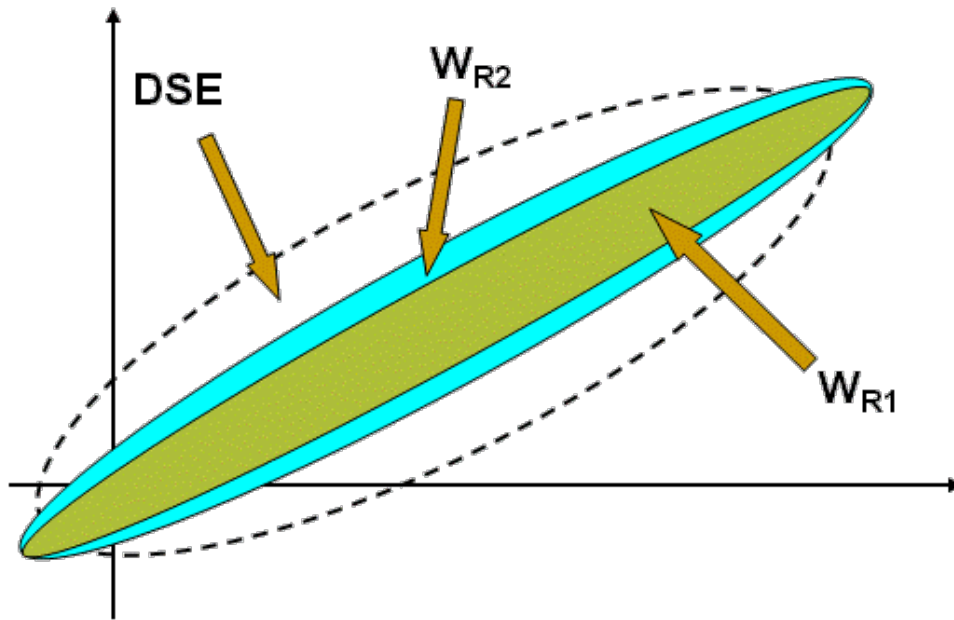


Figure F1b-2.2. Dissipated pseudo strain energy in a loading cycle.

Since 1000 loading cycles were applied to the asphalt mixture specimen, the total DPSE and its components (W_{R1} and W_{R2}) were determined for the 1st, 100th, 250th, 500th, 750th, and 1000th cycles in order to characterize the damage accumulation with the increasing of number load cycles. Figure F1b-2.3 presents the damage accumulation in the asphalt mixture specimen, in which the area within each loop indicates the total DPSE in the corresponding loading cycle. With the increase of loading cycles, the following characteristics can be observed:

- The total damage is increasing since the total DPSE (the area within the loop) is becoming larger;
- The magnitude of the complex modulus is decreasing since the axis of the ellipse is rotating to the horizontal axis direction;
- The phase angle is increasing since the area within the loop is increasing; and
- The pseudo strain is increasing since the loops move from the left to the right.

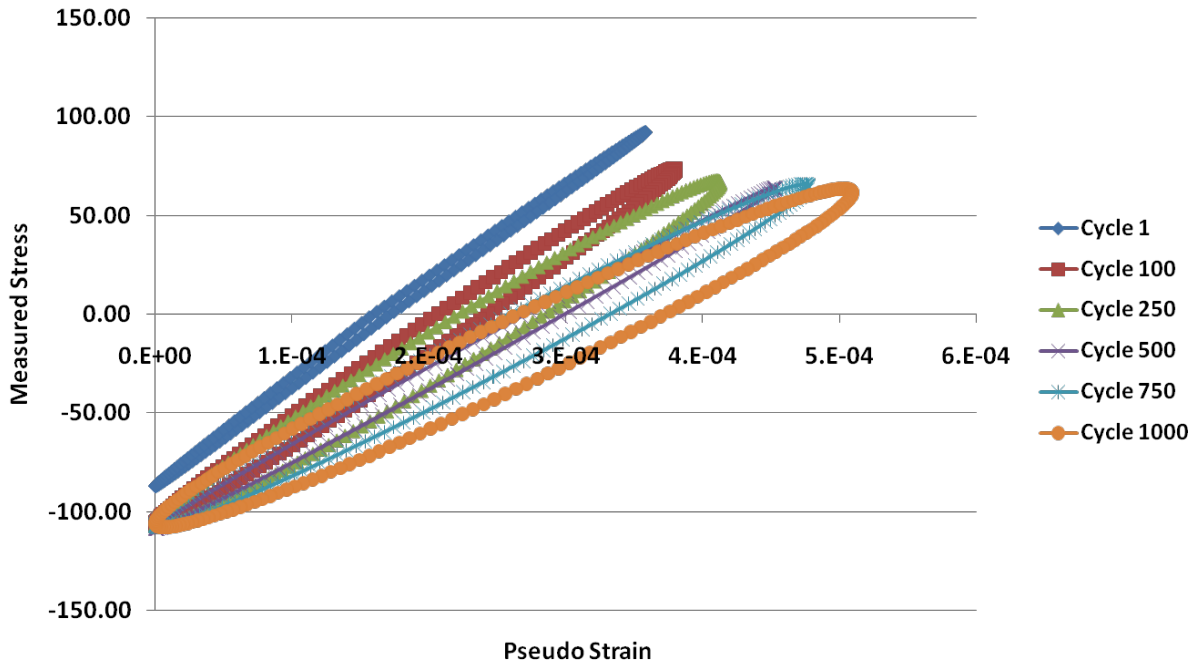


Figure F1b-2.3. Damage accumulation in asphalt mixture specimen with increase of loading cycles.

References

- Luo, X., Luo, R., Lytton, R. L. and Epps Martin, A. (2009a) “A New Perspective of Material Characterization for Asphalt Mixtures under Repeated Tension”, draft available.
- Luo, X., Luo, R., Lytton, R. L. and Epps Martin, A. (2009b) “Further Investigation of Energy Dissipation of Asphalt Mixtures under Repeated Tensile Loading”, draft available.

Significant Results

The controlled-strain RDT test was used to determine the total DPSE and its components: W_{R1} (the DPSE used to develop cracking) and W_{R2} (the DPSE used to develop permanent deformation). It was observed and statistically verified that the material properties when the stress was compressive were different from the material properties when the stress was tensile. The test data were better simulated by differentiating material properties in the different stress states.

A technical presentation was made in the FHWA ETG meeting in Irvine, California, February 2009, on the subject of characterization of properties of asphalt mixtures, including the separation of the DPSE used to develop cracking from the DPSE used to develop permanent deformation.

Significant Problems, Issues and Potential Impact on Progress

A new Material Test System (MTS) used to run the RDT test on asphalt mixture specimens was supposed to be delivered in mid-March. However, the delivery date was postponed to May 2009.

Work Planned Next Quarter

The X-ray Computed Tomography (X-ray CT) will be used to verify the initial crack parameters so that the initial DPSE used to develop cracking will be determined and verified. In addition, the Paris' law parameters will be determined using the RDT test. Beside fracture parameters, the plasticity parameters will be determined using a formulation on plasticity damage accumulation that is under development.

Work Element F1c: Aging

Subtask F1c-1: Critical Review of Binder Oxidative Aging and Its Impact on Mixtures (TAMU)

Work Done This Quarter

There is no literature review work this quarter.

Work Planned Next Quarter

Review of previous work is an ongoing effort.

Subtask F1c-2: Develop Experimental Design (TAMU)

Work Done This Quarter

A draft experimental design was submitted last quarter. Final selection of materials (binder and aggregate) for testing has been determined.

Significant Results

The pilot experiment design was completed, and specimen fabrication (Subtask F1c-4) continued and was completed. Testing of the specimens has been delayed by equipment issues (Subtask F1c-4).

Significant Problems, Issues and Potential Impact on Progress

Further review of the core materials for use in the expanded experiment and of additional field sites for validation is needed.

Work Planned Next Quarter

Conducting the laboratory experiments of the experimental design that use the improved testing protocol (work element F2c) has been delayed by equipment difficulties but will begin in the next quarter. Also, additional field site cores for use in validation of the transport oxidation model and for evaluating the impact of binder oxidation on fatigue will be obtained from WRI.

Subtask F1c-3: Develop a Transport Model of Binder Oxidation in Pavements (TAMU)

Work Done This Quarter

Work this quarter used the transport model to the study of the effect of different climate zones on asphalt binder oxidation in pavements. Annual pavement temperature profiles as a function of depth for the location across the country were generated using available climate data coupled with the pavement temperature prediction model developed in this project. Pavement temperature as a function of time and depth were generated for locations in Arizona, Minnesota, Montana, New York, and Texas. With these temperature profiles, comparison binder oxidation rates in pavements were estimated using binder kinetics and diffusivities for one binder. The resulting calculations provide a quantitative estimate of the differences in binder aging that may be expected in different climates. The simulation was in the year of 1994 beginning from January until December. The yearly aging rate at the various locations ranked from lowest to highest as follows: New York, Montana, Minnesota, Arizona, and Texas (see table F3c-3.1). In all the simulated cases, the fastest aging period occurred during the summer (approximately from May to September), of course, with little aging during the winter).

As an example of the oxidation model calculations, the carbonyl area growth rates for Exxon AC-20 in Texas SH-21 and for the one-year period from January to December in 1994, at two depth ranges is shown in figure F3c-3.1. The oxidation rates in the pavement were rather slow during spring and winter and then increased significantly during the much warmer summer months. Also, the oxidation rate is higher at the surface, primarily because of the higher maximum temperature coupled with the reaction activation energy effect (exponentially higher reaction rate at higher temperatures), rather than because of a different average temperature.

Table F3c-3.1 summarizes carbonyl area (arbitrary units) growth rates measured for two depth ranges for binder recovered from Texas State Highway 21 (SH-21) between Bryan and Caldwell from 1989 to 1992 (Glover 2005). These average aging rates for binder recovered from the top and bottom lifts were determined to be 0.053 and 0.047 CA/year, respectively. Also in the table, aging rates, calculated for the five climate zones mentioned above, and for the binder used in SH-21, are reported. The rates vary from site to site only because of different temperature and solar radiation effects at the different locations. These rates are also shown as CA/year but a separate column also gives the oxidation rate relative to the rate for Texas. Note that the measured and calculated aging rates in Texas differ somewhat, perhaps because the air void characteristics used in the calculation were different from the air void characteristics of the actual pavement.

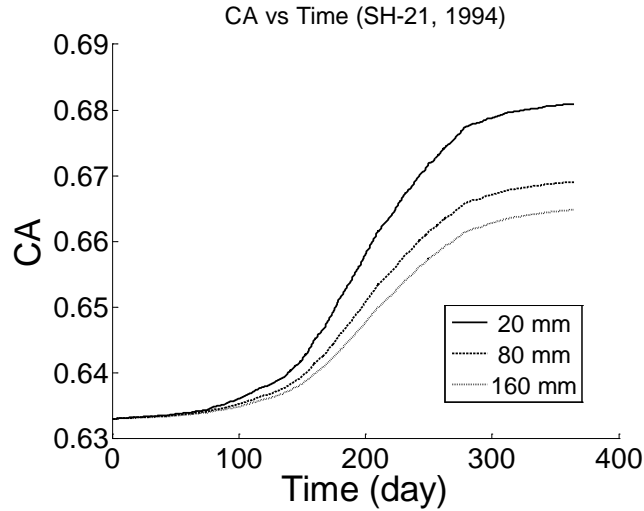


Figure F3c-3.1. Calculated carbonyl area from binder oxidation model at various depths.

Table F3c-3.1. Carbonyl area oxidation rates.

Site	Aging rate (CA/Year)		Aging rate relative to Texas pavement calculation at the top layer	Remark
	Top Layer*	Bottom Layer**		
TX SH-21	0.053	0.047	N/A	Average measured aging rate , 1989 to 1992
NY	0.012	0.007	0.25	Average aging rates calculated from pavement binder oxidation model and pavement temperature prediction model using the climate data from 1994
MT	0.015	0.008	0.31	
MN	0.016	0.010	0.34	
AZ	0.033	0.017	0.69	
TX	0.048	0.032	1.00	

* Top Layer. For TX SH-21 this refers to 0-2 inches below the pavement surface; for the calculations, it refers to 1 inch below the pavement surface

** Bottom Layer. For TX SH-21 this refers to 4-6 inches below the pavement surface; for the calculations, it refers to 6 inches below the pavement surface

Significant Results

Significant progress on model parameter estimation has considerably increased the applicability of the integrated pavement oxidation model. The pavement binder oxidation model provides us with an

important capability of estimating the asphalt binder physical properties in pavements as they change over time due to oxidation and at different pavement depths.

Significant Problems, Issues and Potential Impact on Progress

Further binder oxidation model validation is needed. More actual pavement aging rates need to be compared to model calculations. Pavement cores are available but must be tested for physical properties (subtask F1c-4) before binder aging can be determined. Also, air void characteristic data for the corresponding pavements should be obtained or measured. Higher resolution X-ray CT scans are being evaluated for their ability to provide these air void data. If these air void characteristic data are not available, then parameter estimation methods will be employed.

Work Planned Next Quarter

Even though the binder oxidation model in pavement integrated with pavement temperature prediction model was progressing well, there is a limited availability of asphalt binder oxidation kinetics, which restricts the comparison calculations to only few asphalt binders. An effort will be made to extract the asphalt binder oxidation kinetics from the binder testing data of the binders from Reno, Nevada. These sets of data would be used together with the Nevada pavement temperature generated from pavement temperature prediction model to improve the accuracy of the calculation of the asphalt binder aging in pavement in Nevada region.

Subtask F1c-4: The Effects of Binder Aging on Mixture Viscoelastic, Fracture, and Permanent Deformation Properties (TAMU)

Work Done This Quarter

In this quarter, specimen fabrication for the pilot experiment (Subtask F1c-2) continued and was completed, including 24 AAM samples and 24 AAD samples of unaged, and 24 AAM samples and 24 AAD samples of 6 months aged. The preliminary selection of materials for expanded experiment was determined. Two kinds of binder (Binder 1 and Binder 2) and four types of aggregate were utilized. They are Aggregate 1 (Limestone), Aggregate 2 (Granite), Aggregate 3 (Gravel), and Aggregate 4 (Andesite). Furthermore, a smaller experiment with Binder 1 and Aggregates 3 and 4 was designed to study the effect of aggregate type. An estimate of the quantity for each binder and aggregate type was finished. Additionally, further development of the testing protocol proceeded under work element F2c.

Significant Results

None

Significant Problems, Issues and Potential Impact on Progress

New Linear Variable Differential Transformers (LVDTs) with higher precision have been used since January 2009. The delivery of new MTS equipment was postponed to May 2009.

Work Planned Next Quarter

Begin specimen testing after installation of new equipment.

Subtask F1c-5: Polymer Modified Asphalt Materials (TAMU)

Work Done This Quarter

No activity this quarter.

Work Planned Next Quarter

During the next quarter, polymer modified binders will be obtained for testing.

Work Element F1d: Healing

Subtask F1d-1: Critically Review Previous Work on Healing under FHWA Contracts DTFH61-C-92-00170 and DTFH61-C-99-00022 (TAMU)

Work Done This Quarter

The literature review was continued in this quarter.

Work Planned Next Quarter

This is an ongoing subtask that will be continued through this project.

Subtask F1d-2: Select Materials with Targeted Properties (TAMU)

Work Done This Quarter

In the previous quarter, molecular simulations and literature review were used to identify the key material properties that influence the rate of healing of asphalt binders. A test method to determine the material properties associated with the intrinsic healing function of the healing mechanism was developed. However, the wetting function of the healing mechanism relies on three main properties. First are the viscoelastic properties in the form of the creep compliance parameters, second in the tensile force of bonding between crack faces, and lastly the length of the healing process zone of a cracked surface. The current focus of this research is to determine properties related to the wetting function. While the viscoelastic properties can be determined using standard test methods, surrogate models must be used to evaluate the healing process zone and bonding stresses. Researchers are conducting parametric analysis for the overall healing model as a function of various input material properties. This will facilitate the development of a simplified model for the wetting function.

Work Planned Next Quarter

We will continue to conduct the parametric analysis and evaluation of several different simplified models for the wetting function.

Subtask F1d-3: Develop Experiment Design (TAMU)

Work Done This Quarter

A preliminary experiment design was developed and discussed jointly with researchers from the University of Texas, Texas A&M University, North Carolina State University, and the University of Nebraska. The preliminary discussion was to ensure that there is no duplication of effort amongst various research agencies and the test effort will jointly produce properties that are required for the models that are being developed.

Work Planned Next Quarter

A detailed experiment design to validate the healing model and properties will be developed after making significant progress in subtasks F1d-2 and F1d-4. We anticipate that the experiment design will be developed in the early in the next project year (late Spring).

Subtask F1d-4&5: Investigate Test Methods to Determine Material Properties Relevant to Asphalt Binder Healing (TAMU)

Work Done This Quarter

The work for this task is contingent upon the development of the simplified model in task F1d-2 and future plans are described below.

Work Planned Next Quarter

In the previous quarterly reports we have indicated the development of a test method to determine the intrinsic healing function of the healing mechanism. Based on the results from F1d-2, a similar approach will be used to obtain the parameters related to the wetting function. This will be achieved by measuring the overall healing response (wetting and intrinsic healing) using a crack opening type experiment and then deconvoluting the measured intrinsic healing properties and estimating the remaining material parameters. The test methods to do so will follow closely the methods described in task F1a, but will need to be developed specifically to achieve the objective of this subtask.

Subtask F1d-5: Testing of Materials for model validation* (TAMU)

Work Done This Quarter

No work planned.

Work Planned Next Quarter

Work in this subtask is planned for later after completion of Subtask F1d-3. A preliminary experiment design will be developed specifically for this subtask in addition to F1d-3. This experiment design will allow for partial model validation for only the intrinsic healing function of the healing mechanism.

*Note: Title of the subtask was changed to clarify that the testing in this subtask is not to obtain material properties but to validate the model. The former is accomplished in subtask F1d.4.

Subtask F1d-6: Evaluate Relationship Between Healing and Endurance Limit of Asphalt Binders (UWM)

Work Done This Quarter

The focus last quarter in this subtask was to reduce the variability of results observed in testing with rest periods. The research team appears to have reasonably controlled variation in time sweep tests with no rest periods; however, while running time sweep tests with multiple rest periods, the overall rate of modulus reduction has varied significantly between testing replicates, as is shown in figure F1d-6.1.

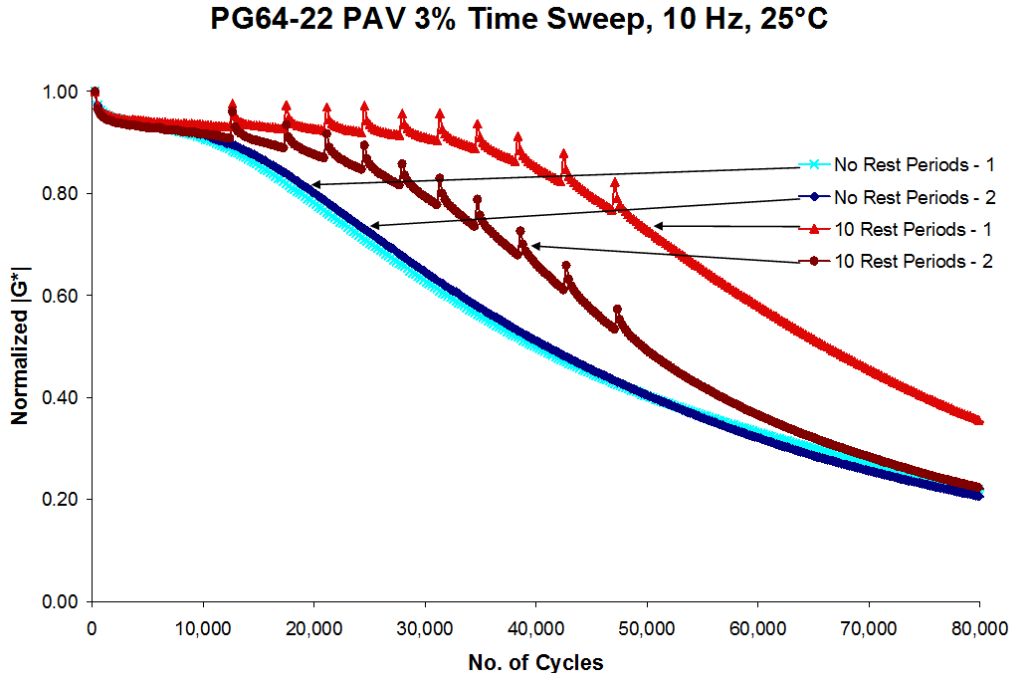


Figure F1d-6.1. Plot. Time sweep tests (with replicates) conducted with and without rest periods.

Upon review of recent literature on the subject of healing of binder fatigue damage (Bhasin et al. 2008, Santagata et al. 2009) it appears that the best available method is to analyze the healing potential of the binder during a single healing event, as opposed to multiple healing events within the same test. The inclusion of multiple events appears to allow a greater opportunity for variability in binder testing. Given this finding, the research team has decided to first try the single event healing testing for this subtask to determine healing characteristics and to evaluate its repeatability before increasing the number of rest periods.

Significant Results

None.

Significant Problems, Issues and Potential Impact on Progress

Variability has caused delay in the selection of new materials and in the testing plan. At this point, a new procedure is being evaluated and, if it is successful, the delay is not likely to affect the end date of this subtask

Work Planned Next Quarter

In coordination with other efforts focused on binder fatigue, a new set of materials is proposed, composed of one neat binder in combination with various additives:

- PG 64-22 unmodified
- PG 64-22 + 4% wt linear styrene-butadiene-styrene (LSBS)
- PG 64-22 + 4% wt LSBS with cross-linking agent
- PG 64-22 + 1.5% wt Elvaloy

Testing will continue to focus on the time sweep procedure. The protocol calling for a single long-duration rest period during each test will be the initial focus to try to minimize the possibility of variability caused by multiple rest periods during a single test. The healing index parameter discussed in the previous quarterly report will continue to be used to evaluate the healing properties of the binders.

Specimens will be tested at equi-stiffness temperatures to isolate any possible effect of differing initial stiffness conditions. Strain-controlled time sweep tests will be performed until a predetermined level of damage is obtained. This will be done by instructing the machine to stop once a lower limit of stress is achieved in each specimen. This is in contrast to determining the location of the rest period during the test from a previous time sweep test with no rest periods, and it is believed that this alternative method may help reduce variability. The rest periods will be consistent for all materials so that a relative ranking of healing performance can be obtained.

Additionally, recent work by Christensen and Bonaquist (2009) has shown that critical information regarding the endurance limit strain level may be obtained from mixture fatigue data using a framework similar in nature to the viscoelastic continuum damage (VECD) model, with a

focus on using reduced cycles to normalize fatigue test results under different testing conditions. The applicability of this concept to asphalt binder fatigue testing will be explored.

The new testing plan described above will be started next quarter, and preliminary results will be presented in the next quarterly report.

Cited References

Bhasin, A., D. N. Little, R. Bommavaram, and K. Vasconcelos, 2008, A Framework to Quantify the Effect of Healing in Bituminous Materials Using Material Properties. *International Journal of Road Materials and Pavement Design*, 9: 219-242.

Christensen, D. W., and R. Bonaquist, 2009, Analysis of HMA Fatigue Data Using The Concepts of Reduced Loading Cycles and Endurance Limit, *Journal of the Association of Asphalt Paving Technologists*, 78.

Santagata, E., O. Baglieri, D. Dalmazzo, and L. Tsantilis, 2009, Rheological and Chemical Investigation on the Damage and Healing Properties of Bituminous Binders. *Journal of the Association of Asphalt Paving Technologists*, 78.

Subtask F1d-7: Coordinate with Atomic Force Microscopic (AFM) Analysis (WRI)

Work Done This Quarter

Correlations were developed relating the viscous properties of SHRP asphalts to temperature dependent pattern formation observed in asphalt thin-film samples studied by atomic force microscopy.

Thermal-Cycle Imaging Of Asphalt Thin-Films by Atomic Force Microscopy.

It is possible to quantify surface entropy effects directly; this is accomplished by observing changes in the ordering of microstructures in thin films of asphalt with powerful imaging techniques. In the case Atomic Force Microscopy (AFM) imaging techniques have been employed to study thermally perturbed asphalts and chromatographic fractions prepared in thin films ($>2\mu\text{m}$) (Pauli et al. 2001; Pauli and Grimes 2003). In most instances these materials exhibit heterogeneity in the surface "microstructure". Loeber (1996), was one of the first investigators to report observing this type of ordered surface phenomena in asphalt materials. In the present work, these features are hypothesized to correspond to surface stress regions where asphalt-wax complexes solidify.

Samples are generally prepared as thin-films, initially spin cast onto glass slide substrates from solution, which vary in film thickness between 600 nm and 1000 nm. In the present work a Quesant Q-Scope™ 250 atomic force microscope equipped with a variable temperature stage was used to image thin films of asphalt in WaveMode™ by AFM as they were heated and cooled via a thermal-cycle. In each experiment the temperature of the sample was incrementally increased then decreased in 3°C increments from ambient temperature to a maximum

temperature. At each incremental heating or cooling step the sample was held constant allowing the sample to thermally equilibrate at that temperatures then imaged,. Height (topography) and phase images were recorded and compared based on asphalt crude source and fraction type.

Specifically, asphalt thin-film samples were prepared by weighing 1.0 ± 0.05 g of SHRP asphalt or asphalt fraction material into 25-mL sample vials and then adding 10.0 ± 0.1 mL of toluene to each vial. Test solutions were then allowed to stand approximately 24 hours to allow for complete dissolution of the sample. After complete dissolution of each sample, a 2.0 μ L “drop” of the solution was spin cast, using an ICL Roto-film spin caster, onto pre-cleaned standard “soda lime” microscope slides at revolution speeds of 600 to 1000 rpm by slowly dispensing the solution from a 10.0- μ L syringe. The solvent was then allowed to completely evaporate by “drying” the films under nitrogen gas in a dry box until imaging could be conducted.

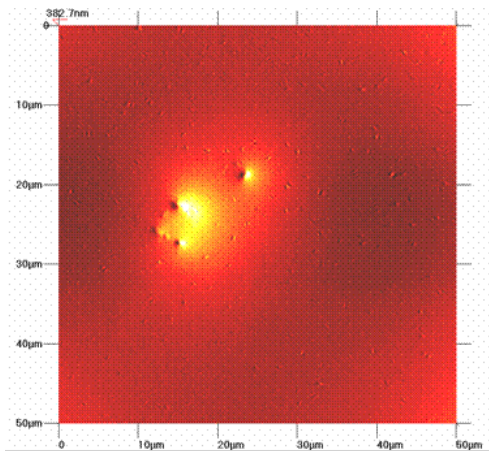
Thin-film sample thicknesses were measured using a Filmetrics F20 instrument. Film thickness measurements were conducted by placing plated films on the F-20 stage then entering initial guesses for both the film thickness and refractive index (RI) into the software, then adjusting both values to optimize the “goodness of fit” readout produced from the measurement. All initial-initial guesses for the film thicknesses were always chosen to be 2.0 μ m, and 1.520 for the initial-initial guess of the refractive index values. All measurements were made in the wavelength range of 500-1000 nm.

All thin-films were imaged using a Quesant QScope™ 250 AFM operated in intermittent-contact mode (WaveMode™). Phase-contrast and height-topography images were captured in the forward and reverse scanning directions. The cantilevers used in the procedure were Mikromasch brand NSC16 cantilevers purchased directly from Quesant Instrument Co., where the average force constant of a set of cantilevers was reported by the manufacturer to be 40 N/m, (i.e., nominal range of 25 to 60 N/m), and the average resonant frequency of a batch of cantilevers was measured to range between 155.5 ± 0.1 kHz to 170.1 ± 0.6 kHz. The average amplitude of oscillation for a batch of cantilever was measured to range between 0.122 ± 0.007 Volts to 0.05 ± 0.01 Volts. The set point force of contact between the cantilever and sample surface was initially always set by the instrument software to -0.5 ± 0.2 Volts. Rates of scan were generally maintained at 1.0 Hz. All scanned images were obtained under ambient pressure (purged under argon gas) at approximately the center of the thin-film “spot” where the film thickness had been previously determined using the F-20 film measurement device.

To perform thermal cycle imaging, sample temperatures were varied based on a calibration curve that was optimized for the sample microscope stage heater. The variable temperature stage was calibrated prior to thermal-cycle imaging in the following manner: a manual control is set to a value between 0 and 800, where a temperature display is read from the controller. However, this is an internal temperature and does not accurately reflect the temperature of the sample. Therefore, a series of measurements were performed to determine the relationship between the controller setting, the controller temperature, and the sample temperature. The sample temperature was measured using a Cole Parmer DigiSense™ Thermistor Probe. The probe was placed on a blank soda lime glass slide to duplicate the same temperatures as would be experienced by an asphalt thin-film. The glass slide was initially positioned on the variable temperature stage, centered over a 3.5-mm-diameter heating pin, which is the heat conducting

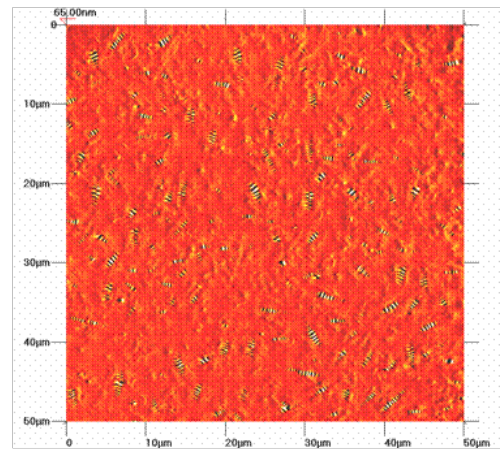
part of the thermal stage of the Quesant QScope-250 AFM that transfers heat to the substrate and sample. Manual control of the thermal stage was varied incrementally in values of 50 from 0 to 400, and then from 400 to 800. Decreasing settings were subsequently varied from 400 to 200 to 100 to 50 and finally back to 0. At each setting, the temperature was allowed to stabilize for approximately 10 minutes. Both the controller temperature setting and the corresponding probe temperature readings were recorded. Values of controller setting were then plotted versus probe temperature to establish a calibration line.

A complete set of WaveMode AFM "thermal-cycle" images of thin-film specimens are depicted in figures F1d-7.1 through F1d-7.6 of the topography of one of the neat SHRP asphalts, AAC-1. In each of these figures the top left image depicts the neat material, the top right image depicts a normal heptane soluble maltene fraction separated from the neat material, and the bottom centered image depicts an IEC neutral fraction separated from the neat material. Inspection of this set of images clearly shows pattern forming phenomena taking place as a function of both temperature and time. Images depicting the temperature dependence of the surface morphology of the IEC-neutral material is particularly interesting in terms of the crystalline patterns that develop, figure F1d-7.3 (40°C-heating), and F1d-7.4 and F1d-7.5, (40°C and 34°C-cooling, respectively). In some of these figures the maltenes images are missing, this is due to the fact that the material became soft and the images only showed a "flat" non-distinct morphology. It is also interesting to point out that in figure F1d-7.6, the size of the "bumble bee" microstructural features decrease when comparing IEC neutral fraction materials to maltenes, and in turn, comparing maltenes to the neat asphalt. The current interpretation of this observation is that the IEC-neutral fraction is much simpler, relatively speaking, in terms of its molecular composition, being mainly composed of a surface layer of waxy material phase separating from the oily material from underneath. The two remaining materials, maltenes and neat asphalt, are more complex still, where resinous materials (i.e., polar aromatic molecules) are present in these samples, and finally, the asphalt contains, in addition to resins, the asphaltenes (polyaromatic hydrocarbons). Thus, the presences of these materials effectively change the original appearance of the base solvent material of the asphalt, in this case, the IEC-neutral material.

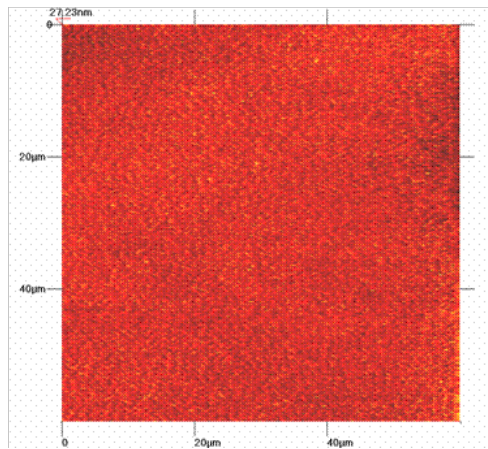


AAC-1-Neat

First images:
prior to thermal
conditioning



AAC-1-Maltenes



AAC-1-Neutrals

Figure F1d-7.1. Tapping mode AFM topography images of a neat asphalt-bitumen thin-film specimen (top left), a normal heptane soluble maltene fraction of the material (top right), and an IEC generated neutral fraction of the original neat material (bottom center). Sample thin-films imaged at 25°C

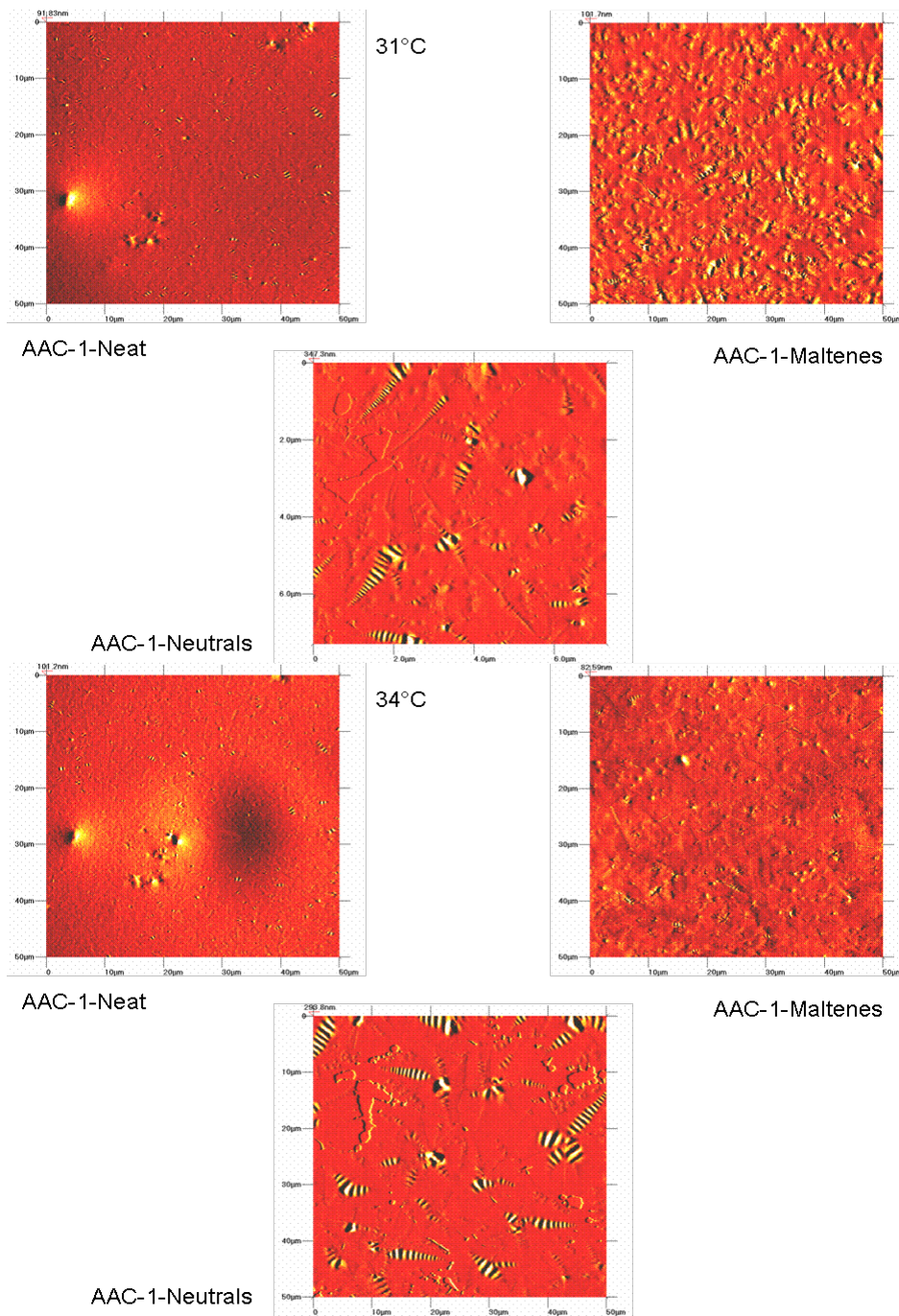


Figure F1d-7.2. Tapping mode AFM topography images of a neat asphalt-bitumen thin-film specimen (top left), a normal heptane soluble maltene fraction of the material (top right), and an IEC generated neutral fraction of the original neat material (bottom center). Top set of three; second heated increment, bottom set of three; third heated increment.

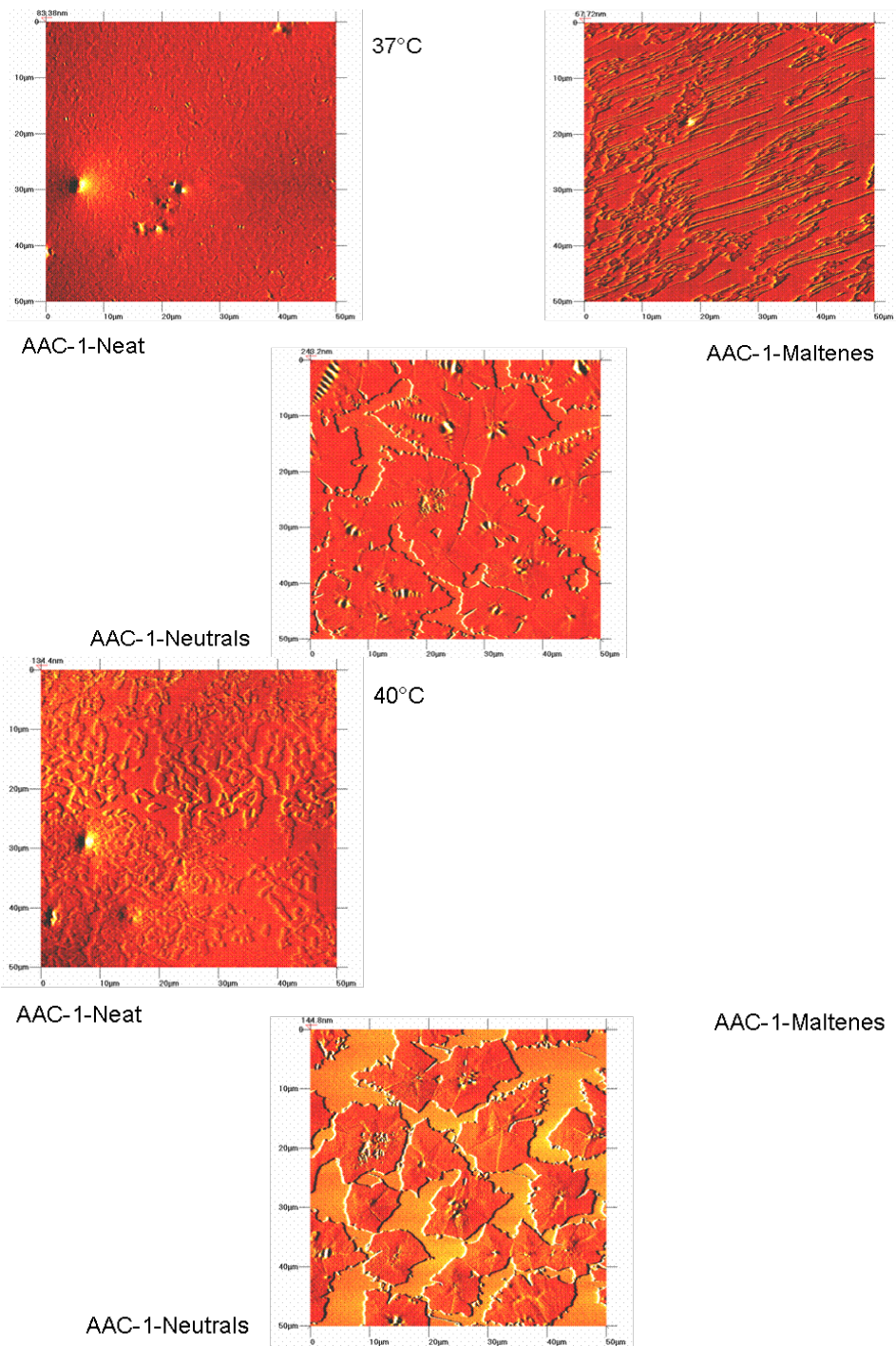
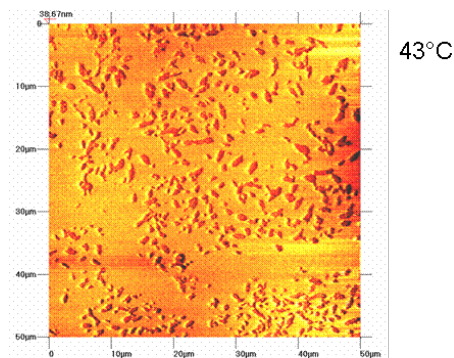
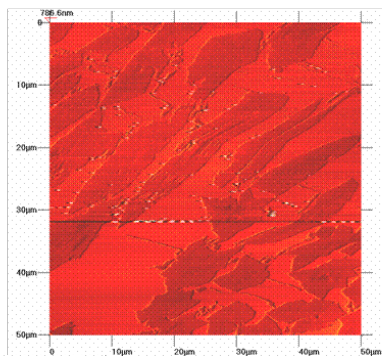


Figure F1d-7.3. Tapping mode AFM topography images of a neat asphalt-bitumen thin-film specimen (top left), a normal heptane soluble maltene fraction of the material (top right), and an IEC generated neutral fraction of the original neat material (bottom center). Top set of three; fourth heated increment, bottom set of three; fifth heated increment.

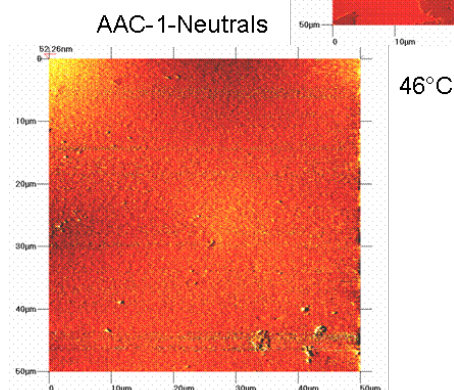


AAC-1-Neat

43°C



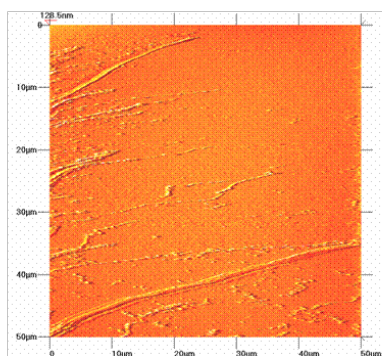
AAC-1-Maltenes



AAC-1-Neat

46°C

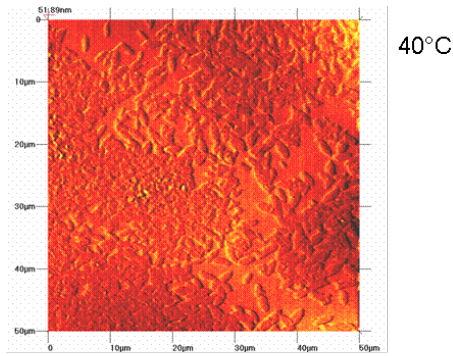
AAC-1-Neutrals



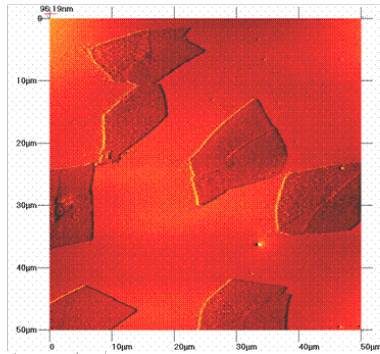
AAC-1-Maltenes

AAC-1-Neutrals

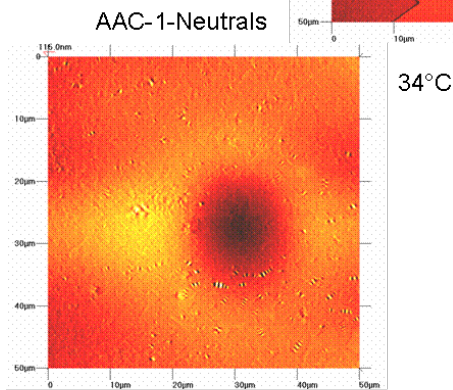
Figure F1d-7.4. Tapping mode AFM topography images of a neat asphalt-bitumen thin-film specimen (top left), a normal heptane soluble maltene fraction of the material (top right), and an IEC generated neutral fraction of the original neat material (bottom center). Top set of three; sixth heated increment, bottom set of three; seventh heated increment.



AAC-1-Neat

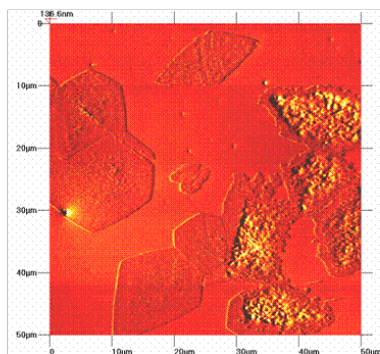


AAC-1-Maltenes



AAC-1-Neutrals

AAC-1-Neat



AAC-1-Maltenes

AAC-1-Neutrals

Figure F1d-7.5. Tapping mode AFM topography images of a neat asphalt-bitumen thin-film specimen (top left), a normal heptane soluble maltene fraction of the material (top right), and an IEC generated neutral fraction of the original neat material (bottom center). Top set of three; first cooling increment, bottom set of three; second cooling increment.

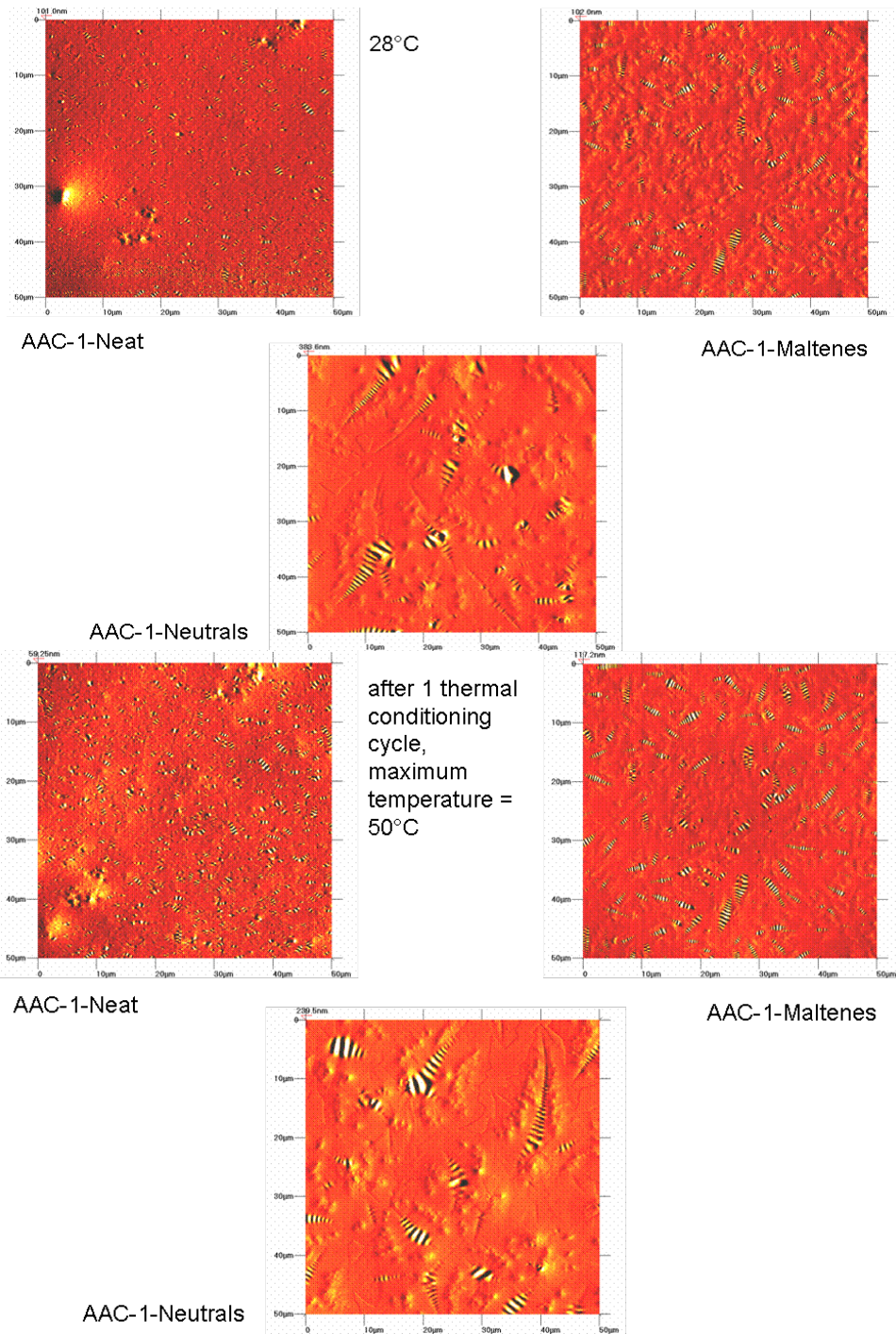


Figure F1d-7.6. Tapping mode AFM topography images of a neat asphalt-bitumen thin-film specimen (top left), a normal heptane soluble maltene fraction of the material (top right), and an IEC generated neutral fraction of the original neat material (bottom center). Top set of three; third cooling increment, bottom set of three; fourth and final cooling increment imaged at 25°C.

Transition temperatures at the "melting" point of the microstructural features were determined for six of the eight SHRP asphalts. The temperature values were determined base on observation of AFM images. Plots were again constructed correlating these temperature values to flow activation energies. Table F1d-7.1 lists phase transition temperatures, $T^{\circ}C$, determined by observations of changes in morphological features in AFM images of 1.0- μm neat asphalt thin-films and flow activation energies of *n*-heptane maltene fraction materials, $E_a(nC_7)$. Figure F1d-7.7, in turn, depicts a plot of flow activation energies of *n*-heptane maltene fraction materials, $E_a(nC_7)$ as a function of lists phase transition temperatures, $T^{\circ}C$,

Table F1d-7.1. Phase transition temperatures of asphalts, $T^{\circ}C$, determined by observations of changes in morphological features in AFM images and flow activation energies of n-heptane maltene fraction material, $E_a(nC_7)$.

Asphalt	$T^{\circ}C$	$E_a(nC_7)$, kcal/mol
AAA-1	---	26
AAB-1	43	30
AAC-1	49	34
AAD-1	35	25
AAF-1	60	38
AAG-1	40	38
AAK-1	40	28
AAM-1	---	38

With the exception of asphalt AAG-1, (based on observation s of changes in surface microstructural morphology, the phase transition in this sample was difficult to judge, which is likely due to the low mass fraction of wax reported for this asphalt), a linear correlation could be drawn through the data points. This data trend again suggests some form of diffusion controlled pattern forming process may be taking place based on the viscosity of the asphalt or maltenes.

Other interesting observations that were made during these experiments are the development of terracing patterns in the thin films after thermal cycles were conducted. Figure F1d-7.8 depict WaveMode AFM topography images of neat SHRP asphalt AAC-1 prepared as a thin-film specimen and imaged directly after thermally heating the sample on a microscope heating stage to 60°C hen cooling under ambient conditions back to room temperature. In this figure, "stair-step" terracing patterns are readily observed over the surface of the film. These patterns are most apparent on the rippled bumble bee microstructures. A simple count of the number of steps (5-7) from high-to-low regions, bottom image of figure F1d-7.8, divided into the total height range of the image (25-nm) would suggest that the surface flow field of the material as it solidifies into place is results in roughly 3-nm to 5-nm step heights. This result suggests that very small clusters of molecules may be moving together in asphalt as it flows, at least at the surface of these thin-films. As a point of reference, the effective diameter of organic molecules in the 500-Dalton to

1000-Dalton molecular weight range are approximately 2-nm to 3-nm, possibly suggesting that asphalts flow like liquids and not like colloids.

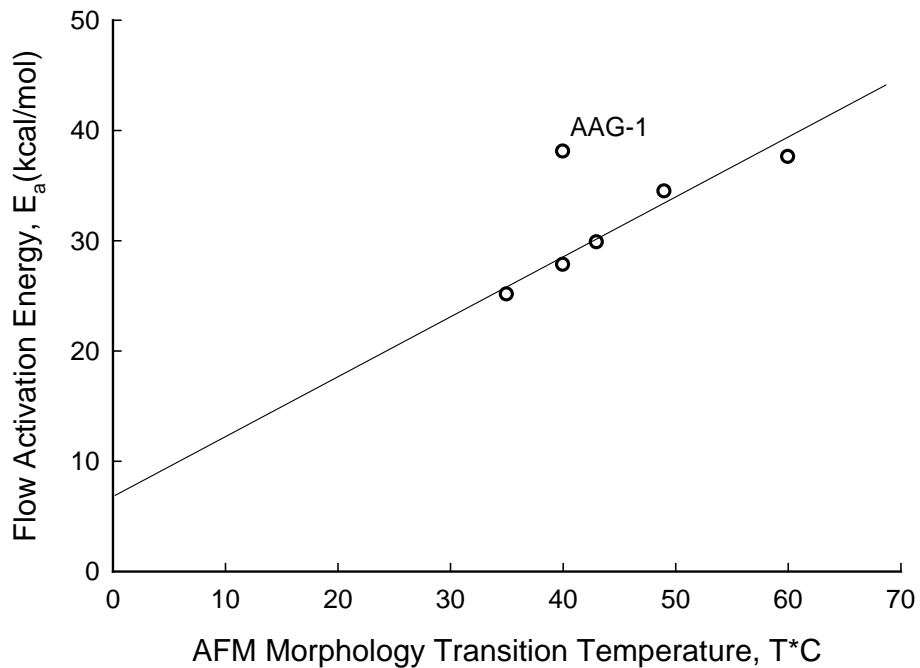


Figure F1d-7.7. Phase transition temperatures, T^* °C, determined by observations of changes in morphological features in AFM images correlated plotted versus the flow activation energies of n-heptane maltene fraction material.

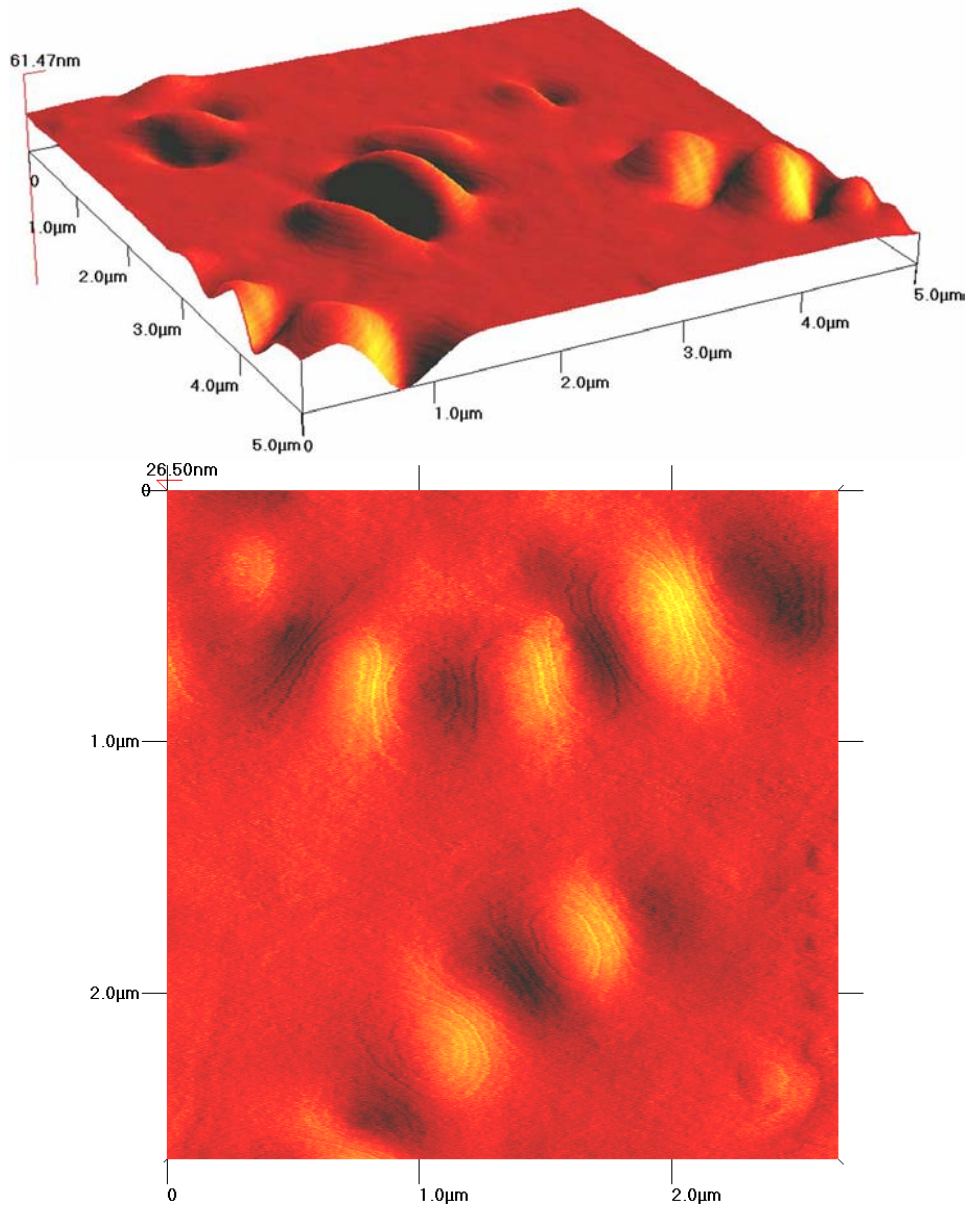


Figure F1d-7.8. WaveMode AFM topography images of neat SHRP asphalt AAC-1 prepared as a thin-film specimen and imaged directly after thermally heating the sample on a microscope heating stage to 60°C then cooling under ambient conditions back to room temperature.

Significant Results

In the work conducted this quarter, asphalt thin films originally prepared from the SHRP core asphalt, and which were subjected to AFM thermal-cycle imaging were analyzed based on changes in morphology as a function of temperature. Close attention was paid to the temperature at which the bee structures tended to “melt away” in the neat asphalt samples. It was speculated

that this temperature constituted a type of phase transition temperature, thus, a correlation was found which related this temperature to that of the activation energy of viscous flow of the n-heptane soluble maltenes. In subtask M2a-2, a detailed model is presented which defines the relationship between phase transition temperature and activation energies of viscous flow of liquids. One interpretation of why this correlation is observed may be related to the phenomena of waxes melting and re-crystallizing in the asphalt. It is presently hypothesized that the bee structures observed by AFM in asphalts and chromatographic fractions of asphalt are closely related to the presence of wax. The correlation depicted in figure F1d-7.7 may correspond to a melting point temperature of wax in asphalt. The interesting point to note is that this melting point is dependent on the viscosity of the asphalt or at least the maltenes phase of the asphalt by the following reasoning: The heats of fusion to melt wax is approximately 3 kcal/mol, whereas the activation energy to move molecules to impart viscosity is measured to be above 20 kcal/mol, thus, it may be that the wax melting and re-crystallization processes are diffusion limited based on the viscosity of the solvent from which the waxes are phase separating from. This phenomena could lend insight to why wax melting is dependent on heating and cooling rates in DSC (differential scanning calorimetric) experiments.

Significant Problems, Issues and Potential Impact on Progress

None.

Work Planned Next Quarter

Analysis of AFM data will continue in the next quarter.

Cited References

Loeber, L., O. Sutton, J. Morel, J.-M. Valleton, and G. Muller, 1996, New direct observations of asphalts and asphalt binders by scanning electron microscopy and atomic force microscopy. *Journal of Microscopy*, 182(1), 32-39.

Pauli, A. T., and W. Grimes, 2003, Surface Morphological Stability Modeling of SHRP Asphalts. *American Chemical Society Division of Fuel Chemistry Preprints*, 48(1): 19-23.

Pauli, A. T., J. F. Branthaver, R. E. Robertson, W. Grimes, and C. M. Eggleston, 2001, Atomic Force Microscopy Investigation of SHRP Asphalts. *American Chemical Society Division of Fuel Chemistry Preprints*, 46(2), 104-110.

Subtask F1d-8: Coordinate Form of Healing Parameter with Micromechanics and Continuum Damage Models (TAMU)

Work Done This Quarter

No work planned for this quarter.

Work Planned Next Quarter

Work on this subtask is scheduled for later years of this research.

CATEGORY F2: TEST METHOD DEVELOPMENT

Work Element F2a: Binder Tests and Effect of Composition (UWM)

Work Done This Quarter

The research team finished analyzing Multiple Stress Creep and Recovery (MSCR) data, started blending the selected binders with the remainder of the additives included in the work plan (Elvaloy AM and Radial SBS, or RSBS), and started aging these materials.

Test results obtained through this work were used in a paper that was accepted for publication and presented at the Association of Asphalt Paving Technologists (AAPT) annual meeting in Minneapolis held March 15-18. This paper, titled “Practical Application of Viscoelastic Continuum Damage Theory to Asphalt Binder Fatigue Characterization,” was co-authored by Carl M. Johnson, Hussain U. Bahia and Haifang Wen.

A series of tests using the newly developed Binder Yield Energy Test (BYET) was carried out to estimate the effects of modifier type and cross-linking on the yield energy values. The initial analysis of the results indicated that the stress-strain behavior and the yielding thresholds are very sensitive to amount of polymer and, in certain cases, the cross-linking. It was also observed that the amount of polymer is more important than the cross-linking and the type of polymer. It was also decided that polyphosphoric acid (PPA)-modified asphalts will be included in future testing to compare to modification with additives.

Significant Results

The Jnr (non-recoverable creep compliance) data for the CRM-based binder at 58 °C, and for the Flint Hills (FH)-based binder at 64 °C are summarized in table F2a.1. The data are shown for the original binder (OB) and for the rolling thin film oven (RTFO)-aged condition, before and after medication with Elvaloy (4170) and linear SBS (LSBS). The concentrations of the Elvaloy were 0.7 and 1.5 %, and the Elvaloy of the SBS were 2% and 4%. These concentrations were used to cause one-grade and two-grade changes for each of the CRM and FH base binders. It can be seen that the changes due to modification are very significant and highly dependent on the additive type. For example, at 3.2 kPa the Jnr for the CRM binder was reduced than 60% at low polymer concentration levels, from 12.09 (neat) to 5.59 (Elvaloy) and 5.25 (LSBS). For the high concentration of polymers Jnr was reduced more than 85%, from 12.09 (neat) to 1.40 (Elvaloy) and 1.96 (LSBS). It was also observed that RTFO causes very high reduction in the Jnr values for all binders.

Table F2a.1. Jnr data for CRM-based binder at 58 °C and FH-based binder at 64 °C.

CRM (PG58-28) Binder Jnr at 58 °C, 1/kPa					
	CRM NEAT OB	CRM 074170 OB	CRM 154170 OB	CRM 2 LSBS OB	CRM 4 LSBS OB
Average at 100 Pa	12.03	4.75	1.50	4.44	0.76
Average at 3200 Pa	12.09	5.79	1.40	5.25	1.96
	CRM NEAT RTFO	CRM 074170 RTFO	CRM 154170 RTFO	CRM 2 LSBS RTFO	CRM 4 LSBS RTFO
Average at 100 Pa	4.05	1.09	0.30	1.09	0.77
Average at 3200 Pa	4.20	1.24	0.30	1.19	0.81
FH (PG 64-22) Binder Jnr at 64 °C, 1/kPa					
	FH NEAT OB	FH 074170 OB	FH 154170 OB	FH 2 LSBS OB	FH 4 LSBS OB
Average at 100 Pa	9.91	1.42	0.90	2.65	1.33
Average at 3200 Pa	10.07	1.62	0.92	3.70	1.90
	FH NEAT RTFO	FH 074170 RTFO	FH 154170 RTFO	FH 2 LSBS RTFO	FH 4 LSBS RTFO
Average at 100 Pa	3.31	0.67	0.36	1.25	0.45
Average at 3200 Pa	3.51	0.75	0.37	1.35	0.48

The percent recovery data from the MSCR test was also obtained for the binders. Examples of the data for the RTFO-aged CRM and FH-based binders are presented in figures F2a.1 and F2a.2, respectively.

The results shown in figures F2a.1 and F2a.2 indicate that for RTFO-aged binders, the highest recovery at 100 Pa and 3200 Pa is exhibited by 1.5% wt Elvaloy 4170 followed by 4% wt LSBS for the CRM binder, and by the 0.7% wt Elvaloy for the FH binder. In addition, 0.7% wt Elvaloy shows more recovery than 2% wt LSBS for both base binders. It is noted that the LSBS-modified binders were not cross-linked and significant changes are expected if cross-linking is used. The work on the cross-linking has already started and will be included in future analysis in this work element.

In addition to the MSCR testing, the testing of the BYET began. Figure 2a.3 depicts example of the results for the same FH and CRM binders discussed earlier, as well as FH binder modified with plastomeric additives (PL1 and PL2). The initial results show significant changes in the yield energy (the vertical scale is logarithmic) when polymers are added. The concentration of the polymer also has a significant effect.

To evaluate the relationship of the yield energy to rheology of these binders, frequency sweep data were also analyzed. Figure F2a.4 depicts the cross-over frequency (the frequency at which $G' = G''$) for the binders. As shown in the figure, there are major differences in the cross-over frequencies, but these differences do not match with the changes in the yield energy. For example, the 4% wt LSBS-modified binder and the 1.5% wt Elvaloy-modified binder show the lowest and highest cross-over frequencies but they show the highest yield energy values.

The initial analysis of MSCR and BYET results point to the importance of differences between rheological and linear viscoelastic properties and damage resistance behavior as measured by MSCR and BYET.

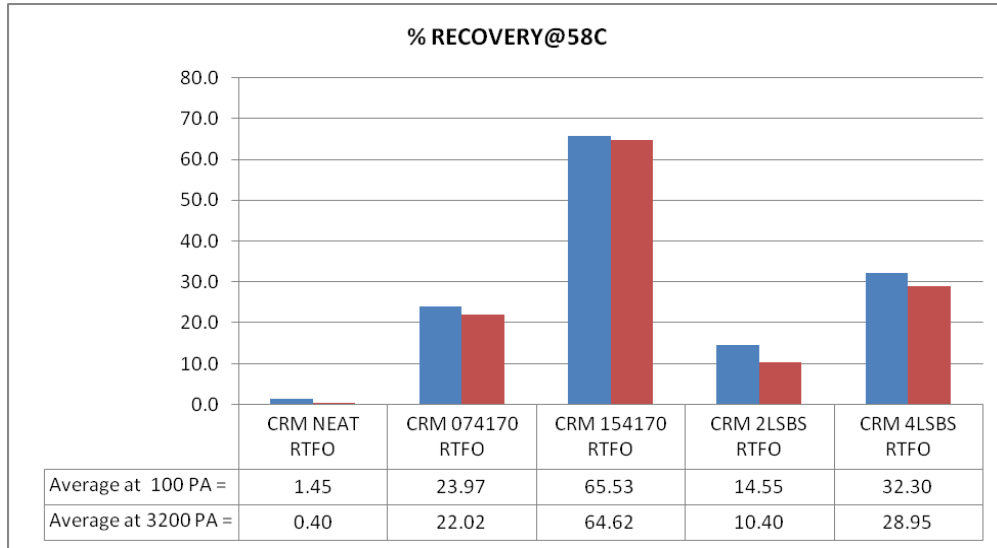


Figure F2a.1. Graph. Elastic recovery data for RTFO-aged CRM-based binder at 58 °C.

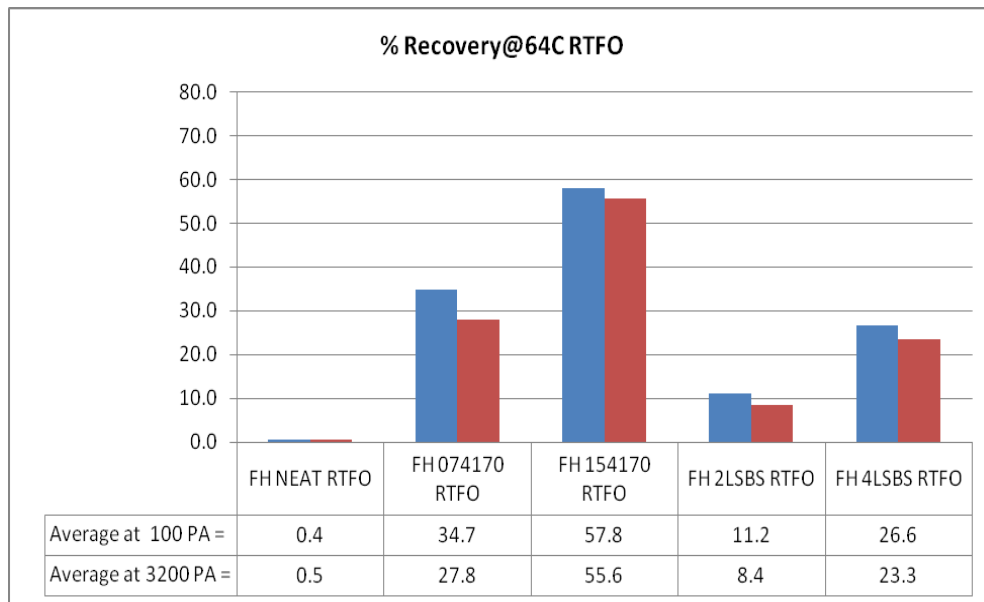


Figure F2a.2. Graph. Elastic recovery data for RTFO-aged FH-based binder at 64 °C.

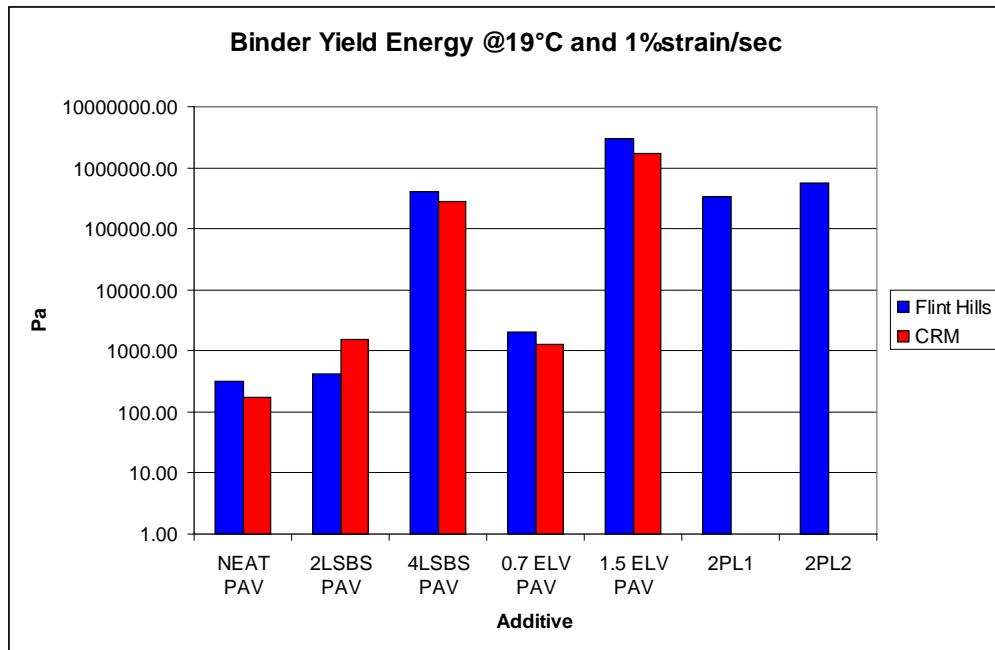


Figure F2a.3. Graph. Binder yield energy data for pressure aging vessel (PAV)-aged binders at 19 °C.

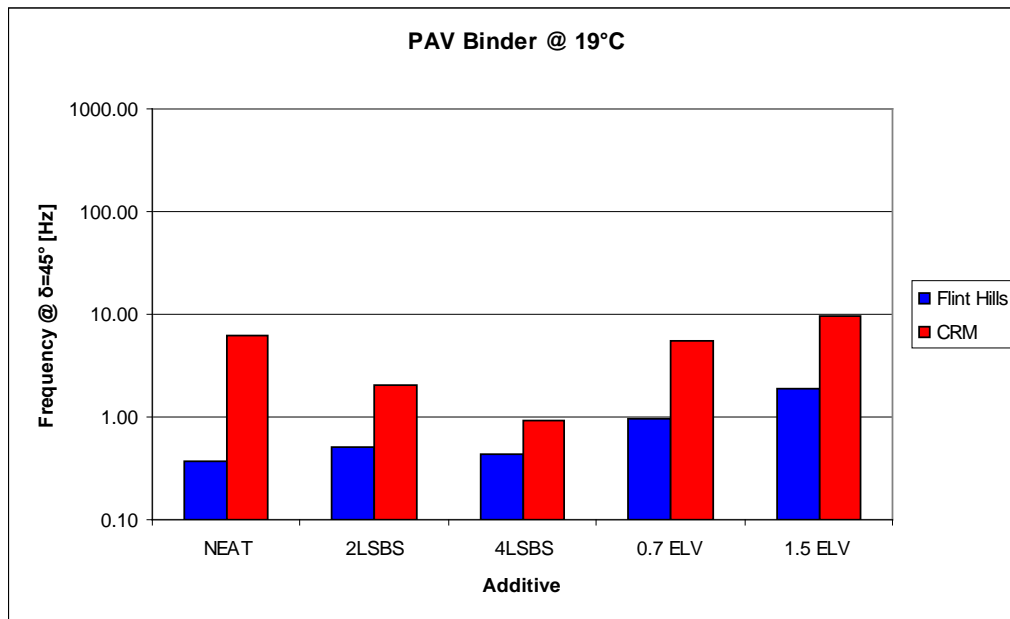


Figure F2a.4. Graph. Binder cross-over frequency for PAV-aged binders at 19 °C.

During this quarter the research team prepared more binders to be tested for the MSCR and BYET:

- CRM + 2% wt RSBS
- CRM + 4% wt RSBS
- FH + 2% wt RSBS
- FH + 4% wt RSBS
- FH + 2% wt LSBS + 2% wt PL1
- FH+ 2% wt LSBS + a cross-linking additive

The research team also conducted Dynamic Shear Rheometer (DSR) testing on original and RTFO materials, and determined the true grades. Examples of the results are presented in tables F2a.2 and F2a.3.

Table F2a.2. Rheological properties of FH-based binder.

	True Grade (TG)									
	Original, G*/sin(δ), kPa				Avg. TG	RTFO, G*/sin(δ), kPa				Avg. TG
	T, °C	Avg.	Standard Deviation	Coeff. of Variation, %		T, °C	Avg.	Standard Deviation	Coeff. of Variation, %	
FH NEAT	64	1.16	0.06	5.51	65.4	64	3.18	-	0.00	66.7
	70	0.55	-	-		70	1.41	-	0.00	
FH + 2 RSBS	64	1.92	0.17	8.84	68.1	70	2.625	0.16	6.20	71.5
	70	0.96	0.02	2.22		76	1.275	0.06	4.99	
FH + 4 RSBS	70	1.93	0.07	3.66	75.7	70	4.12	0.23	5.49	75.5
	76	0.96	0.01	0.74		76	2.08	0.13	6.12	
FH + 0.7 Elv. AM	64	1.49	0.04	2.85	67.9	64	3.715	0.36	9.71	68.5
	70	0.80	0.01	1.77		70	1.865	0.13	7.20	
FH + 1.5 Elv. AM	70	1.10	0.05	4.52	71.0	70	2.385	0.01	0.30	70.9
	76	0.64	0.03	4.42		76	1.33	0.01	1.06	

Table F2a.3. Rheological properties of CRM-based binder.

	True Grade (TG)									
	Original, G*/sin(δ), kPa				Avg. TG	RTFO, G*/sin(δ), kPa				Avg. TG
	T, °C	Avg.	Standard Deviation	Coeff. of Variation, %		T, °C	Avg.	Standard Deviation	Coeff. of Variation, %	
CRM NEAT	58	0.79	0.04	5.37	56.1	58	2.57	-	0.00	59.1
	64	1.71	0.09	5.39		64	1.11	-	0.00	
CRM + 2 RSBS	58	1.57	0.01	0.90	61.5	58	3.75	0.10	2.64	62.5
	64	0.81	0.00	0.09		64	1.845	0.05	2.68	
CRM + 4 RSBS	64	1.72	0.08	4.54	69.7	64	3.79	0.18	4.85	69
	70	0.97	0.03	2.92		70	1.955	0.15	7.60	
CRM + 0.7 Eiv. AM	58	1.07	0.04	3.32	58.6	58	2.9	0.03	0.98	60.2
	64	0.56	0.01	2.53		64	1.485	0.02	1.43	
CRM + 1.5 Eiv. AM	58	1.70	0.04	2.09	63.5	58	3.79	0.14	3.73	63.6
	64	0.95	0.03	2.98		64	2.1	0.1	4.71	

Work Planned Next Quarter

The research team will continue to age materials, perform DSR tests for PAV-aged materials, conduct Bending Beam Rheometer (BBR) tests, fatigue tests, and frequency sweep tests.

Work Element F2b: Mastic (FAM) Testing Protocol (TAMU)

Work Done This Quarter

Improvements to the test protocol to determine fatigue-cracking resistance of FAM specimens using the DMA were made in Subtask F1b-1. Further work on this subtask will be carried out in coordination with the technology development area. The tentative protocol was presented to the mixture ETG at the semi-annual meeting in Reno, NV.

Work Planned Next Quarter

Researchers will coordinate with the technology development work area to further develop the test protocols.

Work Element F2c: Mixture Testing Protocol (TAMU)

Work Done This Quarter

The technical paper on viscoelastic characterization (VEC) test protocol (Luo and Lytton, 2008) was presented in the Transportation Research Board (TRB) AFK50(1) Subcommittee Meeting in the 88th TRB Annual Meeting in Washington, D.C., January 2009. Another presentation entitled “Determine Properties of Asphalt Mixtures Using Experimental and Analytical Methods” was made in the FHWA Expert Task Group (ETG) Meeting in Irvine, California, February 2009. The presentation made in the FHWA ETG meeting included: i) the newly developed test methods characterizing tensile and compressive properties of asphalt mixtures in an undamaged state, ii) how to separate the dissipated pseudo strain energy (DPSE) for fracture damage from the DPSE for permanent deformation developed in asphalt mixtures under repeated direct tensile loading, and iii) progress on the inverse and forward self-consistent micromechanics models (Work Element E1a).

The test protocol on compressive properties of asphalt mixtures was further improved to characterize the anisotropic viscoelastic properties of undamaged asphalt mixtures under compressive loading. The anisotropic properties of asphalt mixtures were interpreted using four parameters including i) the complex creep compliance in the axial direction, ii) the complex Poisson’s ratio in the axial direction, iii) the complex creep compliance in the radial direction, and iv) the complex plane strain bulk compliance in the radial direction. These four parameters were obtained by two test scenarios: i) compressive creep test in the axial direction, and ii) confining creep test in the radial direction. The two test scenarios were completed using the Universal Testing Machine (UTM) and Rapid Triaxial Test (RaTT) Cell. Figure F2c.1 shows the schematic diagram of the two tests.

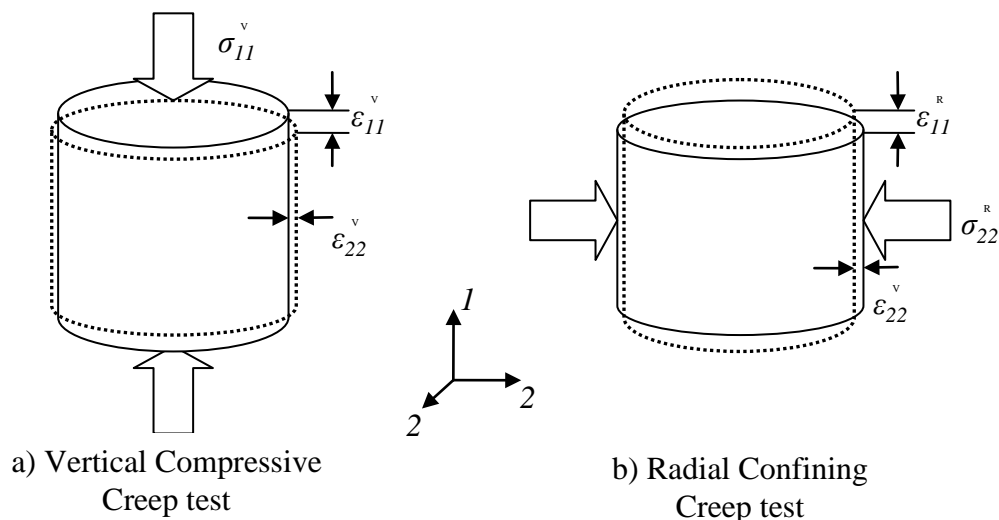


Figure F2c.1 Schematic diagram of two creep tests.

In the first test scenario, a constant axial load was applied to the asphalt mixture specimen without applying confining pressure in the axial direction. The total loading time was 60 seconds. During the loading period, the axial strain and radial strain were measured, which were both functions of time. In the second test scenario, a constant confining pressure was applied to the specimen in the axial direction without applying any axial load. The radial strain was recorded as a function of time. Based on the test data, a set of formulas were derived to determine the aforementioned anisotropic viscoelastic properties (Zhang et al., 2009). The same test scenarios were conducted at three temperatures (10°C, 20°C and 30°C) in order to construct the master curves of the magnitude and phase angle of the complex relaxation modulus and complex Poisson's ratio.

In addition to characterizing asphalt mixtures' properties in an undamaged state, a further investigation was made on the properties of asphalt mixtures in a damaged state under repeated direct tensile (RDT) loading. This investigation was based on the preliminary experimental design and theoretical analysis summarized in the technical report, entitled *Aging Experiment Design Including Revised CMSE* Testing Protocols and Analysis to Characterize Mixture Fatigue Resistance*, which was submitted to the FHWA last quarter. In this investigation, a controlled-strain RDT test was conducted on a lab-mixed-lab-compacted (LMLC) asphalt mixture specimen. Different strain levels (90 and 300 $\mu\epsilon$) were selected to obtain properties of the asphalt mixture specimen in the undamaged and damaged states, respectively. In order to conduct the controlled-strain test, compressive stress must be applied to the asphalt mixture specimen at the end of each loading cycle, as shown in figure F2c.2. It was found that, in the damaged state, when the stress was compressive, the measured properties of the specimen were different from the properties when the stress was tensile (Luo et al. 2009a). More specifically, when the applied stress was compressive, the measured magnitude and phase angle of the complex modulus were different from the magnitude and phase angle of the complex modulus when the stress was tensile. A student's t-test was performed to prove that the two kinds of properties were indeed different from a statistical point of view. By contrast, there was no appreciable difference between the two types of properties if the specimen was in an undamaged state, i.e., the strain level was 90 $\mu\epsilon$.

When determining the damage accumulation in the asphalt mixture specimen under RDT loading, separate models were used to simulate the tensile stress and compressive stress, as well as the corresponding strains, within each loading cycle. These models fit the test data very well, as shown in figure F2c.3. Based on these models, an analytical method was developed to calculate the total DPSE that was used to develop the total damage in the asphalt mixture. The total DPSE was further separated into two components: i) W_{R1} , the DPSE used to develop fracture damage, and ii) W_{R2} , the DPSE used to develop permanent deformation. The Double Meridian Distance (DMD) method was used to verify that the sum of W_{R1} and W_{R2} matched well with the actual measured data (Luo et al. 2009b)

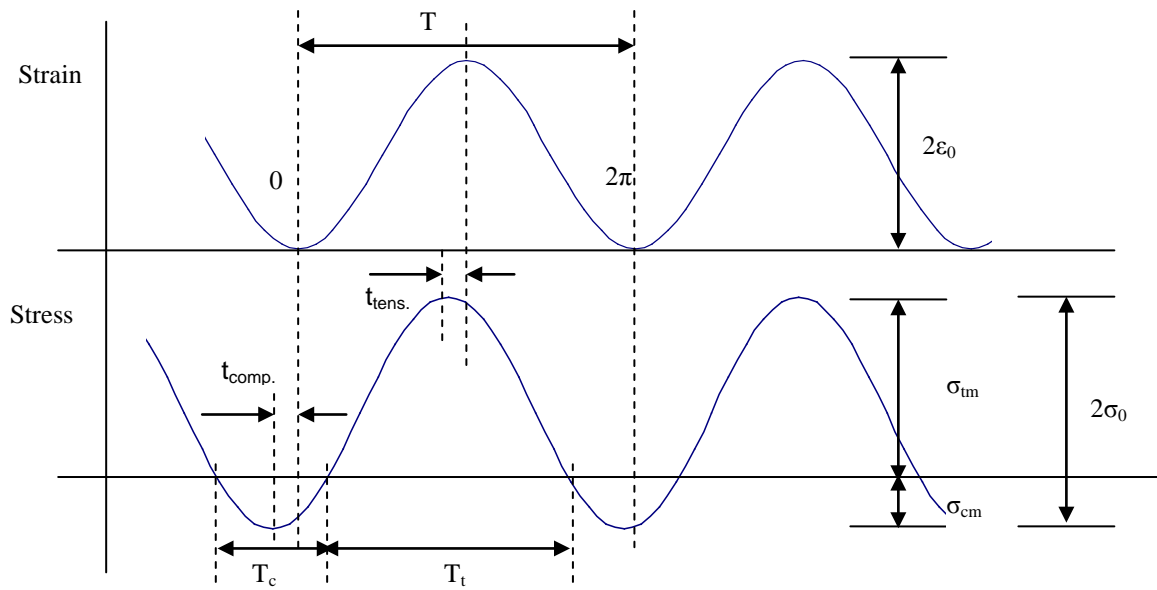


Figure F2c.2 Diagram of Stress and Strain in the Revised RDT Test

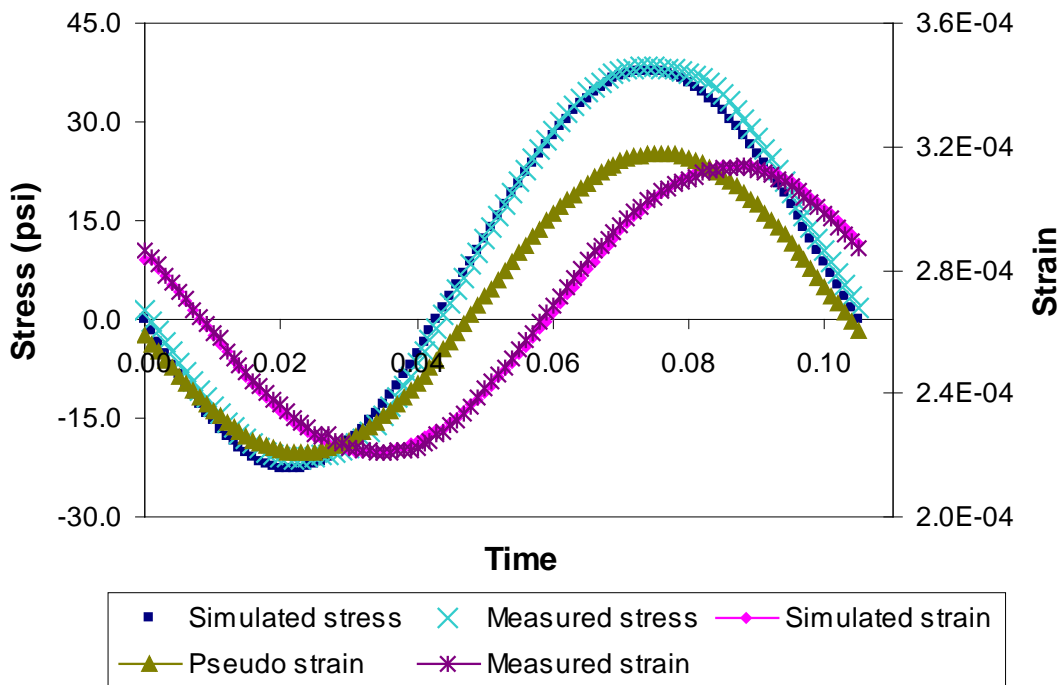


Figure F2c.3 Measured and Modeled Stress/Strain Data at Damaged State

References

Luo, R., and Lytton, R. L. (2008) "Characterization of the Tensile Viscoelastic Properties of an Undamaged Asphalt Mixture." Submitted to *Journal of Transportation Engineering*, American Society of Civil Engineers, under review.

Luo, X., Luo, R., Lytton, R. L. and Epps Martin, A. (2009a) "A New Perspective of Material Characterization for Asphalt Mixtures under Repeated Tension", draft available.

Luo, X., Luo, R., Lytton, R. L. and Epps Martin, A. (2009b) "Further Investigation of Energy Dissipation of Asphalt Mixtures under Repeated Tensile Loading", draft available.

Zhang, Y., Luo, R. and Lytton, R. L. (2009), "Anisotropic Viscoelastic Properties of Undamaged Asphalt Mixtures under Compressive Loading", draft available.

Significant Results

Test protocols were further developed to characterize the anisotropic viscoelastic properties of undamaged asphalt mixtures under compressive loading. A data analysis approach was proposed to determine the creep compliance and complex Poisson's ratio in the axial direction, as well as the creep compliance and plane strain bulk compliance in the radial direction. Tests were conducted under three temperatures in order to construct master curves of the magnitude and phase angle of compliance and Poisson's ratios in both directions.

The CMSE* method was further developed to better characterize the properties of asphalt mixtures in a damaged state using the RDT test protocol. It was observed and statistically verified that the material properties when the stress was compressive were different from the material properties when the stress was tensile. By differentiating material properties in different stress states, the test data were better simulated; in addition, the DPSE used for the fracture damage could be separated from the DPSE used to develop permanent deformation.

A technical paper was presented in the 88th TRB meeting and a presentation including the work that has been accomplished so far was made in the FHWA ETG meeting. Four more technical papers on the work completed for this work element were drafted and will be submitted to technical journals. These papers detailed the mixture testing protocols and data analysis methods that were developed in this quarter and previous quarters.

Significant Problems, Issues and Potential Impact on Progress

New Linear Variable Differential Transformers (LVDTs) with higher precision were received in January 2009. These new LVDTs have been used in the Material Test System (MTS). Problems were identified with the new LVDTs, and one of them was sent back to the manufacture. A new MTS machine was expected to be delivered in mid-March so the tests could be expedited. However, the delivery date of the new MTS was postponed to May 2009.

Work Planned Next Quarter

The test protocol developed to characterize the anisotropic viscoelastic properties of asphalt mixtures will be conducted on more specimens with different asphalt binders and air void contents at different temperatures. The effect of asphalt binder and air void on the undamaged properties of asphalt mixtures will be investigated.

Further analytical method will be developed to model crack initiation and crack propagation in asphalt mixtures. X-ray Computed Tomography will be used to verify the initial crack parameters. Asphalt mixture specimens with different air void contents will be utilized to investigate the effect of air voids on the fracture properties of asphalt mixtures in the damaged state.

Work Element F2d: Tomography and Microstructural Characterization (TAMU)

Work Done This Quarter

Calibration of the creep-and-recovery data to obtain absolute values of force requires the stiffness of the AFM cantilever to be known with a good degree of confidence. A method to measure stiffness of the cantilever by recording its thermal oscillations has been employed to predict stiffness. For obtaining accurate deflection data, closed-loop scanning technique is used. Closed-loop scanning reduces error due to hysteresis and non-linearity of the piezos. Commercially available silicon based calibration standards were used to calibrate the closed-loop scanner. The use of standards is required to ensure that the distance measurements in the AFM are accurate. Currently, improvements are being made to the data acquisition system used to record the thermal oscillations of the cantilever to increase the accuracy of the predicted stiffness.

Significant Results

None

Significant Problems, Issues and Potential Impact on Progress

Some hardware problems were encountered with the thermal k feature of the AFM that is required for calibration. Rectification of these problems is underway.

Work Planned Next Quarter

Work on this task will continue in the next quarter. In the initial phase researchers will try to determine distribution of viscoelastic properties based on the different phases present in the asphalt binder.

Work Element F2e: Verification of the Relationship between DSR Binder Fatigue Tests and Mixture Fatigue Performance (UWM)

Work Done This Quarter

Efforts this quarter were directed toward evaluating the applicability of the viscoelastic continuum damage (VECD) analysis to the results from the monotonic test results of modified asphalts. The research team has made presentations on the results to date at the TRB meeting, the Binder ETG meeting, and the AAPT conference.

Communications with the research team at the University of North Carolina was established this quarter, and a conference call was organized to seek assistance in interpretation of monotonic testing. Testing procedures and samples were shared with Professor Richard Kim’s team, and specific testing protocols are being conducted.

Also this quarter, mixture fatigue testing was initiated to evaluate the relevance of the binder testing being performed. A preliminary experiment was designed using surplus slab compacted specimens from Transportation Pooled Fund (TPF) 5(080): “Investigation of Low Temperature Cracking in Asphalt Pavements”, to prepare beam fatigue specimens. Un-aged binder used to prepare the mixtures was rolling thin film oven (RTFO) aged to simulate the state of binder aging in the beam specimens. The materials are shown in table F2e.1. The goal of this experiment is to verify any relationship between the binder fatigue test methods currently in use and mixture beam fatigue performance. The experimental plan is shown in table F2e.2.

Table F2e.1. Description of the testing materials.

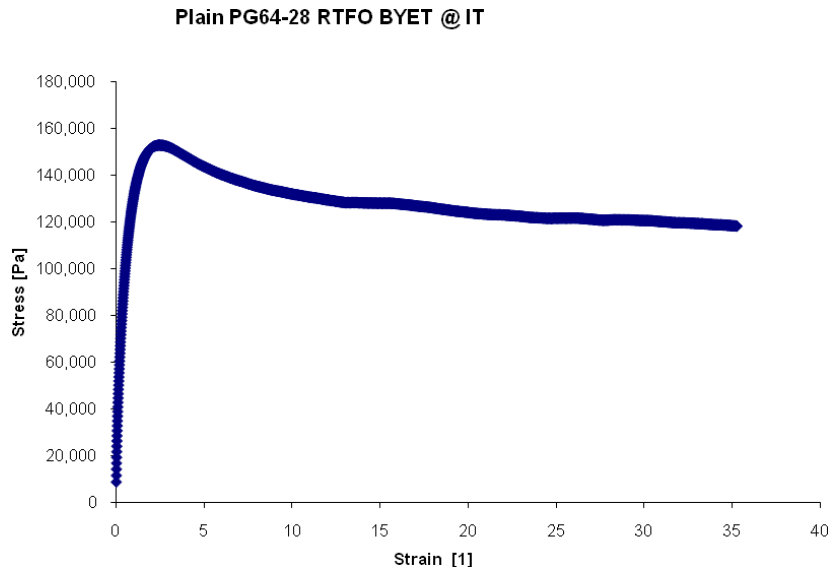
Binder PG Grade	Modifier	Aggregate Type
58-28	None	Limestone
64-28	None	Granite
64-28	Styrene-butadiene-styrene (SBS)	
58-34	Elvaloy	
64-34	Elvaloy	

Table F2e.2. Experimental fatigue testing plan for the TPF-5(080) materials.

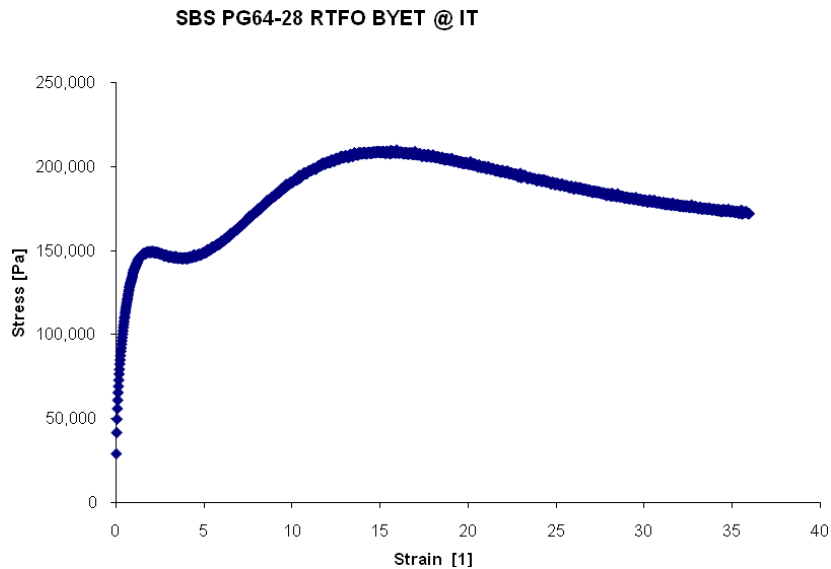
Test Method	Applied Load	Testing Temp(s)	Response Parameters
Frequency Sweep: 0.1 Hz – 30 Hz	0.1% strain	7, 13, 19, 25, 31 °C	Linear viscoelastic $ G^* $ and phase angle spectrum
Time Sweep: 10 Hz	3% strain	SuperPave intermediate temperature (IT), IT-6°C	N_f , VECD $M(D)$ relationship
	5% strain		
Binder Yield Energy Test (BYET)	0.0100/s shear strain rate		Yield Energy, Strain at Max Stress, VECD $M(D)$ relationship
	0.0075/s shear strain rate		
Amplitude Sweep	Stress controlled		VECD $M(D)$ relationship
	Strain controlled		
Mixture Beam Fatigue	500 μ strain controlled	SuperPave IT	N_f (using 50% initial stiffness)

Significant Results

So far, commercially available polymer-modified asphalt binders have shown a distinct behavior under the monotonic loading applied during BYET testing. Typically, most straight-run materials show a single peak stress value, with the material's ability to withstand additional stresses diminishing as the strain in the material continues to increase. However, it appears that some commercially produced polymer-modified binders show this initial peak, and then a secondary larger peak occurs at a higher level of strain. These phenomena are contrasted in figure F2e.1.



(a)



(b)

Figure F2e.1. Graph. Difference in BYET response between (a) straight-run and (b) polymer-modified binders.

Based on discussions with Professor Kim’s group at UNC, the research team at UW–Madison is currently looking at the varying test procedure settings (e.g., varying shear strain rates, temperatures and specimen geometries) in an effort to better explain this behavior. Preliminary data show that the shear rate has an effect on the stress response, but does not affect the presence of this secondary peak, as shown in figure F2e.2.

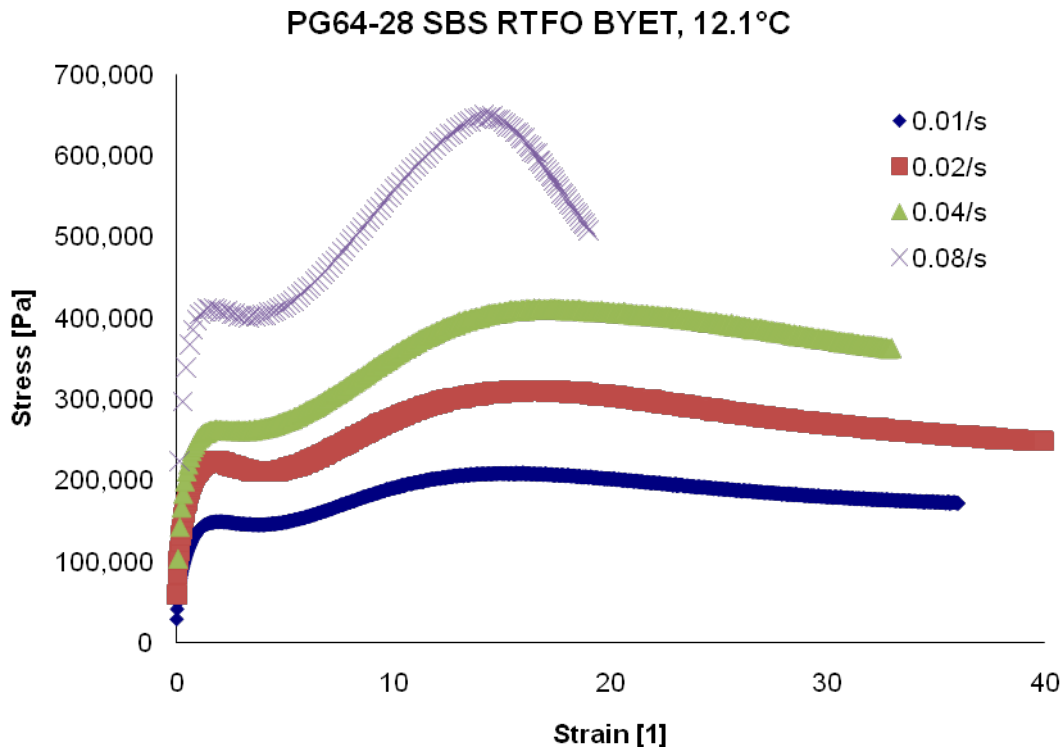


Figure F2e.2. Graph. Effect of shear strain rate on BYET results for an SBS-modified binder.

Significant Problems, Issues and Potential Impact on Progress

The application of VECD analysis to the monotonic test results for modified asphalts appears not to be possible due to strain-hardening observed for a variety of modified asphalts. Unless this issue is resolved, the research team will be forced to look for other alternatives to determine the fatigue damage behavior of binders. This challenge is causing delays in progress and will require changes to the testing plans.

Work Planned Next Quarter

Beam fatigue testing is expected to be completed next quarter, along with BYET and amplitude sweep testing. The findings from this portion of the experiment will be presented in the next quarterly report. Additionally, the findings on the effects of altering testing conditions on BYET results will be presented.

CATEGORY F3: MODELING

Work Element F3a: Asphalt Microstructural Model (WRI)

Work Done This Quarter

A short kick off meeting of the members of the asphalt microstructure modeling team was held in January 2009 during the TRB Meeting in Washington D.C.

Considerable effort was spent in preparation of subcontracts, including proposed budgets, for the anticipated subcontractors on this effort, Virginia Polytechnic Institute (Virginia Tech), the University of Rhode Island, and the National Institute of Standards and Technology (NIST). After subcontracts were drafted they were sent to the respective organization for review. After review by the appropriate organization, the subcontracts were sent to the FHWA Contracting Office for review and approval.

Significant Results

None.

Significant Problems, Issues and Potential Impact on Progress

Significant difficulty was encountered with NIST regarding providing cost share. NIST legal counsel informed WRI that NIST cannot provide cost share. The issue of cost share between different Federal agencies is currently under review at FHWA legal counsel.

Work Planned Next Quarter

It is planned to finalize the subcontract agreements with Virginia Polytechnic Institute and the University of Rhode Island after the subcontract agreements are approved by the FHWA Contracting Office.

Work Element F3b: Micromechanics Model (TAMU)

Subtask F3b-1: Model Development

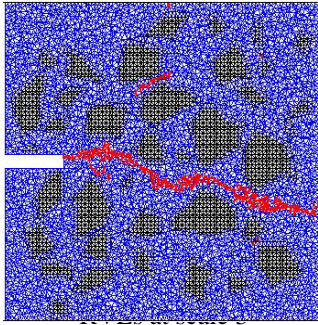
Work Done This Quarter

Lattice Micromechanical Model

Development of the basic lattice micromechanical models is the same as that for Work Element M4a. The progress this quarter in Subtask F3b-1 also benefits the objectives for Work Element M4a. Thus, this part of the report is shown in both areas.

The new lattice modeling engine of multi-scale virtual fabrication and lattice modeling (MS-VFLM) developed in the last quarter is finalized with significant increase in computational efficiency. It has all the functionality of the previous lattice modeling software except the viscoelastic deformation. A sample output from the new MS-LFVM run is shown in the figure, which contains scaling up of fracture energies, sample crack patterns and final load-deflection curve at scale 1. Comparison of efficiency indicates that both tension (TEN) test and single-edge notch (SEN) tests require less than 8 times the previous implementation. The practical implication is that the result shown in the figure takes around 1.1 hours, as opposed to more than 9 hours it took with the previous implementation. This indicates that *virtual testing of laboratory scale specimen can now be done within a reasonable time*. Further reduction of computational cost is currently being investigated. In addition to the computational work, work has initiated on investigating the discrepancy in time-dependency between binder deformation and mastic deformation.

(a)

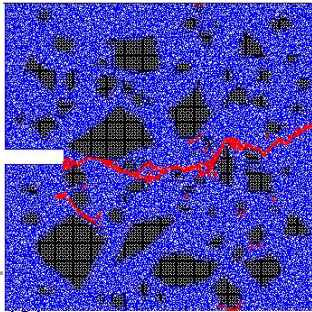


(b)

Specimen No.	1	2	3	4	5
Mastic Cohesion of RVEs (N.mm/mm ²)	0.00150	0.00075	0.00102	0.00099	0.00121
Mastic and Aggregate Adhesion of RVEs (N.mm/mm ²)	0.00064	0.00026	0.00040	0.00038	0.00049

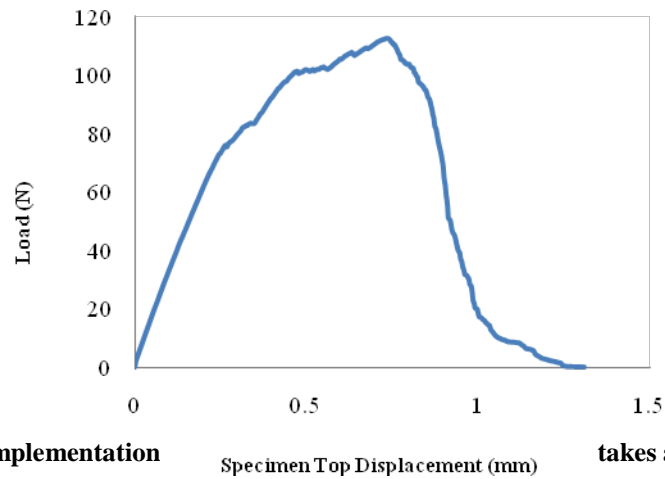
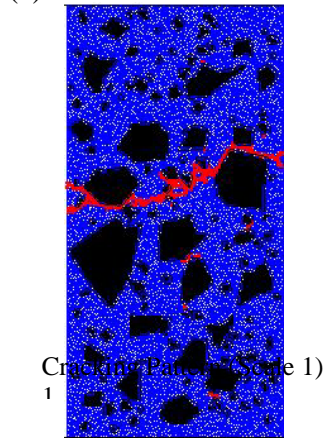


(a)



(b)

Specimen No.	1	2	3	4	5
Mastic Cohesion of RVEs (N.mm/mm ²)	0.04990	0.02207	0.03711	0.02375	0.02706
Mastic and Aggregate Adhesion of RVEs (N.mm/mm ²)	0.02483	0.01092	0.01844	0.01176	0.01342



Sample output from MS-VFLM (the new implementation

Specimen Top Displacement (mm)

takes around

1.1 hours)

Significant Results

Lattice Micromechanical Model

MS-VFLM software is now completely integrated and is more than 8 times more efficient than the previous implementation. This should facilitate practical virtual testing once lattice modeling effort is complete.

Significant Problems, Issues and Potential Impact on Progress

None

Work Planned Next Quarter

Lattice Micromechanical Model

Work will continue on increasing computational efficiency and scaling up from binder deformation behavior to mastic deformation behavior. Modeling of viscoelastic deformation and fracture will also be initiated.

Subtask F3b-2: Account for Material Microstructure and Fundamental Material Properties

Work Done This Quarter

The development of fracture testing system presented in figure F3b-1.1 was continued during this quarter. Fracture test results of asphalt matrix specimens (i.e., fine aggregate matrix: FAM) were then used to determine cohesive zone (CZ) parameters which are implemented into the UNL micromechanics model. In an attempt to identify CZ fracture properties from the matrix fracture testing in a more rigorous way, a 2-D boundary value problem of the fracture testing was numerically simulated by inserting CZ elements in the center of the viscoelastic asphalt matrix specimen.

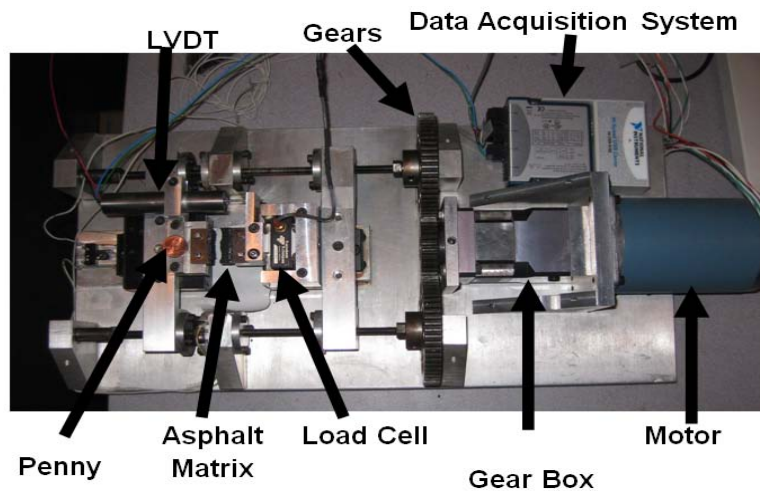


Figure F3b-1.1. Configuration of the fracture testing system.

The CZ properties were determined through a matching process between the simulation and test results. Figure F3b-1.2(a) compares the test results with numerical simulation results to identify the CZ properties. In conjunction with figure F3b-1.2(a), figure F3b-1.2(b) plots the balance of energy from the matrix sample fracture testing. It shows that the internal energy, which is equal to the

external work done, is composed of several sources of energy: the recoverable strain energy, the energy dissipated by the fracture process through the cohesive zones, and the energy dissipated due to material viscoelasticity of the matrix phase. The analysis of figure F3b-1.2(b) infers that the amount of energy dissipated by material viscoelasticity, in this particular case, is minimal compared to the energy dissipated by the fracture process.

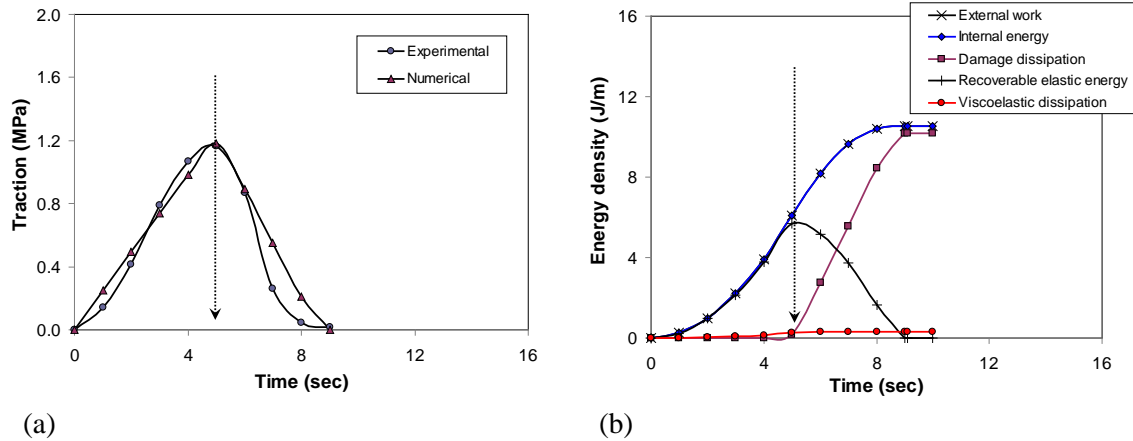


Figure F3b-1.2. Identification of cohesive zone properties: (a) numerical results vs. test results; (b) energy balance from matrix sample fracture simulation.

Figure F3b-1.3 shows a configuration of the uniaxial tensile testing, a digital image obtained from the scanned picture of the asphalt concrete mixture, its finite element mesh generated from the digitized image process, and boundary conditions imposed on the mesh to simulate the uniaxial tensile testing. CZ elements were embedded within the matrix phase neither in aggregate particles nor along the matrix-aggregate interfaces to simulate fracture behavior of the asphalt mixtures at ambient temperature conditions without involving any significant moisture damage. Aggregate particles were modeled as isotropic linear elastic materials, and the asphalt matrix was modeled as isotropic linear viscoelastic. The cohesive zone elements within matrix were modeled using the bilinear traction-separation CZ model.

Figure F3b-1.4(a) present simulation results compared to the uniaxial tensile tests. Experimental results were generally compatible with simulation predictions even before taking any calibrations of the model. Figure F3b-1.4(b) presents the experimental results compared to the simulation results after model calibration. A very good agreement between experimental and numerical simulation results was observed even during a significant portion of the softening part of the curve. An optimization process to obtain the appropriate calibration factors for the cohesive zone fracture parameters (CZ strength T_{max} and CZ fracture energy G_n) was performed. Relatively small calibration shifts were necessary. The calibrated fracture parameters were $1.45T_{max}$ and $0.62G_n$.

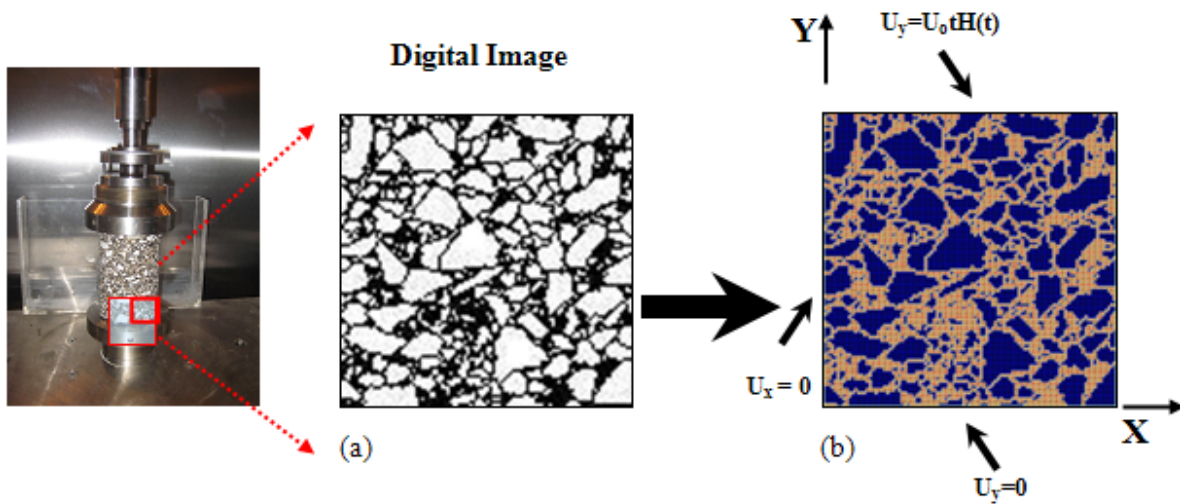


Figure F3b-1.3. Micromechanical simulation of the uniaxial tensile testing: (a) digitization of a scanned image of the specimen; (b) finite element mesh and boundary conditions imposed.

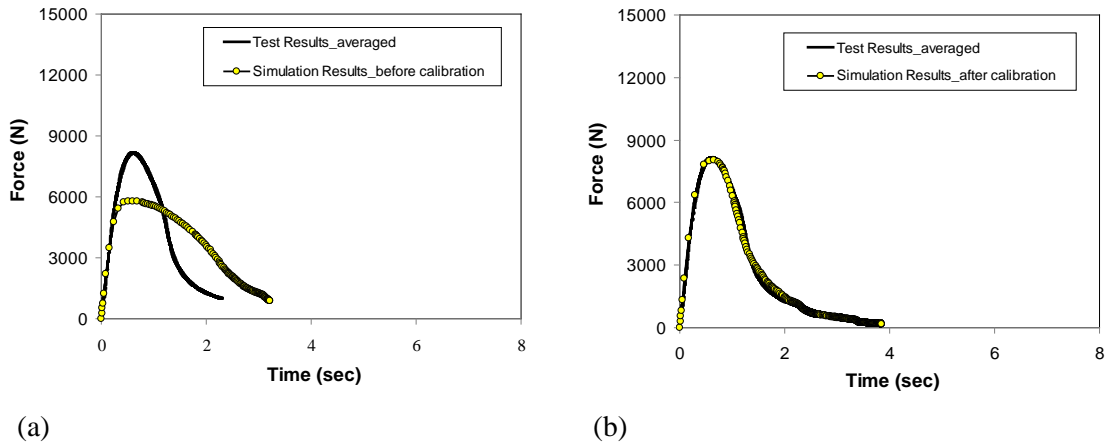


Figure F3b-1.4. Model simulation compared to test results (a) before; (b) after model calibration.

In addition to the model simulation efforts, we have conducted digital image correlation (DIC) analyses of asphalt concrete mixtures under small deformation states in order to experimentally validate the proper dimension of representative volume elements (RVEs) that has been evaluated through a geometrical-numerical process (Kim et al. 2009). In that study (Kim et al. 2009), various geometrical factors such as area fraction, gradation, orientation, and the number of aggregate particles in the heterogeneous asphalt concrete mixtures were considered altogether using two-dimensional actual images of asphalt concrete inner structures. Analysis results indicated that typical dense-graded asphalt concrete mixtures can be characterized for their non-damage effective properties with the approximately 50mm size RVE. Geometrical analysis results to the RVE dimension were then supported by finite element simulations predicting mixture dynamic moduli.

As a further step, during this quarter, the geometrically-numerically determined RVE was verified by experimental tests using the DIC technique.

Two dense-graded Superpave mixtures (19-mm nominal maximum aggregate size) which differ only in the amount of additional hydrated lime (1.0 and 1.5%) were tested in a constant strain rate (0.001 ϵ /sec.) uniaxial tensile mode. Figure F3b-1.5 shows the DIC configuration with the uniaxial tensile testing setup and a magnified view of the asphalt specimen where a total of six trial RVE sections (window sizes ranging from 11.2 mm to 60 mm) was generated for the DIC analysis.

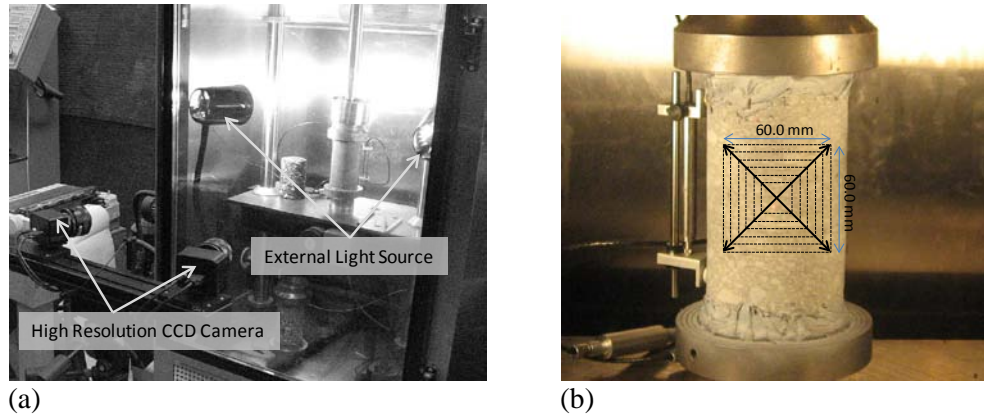
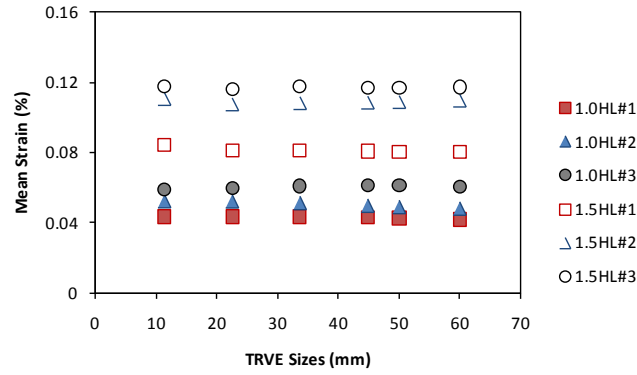
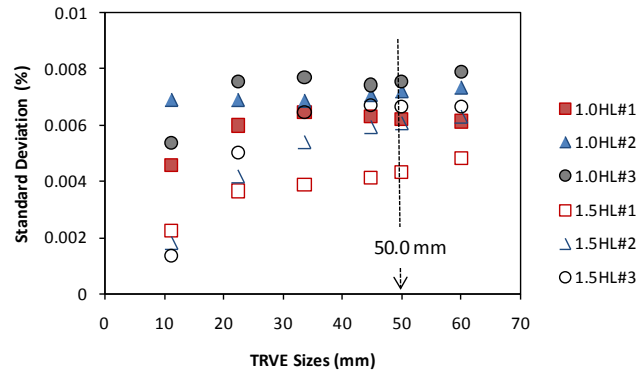


Figure F3b-1.5. (a) DIC configuration of the uniaxial tensile testing; (b) asphalt specimen with six trial RVE sections monitored.

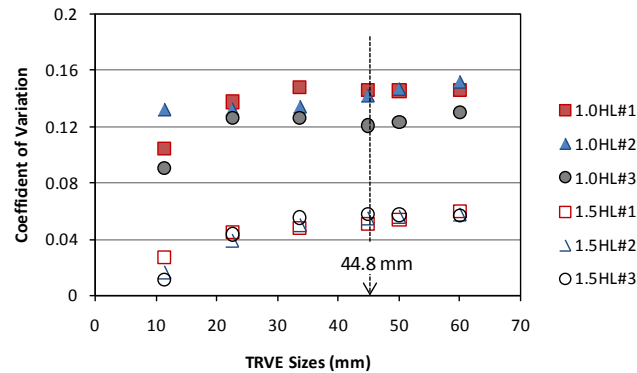
In order to verify the RVE dimension previously defined by the geometrical-numerical approach, strain distributions and their standard deviation on the surface of each specimen are evaluated as Liu (2005) presented. The images of the deformed specimens at the early loading stage up to about 100 $\mu\epsilon$ were only used so that the deformation is in the non-damage state and the strain measurements are not affected by additional heterogeneity such as cracks. Figure F3b-1.6(a) presents mean strains along the loading direction as the trial RVE size increased. The mean strain did not show any clear converging-diverging trends as the trial RVE changed. However, the standard deviation of strains typically increased and stabilized to a value, as the trial RVE size increased. As shown in figure F3b-1.6(b), for the trial RVE size approximately larger than 50 mm, the standard deviation did not vary significantly. The stabilized standard deviation infers that heterogeneous nature of the asphalt concrete mixture reduces and closes to the statistical homogeneity. A similar plot is shown in figure F3b-1.6(c) by taking the coefficient of variation which is simply a ratio of standard deviation to the mean. As expected, the coefficient of variation was not significantly different when the trial RVE size was larger than approximately 40-50 mm. Findings from this analysis were generally consistent with results shown in the previous study (Kim et al. 2009).



(a) Mean Strain vs. Trial RVE Sizes



(b) Standard Deviation of Strains vs. Trial RVE Sizes



(c) Coefficient of Variation vs. Trial RVE Sizes

Figure F3b-1.6. Digital image correlation (DIC) analysis results of asphalt concrete mixtures without damage to experimentally validate the proper dimension of RVE.

Significant Results

Even if both experimental and computational activities pursued by UNL researchers are still in the development-verification stage, some distinct findings could be obtained during this quarter. They can be summarized as follows:

- Computational model simulations with the use of bilinear CZ model and directly-measured componential properties were fairly comparable to experimental results even before model calibration. Strong agreement between simulations and experimental results for the uniaxial tensile testing could be obtained after a low level of calibration in the CZ fracture parameters. However, the predicting power of the model needs to be checked for other cases where different materials and loading conditions are involved.
- The use of a bilinear CZ model with bulk material viscoelasticity considered herein seems to be a potentially promising way at this stage, however further analyses are necessary, because the current bilinear CZ model does not account for rate-dependent fracture behavior which is a characteristics typically observed in asphaltic materials.
- The DIC technique could experimentally validate the proper RVE dimension of typical dense-graded asphalt concrete mixtures where any significant damage is not involved. Statistical homogeneity was obtained from the DIC analyses when the TRVE size was larger than approximately 40-50 mm, which is generally consistent with analysis results from geometrical-numerical approaches presented in the last quarters.

Significant Problems, Issues and Potential Impact on Progress

None

Work Planned Next Quarter

The development of fracture testing system will be continued and testing of different materials and at different testing conditions (e.g., loading rates and temperatures) will be conducted for model verification, calibration, and validation. DIC analyses of asphalt concrete mixtures subjected to cracking will be performed, and any significant findings will be presented.

Mechanical properties of individual mixture components have been estimated by the nano-indentation technique (Khanna et al. 2003). During the last quarter, we have obtained numerous measurements. Test results and any significant findings will be presented next quarter.

Work with Dr. Amit Bhasin at UTA has been initiated to develop a more articulate and scientific protocol in mixing and compaction of the asphalt matrix (i.e., FAM) specimens. Advanced image analysis techniques and finite element computational simulations of mixtures will be incorporated with mechanical test results of FAM specimens produced from different mixing-compaction procedures to finally develop the best protocol of FAM specimen fabrication for the micromechanical modeling.

We will also start to evaluate properties of common materials (binders, matrix, aggregates, and mixtures) selected by ARC modeling teams (TAMU, NCSU, UTA, and UNL). Test results will then be incorporated into the model.

References Cited

Khanna, S. K., Ranganathan, P., Yedla, S. B., Winter, R. M., & Paruchuri, K. (2003). Investigation of nanomechanical properties of the interphase in a glass fiber reinforced polyester composite using nanoindentation. *Journal of Engineering Materials and Technology*, 90-96.

Kim, Y., Lutif, J.E.S., and Allen, D.H. (2009). "Determination of Representative Volume Elements of Asphalt Concrete Mixtures and Their Numerical Validation through Finite Element Method." *Transportation Research Record*, in press.

Liu, C. (2005). "On the Minimum Size of Representative Volume Element: An Experimental Investigation." *Society for Experimental Mechanics*, 45, pp.238-243.

Journal Papers, Conference Proceedings, and Abstracts Produced during This Quarter

F. T. S. Aragão, Y. Kim, J. Lee, and D. H. Allen. "A Micromechanical Model for Heterogeneous Asphalt Concrete Mixtures." *Journal of Materials in Civil Engineering*, under review.

F. T. S. Aragão, Y. Kim, J. Lee, and D. H. Allen. "A Micromechanical Fracture Model for Heterogeneous and Rate-Dependent Asphalt Concrete Mixtures Using the Finite Element Method." 10th U.S. National Congress on Computational Mechanics.

F. T. S. Aragão and Y. Kim. "Modeling Fracture and Failure of Nonlinear, Inelastic Asphalt Concrete Mixtures." 2009 Joint ASCE-ASME-SES Conference on Mechanics and Materials.

Work Element F3c: Development of Unified Continuum Model (TAMU)

Work Done This Quarter

The ARC researchers selected the aggregates and binders that will be used to produce test mixtures. All ARC core aggregates and binders are presented in table F3c-1 and table F3c-2 consequently. Six binder-aggregate combinations will be used to produce mastic and fine asphalt mixtures, while three binder-aggregate combinations will be used to produce full asphalt mixtures as presented in table F3c-3. Among the three binder-aggregate combinations for full asphalt mixtures, one is selected for the first round of experiments to develop the model and fine tune the test protocol. This mixture will be designed using limestone (ARC AG 001) and NuStar Energy binder (ARC BI 001). The remaining two full asphalt mixtures will be tested for further verification of the developed model. The needed amount of binders and aggregates from each ARC team was collected and compiled together as presented in table F3c-4.

Table F3c-1. Core aggregates for ARC.

Aggregate ID	Description	Source	Remarks
ARC AG 001	Limestone	WI	This aggregate has poor moisture damage resistance
ARC AG 002	Granite	CA	SHRP designation RB; regarded as resistant to moisture damage
ARC AG 003	Gravel	AR, also used in TX	Used in NCHRP 9-34; aggregate has poor moisture damage resistance as reported by field and 9-34 protocols but it has very high TSR (AASHTO T283)
ARC AG 004	Andesite	NV	Highly moisture sensitive aggregate; presents challenge in establishing the Superpave mix design

Table F3c-2. Core binders for ARC.

Binder ID	Supplier	Reported Crude Source	Location
ARC BI 001	NuStar Energy	Paulsboro, NJ	Venezuelan
ARC BI 002	Montana Refining OR Exxon-Mobil*	Great Falls, MT or Billings, MT	W. Canadian blend
ARC BI 003	Valero Refining	Benecia, CA	CA Valley & ANS
ARC BI 004	W.Texas Intermediate or Saudi Arabian Medium/Heavy or Gulf Coast*	Valero Refining or another source	To be decided

*WRI to pick one from the possible alternatives in this row

Table F3c-3. Binder-aggregate combinations of test mixtures.

Binders	Aggregates	Mastic and Fine Asphalt Mixtures	Full Asphalt Mixtures
ARC BI 001	ARC AG 001	X	X
	ARC AG 002	X	X
ARC BI 002	ARC AG 001	X	
	ARC AG 002	X	X
ARC BI 003	ARC AG 001	X	
	ARC AG 002	X	

Table F3c-4. Material quantities for ARC.

		NCSU	TAMU	UTA	UNL
Material ID		Amount (kg)	Amount (kg)	Amount (kg)	Amount (kg)
ARC BI 0001		164	938	60	42
ARC BI 0002		88	483	60	25
ARC BI 0003		12	68	60	8
ARC BI 0004		N/A	16	N/A	8
ARC AG 0001	Size 1*	800	3500	N/A	140
ARC AG 0002		1600	7000	N/A	290
ARC AG 0003		N/A	150	N/A	N/A
ARC AG 0004		N/A	150	N/A	N/A
ARC AG 0001	Size 2*	570	2060	220	90
ARC AG 0002		970	3860	220	160
ARC AG 0003		N/A	75	N/A	15
ARC AG 0004		N/A	75	N/A	15
ARC AG 0001	Size 3*	250	780	150	35
ARC AG 0002		390	1425	150	60
ARC AG 0003		N/A	40	N/A	5
ARC AG 0004		N/A	40	N/A	5

* Size 1: passing 19 mm and retained on #16, Size 2: passing #16 and retained on #200, and Size 3: passing #200

The three-dimensional comprehensive constitutive material model was implemented in finite element (FE) code using UMAT in AbaqusTM and has been verified by experimental measurements of creep recovery tests at different temperatures from the Nottingham Database. Finite element analysis of permanent deformation of a pavement structure under repeated loading was conducted. The geometry of pavement structure is sketched in figure F3c.1. A single axial with dual wheels loading with pressure 689.5 kPa was symmetrically applied on the pavement structure, which allows developing a symmetric finite element (FE) model by fixing the horizontal direction on the vertical edge of the mesh to represent the middles of pavement structure.

The asphalt layer material properties were obtained by analyzing the creep-recovery tests at different stress levels and temperatures. Figure F3c.2 shows the recoverable (VE) and permanent (VP) strain contours of transverse crossed the center of loading for different number of cycles (N) at a temperature of 40 °C.

Figure F3c.3 shows the deformation cross over the transverse under the center of loading for different temperatures. This figure shows that the deformation increases with increasing number of loading cycles, and increasing temperatures increases the deformation.

Significant Results

The analysis showed that the model is capable of describing the recovered and permanent responses of asphalt mixtures at different temperatures and stress levels.

Significant Problems, Issues and Potential Impact on Progress

None

Work Planned Next Quarter

The verification of the model will continue during the coming quarter using the Nottingham database. In addition, the analysis of the ALF database from NCSU will start in order to verify the model using this comprehensive database.

Work Element F3d: Calibration and Validation

This work element is planned to start later in the project.

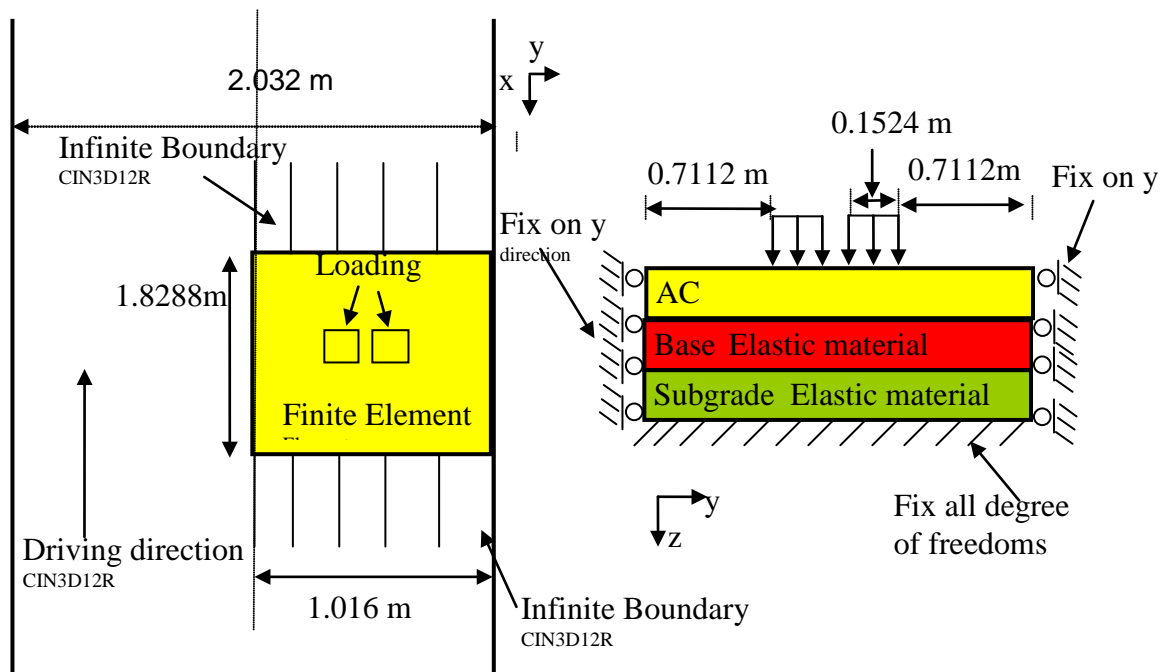


Figure F3c-1. A sketch of the pavement structure.

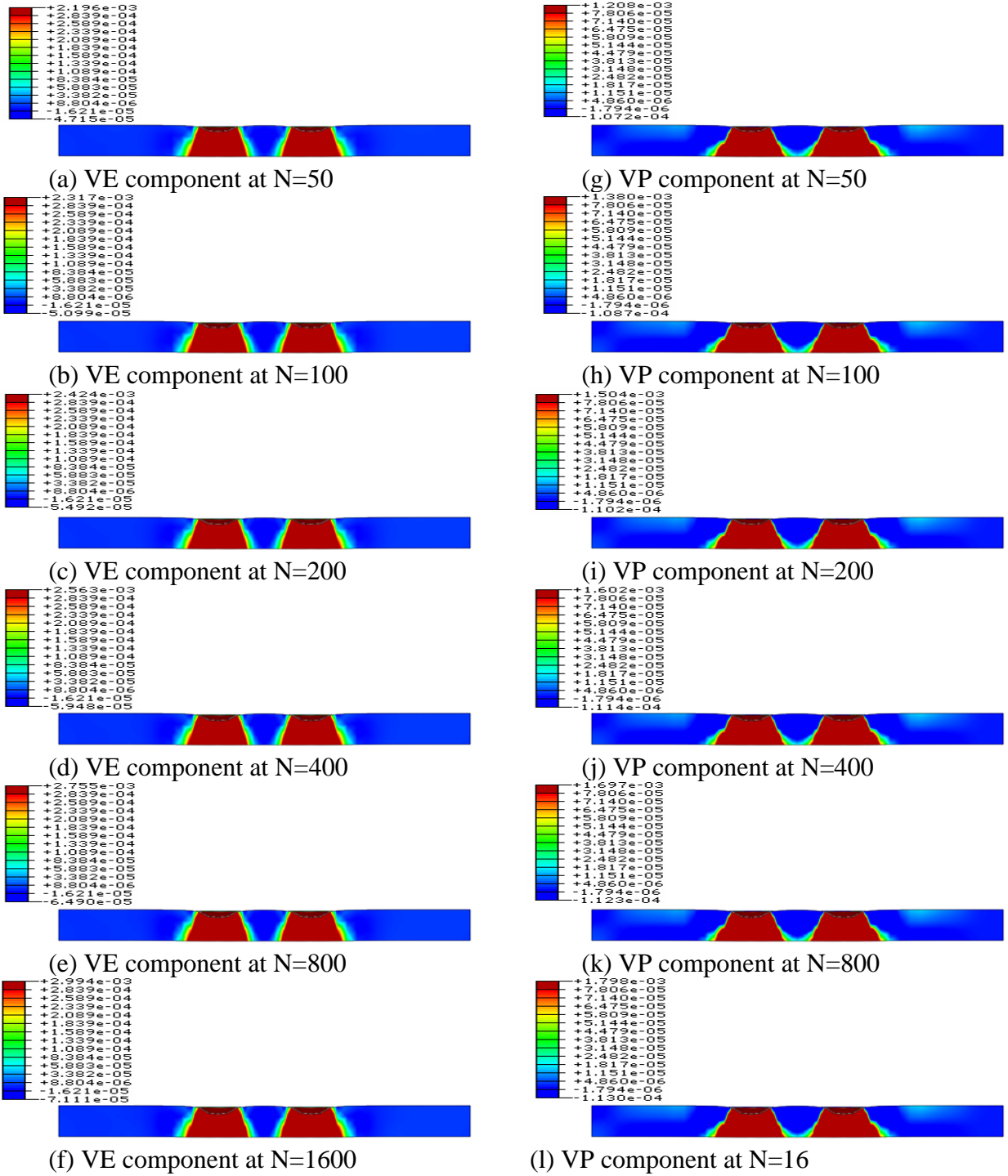
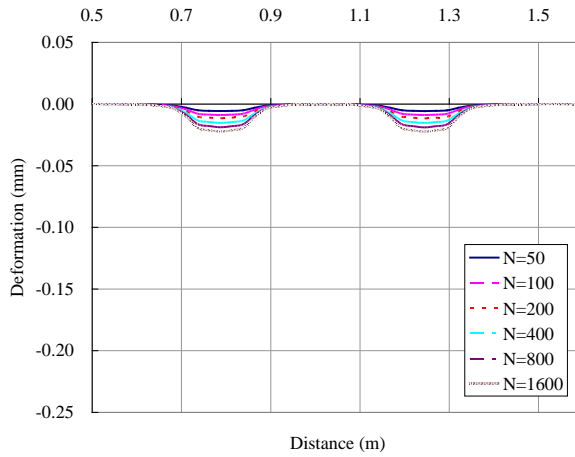
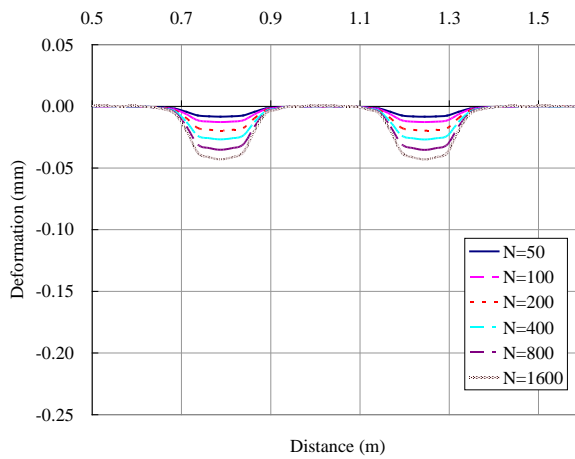


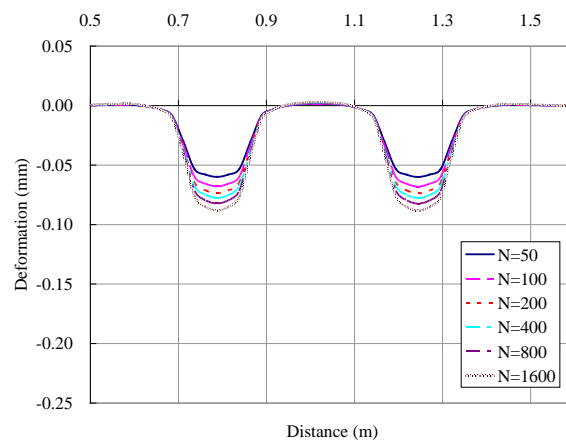
Figure F3c-2. The contours of VE component at N equal to (a) 50, (b) 100, (c) 200, (d) 400, (e) 800, and (f) 1600 and VP components at N equal to (g) 50, (h) 100, (i) 200, (j) 400, (k) 800, and (l) 1600 at temperature 40 °C.



(a) 10 °C



(b) 20 °C



(c) 40 °C

Figure F3c.3. Permanent deformation after number of loading cycles at temperatures of (a) 10, (b) 20, and (c) 40 °C.

Fatigue Year 2		Year 2 (4/08-3/09)												
		4	5	6	7	8	9	10	11	12	1	2	3	
Material Properties														
F1a Cohesive and Adhesive Properties														
F1a-1	Critical review of literature						JP(1)							
F1a-2	Develop experiment design													
F1a-3	Thermodynamic work of adhesion and cohesion													
F1a-4	Mechanical work of adhesion and cohesion													
F1a-5	Evaluate acid-base scale for surface energy calculations													
F1b Viscoelastic Properties														
F1b-1	Separation of nonlinear viscoelastic deformation from fracture energy under cyclic loading										D, JP			M&A,F
F1b-2	Separation of nonlinear viscoelastic deformation from fracture energy under monotonic loading										JP			M&A,F
F1c Aging														
F1c-1	Critical review of binder oxidative aging and its impact on mixtures													
F1c-2	Develop experiment design										D			
F1c-3	Develop transport model for binder oxidation in pavements					P						P		JP
F1c-4	Effect of binder aging on properties and performance													JP,P
F1c-5	Polymer modified asphalt materials													
F1d Healing														
F1d-1	Critical review of literature													
F1d-2	Select materials with targeted properties													
F1d-3	Develop experiment design													
F1d-4	Test methods to determine properties relevant to healing										JP			
F1d-5	Testing of materials													
F1d-6	Evaluate relationship between healing and endurance limit of asphalt binders					DP								DP
F1d-7	Coordinate with AFM analysis													
F1d-8	Coordinate form of healing parameter with micromechanics and continuum damage models													
Test Methods														
F2a Binder tests and effect of composition														
F2a-1	Analyze Existing Fatigue Data on PMA										DP			
F2a-2	Select Virgin Binders and Modifiers and Prepare Modified Binder										DP			
F2a-3	Laboratory Aging Procedures													
F2a-4	Collect Fatigue Test Data					P						JP		
F2a-5	Analyze data and propose mechanisms													P
F2b Mastic testing protocol														
F2b-1	Develop specimen preparation procedures										D			
F2b-2	Document test and analysis procedures in AASHTO format										D			
F2c Mixture testing protocol														
F2c-1	Micro scale physicochemical and morphological changes in asphalt binders													
F2d Tomography and microstructural characterization														
F2d-1	Micro scale physicochemical and morphological changes in asphalt binders													
F2e Verify relationship between DSR binder fatigue tests and mixture fatigue performance														
F2e-1	Evaluate Binder Fatigue Correlation to Mixture Fatigue Data													
F2e-2	Selection of Testing Protocols													
F2e-3	Binder and Mixture Fatigue Testing													
F2e-4	Verification of Surrogate Fatigue Test													P
F2e-5	Interpretation and Modeling of Data													
F2e-6	Recommendations for Use in Unified Fatigue Damage Model													
Models														
F3a Asphalt microstructural model														
F3b Micromechanics model														
F3b-1	Model development													JP
F3b-2	Account for material microstructure and fundamental material properties													
F3c Develop unified continuum model														
F3c-1	Analytical fatigue model for mixture design													
F3c-2	Unified continuum model													JP
F3c-3	Multi-scale modeling													

LEGEND

Deliverable codes

- D: Draft Report
- F: Final Report
- M&A: Model and algorithm
- SW: Software
- JP: Journal paper
- P: Presentation
- DP: Decision Point
- [x]

-  Work planned
-  Work completed
-  Parallel topic

Deliverable Description

- Report delivered to FHWA for 3 week review period.
- Final report delivered in compliance with FHWA publication standards
- Mathematical model and sample code
- Executable software, code and user manual
- Paper submitted to conference or journal
- Presentation for symposium, conference or other
- Time to make a decision on two parallel paths as to which is most promising to follow through
- Indicates completion of deliverable x

Fatigue Year 2 - 5		Year 2 (4/08-3/09)				Year 3 (4/09-3/10)				Year 4 (04/10-03/11)				Year 5 (04/11-03/12)			
		Q1	Q2	Q3	Q4	Q1	Q2	Q3	Q4	Q1	Q2	Q3	Q4	Q1	Q2	Q3	Q4
Material Properties																	
F1a Cohesive and Adhesive Properties																	
F1a-1	Critical review of literature			JP													
F1a-2	Develop experiment design																
F1a-3	Thermodynamic work of adhesion and cohesion																
F1a-4	Mechanical work of adhesion and cohesion					JP	D	F									
F1a-5	Evaluate acid-base scale for surface energy calculations														JP		
F1b Viscoelastic Properties																	
F1b-1	Separation of nonlinear viscoelastic deformation from fracture energy under cyclic loading			D,JP	M&A, F			JP		JP		P		JP,M&A,D		F	
F1b-2	Separation of nonlinear viscoelastic deformation from fracture energy under monotonic loading			JP	M&A, F			JP		JP		P		JP,M&A,D		F	
F1c Aging																	
F1c-1	Critical review of binder oxidative aging and its impact on mixtures																
F1c-2	Develop experiment design			D		F											
F1c-3	Develop transport model for binder oxidation in pavements		P		P, JP		P		P, JP		P		P, JP		D, M&A	F	
F1c-4	Effect of binder aging on properties and performance				JP, P		JP	D	F						JP	D	F
F1c-5	Polymer modified asphalt materials						P				P					D	F
F1d Healing																	
F1d-1	Critical review of literature																
F1d-2	Select materials with targeted properties																
F1d-3	Develop experiment design																
F1d-4	Test methods to determine properties relevant to healing				JP				JP	D	F						
F1d-5	Testing of materials							JP			JP			M&A,D	JP, F		
F1d-6	Evaluate relationship between healing and endurance limit of asphalt binders	DP			DP		DP	JP	DP		JP		P		JP	D	F
F1d-7	Coordinate with AFM analysis																
F1d-8	Coordinate form of healing parameter with micromechanics and continuum damage models											JP				JP,D	F
Test Methods																	
F2a Binder tests and effect of composition																	
F2a-1	Analyze Existing Fatigue Data on PMA			DP													
F2a-2	Select Virgin Binders and Modifiers and Prepare Modified Binder			DP													
F2a-3	Laboratory Aging Procedures																
F2a-4	Collect Fatigue Test Data		P		JP		P		P				JP, D,F				
F2a-5	Analyze data and propose mechanisms				P			P				P			P	D	F
F2b Mastic testing protocol																	
F2b-1	Develop specimen preparation procedures			D													
F2b-2	Document test and analysis procedures in AASHTO format			D													
F2c Mixture testing protocol																	
F2c-1	D, JP	F															
F2d Tomography and microstructural characterization																	
F2d-1	Micro scale physicochemical and morphological changes in asphalt binders							JP			JP	M&A,D	F				
F2e Verify relationship between DSR binder fatigue tests and mixture fatigue performance																	
F2e-1	Evaluate Binder Fatigue Correlation to Mixture Fatigue Data																
F2e-2	Selection of Testing Protocols				DP		DP, D	F									
F2e-3	Binder and Mixture Fatigue Testing																
F2e-4	Verification of Surrogate Fatigue Test				P								D	F, DP			
F2e-5	Interpretation and Modeling of Data																
F2e-6	Recommendations for Use in Unified Fatigue Damage Model															D	F
Models																	
F3a Asphalt microstructural model								JP					JP			M&A	F
F3b Micromechanics model																	
F3b-1	Model development				JP				JP				M&A	D	DP	F, SW	
F3b-2	Account for material microstructure and fundamental material properties											JP				D	F
F3c Develop unified continuum model																	
F3c-1	Analytical fatigue model for mixture design															M&A,D	F
F3c-2	Unified continuum model				JP				JP				M&A	D	DP	F, SW	
F3c-3	Multi-scale modeling											JP	M&A	D		F	

LEGEND

Deliverable codes

- D: Draft Report
- F: Final Report
- M&A: Model and algorithm
- SW: Software
- JP: Journal paper
- P: Presentation
- DP: Decision Point
- [x]

-  Work planned
-  Work completed
-  Parallel topic

Deliverable Description

- Report delivered to FHWA for 3 week review period.
- Final report delivered in compliance with FHWA publication standards
- Mathematical model and sample code
- Executable software, code and user manual
- Paper submitted to conference or journal
- Presentation for symposium, conference or other
- Time to make a decision on two parallel paths as to which is most promising to follow through
- Indicates completion of deliverable x

PROGRAM AREA: ENGINEERED MATERIALS

CATEGORY E1: MODELING

Work element E1a: Analytical and Micro-mechanics Models for Mechanical Behavior of Mixtures (TAMU)

Work Done This Quarter

The technical paper on viscoelastic characterization test protocol (Luo and Lytton, 2008) was presented in the Transportation Research Board (TRB) AFK50(1) Subcommittee Meeting in the 88th TRB Annual Meeting in Washington, D.C., January 2009. Another presentation entitled “Determine Properties of Asphalt Mixtures Using Experimental and Analytical Methods” was made in the FHWA ETG meeting in Irvine, California, February 2009. The presentation made in the FHWA ETG meeting summarized the test protocols developed to characterize the properties of asphalt mixtures in undamaged and damaged states, as well as the progress on the inverse and forward self-consistent micromechanics models.

The test protocol on compressive properties of asphalt mixtures was further developed to characterize the anisotropic viscoelastic properties of undamaged asphalt mixtures under compressive loading. This development has been detailed in Work Element F2c.

The tensile and compressive properties determined using the developed test protocols were taken as input parameters for the inverse and forward self-consistent micromechanics models that were developed and programmed in the previous quarters. The results from the inverse micromechanics model showed that the aggregates exhibited viscoelastic properties instead of elastic, as was reported in the previous quarterly reports. In order to verify the calculation of the micromechanics models, a number of rocks were collected from the same quarry, which was located in San Marcos, Texas, of the aggregates used to make the asphalt mixture specimens. The type of aggregate was Texas limestone. The collected rocks were placed in plastic containers individually with cast cement, as shown in figure E1a.1. After the cement set, each rock was cored into a cylindrical specimen. The diameter of each specimen was approximately 45 mm, and the height of specimens varies with the size of the raw rocks. A height of 67.5 mm (1.5 times of the diameter) was desired in order to reduce the end effect during the compression test conducted on the specimens. Figure E1a.2 illustrates the cylindrical rock specimens; Part (b) of this figure shows a specimen glued with brackets in order to install Linear Variable Differential Transformers (LVDTs).

In order to verify the viscoelastic properties of aggregates, a creep test was conducted on one of the cylindrical rock specimens. As shown in figure E1a.3, the rock specimen was set up in the environmental chamber of the Material Test System (MTS). Three LVDTs were mounted on the brackets glued to the surface of the specimen. A constant load of 9 kN was applied to the specimen for 7,200 seconds (2 hours). The vertical deformation of the specimen was recorded by the three axial LVDTs so the axial strain was determined as a function of time. Calculation results showed that the axial strain rarely changed with time during the 2 hour loading period. In

other words, the rock specimen did not show appreciate viscoelastic properties in the loading duration.



Figure E1a.1. Configuration of coring a cylindrical rock specimen.

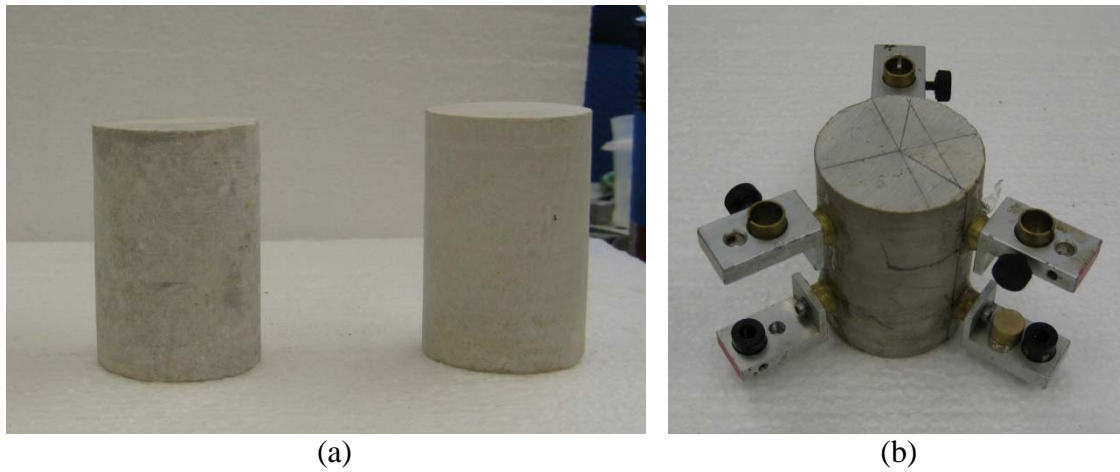


Figure E1a.2. Cylindrical rock specimens.

Despite the fact that the pure rock specimen did not exhibit appreciate viscoelastic properties, the absorption of asphalt binders may make the aggregates viscoelastic. It was found in the previous quarters that the porous aggregates and fines selectively absorbed certain asphalt components. Consequently, it is desired to test the rock specimens with absorbed asphalt components. Before this testing, a pure rock specimen was dried for 24 hours to eliminate possible water inside the specimen. Then the specimen was weighed and soaked in a binder for 32 hours at the mixing temperature used to mix asphalt mixtures. This soaking time was determined based on size of the specimen and the mixing and shipping time at a hot mix asphalt plant. After 32 hour-soaking, the

specimen was cut into two pieces through the middle plane. It is clear in figure E1a.4 that asphalt components have diffused into the middle of the rock specimen.



Figure E1a.3. Configuration of creep test on rock specimen.



Figure E1a.4. Cross section of rock specimen after soaking in asphalt for 32 hours.

References

Luo, R., and Lytton, R. L. (2008). "Characterization of the Tensile Viscoelastic Properties of an Undamaged Asphalt Mixture." Submitted to *Journal of Transportation Engineering*, American Society of Civil Engineers, under review.

Significant Results

Presentations on test protocols characterizing asphalt mixture properties and self-consistent micromechanics models were made in the 88th TRB Annual Meeting and the FHWA ETG meeting.

Texas limestone rocks were collected from the same quarry of aggregates used to make asphalt mixtures in order to check the mechanical properties of rocks. Pure limestone rock did not show appreciable viscoelastic properties. However, it was proved that limestone rocks absorbed asphalt components, which may increase the viscoelasticity of rocks.

Significant Problems, Issues and Potential Impact on Progress

Contradictory to what was expected, the limestone rock did not show appreciate viscoelastic properties during the 2 hour loading time. Possible reasons include: i) load time was too short to reveal the viscoelastic properties; and ii) the LVDTs used in the test did not have high enough resolution to capture the axial deformation of the specimen. However, the rock specimen soaked with asphalt binder is expected to have increased viscoelasticity, which is to be determined in the next quarter.

Work Planned Next Quarter

A number of rock specimens are to be soaked in different asphalt binders for different periods of time. The creep test will be conducted on the specimens with absorbed asphalt components in order to determine the viscoelastic properties of the specimens. After the creep test, the specimen will be cut into halves and the cross sections will be photographed to visually observe the diffusion of asphalt components under natural light and ultraviolet light. In addition, the ablative laser mass spectroscopy will be employed to determine the chromatogram of the asphalt components diffusing into the cross section. The chromatogram will quantify the asphalt components diffusing into the rock specimen.

Work element E1b: Binder Damage Resistance Characterization (DRC) (UWM)

Subtask E1b-1: Rutting of Asphalt Binders

Work Done This Quarter

In the previous quarter, material selection and work plan development were finalized on time. The final work plan includes three separate testing plans for binders, mastics, and mixtures. Laboratory testing this quarter continued following these plans.

The binder and mastic testing included frequency sweep, Repeated Creep and Recovery (RCR) and Multiple Stress Creep and Recovery (MSCR) using the Dynamic Shear Rheometer (DSR). Binder testing progressed with 30% completion of the testing schedule. For mastic testing, it was observed that the testing geometry has an effect on the results that were obtained. Therefore, further investigation on the effect of testing with parallel-plate versus cone-and-plate geometries is being conducted. A complete evaluation of the plate geometry is expected to be conducted in the next quarter.

For the preparation of mixture testing, available aggregate and gradation were identified. The mixtures will be prepared with controlling the percent finer than 75 microns. Therefore, changes in sieve analysis of aggregate masses using pre- and post-washing of fines were determined. This determination was used as a decision point on how mixture preparation should proceed in order to compare mixture, mastic and binder performance.

Significant Results

The asphalt binder testing plan has been prioritized to allow for selection of two binders to be carried into both mastic and mixture testing to complete a full set of tests. These will be used to identify any potential issues and address them appropriately before proceeding to the entire testing matrix. This prioritization has led researchers to focus on binders modified to achieve similar non-recoverable creep compliance (J_{nr}) but differing elastic properties.

For preparation of mastics, the asphalts selected will be mixed with fillers of pulverized limestone, pulverized granite and hydrated lime at a dust-to-binder ratio (DTBR) of 1:1. The 1:1 ratio was chosen for consistency between asphalt mastic testing and asphalt mixture testing, and is not expected to have a significant effect on mix design.

Asphalt binder testing

According to the testing work plan, nine binders were selected for investigation. Testing is completed for three of these binders. A sample of the results obtained is discussed below.

In analyzing the responses of the different binders to the RCR test, J_{nr} was measured. Since the RCR test is conducted for 300 cycles, it is important to investigate the dependency of the calculated J_{nr} on the number of loading cycles. Figure E1b-1.1 shows the values of the J_{nr} at 58 °C for two unmodified binder from two different sources, but with the same performance grade of PG 64. The figure shows the average J_{nr} for the first 10 cycles and the last 10 cycle of

the test. Testing was conducted at multiple stress levels ranging from 0.1 kPa to 30 kPa. The 30 kPa was included because FHWA reported at the Binder ETG meeting in September 2008 that the best correlation with the Accelerated Load Facility performance was found at a stress level of 25.8 kPa.

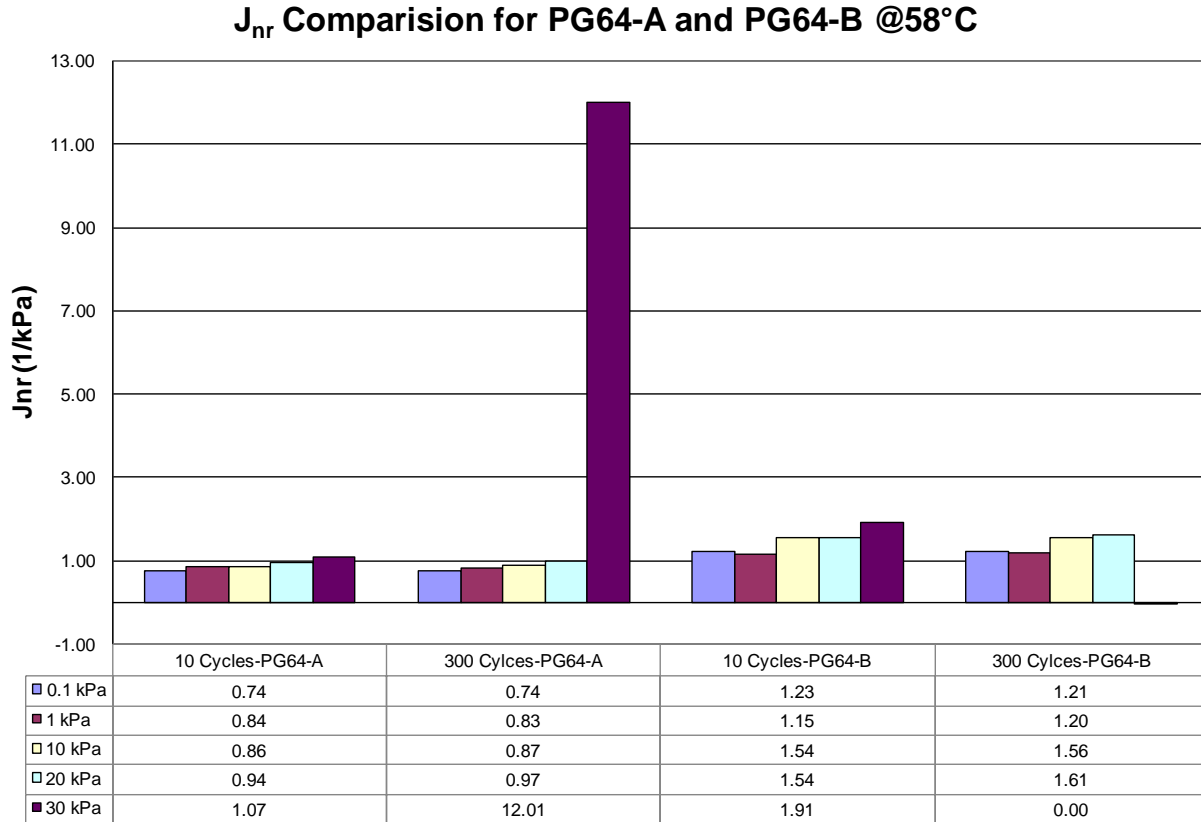


Figure E1b-1.1. Graph. Values of the J_{nr} for unmodified binders of PG 64 at different stresses and numbers of cycles.

As shown in figure E1b-1.1, the average J_{nr} for the first 10 cycles shows minimal increase with the increase in stress level, with a few exceptions at 30 kPa. For the last 10 cycles of the total 300 cycles of testing, the average J_{nr} at 30kPa increased by a large multiplier, and in some cases the sample exhibited unrealistically high J_{nr} values and tertiary-like behavior. Note in figure E1b-1.1, the value of the J_{nr} for the PG 64-B is not listed. This indicates that the samples tested at 300 cycles at 30 kPa reached total failure, resulting in a large value for J_{nr}.

For sensitivity of the testing to changes the temperature, figure E1b-1.2 shows the average J_{nr} for the first 10 cycles and the last 10 cycles when testing at 58°C and 76°C for an styrene-butadiene-styrene (SBS)-modified binder of performance grade PG 76.

J_{nr} for SBS Modified PG76 at 58°C and 76°C

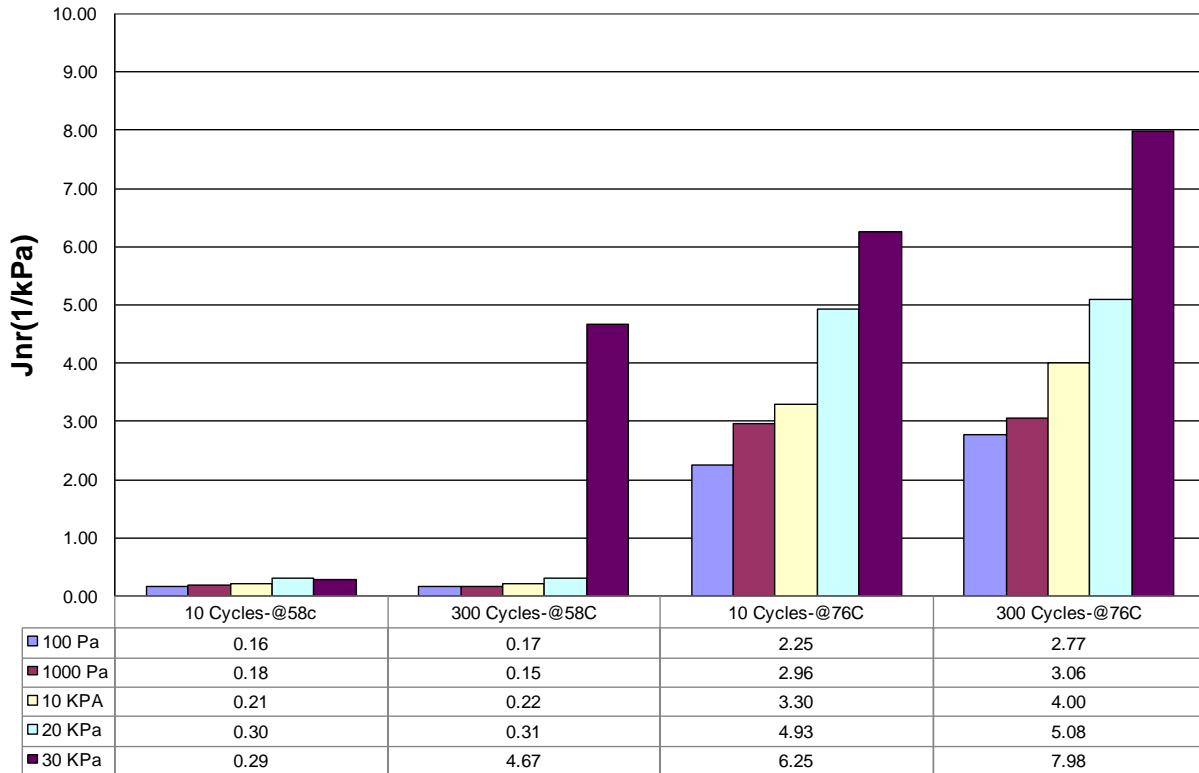


Figure E1b-1.2. Graph. Values of the J_{nr} for SBS-modified binder at 58 °C and 64 °C at different stresses and numbers of cycles.

As shown in figure E1b-1.2, the sensitivity of the SBS modified binder to stress is minimal after 10 cycles of loading at 58 °C. The same trend is still observed after 300 cycles of loading, except when testing at 30 kPa. At 30 kPa the value of the J_{nr} changes from 0.29 kPa^{-1} after 10 cycles to 4.67 kPa^{-1} after 300 cycles. This is an indication of the possibility of the presence of tertiary flow in the specimen at this level of stress and number of cycles. When testing at the high performance grade temperature, the value of the J_{nr} gradually increases as expected. On the other hand, the dependency of the J_{nr} value on the cycle number at the highest stress level is less evident. For example, the maximum change in the J_{nr} value is observed at 27.7%, while at the same stress level at 58 °C, it is about 1500%. Further analysis will take place in the next quarter to quantify such dramatic increase in the J_{nr} at higher stress level to establish the possibility of quantifying tertiary flow behavior.

Regarding the frequency sweep testing, the test was conducted at 58 °C for a frequency range from 0.01 Hz to 100 Hz. As the frequency varied the $G^*/\sin(\delta)$ was measured. Figure E1b.1-3 show the results of the three binders discussed above: two unmodified PG 64 binders and an SBS-modified PG 76 binder.

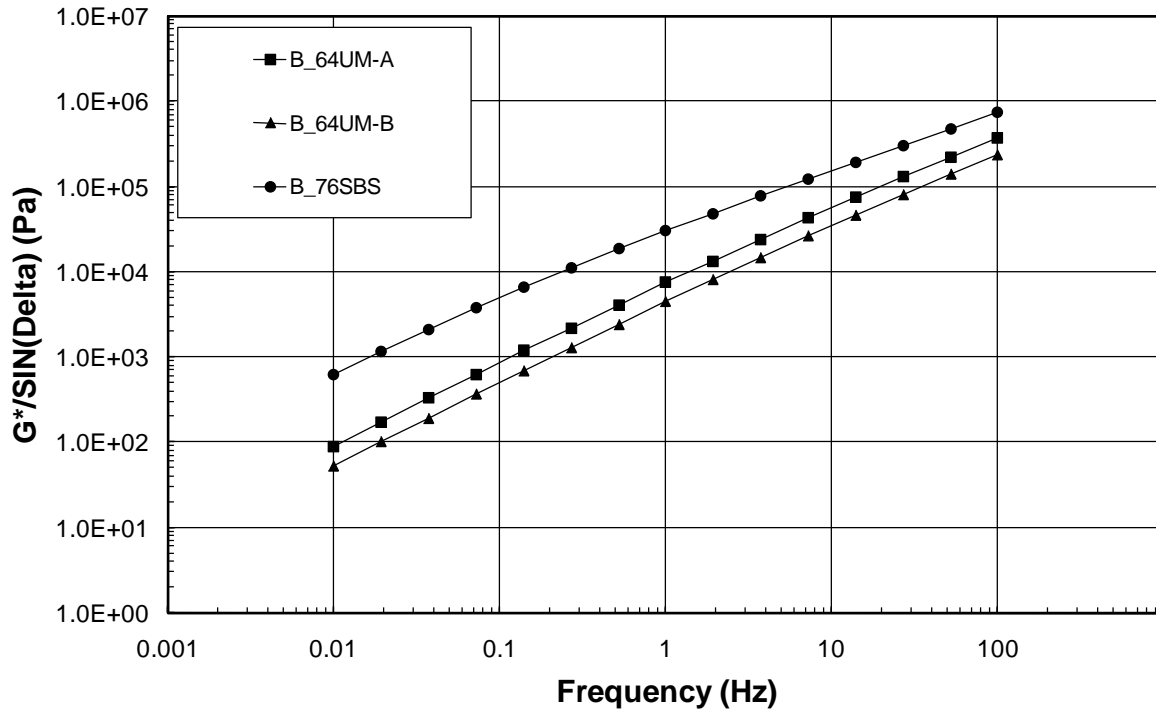


Figure E1b-1.3. Graph. $G^*/\sin(\delta)$ frequency sweep test results for three tested binders.

As shown in figure E1b-1.3, the unmodified binders demonstrate very close values of $G^*/\sin(\delta)$. On the other hand, the SBS-modified PG 76 binder shows higher values of $G^*/\sin(\delta)$ at lower frequencies, approximately one order of magnitude higher than the unmodified binders. As the frequency increases the difference in the $G^*/\sin(\delta)$ decreases, but the higher values for PG 76 are maintained.

Testing of geometry effects was also carried out this quarter. Several binder and mastics were tested using the parallel-plate and the cone-and-plate, and the results were compared. There were significant difficulties in getting reliable data using the cone-and-plate geometry, and in many instances the frequency sweep data showed unrealistic values of phase angle and frequency dependency, particularly at lower frequencies and low stress levels. The need to understand stress sensitivity at various loading rates drove the researchers' interest in frequency sweep testing. This issue is critical because the stress sensitivity could be well related to the accumulated strain rather than the conventional nonlinearity due to stress level. The interest in geometry, on the other hand, was driven by the need to find out if the cone-and-plate is appropriate for mastic testing. It is speculated that due to the smaller gap at the cone tip, testing artifacts interfere with the measurements and that cone-plate should therefore not be used. More will be reported next quarter on these issues.

Mixture testing

In preparation for mixture testing, the mineral aggregate of crushed granite was selected for the preliminary set of mixture testing that will be used to identify any potential issues. The granite source will be used to prepare coarse and fine blends to investigate the gradation effect on

mixture performance. These gradations were prepared to meet specifications for 10 million equivalent single axle loads (ESALs). The mixtures will be prepared with replacing the percent finer than 75 microns with two selected fillers: limestone and granite.

To incorporate the selected mineral fillers in the mix, the need for washing the aggregate was studied. In washing of aggregate samples, two samples of granite were batched according to previous mix design without the P₂₀₀ material and washed according to ASTM C 117-04 to determine if additional loss of fines contributed to mineral dust adhering to larger particles. The total additional loss was approximately 35% fines compared to the value called for in the original mix design. This additional loss was determined to be significant enough to require washing of all aggregate to be used in mixture testing.

Significant Problems, Issues and Potential Impact on Progress

No significant problems have been encountered in the binder testing portion of this subtask. With regard to the mastic testing, the initial results have not matched with expectations based on binder test results, particularly at low stress levels. Mastic behavior appears to be sensitive to DSR plate geometry. Further investigation is being conducted, and updates on the outcomes will be covered in the next quarterly report.

Work Planned Next Quarter

Activities for the next quarter are summarized below:

- Testing of binders will continue according to the test plan.
- Evaluation of the effect of the DSR plate geometry on the mastic testing results will be completed.
- Two binders of similar non-recoverable compliance and different elasticity will be selected and used for mastic and mixture preparation. This is to evaluate the non-recoverable compliance measurements and the percent recovery. This will also serve to confirm the relevance of using the non-recoverable compliance and the percent recovery as indicators of binder quality.
- Data analysis and interpretation of the results will continue.

Subtask E1b-2: Feasibility of Determining Rheological and Fracture Properties of Thin Films of Asphalt Binders and Mastics using Simple Indentation Tests (Year 2 start)

Work Done This Quarter

As described in the Year 3 work plan, the research team refocused this task on the laboratory evaluation of binder viscoelasticity using small-scale indenters (up to 8.5 mm) to measure response at various temperatures. The team began review of the theory behind the use of hemispherical indenters for standard penetration devices. The identification of relevant literature sources will lay the ground for a well-informed experimental plan.

Preliminary testing of binders and mastics was set up using a resilience test with a ball penetration tool (ASTM Standard 5329). The research team determined that the standard ball is too heavy for binder and mastic testing at the high temperature (60°C). A lighter, hemispherical shape was machined, and testing has begun to determine the feasibility of the test and ultimately the relationship to complex shear modulus (G^*) values. The results and the initial literature review are expected to support the new work plan for this task.

Significant Results

The research team compiled a list of 24 sources (publications and textbooks) that will be used to produce a detailed literature review report. The literature search is expected to provide guidance on modeling the results obtained from the indentation testing device to predict fundamental asphalt mechanical properties. The literature ranged from publications authored in 1960 to very recent ones published in 2008. Reviewing publications from this wide of range dates is expected to help map the developments of the theoretical background of rigid ball indentation in viscoelastic materials.

In the meantime, initial testing was conducted on modified and unmodified binder at 25 °C and 60°C with an indenter mass of 70 g. The setup of the test followed that of a regular penetration device. However the penetration needle was replaced by a ball indenter based on ASTM 5329. The schematic in figure E1b-2.1 shows the recommended dimensions included in the ASTM standard.

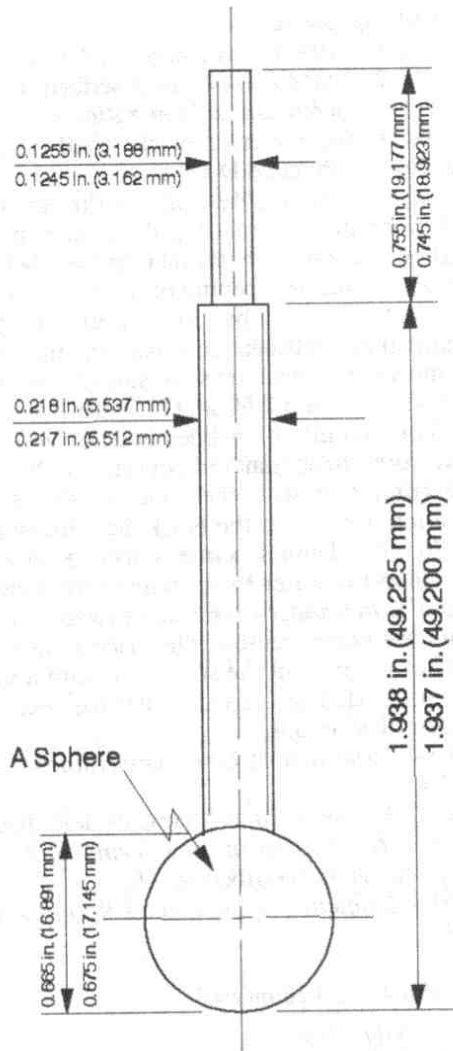


Figure E1b-2.1. Illustration. Schematic of the ball indenter per ASTM 5329.

Attempts to run the test at 60 °C were unsuccessful because the indenter sank rapidly into the asphalt without allowing enough time to record displacement. However, at 25°C displacement occurred at a slow enough rate to allow for recording of data. Figure E1b-2.2 shows the results of testing two modified binder of performance grade PG 70. Binder A was modified with linear styrene-butadiene-styrene (LSBS) polymer and Binder B was modified with Elvaloy. The displacement of the indenter was measured with time until it reached the maximum displacement of 8.5 mm, which is equal to the radius of the sphere. It is important to note that the test was conducted with the sphere lubricated with a mixture of talc powder and glycerin to eliminate the friction between the ball and the specimen surface.

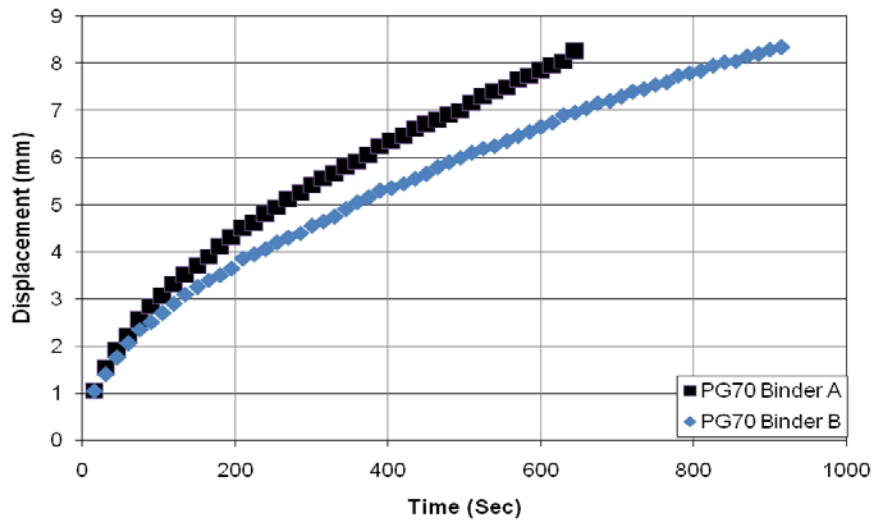


Figure E1b-2.2. Graph. Comparison of indentation results for two PG 70 binders at 25 °C.

As shown in figure E1b-2.2, this procedure can distinguish between different binders by the differing times required to reach the maximum displacement. In tests of an unmodified binder of PG 58, the indenter reached the maximum displacement of 8.5 mm very rapidly, which allowed for fewer data points (15 seconds per recorded data point over 75 seconds). Therefore, modifications have been made to the testing setup to control the indenter's weight.

The modification to the indenter was achieved by decreasing material mass while maintaining the required geometry. The mass of the indenter assembly was reduced from 70 grams for the original assembly to 25 grams for the new assembly. In addition, the new assembly allows the addition of dead weights in increments of 5 grams to bring the assembly to a maximum of 225 grams. This allows for adjusting the indenter's weight to accommodate testing at a range of temperatures. Figure E1b-2.3 shows the indentation assembly. A comparison of the standard indenter and the modified indenter is shown in figure E1b-2.4.



Figure E1b-2.3. Photograph. The indentation assembly showing the ball and the micrometer gauge.



Figure E1b-2.4. Photograph. The standard indenter and the modified indenter.

The modified indenter is made with a half sphere to minimize the mass. There is no need for a full sphere, since the displacement is only measured up to a maximum depth equal to the radius of the half sphere.

Based on the initial preliminary literature search, the creep compliance of the specimens can be calculated using the following equation (Lee and Radok 1960):

$$J(t) = \frac{16\sqrt{R}[\alpha(t)]^{3/2}}{3p}$$

Where

$J(t)$ is creep compliance at time t ,
 R is the radius of the sphere or half sphere,
 $\alpha(t)$ is displacement at time t , and
 p is the indentation force.

This model assumes the following points:

- The material of the sample is an incompressible viscoelastic one.
- The rigidity on the ball is magnitudes higher than that of the sample.
- There is no friction between the ball and the sample.
- The displacement does not exceed the radius of the ball.

For the modified binders discussed in figure E1b-2.2, the creep compliance is shown in figure E1b-2.5

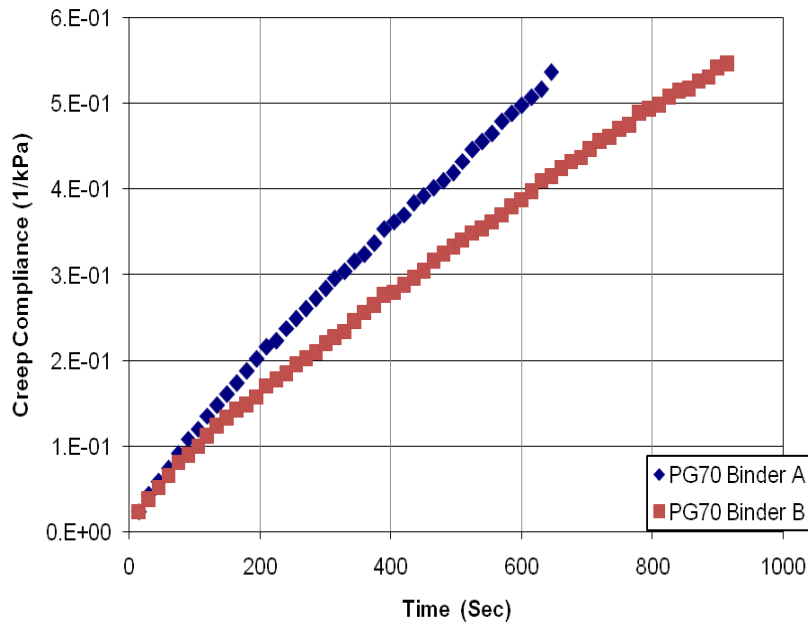


Figure E1b-2.5. Graph. Calculated creep compliance of PG 70 modified binders.

Figure E1b-2.5 shows that this device can distinguish between two binders although they have the same PG grade. This indicates the potential of using this testing setup to estimate the creep compliance of different binders.

Significant Problems, Issues and Potential Impact on Progress

None.

Work Planned Next Quarter

Next quarter, the following tasks will be conducted:

- The literature review and the testing plan for this research will be finalized.
- Testing of a range of binders and mastics will be conducted using the indentation device to calculate the creep compliance. The following variables will be included:
 1. Binder type
 2. Mastic filler type
 3. Temperature
 4. Indenter weight
- Analytical modeling will begin for deriving the complex shear modulus from the indentation test. The results will be compared to the measured Dynamic Shear Rheometer values for validation.

Cited References

Lee, E. H., and J. R. M. Radok, 1960, The Contact Problem for Viscoelastic Bodies. *Journal of Applied Mechanics*, 27: 438-444.

Work Element E1c: Warm and Cold Mixes

Subtask E1c-1: Warm Mixtures

Work Done This Quarter

Work focused on measuring the effects of warm mix asphalt (WMA) additives on asphalt binder rheological properties and mixture workability. Activities involved inclusion of a surfactant-based WMA additive and a coarse-graded mix design into the testing matrix. Testing has been completed of the new additive and results have been compared to other additives. Some efforts were directed toward a literature review on tribology (the study of lubrication) to investigate new test methods to measure lubrication effects of WMA additives on the asphalt binder's contribution to mixture workability. Work in this research study and others has shown that WMA additives have little effect on viscosity, particularly in the case of mineral-based and surfactant additives. Based on this review, the research team decided to modify the testing apparatus used for standard ASTM D5183-05, which is now used in the oil industry to measure lubrication properties with a four-ball fixture, so that the test can be conducted with the Dynamic Shear Rheometer (DSR).

A substantial effort was also put into synthesizing all research results collected to date in an interim report. The report includes the experimental results related to the effects of WMA additives on binder properties and mixture workability, and also a literature review on tribology. The interim report is currently under review and will be submitted next quarter.

Presentations

Dr. Elie Hajj of the University of Nevada, Reno (UNR) gave a presentation updating progress on this task to the FHWA Mixtures ETG on February 27.

Dr. Hussain Bahia of the University of Wisconsin–Madison and Dr. Hajj of UNR gave a similar presentation to the Manitoba Infrastructure and Transportation Department. The purpose of this presentation was to generate discussion regarding collaboration on a WMA field project. Based on these discussions, it was decided that the ARC will conduct similar experiments on the materials planned for use in the Manitoba project.

Significant Results

Effect of WMA additives on binder rheological properties

The effects of wax- and surfactant-based additives on high-, intermediate- and low-temperature binder properties were investigated for a PG 64-22 neat and PG 76-22 polymer-modified binder. Results show that for the PG 64-22 base binder, the addition of Sasobit results in a bump of one PG grade, while the surfactant does not change the grade of the binder. Conversely, results for the PG 76-22 base binder show that the addition of the surfactant reduces the high temperature PG grade, and the addition of Sasobit has no significant effect on the grade. High-temperature effects were further investigated using the non-recoverable creep compliance (J_{nr}) and stress sensitivity parameters defined in ASTM D7405, “Standard Test Method for Multiple Stress Creep and Recovery (MSCR) of Asphalt Binder Using a Dynamic Shear Rheometer.” Results are presented in figure E1c-1.1. Tests were conducted at 64 °C for the binders made with the PG-64 grade and at 76 °C for the binders made with the PG-76 grade.

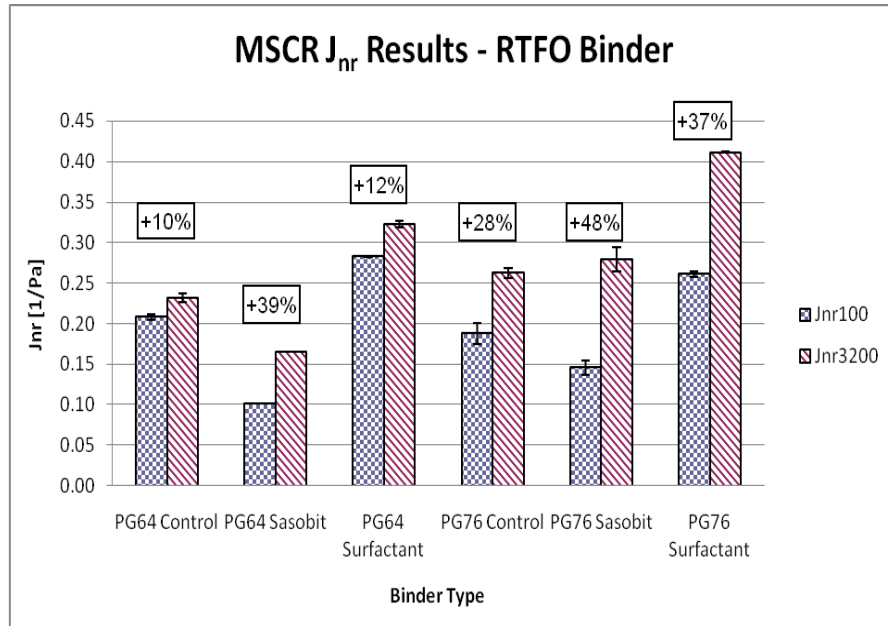


Figure E1c-1.1. Graph. Non-recoverable compliance (J_{nr}) results from MSCR testing, with percent J_{nr} increase from 100 Pa loading to 3200 Pa loading.

The results indicate that the Sasobit improves the properties related to the MSCR by decreasing the J_{nr} while the surfactant causes a non-favorable increase in the J_{nr} value. Stress sensitivity was also evaluated using the percent difference between the 100 Pa and 3200 Pa stress levels, shown in figure E1c-1.1 as a percent increase relative to the 100 Pa value. For both binders, there appears to be a significant increase in the stress sensitivity compared to the original binders. Work currently being performed by FHWA suggests a J_{nr} less than 0.4 (%/Pa) or 4.0 kPa⁻¹, as a possible specification limit at the climatic grade. It is expected that all the binders shown in figure E1c-1.1 will meet this requirement if tested at 64 °C for the PG 64 base binder, and if tested at 70 °C for the PG 76 binders. There is a trend, however, that the additives increase stress sensitivity and that the surfactant actually increases the J_{nr} value.

Evaluation of resistance to fatigue was conducted using the Superpave parameter of G**sin*(δ). The values of this parameter were similar for the base and Sasobit-modified binders for both binder grades; however, the surfactant showed significantly lower values of the parameter (more than 45%). In subsequent quarters, more advanced methods of binder fatigue characterization and mixture testing will be used to verify these differences and quantify their impact on the mix.

The effect of WMA on the binder low-temperature properties was investigated using the Bending Beam Rheometer (BBR) parameters for stiffness (S(60)) and m-value (m(60)). Results presented in figure E1c-1.2 show that the addition of Sasobit causes some increases in stiffness and also reductions in m-value. However, these changes in low-temperature properties did not adversely affect the low-temperature PG grade of any of the WMA-modified binders. The results for the surfactant, on the other hand, show a reduction in stiffness and a substantial increase in the m-value. The effects of Sasobit on physical hardening was also investigated by placing BBR specimens in the bath at -12 °C and testing after curing times of 1, 5 and 24 hours. Results to

date show no significant increase in stiffness or m-value over time, so it cannot be confirmed that use of Sasobit causes additional physical hardening in binders at low temperatures. The data collected to date are limited in types of binders and more testing is needed before final conclusions can be drawn.

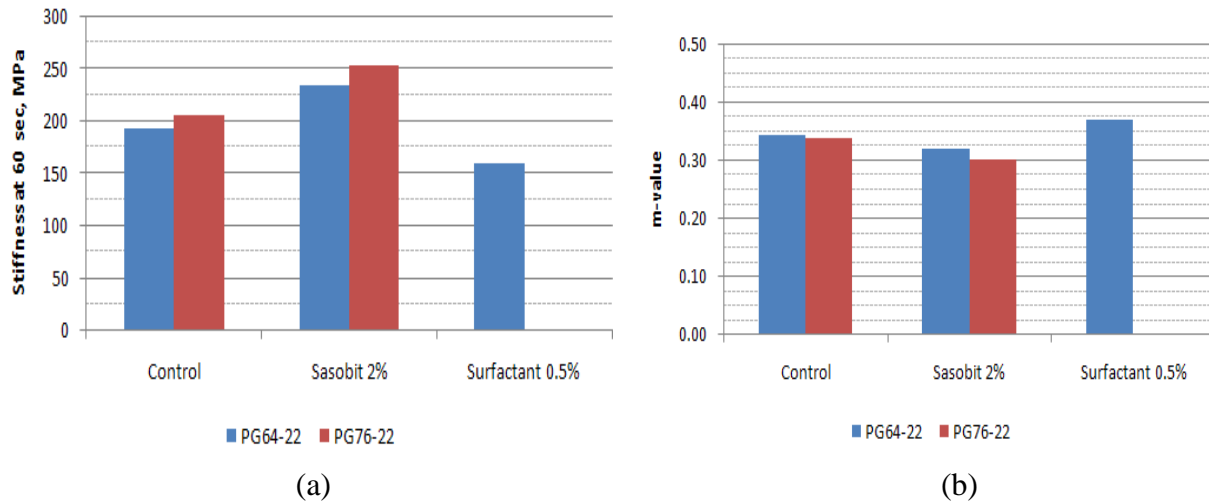


Figure E1c-1.2. Graphs. Effect of WMA additives at -12 °C on low-temperature properties (a) S(60) and (b) m(60).

Effect of WMA additives on mixture workability

Work focused on completion of the test matrix developed for a fine-graded, granite mix design (E-10) using the neat and polymer-modified binders. The experimental matrix is shown in table E1c-1.1. Two main evaluation parameters were used:

- Percent air voids at Superpave gyration levels (N_{ini} , N_{des} , N_{max}).
- Construction Force Index (CFI). The pressure distribution analyzer (PDA) plate measures the resistive force during compaction from 88% G_{mm} to 92% G_{mm} .

Table E1c-1.1. Summary of experimental factors for testing completed to date.

Variable	Values	Levels
Compaction Temperature (°C)	90	3
	110	
	135	
Compaction Pressure	600	2
	300	
Binder Grade	PG 64-22	2
	PG 76-22	
Additive Type	Control	3
	Advera	
	Revix	
Aggregate Type	Granite	1
NMAS	19.5	1
Gradation	Fine	1
	Two Replicates	2
	Total Mixes	72

The summary of air voids over the compaction temperatures specified in table E1c-1 for the mix prepared with the PG 76-22 binder and compacted at 600 kPa is shown in figure E1c-1.3.

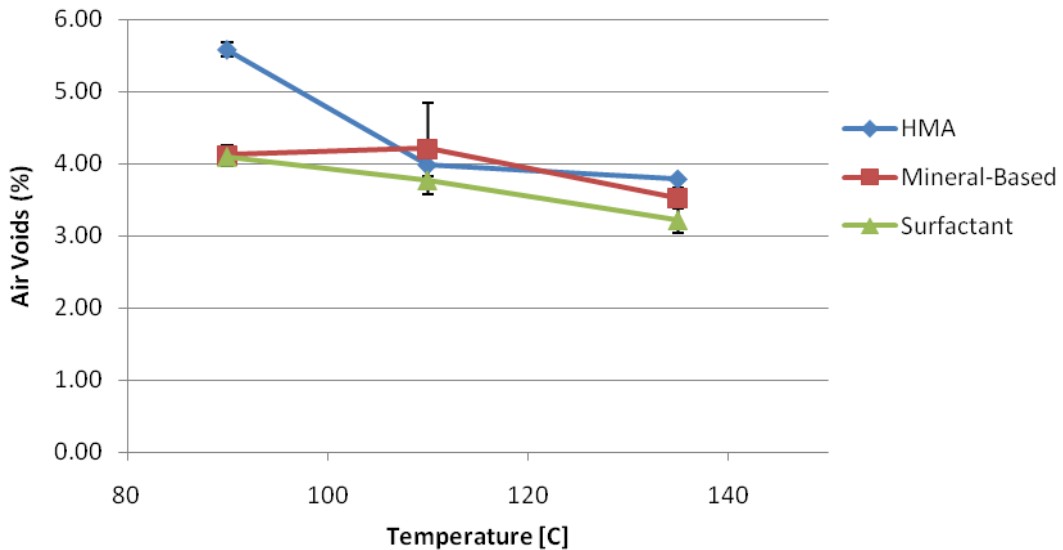


Figure E1c-1.3. Graph. Comparison of air voids at N_{des} (100) versus compaction temperatures for PG 76 binder.

Results shown in figure E1c-1.3 indicate that above the 90 °C compaction temperature, there is little difference in air voids between the control mix (HMA) and those prepared with warm mix additives (mineral-based and surfactant). At 90 °C, however, the WMA mixes show significant improvement in workability, with both WMA mixes exhibiting air void levels approximately 1.5% lower than the HMA. This trend was also verified with data collected from the PDA during specimen compactions, as shown in figure E1c-1.4.

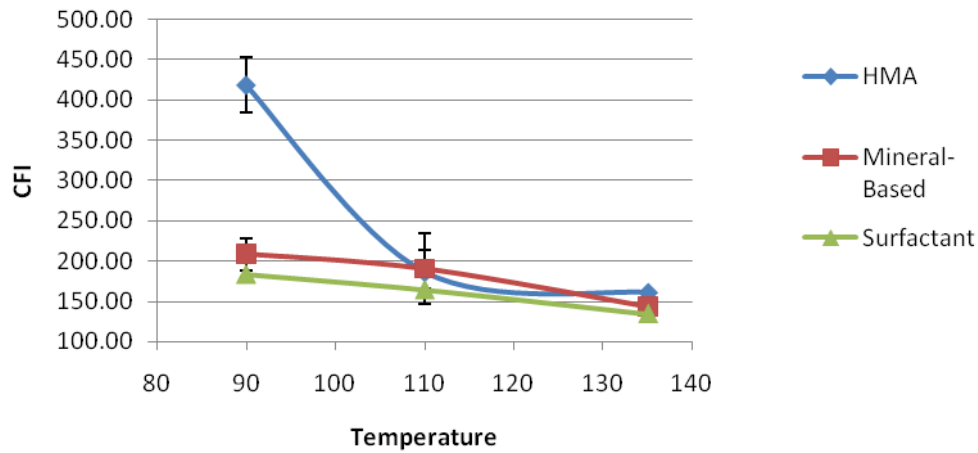


Figure E1c-1.4. Graph. Comparison of CFI data for PG 76 mixtures compacted at 600 kPa.

Similar trends were observed for mixes prepared with the PG 64-22 binder and compacted at 600 kPa. More detailed results will be available in the interim report.

The samples compacted at 300 kPa did not show the same trends, as the difference in air voids was not clear even at 90 °C. Figures E1c-1.5 and E1c-1.6 show the differences in air voids between the WMA and HMA at all compaction temperatures.

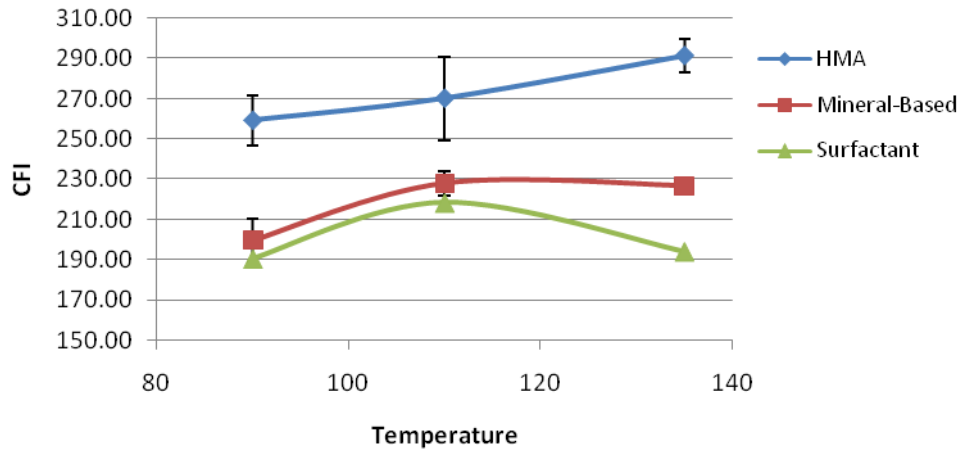


Figure E1c-1.5. Graph. Comparison of air voids at N_{des} (100) versus compaction temperatures for PG 64 binder at 300 kPa pressure.

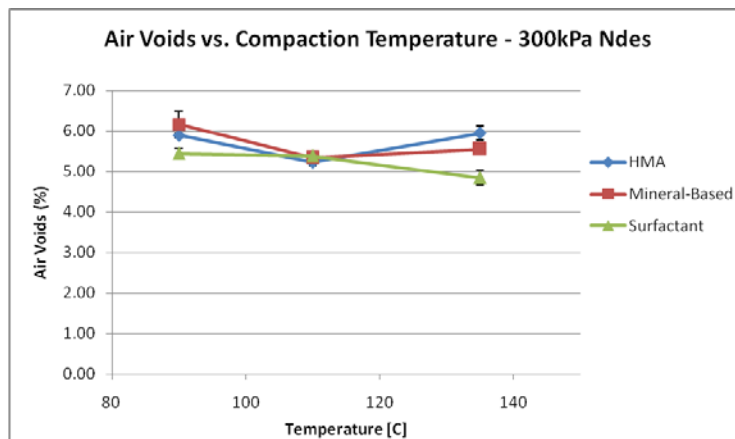


Figure E1c-1.6. Graph. Comparison of air voids at N_{des} (100) versus compaction temperatures for PG 76 binder at 300 kPa pressure.

There appeared, however, to be a slight but consistent decrease in air voids for the mixes with PG 64 binder. To further investigate this, the CFI data were analyzed as shown in figure E1c-1.7. The CFI parameter results for the PG 64-22 binder show somewhat enhanced workability (lower CFI values) for WMA mixes. The difference is approximately 15% of the HMA CFI values within the shown temperature range. It is not clear yet whether or not this difference has a significant practical impact. More data will be collected to explore the significance of this difference.

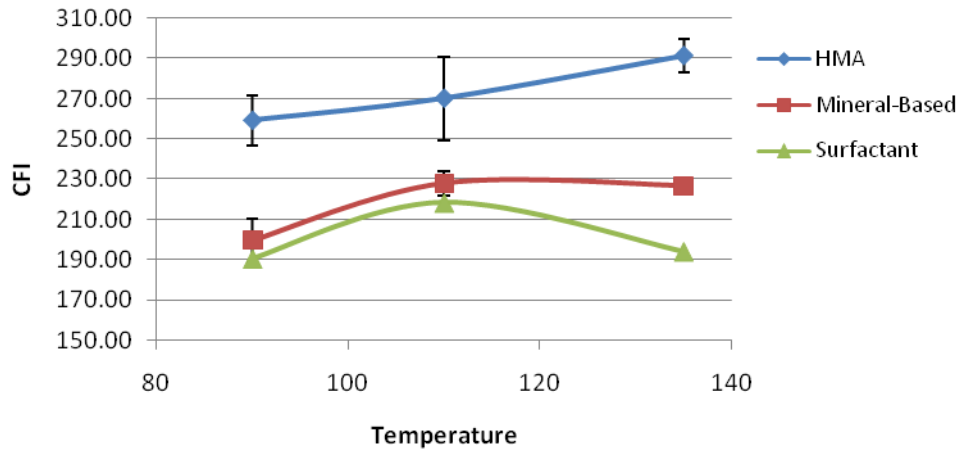


Figure E1c-1.7. Graph. Comparison of CFI data for PG 64 mixtures compacted at 300 kPa.

In addition to the testing of the fine-graded mixtures, a coarse-graded mix design was prepared to investigate the effects of gradation on the threshold at which the benefit from warm mix additives is realized. As a frame of reference, the mix design used in the previously presented data had approximately 65% of the aggregate gradation passing the No. 4 sieve. The coarse mix design has 45% passing the No. 4 sieve. To date, mixes have been tested across all temperatures and compaction temperatures for HMA and the surfactant-based WMA. Examples of the data for the PG 64-22 binder are shown in figure E1c-1.8. This figure indicates that there are minor effects at higher binder temperatures, but some important effects are observed at 90 °C. More work is needed before findings regarding the coarse-graded mixture can be drawn.

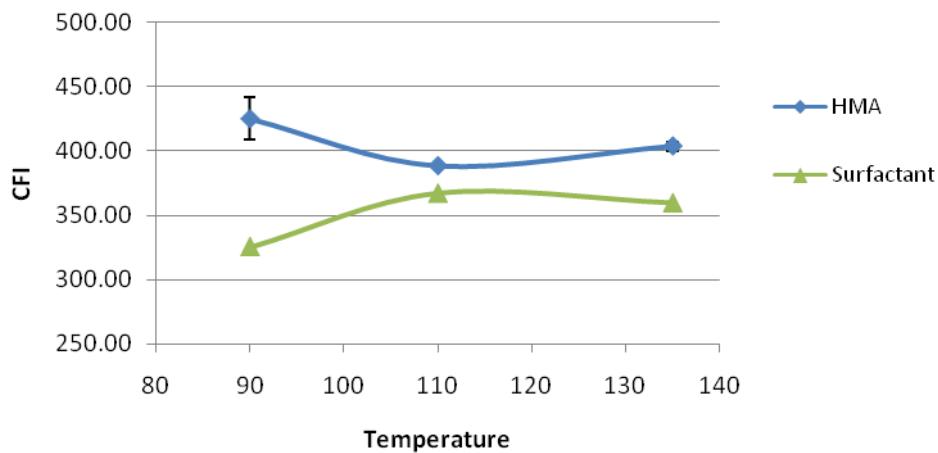


Figure E1c-1.8. Graph. Comparison of CFI data for coarse PG 64 mixtures compacted at 600 kPa.

Significant Problems, Issues and Potential Impact on Progress

Mixture performance testing was delayed six months for work plan changes regarding the type of WMA additives that should be used in the testing. Also, winter conditions and lack of access to aggregates have caused delays. The aggregate source is now open for the season. Materials collection and sending of samples to UNR will be complete by April 30.

The addition of the coarse mix design to the workability testing matrix delayed progress by approximately one month. This should not affect overall progress.

Work Planned Next Quarter

The research team will submit an interim report early next quarter to FHWA. Upon approval, the report will be shared with various partners from the industry as well as federal and state agencies.

Efforts will continue toward finishing the experimental plan presented in the Year 3 work plan, including evaluation of the coarse mix design. The investigation will also extend to foamed asphalt mixes using recommendations developed in the binder evaluation.

The data collected will be analyzed using the workability measures presented in NCHRP project 9-43, "Mix Design Practices for Warm Mix Asphalt." Results will be compared to the CFI data collected to verify the findings of the NCHRP study or provide further recommendations.

Performance testing will start at UNR and will include evaluation of the effects of warm mix additives on resistance to rutting, fatigue and thermal cracking.

There have been some questions as to whether a bump in the high-temperature PG grade of the binder specified in the mix design is needed. The reason for concern is that lower production temperatures lead to less short-term aging of the binder, which in turn makes the mix more susceptible to rutting. This concern will be evaluated by testing high-temperature performance of mixtures compacted at 135°C and 90°C, the same temperature range that showed performance differences in the workability testing.

Subtask E1c-2: Improvement of Emulsions' Characterization and Mixture Design for Cold Bitumen Applications

Work Done This Quarter

Emulsion construction properties

Efforts this quarter were focused on developing laboratory procedures to quantify the curing rate and development of bond strength. Two potential testing devices were evaluated: the first includes using the Dynamic Shear Rheometer (DSR) to measure the change in G^* and strain tolerance using a strain sweep procedure at intermediate temperatures, and the second uses the Pneumatic Adhesion Tensile Testing Instrument (PATTI) to measure bond strength development. The relevance of the results from these tests is being evaluated by comparing them

to the mass loss measured in the ASTM D7000 sweep test. Based on initial analysis, results from both tests correlate well with performance measured in the sweep test; therefore, the research team will need to decide which test to recommend for implementation after sufficient testing has been completed.

Emulsion residue properties

The research team has addressed all of the comments provided by TRB committee AFK 50 on the paper submitted for evaluating the newly proposed evaporative residue recovery procedure. The revised paper is being summarized for submission to the project advisory group and FHWA. The document will state and justify the research team's intent to use the new recovery method in its research. The research team is also collaborating with the Federal Lands study that is evaluating the rheological properties of polymer-modified emulsions. Four modified emulsions were sampled from the field; high-, intermediate- and low-temperature rheological properties were measured; and results of these tests were shared with the research team. Data analysis is currently in progress, with the intent of using the results of this initial data set to justify the use of candidate tests and analysis methods for measuring emulsion residue properties for this project.

Energy analysis

The literature review document discussed in the ARC Q4 2008 report was finalized. The document was then further summarized and presented as a research needs white paper to promote technology transfer and give interested parties an idea of the research team's motivation for researching energy consumption under this subtask. The white paper, titled "Sustainable Asphalt Pavements: Technologies, Knowledge Gaps and Opportunities," was submitted to FHWA and is available for download at <http://www.uwmarc.org/files/MARC-Sustainable-Asphalt-Pavements-white-paper.pdf>.

Presentations

The following presentations were given this quarter:

- TRB Poster Session 541: Tests, Evaluation and Stability of Various Modified Asphalt Binders Used in Hot Mix Asphalt and Surface Treatments, "Rheological Evaluation of Emulsion Residues Recovered Using Newly Proposed Evaporative Techniques," by Andrew Hanz, January 13.
- TRB Sessions 777/791: Advances in Pavement Chip Seals, "Current and Future Chip Seal Use in the United States: Materials Research and Challenges," by Hussain Bahia, January 15.
- AEMA-ARRA-ISSA Annual Meeting, "Overview of the Asphalt Research Consortium Studies on Emulsions," by Hussain Bahia, February 20.

Significant Results

Adhesion and DSR testing

Testing focused on the effects of aggregate mineralogy and environmental conditions on the gains in the bond strength of the emulsion over time. Aggregate mineralogy was evaluated using three aggregate types: granite, soft limestone and diabase. The research team plans to add a hard limestone in the near future to fully investigate the impacts of both aggregate mineralogy and

porosity on development of emulsion rheological properties. Comparison of tensile strength values for curing times of 2, 6 and 24 hours for the previously mentioned aggregate types are provided in figure E1c-2.1.

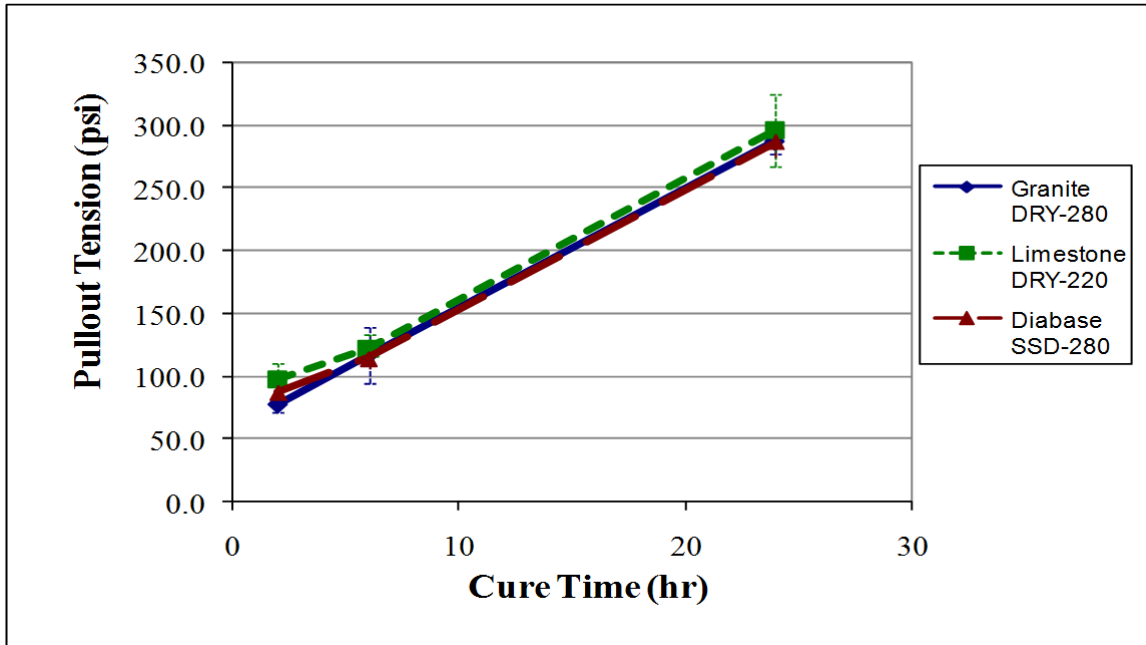


Figure E1c-2.1. Graph. Effect of aggregate type on development of emulsion bond strength for CRS-2 emulsion (35 °C, 15% relative humidity).

Figure E1c-2.1 demonstrates that for this emulsion (CRS-2), there is no effect of aggregate type on pullout tension. This trend is consistent among all combinations of curing conditions used in this study. Thus far, all materials have exhibited adhesive failures at the 2-hour curing time; the failure mode transitions to cohesive failure at the 6- and 24-hour curing times. Before drawing any firm conclusions, additional emulsions and the fourth aggregate type (hard limestone) should be evaluated.

Curing conditions were controlled using a recently acquired humidity chamber. Two levels of temperature (15 °C and 35 °C) and humidity (30% and 70%) were selected, with all four possible combinations tested. Figure E1c-2.2 shows the effect of curing conditions for limestone aggregate.

Figure E1c-2.2 indicates that, as expected, curing temperature and humidity both significantly affect the development of bond strength. The consistency of the test results with expectation is important, demonstrating that the test procedure developed is adequately sensitive to show expected changes in material behavior.

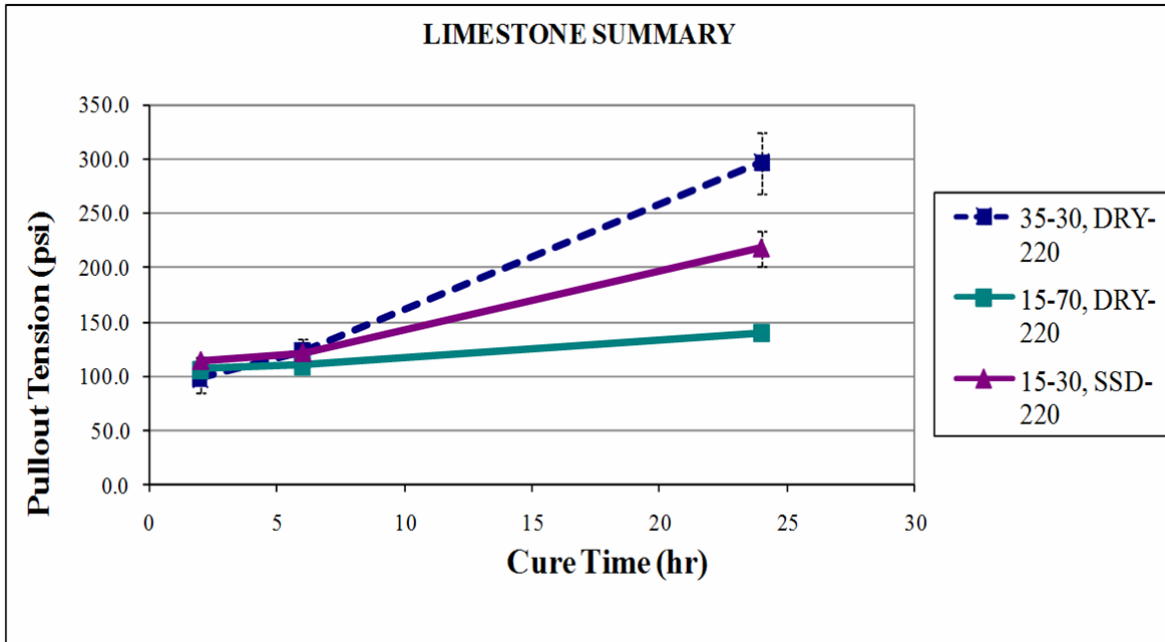


Figure E1c-2.2. Graph. Effects of curing conditions on development of emulsion bond strength. At the time of publication, the sample cured at 35 °C and 70% humidity was unavailable to include in this graph. (The legend indicates curing temperature (°C), percent humidity, surface moisture condition (air dry or saturated surface dry), and roughness level.)

DSR testing using a strain sweep procedure with 25 mm parallel plate geometry was used to measure the curing rate of the emulsion in terms of development of stiffness and strain tolerance. The emulsion was cured on a granite substrate at curing conditions of 15 °C and 30% relative humidity. The material was sampled after 2, 6 and 24 hours and tested. The specifics of the sample preparation and test procedure are provided in the International Symposium on Asphalt Emulsion Technology (ISAET) paper referenced in the ARC Q3 2008 report. Like the results shown in that paper as well as the PATTI results previously presented, DSR testing results showed sensitivity to curing time (Hanz et al. 2008a). Specific results are given in correlations between DSR testing and sweep test results provided in later sections of this report.

Sweep test results and comparison to PATTI and DSR testing results

The sweep test was conducted using granite aggregate chips with 100% passing the 9.5 mm sieve and 1% passing the No. 4 sieve. Aggregate gradations, sample preparation and testing were conducted using the ASTM D7000 sweep test procedure. Samples were cured using the same environmental conditions and tested at the same curing times as the previously reported DSR and PATTI tests. Results are presented in figure E1c-2.3. At the time of this report, only one replicate for each curing condition was available.

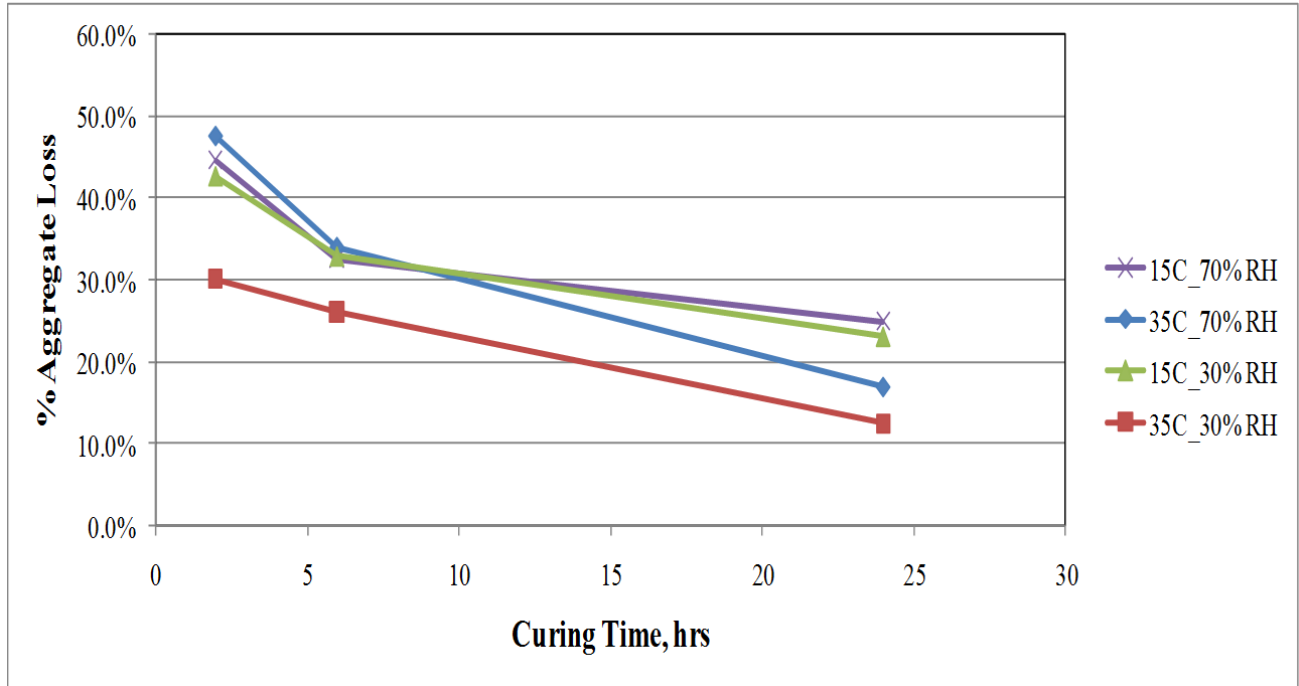


Figure E1c-2.3. Graph. Effect of curing conditions (temperature and humidity) on development of emulsion bond strength.

Results presented in figure E1c-2.3 show sensitivity to both curing temperature and humidity. Results also show sensitivity to curing time, consistent with results presented in the ARC Q4 2008 report. Initial results are promising in that they are consistent with the DSR and PATTI tests used to evaluate the components of the sweep test system. This consistency allows for comparison of the tests used on the aggregate/emulsion components to performance as measured by the sweep test. A comparison of sweep test results and the strain tolerance as measured by the linear viscoelastic limit (10% reduction in G^*) and the failure strain (50% reduction in G^*) is provided in figure E1c-2.4. A comparison of the development of stiffness as measured by $G^*/\sin(\delta)$ at 12% strain is provided in figure E1c-2.5. Curing conditions for the CRS-2 emulsion were 15°C and 30% humidity.

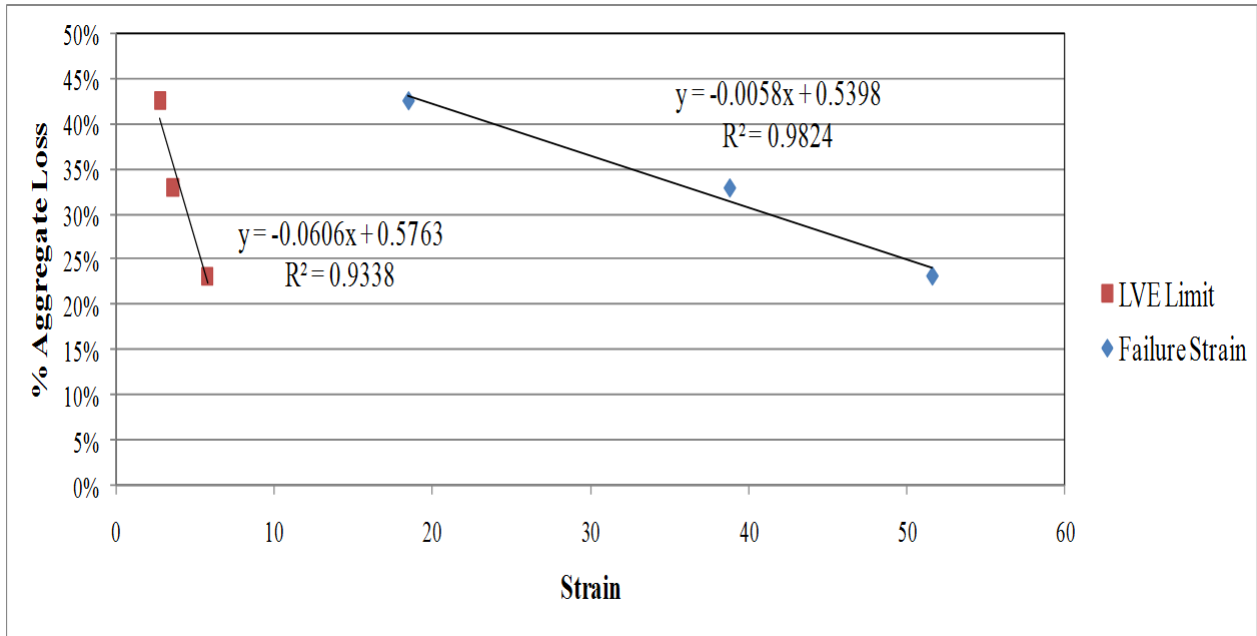


Figure E1c-2.4. Graph. Comparison of measured strain tolerance parameters linear viscoelastic limit and failure strain to performance. Values were measured by the ASTM D7000 sweep test.

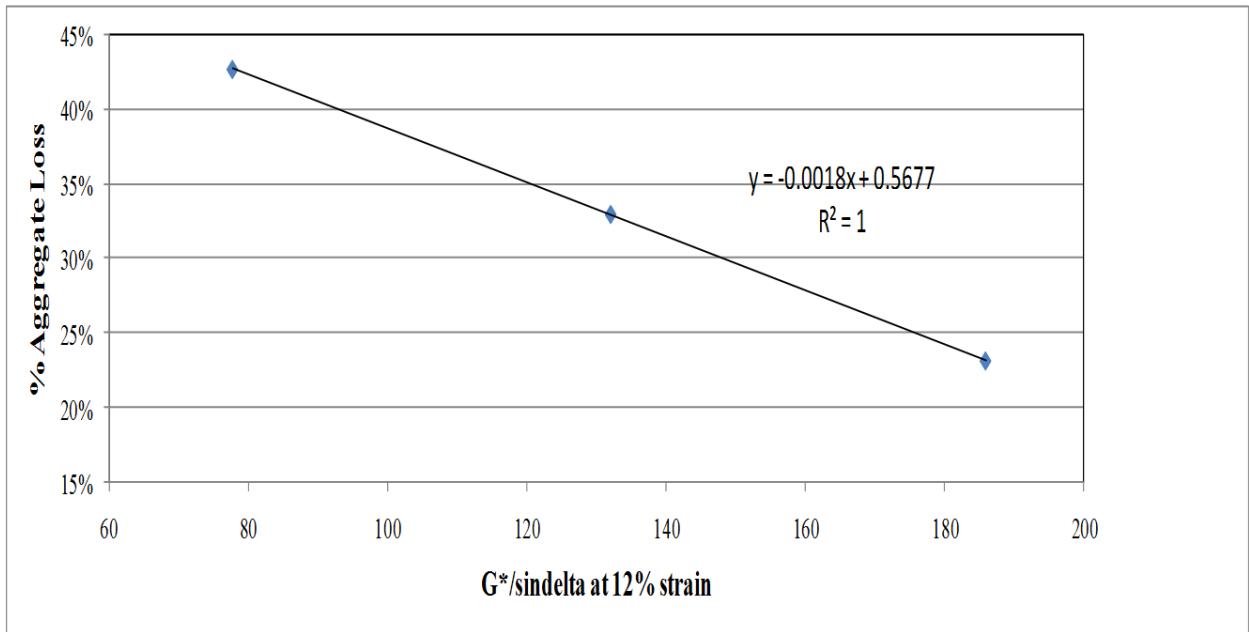


Figure E1c-2.5. Graph. Comparison of permanent deformation resistance to performance as measured by the ASTM D7000 sweep test.

Although sample size is small, there are strong correlations between chip seal performance, as measured by aggregate loss using the sweep test, and the emulsion parameters of strain tolerance and G^* , as defined in Hanz et al. (2008b). Further testing is needed to explore correlations between different aggregate and emulsion types. Specific materials were provided in the Year 3 work plan. These preliminary results show promise that the test developed for direct measurement of emulsion properties during curing using the DSR relates well to the performance of the chip seal system in the sweep test. Similar relationships were also evaluated for the PATTI test as presented in figure E1c-2.6.

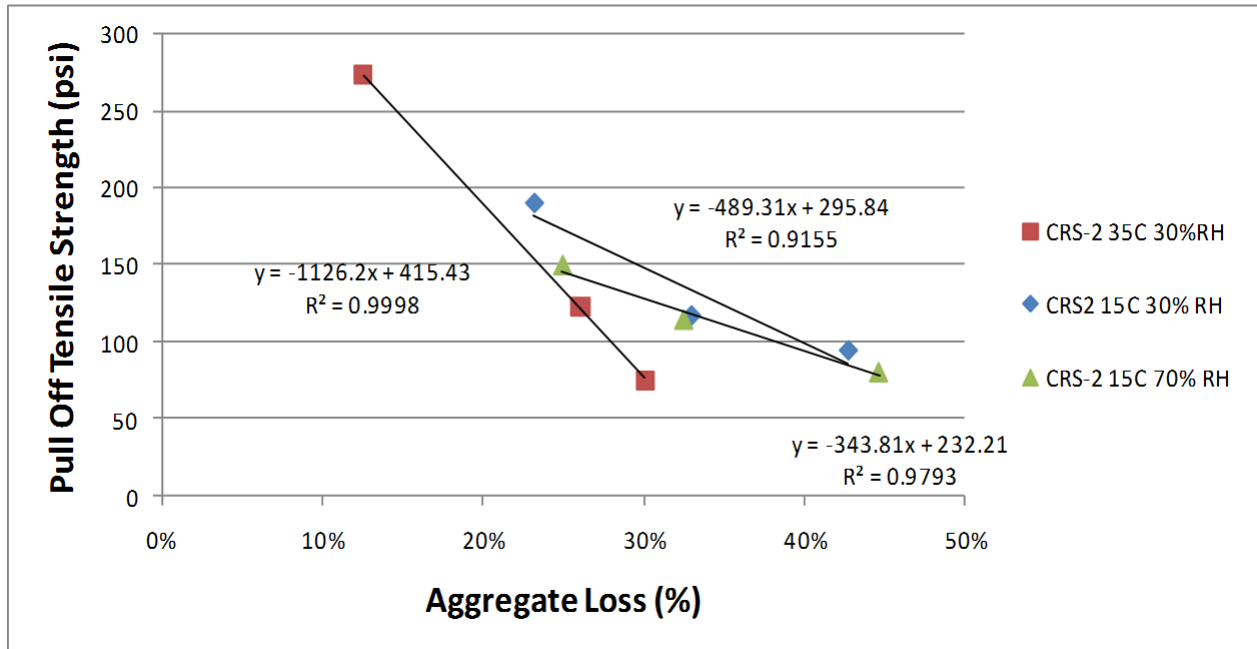


Figure E1c-2.6. Graph. Comparison of pulloff tensile strength to performance as measured by the ASTM D7000 sweep test.

Results in figure E1c-2.6 show the relationship between pulloff tensile strength and aggregate loss for a CRS-2 emulsion with a granite aggregate at various curing conditions. Correlations were very strong for all three curing conditions tested. Furthermore, the effect of temperature and humidity on the development of performance properties is clearly shown by the difference in the slopes of the various regression lines. The figure, however, does not show a consistent relationship between aggregate loss and pulloff strength because the results presented in figure E1c-2.6 include three curing times. Figure E1c-2.7 shows the same data provided in figure E1c-2.6 grouped by curing time instead of curing conditions.

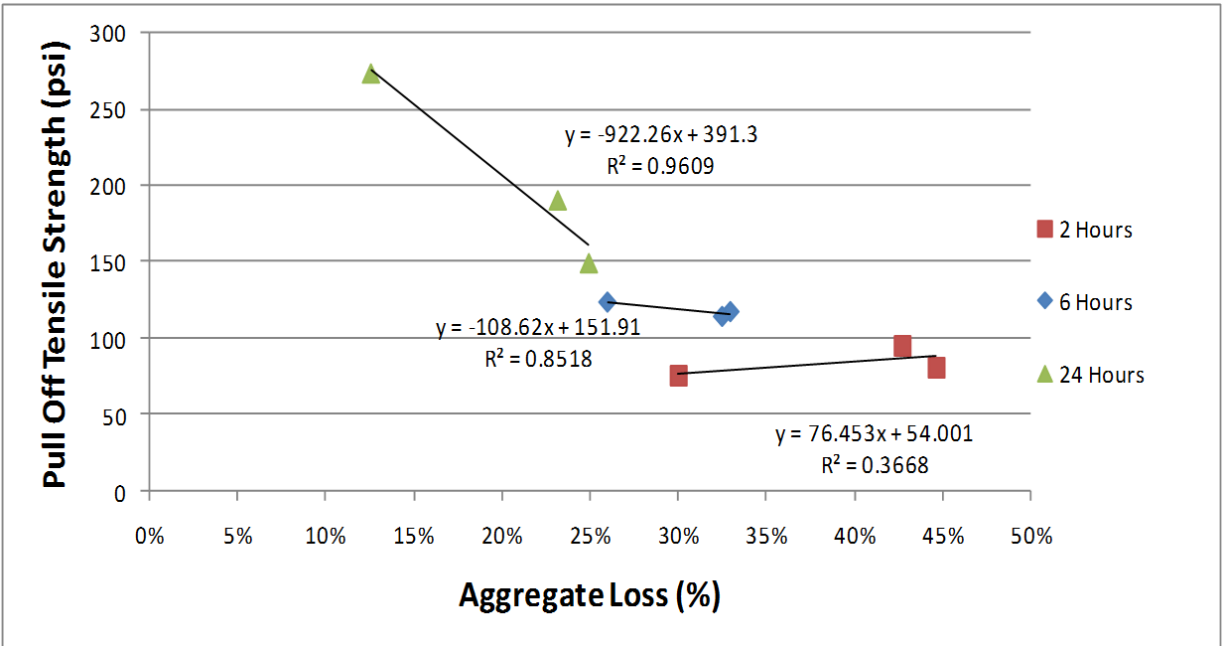


Figure E1c-2.7. Graph. Comparison of pulloff tensile strength to performance as measured by the ASTM D7000 sweep test at equivalent curing times.

Figure E1c-2.7 indicates that after two hours of curing, there is no relationship between aggregate loss and pulloff tensile strength, as noted by a 15% change in aggregate loss with little change in pulloff tensile strength. Similar results are shown after 6 hours of curing. However, after 24 hours of curing there is a strong relationship, clearly showing a range in performance in terms of both aggregate loss and pulloff strength. As more emulsions and aggregate combinations are tested, the data will be able to show if and how the relationship after 24 hours of curing is affected by different materials.

These preliminary findings confirm the earlier statement that a decision point is needed to select which test method to further evaluate and integrate into current practice. The decision will be based on results from the tests performed using a wider range of aggregate and emulsion types. Attempts will also be made to correlate laboratory results to field tests. The PATTI is promising because it is a much more practical device that costs significantly less than a DSR.

Significant Problems, Issues and Potential Impact on Progress

PATTI testing procedural issues reported last quarter have been resolved.

The literature review report for this work element was delayed. The research team felt it would be more productive to work on an interim report next quarter and include a white paper with the experimental test results and analysis. The white paper would address selection of an evaporative residue recovery method and include adequate background information.

It is premature to decide which test to use to quantify curing rate. Only one emulsion type was tested due to delays in procuring an environmental chamber. Evaluation of two or three additional emulsion types is needed before the DSR or PATTI test can be selected. It is hoped the decision can be made at the end of next quarter.

Work Planned Next Quarter

Work will continue in the following areas:

Emulsion construction properties

Work will continue on executing the experimental design provided in the Year 3 work plan. A testing protocol will be developed to investigate how the laboratory tests correlate to field performance.

Emulsion residue properties

Data from the Federal Lands study will be analyzed and used to develop a residue testing plan for high-, intermediate- and low-temperature performance of emulsion residues. Tests will be conducted on residues for emulsions collected in the study and on the base binders. A database will be developed to allow for comparison of the properties.

Energy analysis

Work will focus on identifying and scheduling site visits for data collection to verify and/or adjust current inputs needed for energy consumption and emissions models.

Advisory group

The project advisory group will convene on April 10, 2009, for a progress update and technical discussion to prioritize future research objectives.

Cited References

Hanz, A., Z. Arega, and H. Bahia, 2008a, Advanced Methods for Quantifying Emulsion Setting and Adhesion to Aggregates. Submitted to the International Symposium on Asphalt Emulsion Technology (ISAET). Work was presented at the ISAET conference in Arlington, Virginia, September 25, 2008.

Hanz, A., Z. Arega, and H. Bahia, 2008b, Rheological Characterization of Emulsion Residues Recovered Using Newly Developed Evaporative Techniques. Accepted for poster presentation.

CATEGORY E2: DESIGN GUIDANCE

Work element E2a: Comparison of Modification Techniques (UWM Year 2 start)

Work Done This Quarter

The research team composed a materials request letter (copied below) and submitted it to the suppliers and manufacturers listed in table E2a.1. Only one positive response has been received as of the date of this report. Follow up by phone and e-mail is under way.

The research team has also identified the following generic technologies to be included in the work element:

- Elastomeric modifiers: styrene-butadiene-styrene (SBS), styrene-butadiene rubber (SBR) and Elvaloy
- Plastomeric modifiers: ethylene vinyl acetate (EVA) and polyethylene (PE)
- Chemical modification: polyphosphoric acid (PPA) and oxidation
- Combinations three kinds of modification of the above

There is very limited production of the EVA- and PE-modified binders in the United States. Thus, some of these binders will be produced by the research team in the laboratory.

During the most recent Binder ETG, Dr. John D'Angelo presented significant data showing the effect of heating and cross linking of polymers on the results of the Multiple Stress Creep and Recovery test. Also, Dr. Jeff Rowe of Abtech presented data on a large study on waxes that appears to be sponsored by FHWA. The research team has started reviewing these significant results to determine how this work element could or could not be aligned with these activities. It is expected that the research team will propose a meeting with the main researchers conducting these two studies to share ideas on how to organize the findings and how to coordinate this work elements with these efforts. The end of June or first part of July is a target date.

Table E2a.1. Manufacturers invited to participate in this research effort.

Company	Sent e-mail	Accepted
Nustar	X	
Holly Asphalt	X	
Seneca Chicago	X	
United Refining	X	
ConocoPhillips	X	
Kraton	X	
Marathon	X	
BitMat	X	
Mathy Construction	X	
Paramount Petroleum	X	
Payne and Dolan	X	
Valero Oil	X	
Honeywell	X	X
Vance Brothers	X	

Significant Results

The review of ongoing work clearly indicates that the method of production of polymer-modified asphalts plays a significant role in defining critical performance of binders. It is not clear from information reviewed to date how important cross-linking is and whether the elasticity resulting from cross-linking is important for damage resistance.

Significant Problems, Issues and Potential Impact on Progress

The industry response to the request for participation in this work was surprisingly weak. The research team hopes this will change significantly with more direct contact between the researchers and the manufacturers.

Work Planned Next Quarter

The research team will work on securing more involvement from the manufacturers in this project and obtaining the materials needed for testing. A meeting with researchers conducting similar work at FHWA and other organizations will be coordinated to discuss possible collaboration.

Work element E2b: Design System for HMA Containing a High Percentage of RAP Material (UNR)

Work Done This Quarter

This work element is a joint project between University of Nevada, Reno and University of Wisconsin–Madison. The data for the physical properties of the various extracted aggregates were analyzed. Additionally, FHWA completed the AIMS testing for both the Nevada-Andesite and the California-Handley Ranch aggregates.

The experimental plan for checking the impact of mixing on the properties of the aggregates was completed. The virgin aggregates were mixed with water (no asphalt) in the mixer and their properties were re-evaluated.

The overall experimental plan remained unchanged from the previous quarter except for the addition of one softer binder. This third recycled asphalt pavement (RAP) binder added to the project is a PG 58-34 from Murphy Oil. Analytical and procedural changes in the testing are described below.

A new approach was developed and put in place to analyze the Bending Beam Rheometer (BBR) stiffness and m-values. Instead of using blending charts and binder-mortar correlation to back calculate the percent of aged binder in RAP aggregates, the new approach determines the limit of percentage RAP binder in the blended binder based on the mortar results. The testing of mortars is performed at a testing temperature of 0°C. An Excel spreadsheet was developed to support this new analysis approach which does not require the creation of binder-mortar correlation equations.

Procedurally, the preparation of the mortar was changed this quarter. Instead of using fresh and pressure aging vessel (PAV)-aged binder, the mortars are prepared using only PAV-aged binder.

The testing load used in the procedure has also been increased from 4000 mN to 4500 mN to produce significant deflections for harder RAP mortars. Since the testing temperature for the mortars is 0°C, the PAV-aged binders are tested at three different temperatures, with one of them equal to 0°C to relate to the mortar samples.

The RAP gradation for producing the mortar also changed. Only three sieves (#30, #50 and #100) are used to produce a mixture following the maximum density gradation line. This approach has the advantage of limiting the amount of binder used and distributing aggregates to minimize entrapped air voids observed earlier.

Significant Results

The research team developed and finalized a new mortar preparation and sampling procedure that include only three sieve sizes. The gradation changes resulted in more consistent BBR stiffness and m-values.

A new approach to analyze the BBR data obtained from testing mortar samples is introduced. The approach includes the following steps:

1. Test the fresh binder intended for mixing with RAP after PAV aging at three temperatures using the BBR. The temperatures should include two that capture the specification limits of $S = 300$ MPa and $m = 0.300$. The third temperature should be 0.0 °C, at which a reduced loading in the BBR may be used.
2. Sieve the RAP on the # 30, #50 and #100 and combine in proportions that follow the maximum density line. This is called Select RAP (SRAP). Determine the binder content in SRAP using the ignition oven.
3. Use aggregates retained from the ignition oven to combine RAP aggregates at similar proportions of the SRAP in step 2.
4. Mix the SRAP (from step 2) and the aggregates for the RAP (step 3) with PAV -aged fresh binder to produce SRAP mortar and PAV RAP (PRAP) mortar. Use enough amounts of the PAV-aged binder to get the total binder content in both mortars to 25% by weight of SRAP and/or RAP.
5. Test 2 replicates of the SRAP mortar and 2 replicates of the PRAP at 0.0 °C.
6. Input the BBR results for all 6 loading times for the 2 mortars and the PAV binder tested at 0.0 °C in the spreadsheet RAPBA (RAP Binder Analysis). Also, input the binder content in RAP and the new HMA mixture containing this RAP for the project; the total binder percentage in mortar; the $S(60)$ and $m(60)$ for the PAV binder at the other two temperatures; and the target PG grade for the project.
7. RAPBA automatic calculation should output the allowable RAP content chart for the specific new HMA mixture in the project.

An example of the analysis using the new approach is shown in figure E2b.1. The plot shows the maximum amount of RAP (noted as SRAP on the vertical axis) that can be blended in a new HMA mix with a fresh binder to achieve a target PG grade (on the horizontal axis). The results show the maximum allowed using both the S and the m value limits.

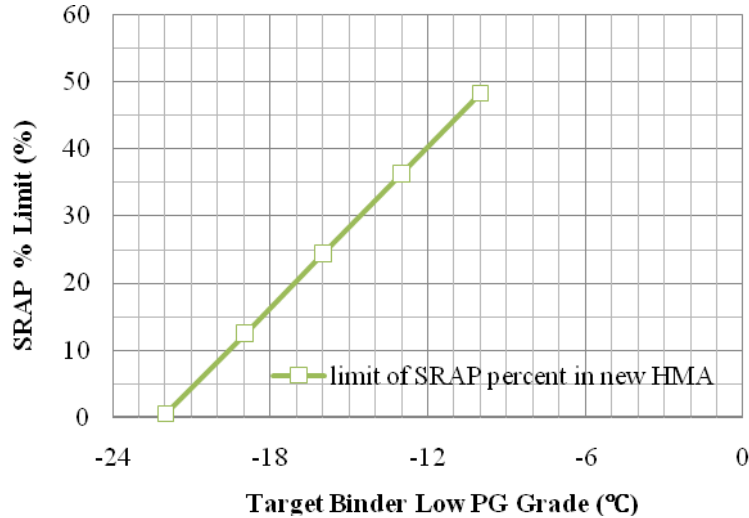


Figure E2b.1. Graph. Limit of percentage of RAP binder in blended binder based on different target low-temperature PG grades.

This quarter, the effect of mixing time of the RAP with the PAV binder was also evaluated. The purpose of this experiment was to evaluate if longer mixing time changes the BBR results for the mortars. In addition, a study of the effect of gradation of RAP used in the mortars and the number of sizes to be included in the mortar began. Results of both of these testing activities are being analyzed and it is expected that the analysis will be ready by next quarter.

The research team made two observations in relation to mortar preparation:

- While mortar preparation will not be as quick or as simple as BBR binder beam preparation, the selection of size of RAP in mortar could simplify the mortar sample preparation procedure and result in minimizing preparation time.
- Only one PAV binder content was used to prepare the mortars. To develop a consistent test method, different PAV binder contents should be considered. Increasing the content could make the process of producing samples much easier.

Significant Problems, Issues and Potential Impact on Progress

None.

Work Planned Next Quarter

Next quarter, the research team will run a complete experiment with three binders of different grades and four RAP sources, as described in the experimental design included in the work plan. Collected data will be analyzed according to the new approach described in this quarterly report. The Excel spreadsheet to support the analysis will also be finalized.

For the selected best extraction procedure, the research team will evaluate the impact of solvent types on the aggregate properties.

Work element E2c: Critically Designed HMA Mixtures (UNR)

Work Done This Quarter

The UNR team analyzed the calculated deviator and confining stresses from the 3D-Move responses of the PG64-22, PG58-22, and PG52-22 mixtures under the moving 18-wheel truck at 60, 40, 20 (with and without braking), and 2 mph (with braking).

The requested field HMA mixtures from the WesTrack sections that experienced early rutting were received from the material reference library (MRL) for laboratory evaluation. The WesTrack mixtures are under evaluation for permanent deformation characteristics.

Significant Results

Figures E2c.1 and E2c.2 show the calculated maximum deviator and confining stresses in the PG58-22 HMA layers under the non-braking and braking tandem driving axle, respectively. Furthermore, table E2c.1 shows the maximum stresses along with the sum of the maximum deviator and confining stresses (i.e. total vertical stress).

Additionally, the time of loading in the HMA layer at 2 inches below the pavement surface was calculated for all the mixes under both non-braking and braking conditions. The time of loading was determined by best fitting a sinusoidal wave shape for the deviator stress pulse that was calculated from the octahedral shear stress (τ_{oct}) under a moving 18-wheel truck at different speeds and temperatures.

The data for the pulse time for all three mixtures were combined and a general relationship between the loading time at 2 inches below the pavement surface and vehicle speed and temperature was established for the non-braking and braking conditions. The pavement thickness did not have a statistically significant impact on the pulse time at 2 inches below the pavement surface. Fitting parameters (R^2) of 0.983 and 0.999 were found for the non-braking and braking conditions, respectively.

Non-braking conditions (temperature between 40 and 70°C and speed between 20 and 60 mph):

$$\log(t) = -0.66540 - 0.00353*Temp - 0.02360*Speed + 0.000154*(Speed)^2 \quad (1)$$

Braking conditions (temperature between 40 and 70°C and speed between 2 and 20 mph):

$$\log(t) = -0.23603 - 0.00038674*Temp - 0.05531*Speed \quad (2)$$

where,

t = deviator stress pulse time at 2 inches below pavement surface in seconds

$Temp$ = pavement temperature in °C

$Speed$ = vehicle speed in mph

Table E2c.2 shows an example of the estimated pulse time at 2-inch below the pavement surface under the driving tandem axles of an 18-wheel truck at a travelling speed of 20 and 60 mph without braking and 2 and 20 mph with braking.

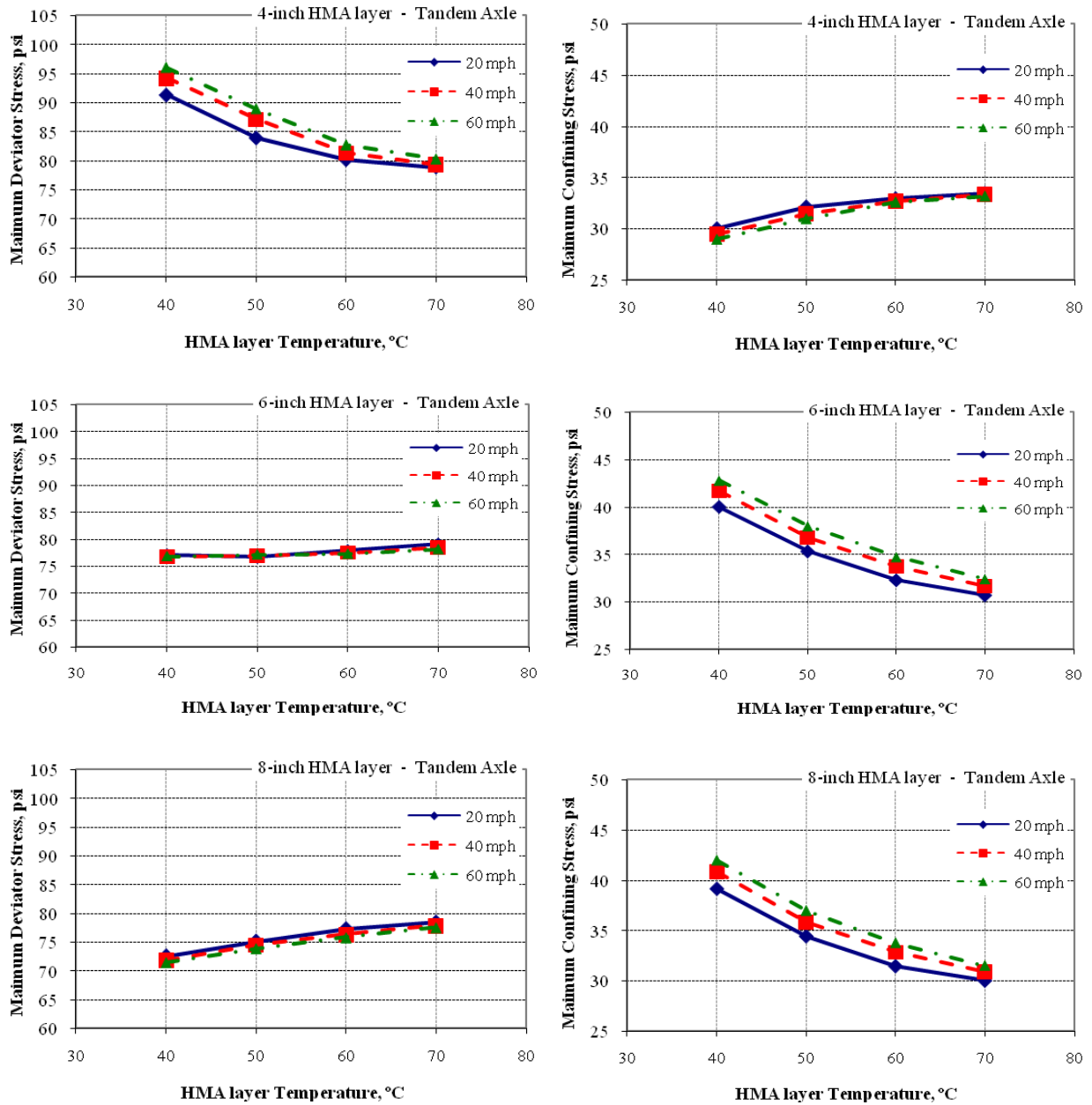


Figure E2c.1. Maximum deviator and confining stresses at 2-inch below the pavement surface of the PG58-22 mix

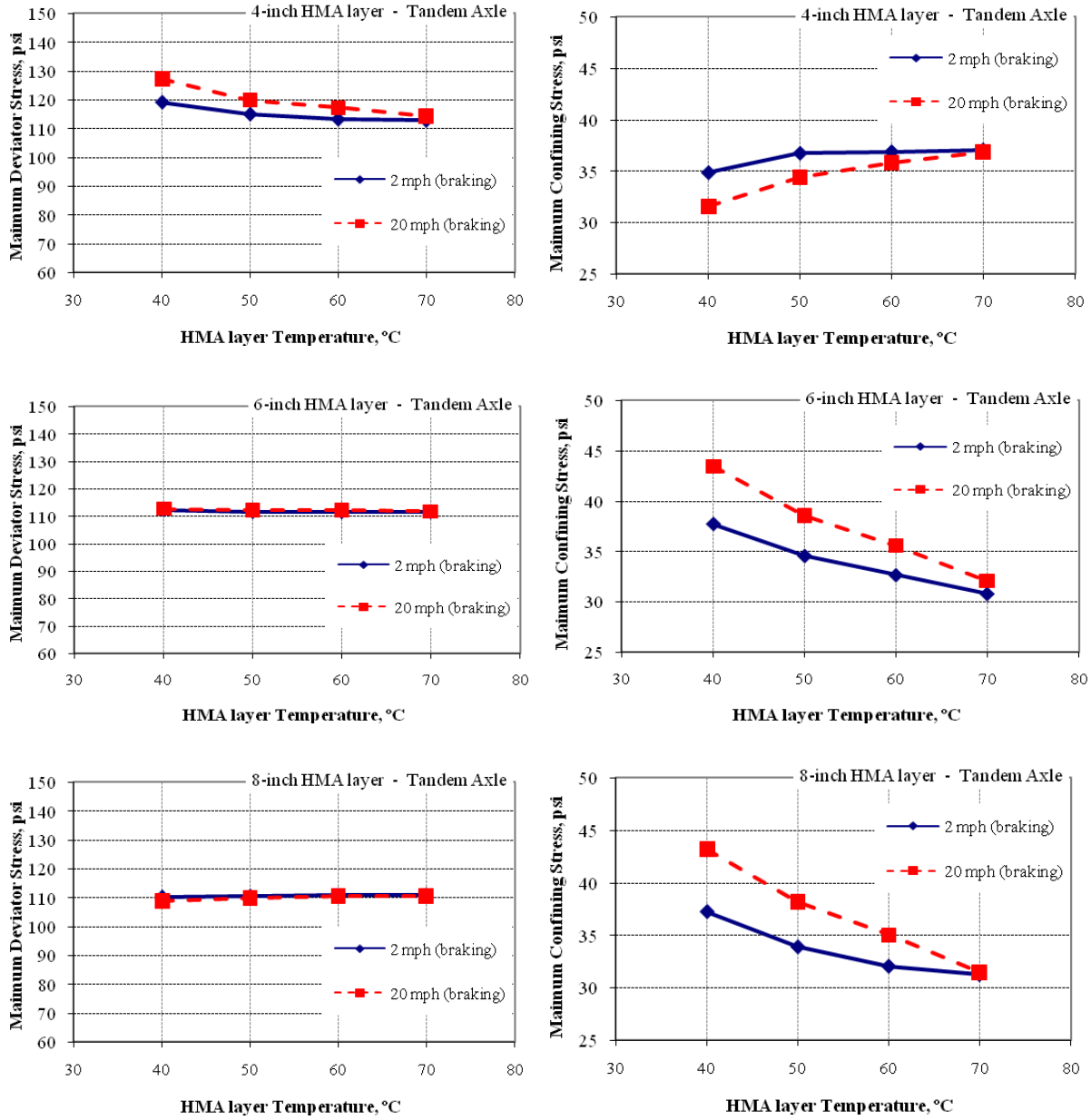


Figure E2c.2. Maximum deviator and confining stresses at 2-inch below the pavement surface under braking conditions of the PG58-22 mix

Table E2c.1. Summary of the maximum deviator and confining stresses at 2” below the pavement surface of the PG58-22 mix.

HMA layer temperature (°C)	HMA layer thickness (in)	18-wheel traveling speed (mph)	Max deviator stress, σ_d (psi)	Max confining stress, σ_c (psi)	Total vertical stress, $\sigma_d + \sigma_c$ (psi)	
40	4	2 (braking)	119	35	154	
		20 (braking)	127	32	159	
		20	91	30	121	
		40	94	30	124	
	6	60	96	29	125	
		2 (braking)	112	38	150	
		20 (braking)	113	44	156	
		20	77	40	117	
	8	40	77	42	118	
		60	77	43	120	
		2 (braking)	110	37	147	
		20 (braking)	109	43	152	
50	4	20	73	39	112	
		40	72	41	113	
		60	72	42	114	
		2 (braking)	115	37	152	
	6	20 (braking)	120	34	154	
		20	84	32	116	
		40	87	31	119	
		60	89	31	120	
	8	2 (braking)	112	35	146	
		20 (braking)	112	39	151	
		20	77	35	112	
		40	77	37	114	
60	6	60	77	38	115	
		2 (braking)	110	34	144	
		20 (braking)	110	38	148	
		20	75	34	110	
	8	40	75	36	110	
		60	74	37	111	
		2 (braking)	113	37	150	
		20 (braking)	117	36	153	
	70	4	20	80	33	113
			40	81	33	114
			60	83	33	115
			2 (braking)	112	33	144
6		20 (braking)	112	36	148	
		20	78	32	110	
		40	78	34	111	
		60	77	35	112	
8		2 (braking)	111	32	143	
		20 (braking)	111	35	146	
		20	77	31	109	
		40	76	33	109	
40	4	60	76	34	110	
		2 (braking)	113	37	150	
		20 (braking)	114	37	151	
		20	79	34	112	
	6	40	79	33	113	
		60	80	33	114	
		2 (braking)	112	31	142	
		20 (braking)	112	32	144	
	8	20	79	31	110	
		40	78	32	110	
		60	78	32	111	
		2 (braking)	111	31	142	
8	20 (braking)	111	32	142		
	20	79	30	109		
	40	78	31	109		
	60	78	32	109		

Table E2c.2. Estimated pulse time at 2 inches below pavement surface.

HMA layer temperature (°C)	18-wheel travelling speed (mph)	Loading time at 2" below pavement surface (seconds)
52	2 (braking)	0.4298
	20 (Braking)	0.0434
	20	0.0550
	60	0.0195
58	2 (braking)	0.4275
	20 (Braking)	0.0432
	20	0.0524
	60	0.0185
64	2 (braking)	0.4252
	20 (Braking)	0.0430
	20	0.0499
	60	0.0177

Significant Problems, Issues and Potential Impact on Progress

The 3D-Move runs are taking more time than what was anticipated because of limitations in the number of computers that can be used. Delay is expected to complete all the runs described in the experimental plan of this work element.

Work Planned Next Quarter

The calculations of the 3D-Move model will continue to cover all the loading conditions that were described in the experimental plan for this work element.

Evaluate the field HMA mixtures from the WesTrack sections in the laboratory for permanent deformation characteristics under the repeated load triaxial test.

Work element E2d: Thermal Cracking Resistant Mixes for Intermountain States (UNR & UWM)

Work Done This Quarter

This work element is a joint project between University of Nevada Reno and University of Wisconsin–Madison. Efforts at UNR this quarter include parts of Subtask E2d-1, “Identify Field Sections,” and Subtask E2d-3, “Identify an Evaluation and Testing System.” These are described below.

The UNR team completed the analyses of the air and pavement temperature profiles data from the LTPP Seasonal Monitoring Program (SMP) and Westrack pavement sections.

The long-term oven aging process continued for the following binders as described in the experimental plan for this work element:

- Unmodified PG64-22
- Polymer modified PG64-28 (using the same PG64-22 crude source) that meets the specs of UT, NV, and CA.
- PG64-22 + 3% SBS
- PG64-22 + 10% hydrated lime
- PG64-22 + 20% hydrated lime

Additionally, the aged binders were tested for their rheological properties.

The experimental plan to evaluate the impact of aggregate absorption on the long-term aging properties of the binder in the HMA mix was started for two aggregate sources. HMA mixes were prepared for the PG64-22 and PG64-28 asphalt binders.

Efforts at UW–Madison this quarter include parts of Subtask E2d-2, “Identify the Causes of the Thermal Cracking,” and Subtask E2d-3, “Identify an Evaluation and Testing System.” These are described below.

The Single-Edge Notched Bending (SENB) equipment has been prepared with all electronic and pneumatic connections. New software has also been created to acquire data.

Fourier transform infrared (FTIR) spectroscopy tests have been performed on a first set of binders aged at UNR. Tests were performed on equipment located at UW–Madison’s Department of Physics.

The Asphalt Binder Cracking Device (ABCD) test has been performed on some mastics to verify the suitability of this test.

The development of a new type of dilatometric cell for glass transition temperature (T_g) measurement continued, but with many challenges. To meet progress requirements, the development of the new cells was put on hold and the original type of dilatometric cell was used to collect critically-needed data. Collection of the mixture T_g measurements also started. The system for measuring the mixture T_g appears to be working satisfactorily and is giving reliable data. The work on the mixture T_g measurements is being closely coordinated with the Transportation Pooled Fund study led by the University of Minnesota.

Significant Results

The UNR-team completed the calculations for the pavement temperature rates for all the LTPP SMP sections. Figure E2d.1 shows the results for the average daily and hourly cooling and warming temperature rates in Battle Mountain, Nevada and Estelline, Texas. A table

summarizing the determined minimum and maximum air and pavement temperature along with the calculated air and pavement temperature rates was prepared.

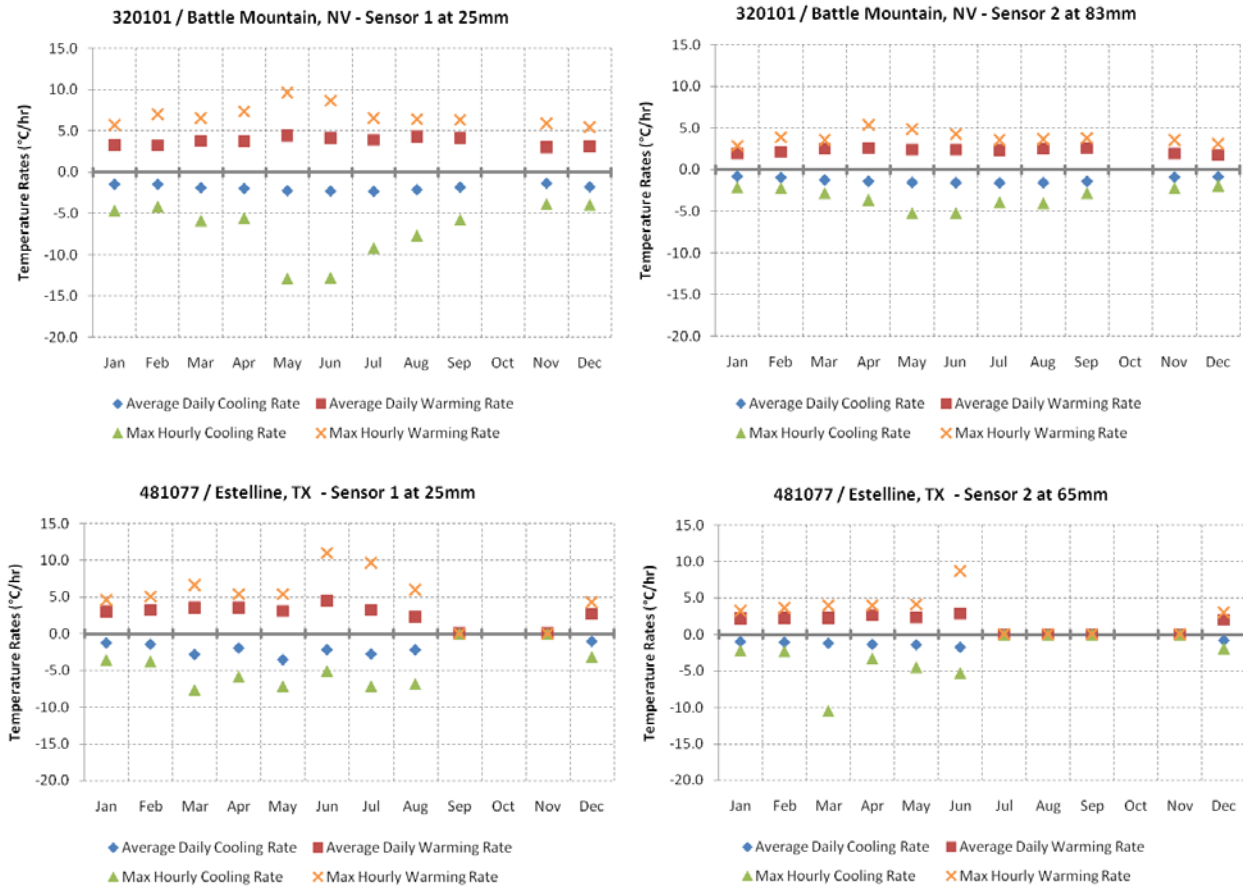


Figure E2d.1. Daily and hourly cooling and warming temperature rates in Battle Mountain, Nevada and Estelline, Texas.

Figure E2d.2 shows the measured $G \cdot \sin \delta$ for the aged PG64-22 asphalt binder at different temperatures and aging times. Similar data are produced for the other aged asphalt binders. Figure E2d.3 shows the measured $S(t)$ and m -value for the aged PG64-22 asphalt binder at 85°C and at various aging times. Similar data are produced for the other aged asphalt binders.

The multiple stress recovery (MSCR) test was conducted on the aged asphalt binders according to AASHTO TP70-07 using a creep stress of 3.2 and 10 kPa. Figure E2d.4 shows the J_{nr} for the PG64-22 and PG64-28 asphalt binders at different aging times.

Results of FTIR tests for measuring the carbonyl peak growth on the aged binders are shown in figure E2d.5. UNR will take the next step in providing the initial analysis of these data.

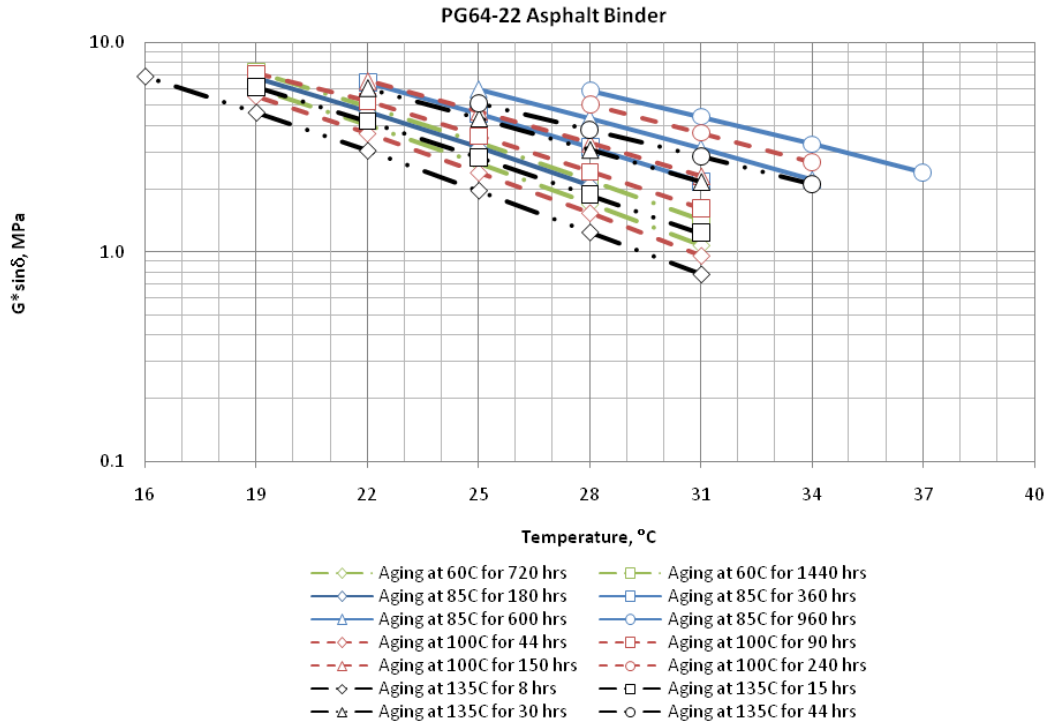


Figure E2d.2. $G^* \sin \delta$ for the PG64-22 at various temperatures and curing times.

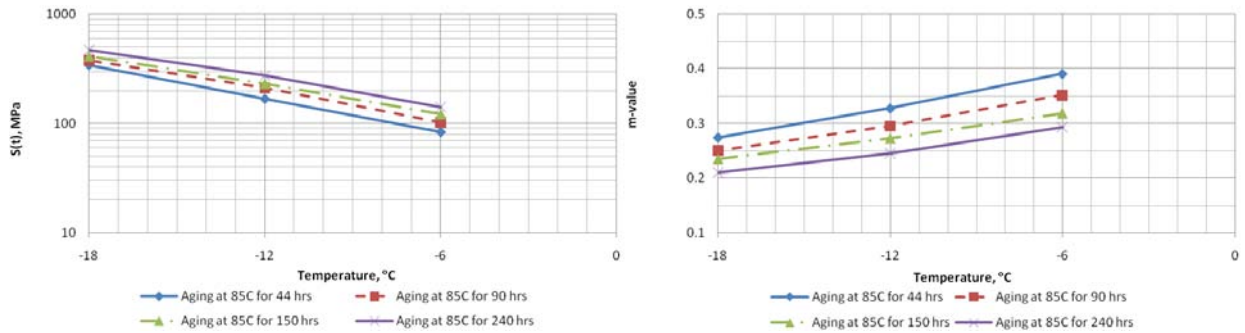


Figure E2d.3. BBR test results for the PG64-22 at 85°C aging time and various curing times.

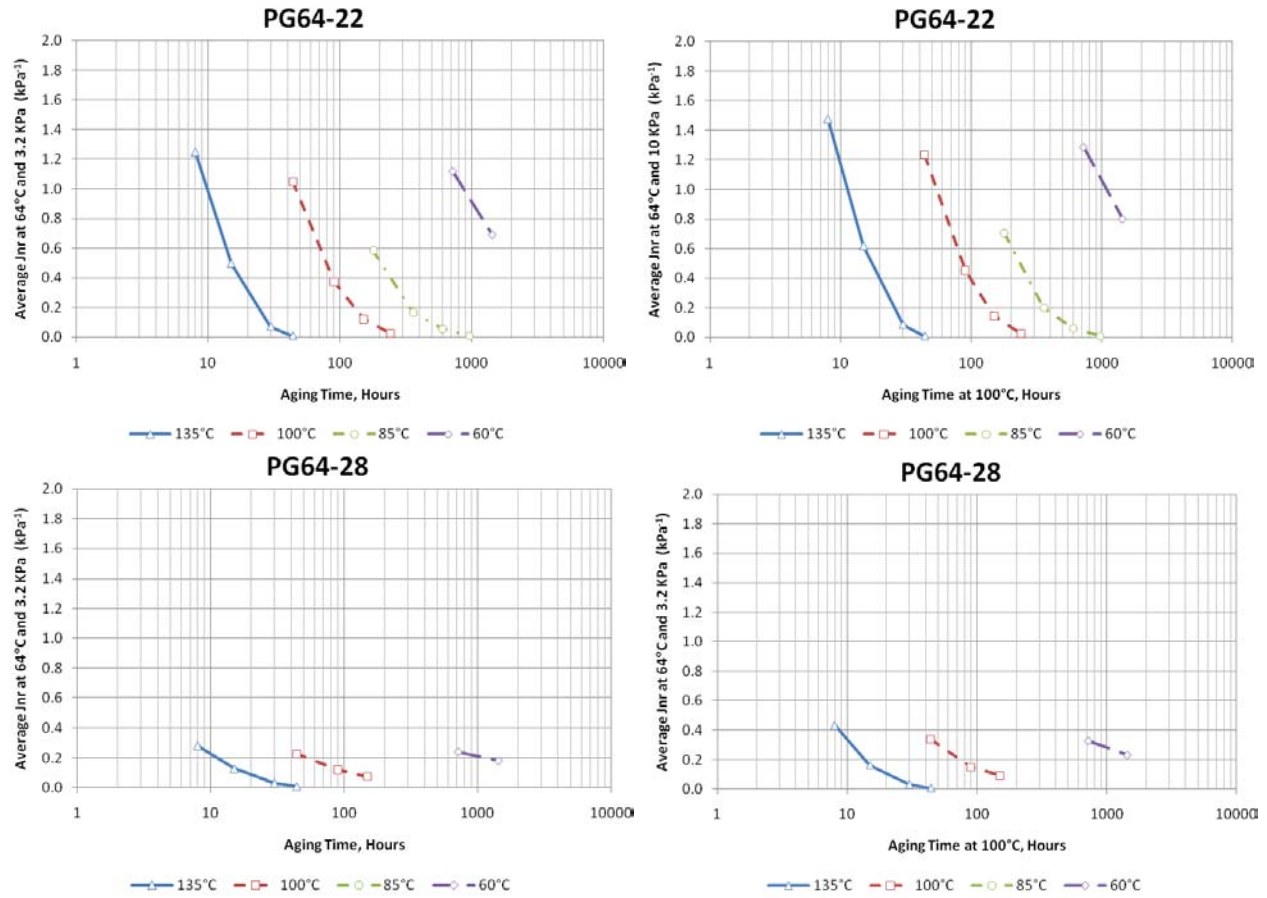


Figure E2d.4. Jnr of the PG64-22 and PG64-28 asphalt binders from the MSCR test.

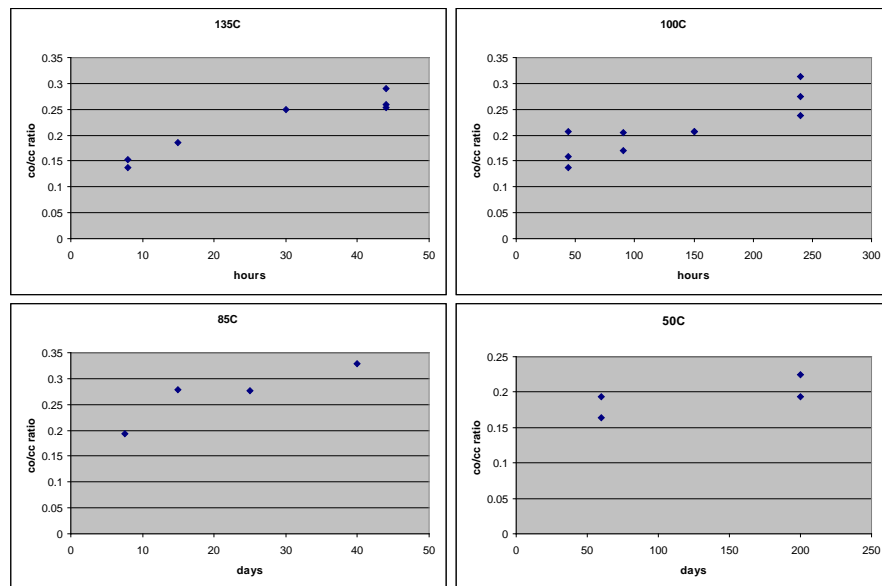


Figure E2d.5. Results of FTIR spectroscopy tests for binders aged at four different temperatures.

The SENB device is working and the experimental plan will start as soon as the data acquisition system is optimized. Problems with friction in the shaft lodging have been solved.

The problem with the connection of the pressure sensors to the original type of dilatometric cells was solved, and the automatic acquisition of the data is now working.

Results of the mixture T_g testing in heating and cooling for a trial sample is shown in figure E2d.6. The results show a variation in the T_g values and the coefficients of volume change in cooling and in heating.

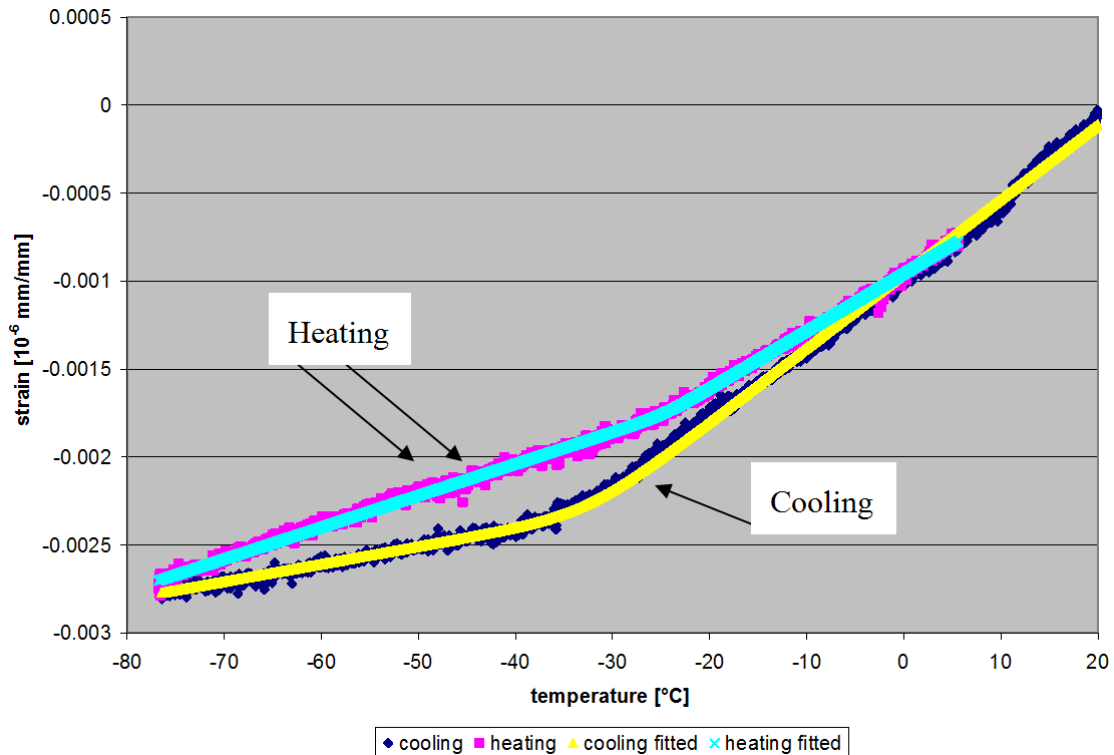


Figure E2d.6. Graph. Example of mixture glass transition measurements.

Significant Problems, Issues and Potential Impact on Progress

The investigation on the impact of TSRST specimen size and shape has been delayed because of the limited availability of the equipment and the extensive use of liquid nitrogen as a cooling agent. The existing TSRST equipment set-up at UNR is in the process to be upgraded with a chiller and a control unit based on compressed air to replace the liquid nitrogen cooling agent.

Work Planned Next Quarter

Continue the aging process of binders and continue measuring the properties of the aged binders.

Continue the work on the impact of aggregate absorption on the aging of the asphalt binder. Further calibration tests of the new type of dilatometric cell will be performed with different gaskets to obtain a constant curve and to carry out the experimental plan. The testing will resume for the binders aged with different procedures.

The new software for the SENB device will be completed as soon as possible, and the equipment will be used to test binders and mixtures.

Work element E2e: Design Guidance for Fatigue and Rut Resistance Mixtures (AAT)

Work Done This Quarter

Work was initiated this Quarter on modifying the preliminary experimental designs to incorporate the core asphalts, aggregates, and modifiers.

Significant Results

Improvements have been identified for the following models developed in NCHRP Project 9-25:

- (1) Hirsch Model for dynamic modulus,
- (2) Resistivity Model for rutting resistance,
- (3) Continuum Damage Fatigue Model
- (4) Permeability Model

Preliminary experimental plans have been developed to address the needed model improvements.

Significant Problems, Issues and Potential Impact on Progress

This work element is approximately 6 months behind the proposed Year 2 schedule. This delay can be made up during the remaining years for the project by accelerating the laboratory testing schedule.

Work Planned Next Quarter

Final experimental designs will be prepared using the final core materials selected by the Asphalt Research Consortium.

Engineered Materials Year 2	Year 2 (4/2008-3/2009)												Team	
	4	5	6	7	8	9	10	11	12	1	2	3		
(1) High Performance Asphalt Materials														
E1a: Analytical and Micro-mechanics Models for Mechanical behavior of mixtures														TAMU
E1a-1: Analytical Micromechanical Models of Binder Properties										P	JP	P		
E1a-2: Analytical Micromechanical Models of Modified Mastic Systems										P	JP	P		
E1a-3: Analytical Models of Mechanical Properties of Asphalt Mixtures			P	P	JP					P	JP	P		
E1a-4: Analytical Model of Asphalt Mixture Response and Damage										P	JP	P		
E1b: Binder Damage Resistance Characterization														UWM
E1b-1: Rutting of Asphalt Binders														
E1b-1-i. Literature review														
E1b-1-ii. Select Materials & Develop Work Plan			DP, P						P					
E1b-1-iii. Conduct Testing									P					
E1b-1-iv. Analysis & Interpretation								JP		P				JP
E1b-1-v. Standard Testing Procedure and Recommendation for Specifications														
E1b-2: Feasibility of Determining rheological and fracture properties of thin films of asphalt binders and mastics using simple indentation tests														UWM
E1b-2-i. Literature Review														
E1b-2-ii. Proposed SuperPave testing modifications or new testing														
E1b-2-iii. Preliminary testing and correlation of results														
E1b-2-iv. Feasibility of using indentation tests for fracture and rheological testing														
E2a: Comparison of Modification Techniques														UWM
E2a-1: Identify modification targets and material suppliers														DP
E2a-2: Test material properties														
E2a-3: Develop model to estimate level of modification needed and cost index														
E2a-4: Write asphalt modification guideline/report on modifier impact over binder properties														
E2c: Critically Designed HMA Mixtures														UNR
E2c-1: Identify the Critical Conditions								JP						D
E2c-2: Conduct Mixtures Evaluations														
E2c-3: Develop a Simple Test														
E2c-4: Develop Standard Test Procedure														
E2c-5: Evaluate the Impact of Mix Characteristics														
E2d: Thermal Cracking Resistant Mixes for Intermountain States														UWM/UNR
E2d-1: Identify Field Sections														D
E2d-2: Identify the Causes of the Thermal Cracking														
E2d-3: Identify an Evaluation and Testing System														
E2d-4: Modeling and Validation of the Developed System														
E2d-5: Develop a Standard														
E2e: Design Guidance for Fatigue and Rut Resistance Mixtures														AAT
E2e-1: Identify Model Improvements														
E2e-2: Design and Execute Laboratory Testing Program														
E2e-3: Perform Engineering and Statistical Analysis to Refine Models														
E2e-4: Validate Refined Models														
E2e-5: Prepare Design Guidance														
(2) Green Asphalt Materials														
E2b: Design System for HMA Containing a High Percentage of RAP Material														UNR
E2b-1: Develop a System to Evaluate the Properties of RAP Materials								JP						
E2b-2: Compatibility of RAP and Virgin Binders														
E2b-3: Develop a Mix Design Procedure														
E2b-4: Impact of RAP Materials on Performance of Mixtures														
E2b-5: Field Trials														
E1c: Warm and Cold Mixes														UWM
E1c-1: Warm Mixes														
E1c-1-i. Effects of Warm Mix Additives on Rheological Properties of Binders														
E1c-1-ii. Effects of Warm Mix Additives on Mixture Workability and Stability								P				D	DP	F
E1c-1-iii. Mixture Performance Testing														
E1c-1-iv. Develop Revised Mix Design Procedures														
E1c-1-v. Field Evaluation of Mix Design Procedures and Performance Recommendations														
E1c-2: Improvement of Emulsions' Characterization and Mixture Design for Cold Bitumen Applications														
E1c-2-i. Review of Literature and Standards								JP, P						
E1c-2-ii. Creation of Advisory Group														
E1c-2-iii. Identify Tests and Develop Experimental Plan														P, DP
E1c-2-iv. Develop Material Library and Collect Materials														
E1c-2-v. Conduct Testing Plan														
E1c-2-vi. Develop Performance Selection Guidelines														
E1c-2-vii. Validate Guidelines														
E1c-2-viii. Develop CMA Mix Design Procedure														
E1c-2-ix. Develop CMA Performance Guidelines														

Deliverable codes
D: Draft Report
F: Final Report
M&A: Model and algorithm
SW: Software
JP: Journal paper
P: Presentation
DP: Decision Point

Deliverable Description
Report delivered to FHWA for 3 week review period.
Final report delivered in compliance with FHWA publication standards
Mathematical model and sample code
Executable software, code and user manual
Paper submitted to conference or journal
Presentation for symposium, conference or other
Time to make a decision on two parallel paths as to which is most promising to follow through



Engineered Materials Year 2 - 5	Year 2 (4/08-3/09)				Year 3 (4/09-3/10)				Year 4 (04/10-03/11)				Year 5 (04/11-03/12)				Team		
	Q1	Q2	Q3	Q4	Q1	Q2	Q3	Q4	Q1	Q2	Q3	Q4	Q1	Q2	Q3	Q4			
(1) High Performance Asphalt Materials																			
E1a: Analytical and Micro-mechanics Models for Mechanical behavior of mixtures																	TAMU		
E1a-1: Analytical Micromechanical Models of Binder Properties				P,JP	JP	P	P	JP	M&A	D	F,SW								
E1a-2: Analytical Micromechanical Models of Modified Mastic Systems				P,JP	JP	P	P		M&A	JP	D	F,SW							
E1a-3: Analytical Models of Mechanical Properties of Asphalt Mixtures	P	P,JP		P,JP	JP	P	P	M&A		D	SW,JP	F							
E1a-4: Analytical Model of Asphalt Mixture Response and Damage				P,JP	JP	P	P		M&A	D	F,JP	SW							
E1b: Binder Damage Resistance Characterization																			
E1b-1: Rutting of Asphalt Binders																	UWM		
E1b-1-1: Literature review																			
E1b-1-2: Select Materials & Develop Work Plan	DP, P			P															
E1b-1-3: Conduct Testing				P				JP		P									
E1b-1-4: Analysis & Interpretation			JP	P	JP			JP		P			JP						
E1b-1-5: Standard Testing Procedure and Recommendation for Specifications											P		DP	P	D	JP	F		
E1b-2: Feasibility of Determining rheological and fracture properties of thin films of asphalt binders and mastics using simple indentation tests																			
E1b-2i. Literature Review							D												
E1b-2ii. Proposed SuperPave testing modifications or new testing devices							P												
E1b-2iii. Preliminary testing and correlation of results											D								
E1b-2iv. Feasibility of using indentation tests for fracture and rheological properties								JP		P		F							
E2a: Comparison of Modification Techniques																			
E2a-1: Identify modification targets and material suppliers				DP				DP										UWM	
E2a-2: Test material properties										P									
E2a-3: Develop model to estimate level of modification needed and cost index																			
E2a-4: Write asphalt modification guideline/report on modifier impact over binder properties																			
E2c: Critically Designed HMA Mixtures																			
E2c-1: Identify the Critical Conditions			JP		D			JP	D	F								UNR	
E2c-2: Conduct Mixtures Evaluations										D	D, F	JP				D, F	JP		
E2c-3: Develop a Simple Test																D, F			
E2c-4: Develop Standard Test Procedure																D, F			
E2c-5: Evaluate the Impact of Mix Characteristics																	D, F		
E2d: Thermal Cracking Resistant Mixes for Intermountain States																			
E2d-1: Identify Field Sections				D, F	D			D	F									UWM/UNR	
E2d-2: Identify the Causes of the Thermal Cracking								DP	JP	DP, D									
E2d-3: Identify an Evaluation and Testing System															D, F	JP			
E2d-4: Modeling and Validation of the Developed System																	D, F		
E2d-5: Develop a Standard																	D, F		
E2e: Design Guidance for Fatigue and Rut Resistance Mixtures																			
E2e-1: Identify Model Improvements																		AAT	
E2e-2: Design and Execute Laboratory Testing Program																			
E2e-3: Perform Engineering and Statistical Analysis to Refine Models																			
E2e-4: Validate Refined Models																			
E2e-5: Prepare Design Guidance																			
(2) Green Asphalt Materials																			
E2b: Design System for HMA Containing a High Percentage of RAP Material																			
E2b-1: Develop a System to Evaluate the Properties of RAP Materials			JP					D	D, F	D								UNR	
E2b-2: Compatibility of RAP and Virgin Binders																D, F	JP		
E2b-3: Develop a Mix Design Procedure											D					D, F	JP		
E2b-4: Impact of RAP Materials on Performance of Mixtures																	D, F		
E2b-5: Field Trials																	D, F		
E1c: Warm and Cold Mixes																			
E1c-1: Warm Mixes																			
E1c-1i. Effects of Warm Mix Additives on Rheological Properties of Binders.																		UWM	
E1c-1ii. Effects of Warm Mix Additives on Mixture Workability and Stability																		UWM	
E1c-1iii. Mixture Performance Testing			P	D	F, DP													UWM/UNR	
E1c-1iv. Develop Revised Mix Design Procedures									JP		P, DP							UWM/UNR	
E1c-1v. Field Evaluation of Mix Design Procedures and Performance Recommendations																JP	D	P, F	UWM/UNR
E1c-2: Improvement of Emulsions' Characterization and Mixture Design for Cold Bitumen Applications																			
E1c-2i. Review of Literature and Standards																		UWM	
E1c-2ii. Creation of Advisory Group				JP, P, D	F			D	D										
E1c-2iii. Identify Tests and Develop Experimental Plan								P, DP	D		D								
E1c-2iv. Develop Material Library and Collect Materials.																			
E1c-2v. Conduct Testing Plan									JP	D	P								
E1c-2vi. Develop Performance Selection Guidelines													JP	D	P, F				
E1c-2vii. Validate Guidelines									D							JP	P		
E1c-2viii. Develop CMA Mix Design Procedure																P			
E1c-2ix. Develop CMA Performance Guidelines																JP	D	F	

Deliverable codes
D: Draft Report
F: Final Report
M&A: Model and algorithm
SW: Software
JP: Journal paper
P: Presentation
DP: Decision Point

Deliverable Description
Report delivered to FHWA for 3 week review period.
Final report delivered in compliance with FHWA publication standards
Mathematical model and sample code
Executable software, code and user manual
Paper submitted to conference or journal
Presentation for symposium, conference or other
Time to make a decision on two parallel paths as to which is most promising to follow through

Work planned
Work completed
Parallel topic
Delayed

PROGRAM AREA: VEHICLE-PAVEMENT INTERACTION

CATEGORY VP1: WORKSHOP

Work element VP1a: Workshop on Super-Single Tires

This work element is complete.

CATEGORY VP2: DESIGN GUIDANCE

Work element VP2a: Mixture Design to Enhance Safety and Reduce Noise of HMA (UWM)

Work Done This Quarter

Preliminary testing of laboratory-prepared gyratory specimens and field testing was performed during this quarter. The average depth of pavement surface macrotexture was compared with surface frictional properties. Pavement surface macrotexture was measured in accordance with ASTM E965 using the sand patch method to determine average depth. The test procedure for the sand patch method involves spreading a known volume of material (sand) on a pavement surface that has been cleaned and dried. The diameter of the area covered by the material is then measured and an average depth is calculated according to the following equation:

$$V = (\pi d^2)/4$$

Where

V is the volume of material (sand) used (mm^3), and
d is the measured diameter of the spread material (mm).

This technique is intended to provide information regarding macrotexture without consideration of microtexture characteristics or frictional properties. A British Pendulum Skid Resistance Tester was used to determine frictional properties of pavement surface. An adaptation to the pendulum device was manufactured at the University of Wisconsin–Madison to elevate the device for use with gyratory compacted specimens for laboratory testing. (The device may be simply removed from the pedestal to take field measurements of pavement surfaces.) The Wessex S885 Skid Tester used in this experiment is shown with the pedestal adaptor in figure VP2a.1.

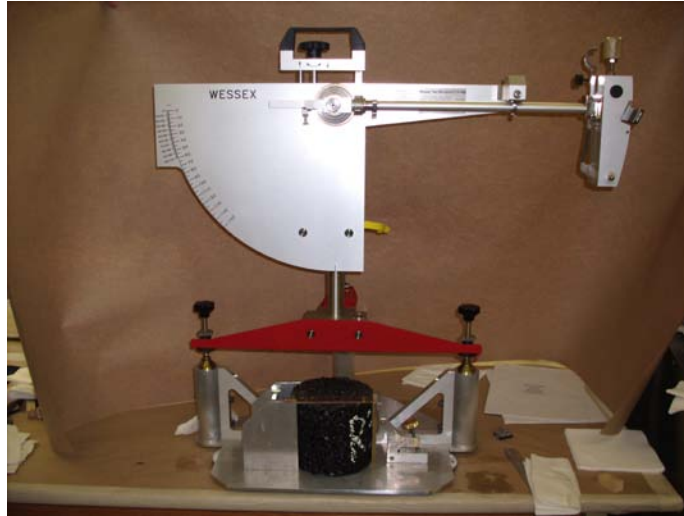


Figure VP2a.1 Photograph. Wessex S885 Skid Resistance Tester and adaptive pedestal used to determine British Pendulum Number (BPN) of gyratory compacted specimens in a laboratory setting.

Sand patch data were collected for specimens listed in the matrix of table VP2a.1 and a chosen representation from these samples were used for preliminary data collection with the pendulum. The pavements tested for macrotexture depth cover a range of variables such as nominal maximum aggregate size (NMAS), aggregate type, design equivalent single axle loads (ESALs), binder PG, base material (of field tests), and compaction temperature and pressure.

Table VP2a.1. Specimen testing matrix.

NMAS	Agg. Type	Design ESALs	Binder PG	Base	Compaction Temperature & Pressure					
					600 kPa 120 °C	600 kPa 90 °C	600 kPa 60 °C	300 kPa 120 °C	300 kPa 90 °C	300 kPa 60 °C
19 mm	LS	E-1	58-28	CABC	X	X	X	X	X	X
		E-3	64-22	Milled AC	X	X	X	X	X	X
				CABC	X	X	X	X	X	X
				CABC	X	X	X	X	X	X
	E-10	64-22	CABC	X	X	X	X	X	X	
GV	E-10	58-28	Rubb. PCC	X	X	X	X	X	X	
12.5 mm	LS	E-1	58-28	Milled AC	X	X	X	X	X	X
			64-22	Pulverized AC	X	X	X	X	X	X
		E-3	58-28	Pulverized AC	X	X	X	X	X	X
	GV	E-1	58-28	Milled AC	X	X	X	X	X	X
				Milled AC	X	X	X	X	X	X
		E-10	58-28	Dowel PCC	X	X	X	X	X	X
				Dowel PCC	X	X	X	X	X	X
			58-28	Rubb. PCC	X	X	X	X	X	X

LS =Limestone, GV=Gravel

Significant Results

Mean texture depth (MTD) results from sand patch method, listed in table VP2a.2, exhibit a significant range of values regardless of the sorting variable. This variation is depicted in figure VP2a.2. Thus, surface frictional properties were determined for several specimens to verify the wide range of values. This testing was performed with a Wessex S885 Skid Tester British Pendulum device in accordance with ASTM E303.

Table VP2a.2. Values of mean texture depth (MTD) measured with the sand patch method.
(Highlighted specimens are those initially tested to determine surface friction.)

Design ESALs	Project	NMAS (mm)	Compaction		Mean MTD (mm)	Std Dev σ (mm)	COV
			Temp. (°C)	Press. (kPa)			
E-1	STH-44	12.5	60	300	0.32	0.03	8.3%
E-1	STH-77	12.5	60	300	0.17	0.00	0.0%
E-10	I-39 M	12.5	60	300	0.26	0.02	8.4%
E-3	US-8	12.5	60	300	0.29	0.03	8.8%
E-1	STH-77	12.5	90	300	0.22	0.02	8.5%
E-1	STH-44	12.5	120	300	0.30	0.01	4.5%
E-10	I-39 M	12.5	120	300	0.22	0.02	7.1%
E-3	STH-96	12.5	120	300	0.24	0.01	4.5%
E-1	STH-77	12.5	120	600	0.19	0.01	2.9%
E-10	I-39 M	12.5	120	600	0.26	0.01	4.1%
E-10	I-39 M	12.5	120	600	0.24	0.03	10.8%
E-3	US-8	12.5	120	600	0.19	0.01	3.8%
E-1	STH-33	19	60	300	0.30	0.02	5.2%
E-10	SH-181	19	60	300	0.35	0.01	2.9%
E-10	US-53	19	60	300	0.46	0.10	22.3%
E-1	STH-33	19	60	600	0.21	0.01	4.6%
E-10	SH-181	19	60	600	0.35	0.02	4.8%
E-3	US-18 BM	19	75	250	0.48	0.04	8.8%
E-3	US-18 BM	19	105	250	0.44	0.02	5.6%
E-3	US-18 BM	19	105	600	0.44	0.03	5.8%
E-1	STH-33	19	120	600	0.26	0.03	12.2%
E-10	SH-181	19	120	600	0.43	0.01	3.2%
E-10	US-53	19	120	600	0.44	0.06	12.8%

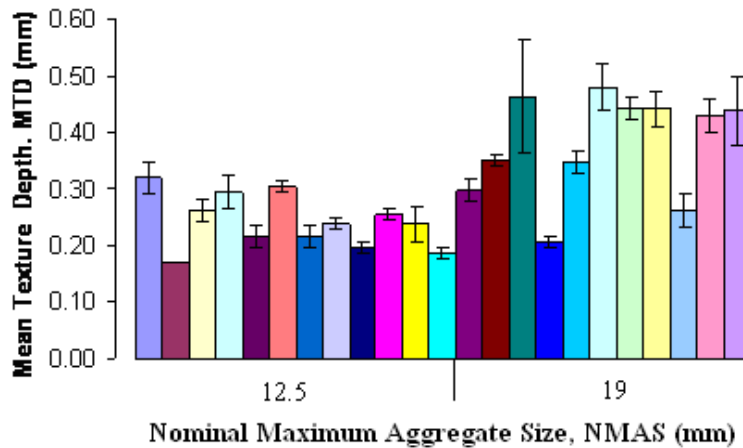


Figure VP2a.2. Graph. Variation of MTD obtained from sand patch method.

The highlighted specimens in table VP2a-2 represent those chosen for initial testing with the British Pendulum to determine surface friction. The six specimens chosen were compacted at the listed temperature and pressure using the gyratory compactor with dimensions of 150 mm (h) by 150 mm (d). This selection was chosen as representative because they cover three design ESAL categories, both NMAS categories, two aggregate types, several temperatures and pressure and, most critically, three levels of MTD. Of the six samples selected, two were of high MTD values, two mid-range, and two low to see if a similar trend could be derived from BPN. The representative set yielded the BPN values seen in table VP2a.3 as well as the corresponding coefficient of friction determined using the BPN. Samples were tested under laboratory conditions of room/surface temperature of 24 °C.

Table VP2a.3. Friction measurements in terms of BPN for selected mixtures.

Design ESALs	Project	NMAS (mm)	Compaction		Average BPN	σ	COV	Coefficient of Friction
			Temp. (°C)	Press. (kPa)				
E-10	US-53	19	60	300	70.33	0.58	0.82	82
E-3	US-18 BM	19	75	250	73.67	1.15	1.57	87
E-1	STH-44	12.5	120	300	65.67	0.58	0.88	76
E-1	STH-33	19	60	300	66.00	0.00	0.00	76
E-1	STH-77	12.5	120	600	54.67	0.58	1.06	60
E-1	STH-77	12.5	60	300	59.67	0.58	0.97	68

A positive correlation was identified between the MTD and BPN values obtained for these six specimens and can be clearly seen in figure VP2a.3.

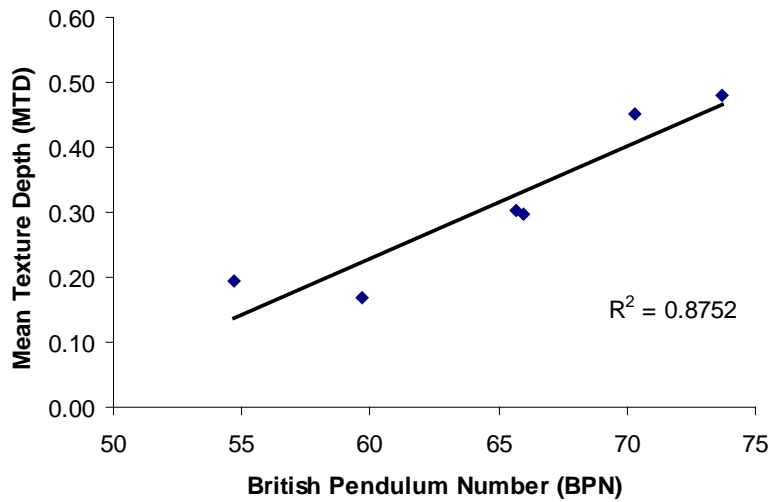


Figure VP2a.3. Graph. MTD versus BPN for representative data set.

Although the correlation is promising, it is clear from the plot that the representative set is relatively small in number. The remaining samples that underwent sand patch testing will be tested for surface frictional characteristics with the pendulum device and other methods. It is rather surprising to see the strong relationship between the MTD and the BPN, since the first represents macrotexture and the second represents microtexture.

Significant Problems, Issues and Potential Impact on Progress

The only problem encountered was that the pendulum cannot be used for testing samples in the dry condition. The specification for pendulum testing calls for wet conditions, but it was the hope of the research team to also determine BPN under dry conditions to compare with MTD data. However, pendulum testing was not able to distinguish between any of the six samples under dry conditions, as all reported roughly the same BPN. This, in turn, yielded the same coefficient of friction. This issue will not have impact on progress of this task. Further pendulum testing will be performed under wet conditions only.

Work Planned Next Quarter

Work next quarter will include finalizing BPN data collection for a full analysis in conjunction with MTD data. Also next quarter, the group would like to make significant progress on additional testing methods such as the Circular Track Meter (CTMeter, ASTM E2157) and the Dynamic Friction Tester (DFTester, ASTM E1911).

The issue of surface abrasion due to traffic will also be studied next quarter. This issue was mentioned before regarding the MTD measurements. With the pendulum sample holder developed, testing to study the effect of abrasion will begin using a circular rotating abrasion device.

Cited References

ASTM E965-06 (Reapproved 2006): Standard Test Method for Measuring Pavement Macrotexture Depth Using a Volumetric Technique.

ASTM E303: Standard Test Method for Measuring Surface Frictional Properties Using the British Pendulum Tester.

ASTM E2157-01 (Reapproved 2005): Standard Test Method for Measuring Pavement Macrotexture Properties Using Circular Track Meter.

ASTM E1911-09: Standard Test Method for Measuring Paved Surface Frictional Properties Using the Dynamic Friction Tester.

CATEGORY VP3: MODELING

Work element VP3a: Pavement Response Model to Dynamic Loads (UNR Year 2 start)

Work Done This Quarter

Worked on the 3D-Move model to make it a menu-driven software.

Worked on converting the non-uniform tire-pavement contact pressure distribution measurements from the Nevada Automotive Test Center (NATC) into a standard form to be implemented in the 3D-Move model.

Significant Results

Developed additional input modules for the 3D-Move user friendly interface.

Significant Problems, Issues and Potential Impact on Progress

Michelin will most probably not share their measured non-uniform contact stress data with the pavement design community.

CSIR is not in a position to share existing Stress-in-Motion (SIM) data since they are working on a similar database for their National Roads Agency (SANRAL) in South Africa.

Work Planned Next Quarter

Continue working on the 3D-Move model to make it a menu-driven software.

Continue collecting and developing the database for non-uniform tire/pavement contact pressure distribution.

Vehicle-Pavement Interaction Year 2	Year 2 (4/2008-3/2009)												Team	
	4	5	6	7	8	9	10	11	12	1	2	3		
(1) Workshop														
VP1a: Workshop on Super-Single Tires														UNR
(2) Design Guidance														
VP2a: Mixture Design to Enhance Safety and Reduce Noise of HMA														UWM
VP2a-1: Evaluate common physical and mechanical properties of asphalt mixtures with enhanced frictional skid characteristics														
VP2a-2: Evaluate pavement macro- and micro-textures and their relation to tire and pavement noise-generation mechanisms														
VP2a-3: Develop a laboratory testing protocol for the rapid evaluation of the macro and micro-texture of pavements						M&A							P	
VP2a-4: Run parametric studies on tire-pavement noise and skid response								JP						
VP2a-5: Establish collaboration with established national laboratories specialized in transportation noise measurements. Gather expertise on measurements and analysis														
VP2a-6: Model and correlate acoustic response of tested tire-pavement systems														
VP2a-7: Proposed optimal guideline for design to include noise reduction, durability, safety and costs														
(3) Pavement Response Model Based on Dynamic Analyses														
VP3a: Pavement Response Model to Dynamic Loads														UNR
VP3a-1: Dynamic Loads														
VP3a-2: Stress Distribution at the Tire-Pavement Interface														
VP3a-3: Pavement Response Model														
VP3a-4: Overall Model														

Deliverable codes

D: Draft Report
 F: Final Report
 M&A: Model and algorithm
 SW: Software
 JP: Journal paper
 P: Presentation
 DP: Decision Point

Deliverable Description

Report delivered to FHWA for 3 week review period.
 Final report delivered in compliance with FHWA publication standards
 Mathematical model and sample code
 Executable software, code and user manual
 Paper submitted to conference or journal
 Presentation for symposium, conference or other
 Time to make a decision on two parallel paths as to which is most promising to follow through

 Work planned
 Work completed
 Parallel topic

Vehicle-Pavement Interaction Years 2 - 5

	Year 2 (4/08-3/09)				Year 3 (4/09-3/10)				Year 4 (04/10-03/11)				Year 5 (04/11-03/12)				Team
	Q1	Q2	Q3	Q4	Q1	Q2	Q3	Q4	Q1	Q2	Q3	Q4	Q1	Q2	Q3	Q4	
(1) Workshop																	
VP1a: Workshop on Super-Single Tires																	UNR
(2) Design Guidance																	
VP2a: Mixture Design to Enhance Safety and Reduce Noise of HMA																	UWM
VP2a-1: Evaluate common physical and mechanical properties of asphalt mixtures with enhanced frictional skid characteristics					DP												
VP2a-2: Evaluate pavement macro- and micro-textures and their relation to tire and pavement noise-generation mechanisms					DP												
VP2a-3: Develop a laboratory testing protocol for the rapid evaluation of the macro and micro-texture of pavements		M&A		P													
VP2a-4: Run parametric studies on tire-pavement noise and skid response			JP			JP		D									
VP2a-5: Establish collaboration with established national laboratories specialized in transportation noise measurements. Gather expertise on measurements and analysis																	
VP2a-6: Model and correlate acoustic response of tested tire-pavement systems										JP	D	F					
VP2a-7: Proposed optimal guideline for design to include noise reduction, durability, safety and costs											D	P, F					
(3) Pavement Response Model Based on Dynamic Analyses																	
VP3a: Pavement Response Model to Dynamic Loads																	UNR
VP3a-1: Dynamic Loads									D, F	JP							
VP3a-2: Stress Distribution at the Tire-Pavement Interface									D, F	JP							
VP3a-3: Pavement Response Model						SW, v, β							SW, JP				
VP3a-4: Overall Model													D	F			

Deliverable codes

- D: Draft Report
- F: Final Report
- M&A: Model and algorithm
- SW: Software
- JP: Journal paper
- P: Presentation
- DP: Decision Point

Deliverable Description

- Report delivered to FHWA for 3 week review period.
- Final report delivered in compliance with FHWA publication standards
- Mathematical model and sample code
- Executable software, code and user manual
- Paper submitted to conference or journal
- Presentation for symposium, conference or other
- Time to make a decision on two parallel paths as to which is most promising to follow through



PROGRAM AREA: VALIDATION

CATEGORY V1: FIELD VALIDATION

Work element V1a: Use and Monitoring of Warm Mix Asphalt Sections (Year 1 start)

Work Done This Quarter

No activity this quarter.

Significant Results

Warm mix sections were placed at the East Entrance to Yellowstone National Park in the Fall of 2007.

Significant Problems, Issues and Potential Impact on Progress

None.

Work Planned Next Quarter

No activity planned.

Work element V1b: Construction and Monitoring of additional Comparative Pavement Validation sites (Year 1 start)

Work Done This Quarter

The ARC and Manitoba Infrastructure & Transportation are preparing to construct two new comparative pavement performance sites in the province of Manitoba, Canada. The first site is on provincial highway 14 between Plum Coulee and Winkler. The project involves milling 25 mm of the existing 100 mm pavement, using the RAP in the first 50 mm lift of new construction with three Warm-mix additives and a conventional hot-mix control section, and a surface 50 mm lift using virgin materials with the Warm-mix additives and hot-mix control section. The RAP content of the first lift will be 30 – 32 percent. The total project length is about 14 km (8.7 miles) with about 3 km (1.75 miles) of each of the Warm-mix additives, Sasobit, Advera, Evotherm DAT, and the hot-mix sections. The ARC and Manitoba I&T will conduct material property testing of the RAP, aggregate, and asphalt and formulate mix designs for the 30% RAP lower lift and the virgin top lift materials. The data obtained on the materials and mixes will determine the recommended placement temperatures of the Warm-mix materials. If laboratory data on the control hot-mix indicates that lower placement temperatures are possible, an additional test section may be included as a side-by-side comparison with the hot-mix placed at normal mixing and compaction temperatures.

Prior to construction, the ARC and Manitoba I&T will identify pertinent areas for performance monitoring sections and conduct distress surveys of those areas so that the influence of existing pavement distress can be evaluated on the new materials.

The second comparative pavement performance site is on provincial highway 8 between Gimli and Hnaua. The total project length is about 28 km (17 miles) but the ARC sections will be placed in 14 km (8.7 miles) of the southern part of the project. The existing pavement was milled and recycled in the Fall of 2008 using a ratio of 70% RAP and 30% new material in two 50 mm lifts.

The ARC sections will be constructed over the 70% RAP material placed last fall using two 50 mm lifts with conventional hot-mix, 15% RAP, 40% RAP with no grade change for the new asphalt, and 40% RAP with a grade change.

Significant Results

None.

Significant Problems, Issues and Potential Impact on Progress

None.

Work Planned Next Quarter

It is planned to conduct a pre-construction distress survey and monitoring of the proposed sections on PH14 prior to the milling operations.

CATEGORY V2: ACCELERATED PAVEMENT TESTING

Work element V2a: Accelerated Pavement Testing including Scale Model Load Simulation on Small Test Track (Later start)

Work Done This Quarter

No activity this quarter.

Significant Results

None.

Significant Problems, Issues and Potential Impact on Progress

None.

Work Planned Next Quarter

No activity planned.

Work element V2b: Construction of Validation Sections at the Pecos Research & Testing Center (Later start)

This work element is included to indicate that this may be a possibility for accelerated pavement testing for ARC research because it is a facility in the TAMU system.

CATEGORY V3: R&D VALIDATION

Work element V3a: Continual Assessment of Specifications (UWM)

Work Done This Quarter

Work last quarter focused on elastic recovery using the ductilometer at 25°C to evaluate correlations with the Multiple Stress Creep and Recovery (MSCR) test results. New data were generated to examine the benefits of replacing the elastic recovery with the percent recovery from the MSCR test at various stress levels.

A survey on limits on elastic recovery at different state departments of transportation (DOTs) was obtained. The new data generated in the laboratory was used to convert the elastic recovery thresholds specified by the DOTs into MSCR percent recovery limits.

A testing plan was developed to examine the correlation of the MSCR percent recovery on mixture performance. This plan compares two binders with the same nonrecoverable compliance but with different percent recoveries. This initial experiment was developed to assess the value of including the MSCR percent recovery as a binder characterizing criterion in addition to the nonrecoverable compliance that is already being used. The mixtures will be tested to evaluate their permanent deformation resistance using the simple performance test procedure.

Work on the development of the Single-Edge Notched Bending (SENB) test to measure fracture properties was also completed. The prototype encountered some challenges in testing mastics. More work is being conducted to fine-tune the compliance of the testing frame to minimize discrepancy in the results. In the meantime, the University of Wisconsin–Madison laboratory received the Asphalt Binder Cracking Device (ABCD). A number of tests were conducted to evaluate this device. The testing was conducted on asphalt binders as well as mastics.

Significant Results

For the MSCR study, different binders were included and tested at 58 °C and 64 °C. The binders were selected so that they covered a wide range of percent recoveries. At 58 °C, the percent recoveries ranged from 3.3% to 90.3%. At 64 °C, the range was from 1.5% to 89.6%. For the

nonrecoverable compliance (Jnr), the range was 0.05 kPa⁻¹ to 4.17 kPa⁻¹ at 58 °C, and 0.06 kPa⁻¹ to 7.74 kPa⁻¹ at 64 °C. The correlation of the MSCR percent recovery and Jnr with the elastic recovery measured at 25 °C using AASHTO T301 (“Standard Method of Test for Elastic Recovery Test of Asphalt Materials by Means of a Ductilometer”) followed the same trend found in literature. Figures V3a.1 and V3a.2 show the correlations found between the MSCR results and the elastic recovery of the binders.

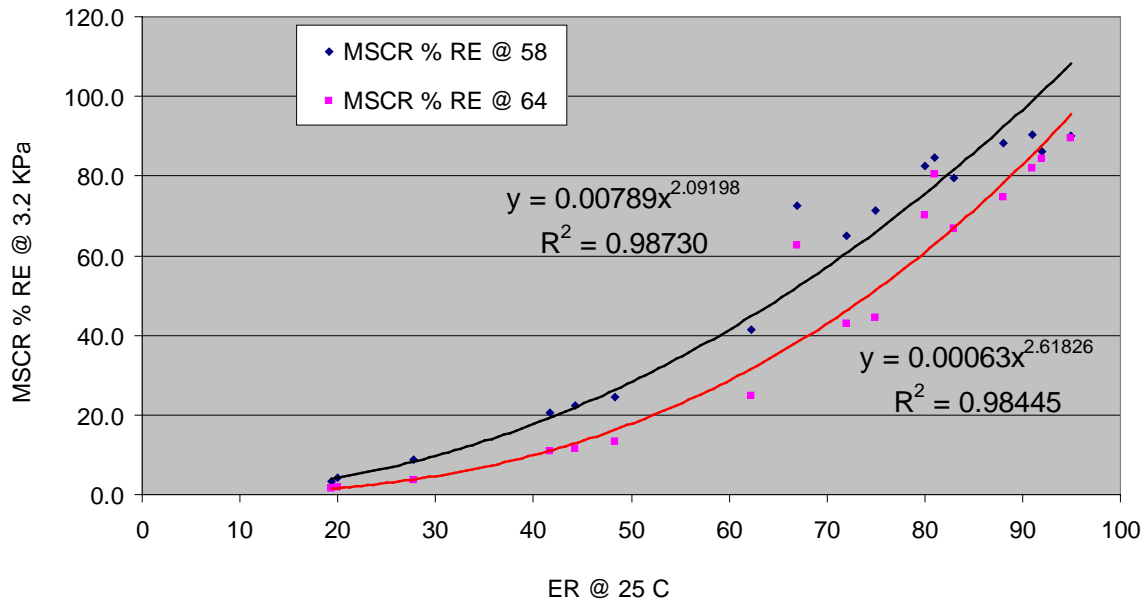


Figure V3a.1. Graph. Correlation between elastic recovery (ER) at 25°C and MSCR percent recovery (% RE).

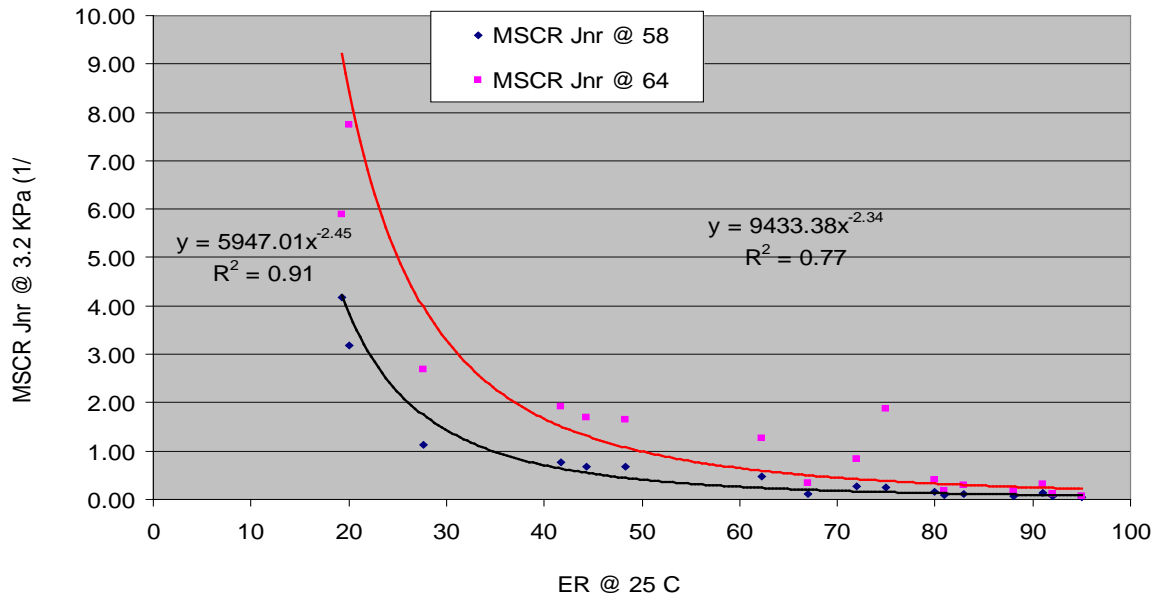


Figure V3a.2. Graph. Correlation between elastic recovery at 25 °C and MSCR nonrecoverable compliance (Jnr).

The survey of the different state DOTs showed that 20 agencies specify minimum values for the elastic recovery of binders, as shown in figure V3a.3. The minimum values typically vary within individual states depending on the PG grade of the binder used. However, for the state of Illinois the minimum value of the elastic recovery is dependent on the type of modification used. Therefore, figure V3a.3 shows two minimum values for Illinois.

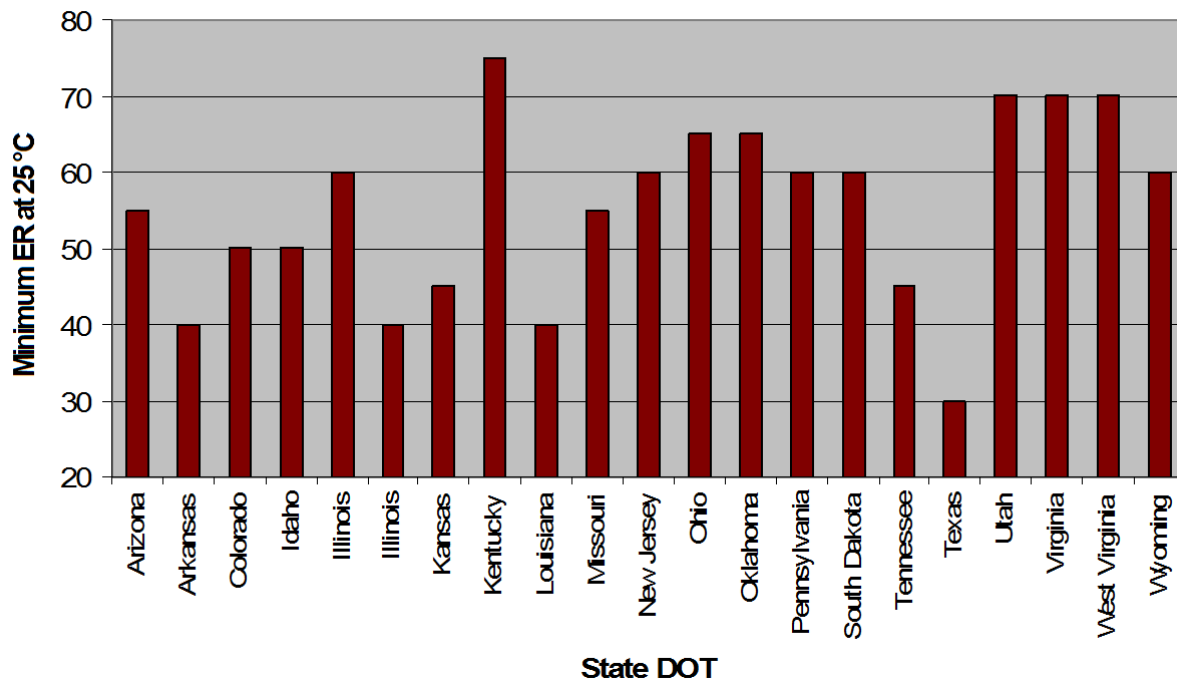


Figure V3a.3. Graph. Minimum elastic recovery values specified by state DOTs.

The translation of the elastic recovery limits to MSCR percent recovery is obtained using the fitted equations shown in figure V3a.1. The values of the MSCR percent recovery corresponding to the DOTs' limits are plotted in figure V3a.4.

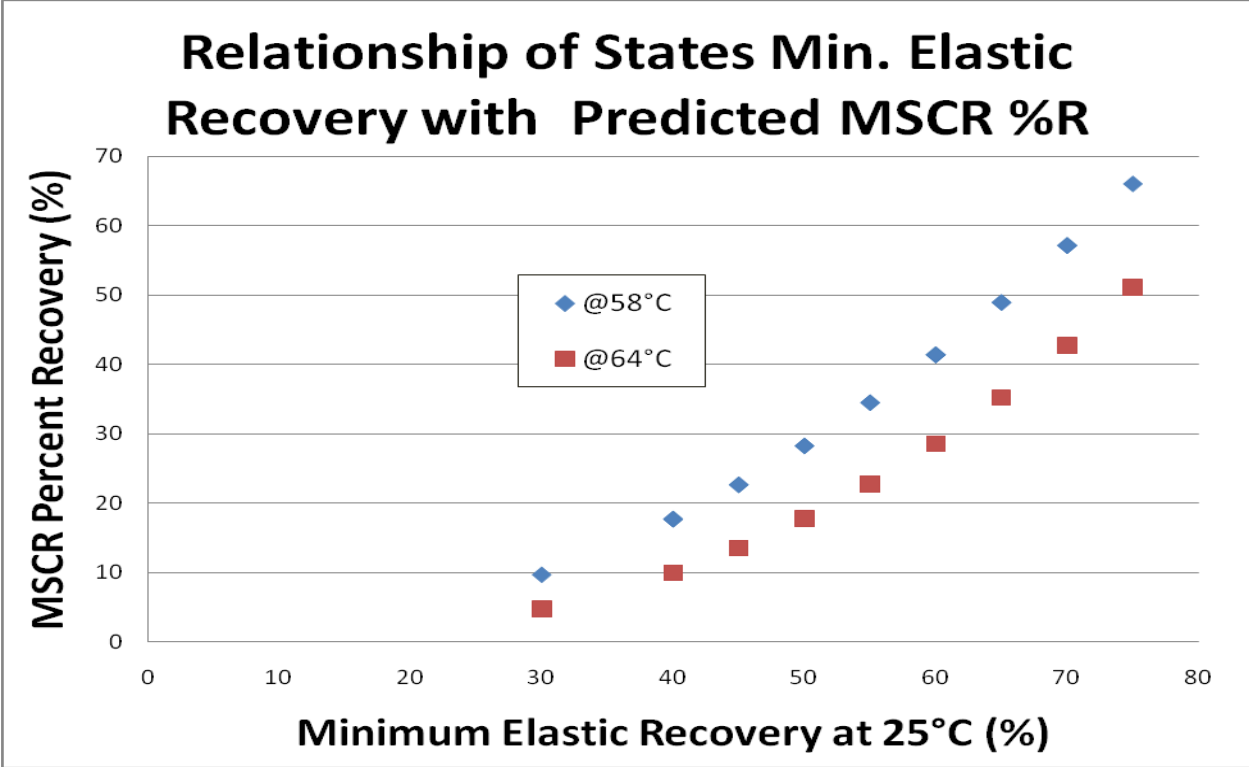


Figure V3a.4. Graph. State DOTs' minimum elastic recovery requirements and the corresponding MSCR percent recovery.

As mentioned earlier, the SENB testing still needs fine-tuning. In the meantime, the ABCD device was used to measure the low-temperature fracture temperatures for different binders and mastics. This serves to evaluate the sensitivity of the device to different materials. Figure V3a.5 shows a summary of the data collected by the ABCD. Results indicate that the ABCD shows good sensitivity to the different materials used and can distinguish between different binders and mastics.

The ABCD testing device now available to the research team is on loan to UW–Madison, and the time period of its availability is currently under negotiation.

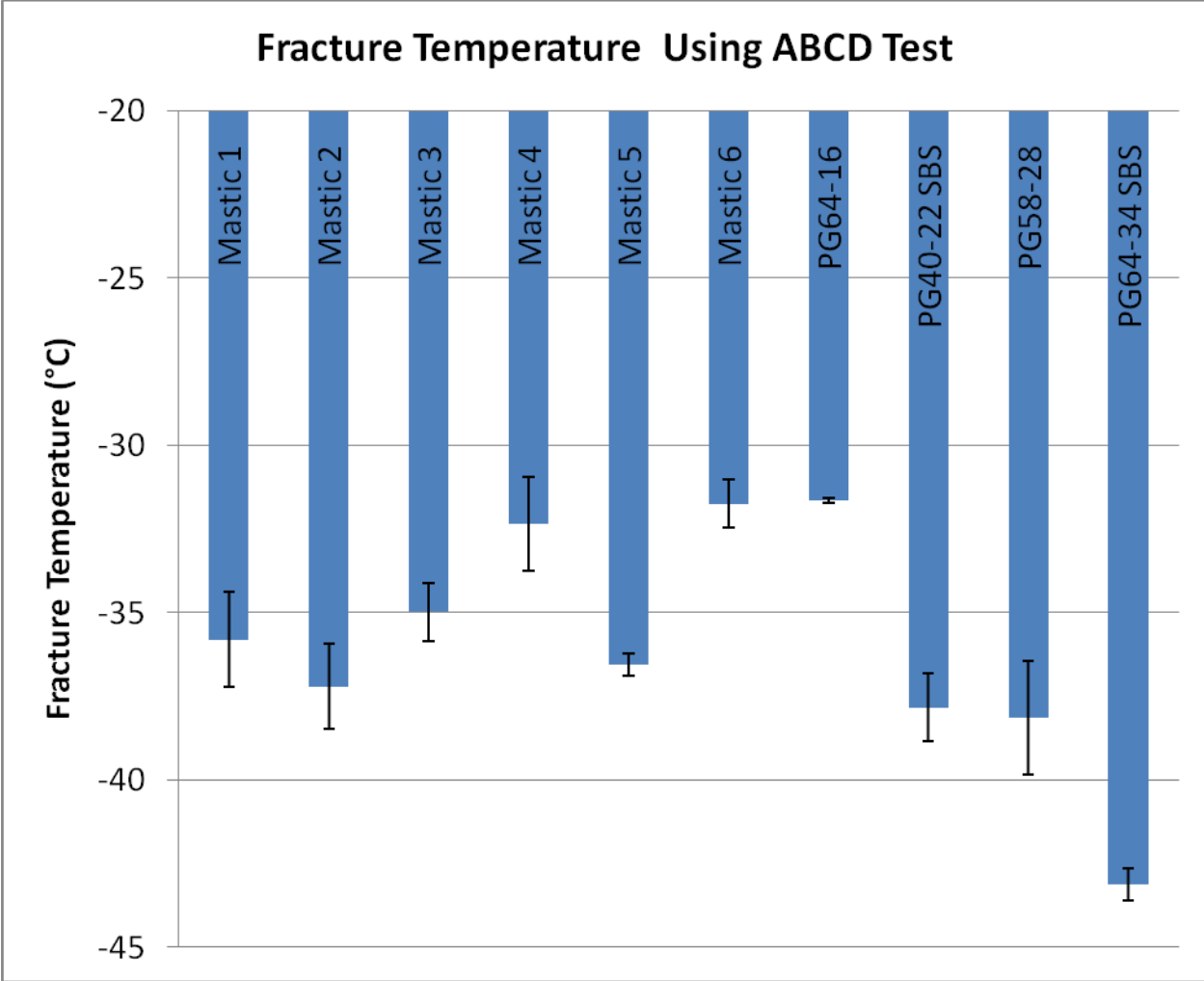


Figure V3a.5. Graph. Binder and mastic fracture temperatures from the ABCD test.

Significant Problems, Issues and Potential Impact on Progress

None.

Work Planned Next Quarter

Work will continue on analyzing the MSCR results at various stress levels and on determining the importance of percent recovery. Mixture testing is scheduled to begin.

Work will also start on the collection of data for the binder fracture test results and on the analysis of a parameter to use as part of the binder specification for low-temperature cracking.

Work element V3b: Validation of the MEPDG Asphalt Materials Models Using New MEPDG Sites and Selected LTPP Sites (UNR, UWM)

Subtask V3b-1: Design and Build Sections (Start Year 1, Year 2, and Year 3)

Work Done This Quarter

None.

Significant Results

None.

Significant Problems, Issues and Potential Impact on Progress

Only three agencies have committed to the construction of MEPDG sites: the Washoe RTC in northern Nevada in 2008, The South Dakota DOT in 2009/2010, and the Wisconsin DOT in 2009. The researchers are facing significant hesitation from the DOTs to use the MEPDG to design and construct HMA pavements. The level of this work element may have to be reduced.

Work Planned Next Quarter

Continue discussions with the states to select field sections for the MEPDG validation sites.

Subtask V3b-2: Additional Testing (Start Year 2, Year 3, and Year 4)

Work Done This Quarter

This work element is to provide additional testing for states that commit to MEPDG validation sites.

Work Planned Next Quarter

None.

Subtask V3b-3: Select LTPP Sections (Start Year 1 thru Year 5)

Work Done This Quarter

Sampling of the binders listed in table V3b-3.1 was completed, and the research team began aging previously sampled binders. The highlighted binders in table V3b-3.1 were selected for preliminary evaluation of current binder fatigue test methods to investigate possible correlation to available LTPP fatigue data. The experimental matrix is shown in table V3b-3.2. This matrix will first be used only for a small set of binders to determine the value in conducting all these tests and to identify any challenges. The research team has scheduled a meeting with a task

group from the Binder ETG in early April to discuss the plan and collect feedback on this testing plan.

Table V3b-3.1. LTPP binders selected for fatigue cracking investigation.

Agency	Exp. No.	SHRP ID	Climate Zone	Fatigue Cracking - m ²	Sample Location	Sample Type
CT	9A	90902	WF	0		AC PG 64-28
MT	9	300903	DF	0		64-22
NC	9A	370901	WN	0	BC01A01	AC-20
NC	9A	370902	WN	0	BC01A02	64-22
NC	9A	370903	WN	0	BC01A03	70-22
NC	9A	370962	WN	0	BC01A62	PG 76-22
WI	9	550903	WF	0		58-72
CT	9A	90960	WF	0.8		AC-10
CT	9A	90961	WF	2.1		PG 58-34
FL	9A	120902	WN	2.2		PG 64-16
NC	9A	370961	WN	3.7	BC01A61	PG 76-22
CT	9A	90962	WF	4.3		PG 58-28
CT	9A	90903	WF	5		PC PG 64-22
PQ	A9	89A902	WN	6.7		52-40
PQ	A9	89A901	WN	8.8		52-34
NJ	9A	340902	WF	11.4	BC01A02	58-28
NC	9A	370963	WN	12.7	BC01A63	AC20
NM	9	350903	DN	15.7		58-22
NC	9A	370965	WN	17.7	BC01A65	PG 16-23
NM	9	350902	DN	32		64-22
MO	9A	290963	WF	37.9	BC02A63	64-16
NJ	9A	340901	WF	49.5	BC01A01	64-22
NC	9A	370964	WN	51.1	BC01A64	PG 76-22
MO	9A	290901	WF	51.6	BC02A01	64-28
NE	9	310902	DF	65.5		AC
NC	9A	370960	WN	73.1	BC01A60	PG 76-22
MT	9	300902	DF	76.2		64-34
NE	9	310903	DF	175.5		AC
NJ	9A	340961	WF	178.8	BC01A61	78-28
AZ	9A	04B901	DN	328		AC BINDER
AZ	9A	04B903	DN	337.9		AC-40,PG 70-10

These four binders were selected for preliminary investigations.

All are currently being aged in the rolling thin film oven (RTFO).

Table V3b-3.2. Experimental fatigue testing plan for the initial set of LTPP binders.

Test Method	Applied Load	Testing Temp(s)	Response Parameters
Frequency Sweep: 0.1 Hz – 30 Hz	0.1% strain	6, 19, 24, 36 °C	Linear viscoelastic $ G^* $ and phase angle spectrum
Time Sweep: 10 Hz	3% strain	SuperPave intermediate temperature (IT), IT-6 °C	N_f , viscoelastic continuum damage (VECD) $M(D)$ relationship
	5% strain		
Binder Yield Energy Test	0.080/s shear strain rate		Yield Energy, Strain at Max Stress, VECD $M(D)$ relationship
	0.010/s shear strain rate		
Amplitude Sweep	Stress controlled		VECD $M(D)$ relationship
	Strain controlled		

The frequency sweep testing will be used to generate master curves to determine linear viscoelastic properties over a range of temperatures and frequencies. The data can then be used as input to the damage modeling of the time sweep, amplitude sweep and Binder Yield Energy Test (BYET) results.

The four binders selected for the initial investigation were chosen to represent the extreme cases of fatigue performance. Both RTFO-aged and pressure aging vessel (PAV)-aged materials will be used to determine what level of aging provides the strongest correlation with field performance data.

Significant Results

None.

Significant Problems, Issues and Potential Impact on Progress

The problems encountered in work element F2e in applying the VECD analysis to the results of modified binders is leading to uncertainty in testing procedures for the LTPP binders. The research team is hopeful that these issues will be resolved soon, but if these issues persist, some changes in the timetable and approach of this subtask could become necessary.

Work Planned Next Quarter

Preliminary testing will begin following the testing plan shown in table V3b-3.2. Binder aging will continue on the other binders as well so that when the preliminary testing is complete, the testing program can be expanded without interruption. A presentation is planned for the proposed binder fatigue task group meeting April 8-9 in Minneapolis. This meeting is intended to take the

place of the presentation shown as occurring in January 2009 in the Year 2 Gantt chart for this subtask.

Subtask V3b-4: Testing of Extracted Binders from LTPP Sections

Work Done This Quarter

No activity planned.

Subtask V3b-5: Review and Revisions of Materials Models (Year 4, and Year 5)

Work Done This Quarter

No activity planned.

Subtask V3b-6: Evaluate the Impact of Moisture and Aging (Year 4, and Year 5)

No work planned.

Validation Year 2	Year 2 (4/2008-3/2009)											Team	
	4	5	6	7	8	9	10	11	12	1	2		3
(1) Field Validation													
V1a: Use and Monitoring of Warm Mix Asphalt Sections													WRI
V1b: Construction and Monitoring of additional Comparative Pavement Validation sites													WRI
(2) Accelerated Pavement Testing													
V2a: Accelerated Pavement Testing including Scale Model Load Simulation on small test track (This work element will include all accelerated pavement testing)													WRI
V2b: Construction of validation sections at the Pecos Research & Testing Center													WRI
(3) R&D Validation													
V3a: Continual Assessment of Specification													UWM
V3a-1: Evaluation of the PG-Plus practices and the motivations for selecting the "plus" tests.							P				D	F	
V3a-2: Detailed analysis of all PG-Plus tests being proposed or in use today, documentation of benefits and costs of these tests, and comparison with new tests											P		
V3a-3: Development of protocols for new binder tests and database for properties measured													
V3a-4: Development of specification criteria for new tests based on field evaluation of construction and performance													
V3a-5: Interviews and surveys for soliciting feedback on binder tests and specifications												JP	
V3b: Validation of the MEPDG Asphalt Materials Models and Early Verification of Technologies Developed by ARC using new MEPDG Sites and Selected LTPP sites													UNR/UWM/WRI
V3b-1: Design and Build Sections													UNR
V3b-2: Additional Testing													
V3b-3: Select LTPP Sites to Validate New Binder Testing Procedures											P		UWM
V3b-4: Testing of Extracted Binders from LTPP Sections													
V3b-5: Review and Revisions of Materials Models													
V3b-6: Evaluate the Impact of Moisture and Aging													

Deliverable codes

- D: Draft Report
- F: Final Report
- M&A: Model and algorithm
- SW: Software
- JP: Journal paper
- P: Presentation
- DP: Decision Point

Deliverable Description

- Report delivered to FHWA for 3 week review period.
- Final report delivered in compliance with FHWA publication standards
- Mathematical model and sample code
- Executable software, code and user manual
- Paper submitted to conference or journal
- Presentation for symposium, conference or other
- Time to make a decision on two parallel paths as to which is most promising to follow through

 Work planned
 Work completed
 Parallel topic

Validation Years 2 - 5	Year 2 (4/08-3/09)				Year 3 (4/09-3/10)				Year 4 (04/10-03/11)				Year 5 (04/11-03/12)				Team
	Q1	Q2	Q3	Q4	Q1	Q2	Q3	Q4	Q1	Q2	Q3	Q4	Q1	Q2	Q3	Q4	
(1) Field Validation																	
V1a: Use and Monitoring of Warm Mix Asphalt Sections																	WRI
V1b: Construction and Monitoring of additional Comparative Pavement Validation sites																	WRI
(2) Accelerated Pavement Testing																	
V2a: Accelerated Pavement Testing including Scale Model Load Simulation on small test track																	WRI
V2b: Construction of validation sections at the Pecos Research & Testing Center																	WRI
(3) R&D Validation																	
V3a: Continual Assessment of Specification																	UWM
V3a-1: Evaluation of the PG-Plus practices and the motivations for selecting the "plus" tests.		P		D, F													
V3a-2: Detailed analysis of all PG-Plus tests being proposed or in use today, documentation of benefits and costs of these tests, and comparison with new tests				P	D												
V3a-3: Development of protocols for new binder tests and database for properties measured						JP				P							
V3a-4: Development of specification criteria for new tests based on field evaluation of construction and performance						D		P	P			JP	P		JP		
V3a-5: Interviews and surveys for soliciting feedback on binder tests and specifications									P		JP		P		D	F	
V3b: Validation of the MEPDG Asphalt Materials Models and Early Verification of Technologies Developed by ARC using new MEPDG Sites and Selected LTPP sites																	UNR/UWM
V3b-1: Design and Build Sections												D, F					
V3b-2: Additional Testing																	
V3b-3: Select LTPP Sites to Validate New Binder Testing Procedures						DP		P		JP		P			D	F	
V3b-4: Testing of Extracted Binders from LTPP Sections																	
V3b-5: Review and Revisions of Materials Models																	
V3b-6: Evaluate the Impact of Moisture and Aging																	

Deliverable codes

D: Draft Report
 F: Final Report
 M&A: Model and algorithm
 SW: Software
 JP: Journal paper
 P: Presentation
 DP: Decision Point

Deliverable Description

Report delivered to FHWA for 3 week review period.
 Final report delivered in compliance with FHWA publication standards
 Mathematical model and sample code
 Executable software, code and user manual
 Paper submitted to conference or journal
 Presentation for symposium, conference or other
 Time to make a decision on two parallel paths as to which is most promising to follow through

 Work planned
 Work completed
 Parallel topic

PROGRAM AREA: TECHNOLOGY DEVELOPMENT

Work element TD1: Prioritize and Select Products for Early Development (Year 1)

Work Done This Quarter

This work element has been completed.

Significant Results

Six early technology development projects have been identified and all have received favorable ratings from the ETGs.

Significant Problems, Issues and Potential Impact on Progress

None.

Work Planned Next Quarter

None.

Work element TD2: Develop Early Products (Year 2)

Work Done This Quarter

Work continued on the Simplified Continuum Damage Fatigue project. The research team continued preparing a draft standard test method for Simplified Continuum Damage Fatigue Testing. This method is in the format of an AASHTO standard test method. It describes the testing and analysis that are required to generate fatigue curves for asphalt concrete mixtures. The accompanying spreadsheet for the analysis has been improved. The draft standard method is approximately 90 percent complete.

The research team is working with Interlaken Technology Corporation to modify NCHRP's Asphalt Mixture Performance Tester to perform the continuum damage fatigue testing. This equipment was purchased by NCHRP in NCHRP Project 9-29. It is being used by AAT on Phase VI of NCHRP Project 9-29. Interlaken completed the development tension grips for the AMPT, and the necessary hardware to glue specimens for the test. Work was initiated on software for controlled stress and controlled strain tension-compression testing and data acquisition.

Dr. Donald Christensen made a brief presentation about the Simplified Continuum Damage Fatigue analysis methodology at the Mixture and Construction Expert Task Group. He presented a journal paper about the analysis methodology at the annual meeting of the Association of Asphalt Paving Technologists.

Significant Results

An improved method was developed for analysis of continuum damage fatigue data. Two new and very useful concepts were included in the improved method. The first is the concept of reduced loading cycles. Reduced loading cycles can be used as a much simpler alternative to the continuum damage parameter, S , in developing damage functions for asphalt concrete mixtures. The second concept introduced in the improved analysis approach is that of effective strain, which is the applied strain minus the endurance limit. This innovation in continuum damage analysis allows for the calculation of endurance limits from relatively limited fatigue data, and is a much quicker and more elegant approach to this problem than performing flexural fatigue tests over a range of strains for weeks or even months.

Significant Problems, Issues and Potential Impact on Progress

None.

Work Planned Next Quarter

The draft standard test method for the simplified continuum damage fatigue test will be completed. The software for the NCHRP AMPT equipment will also be completed. The test method and equipment will be applied to fatigue data from several mixtures. A ruggedness testing plan for the simplified continuum damage fatigue test will be developed.

Work element TD3: Identify Products for Mid-Term and Long-Term Development (Years 2, 3, and 4)

Work Done This Quarter

The research team continued to review interim research products to identify potential mid-term and long-term development projects.

Significant Results

None.

Significant Problems, Issues and Potential Impact on Progress

None.

Work Planned Next Quarter

The research team will continue to review interim research products to identify potential mid-term and long-term development projects.

Work Element TD4: Develop Mid-Term and Long-Term Products (Years 3, 4, and 5)

This activity is planned for later in the project.

PROGRAM AREA: TECHNOLOGY TRANSFER

CATEGORY TT1: OUTREACH AND DATABASES

Work element TT1a: Development and Maintenance of Consortium Website (Duration: Year 1 through Year 5)

Work Done This Quarter

The ARC website was maintained and updated. The ARC year 3 work plan and the ARC quarterly technical progress report, Oct 1- Dec 31, were uploaded to the ARC website.

Work Planned Next Quarter

Continue maintaining and updating the ARC website.

Work element TT1b: Communications (Duration: Year 1 through Year 5)

Work Done This Quarter

The fourth ARC Newsletter was published in March 2009.

Work Planned Next Quarter

None.

Work element TT1c: Prepare Presentations and Publications

Work Done This Quarter

Presentations

H. U. Bahia and A. Faheem, "Transition from Elastic Recovery to MSCR Test – Update on the ARC Studies," Rocky Mountain Asphalt User-Producer Group Meeting; March 24, 2009.

H.U. Bahia, "ARC Update on Warm Mix Research," Presentation to the Manitoba Infrastructure and Transportation Materials Engineering Branch; March 17, 2009.

H. U. Bahia, "Binder Fatigue Task Group Update," FHWA Asphalt Binder Expert Task Group; April 8, 2009.

H. U. Bahia, A. Hanz, Z. Arega, and T. Miller, "Rheological Evaluation of Bitumen Emulsions During Curing and Setting," SAT/RMPD/CSIR Seminar, Pretoria, R. of South Africa; March 4, 2009.

H. U. Bahia, A. Hanz, Z. Arega, and T. Miller, "Overview of the Asphalt Research Consortium (ARC) Studies on Emulsions," AEMA-ARRA-ISSA Annual Meeting; February 20, 2009.

H. U. Bahia and E. Hajj, "ARC Update - Engineered Materials," FHWA Fundamental Properties and Advanced Models Expert Task Group, Irvine, California, February 23-24, 2009.

H. U. Bahia, "ARC Update - Binder Fatigue," FHWA Asphalt Binders Expert Task Group, Irvine, California, February 24, 2009.

H. U. Bahia, "Emulsion Materials Advances for Improving Design and Performance of Chip Seals," Wisconsin County Highway Association Meeting; January 28, 2009.

H. U. Bahia and A. Hanz, "Advanced Methods for Testing Emulsions," Presented at the 88th Annual Meeting of the Transportation Research Board; January 15, 2009.

A. Faheem, "Conceptual Phenomenological Model For Interaction Of Asphalt Binders With Mineral Fillers," Presented at the 84th Annual Meeting and Technical Sessions of the Association of Asphalt Paving Technologists; March 18, 2009.

C. M. Johnson, H. Wen, and H. U. Bahia, "Practical Application of Viscoelastic Continuum Damage Theory to Asphalt Binder Fatigue Characterization," Presented at the 84th Annual Meeting and Technical Sessions of the Association of Asphalt Paving Technologists; March 17, 2009.

Drs. Dallas Little, Eyad Masad, Rashid Abu Al-Rub, Bob Lytton, and Rong Luo, "Update on ARC Modeling Activities and Deliverables", FHWA Fundamental Properties and Advanced Models Expert Task Group, Irvine, California, February 23-24, 2009.

Dr. Elie Hajj, "Update - Work Element E2c: Critically Designed HMA Mixtures," and "Update - Subtask V3b-1: Design and Build Sections", FHWA Fundamental Properties and Advanced Models Expert Task Group, Irvine, California, February 23-24, 2009.

Dr. Elie Hajj "Update - Work Element E2c: Critically Designed HMA Mixtures", "Update Work Element E2d: Thermal Cracking Resistant Mixes for Intermountain States", and "Update - Subtask E1c-1: Warm Mixtures." *FHWA Asphalt Mixture & Construction Expert Task Group*, Irvine, California, February 26, 2009.

Poster Sessions

E. Bautista, S. Mangiafico, H. Bahia, and T. Ma, "Evaluation of Rheological Properties of binder in RAP without Extraction and Recovery," *Presented during Poster Session*, 88th Annual Meeting of the Transportation Research Board; Washington, D.C., 2009.

A. Hanz, Z. Arega, and H. Bahia, "Rheological Evaluation of Emulsion Residues Recovered Using Newly Proposed Evaporative Techniques," *Presented during Poster Session, 88th Annual Meeting of the Transportation Research Board; Washington, D.C., 2009.*

C. Daranga, C. Clopotel, A. Mofolasayo, and H. Bahia, "Storage Stability and Effect of Mineral Surface on Polyphosphoric Acid (PPA) Modified Asphalt Binders," *Presented during Poster Session, 88th Annual Meeting of the Transportation Research Board; Washington, D.C., 2009.*

Work Planned Next Quarter

ARC members will continue to make presentations on ARC research and progress at various meetings. Publications will be prepared as the research warrants.

Work element TT1d: Development of Materials Database (Duration: Year 2 through Year 5)

Work Done This Quarter

Continued the work on developing the Microsoft Access database tables according to the ERD diagram. Continued working on converting the ARC website from a static to a dynamic web site using the Microsoft Active Server Pages (ASP.NET) web application.

Significant Results

Most of the database design has been implemented in the actual test and production servers. A basic authentication system has been created so that UNR and other designated users can interact with the ASP application and the database. A more refined system is in the works but a basic system is implemented so that UNR can begin entering data.

The production web site has been implemented. The production site will contain the tested applications that UNR and others will use. The application on this site is able to authenticate users and interact with the SQL server database.

Forms are being created to enter material and material properties and building the application business logic, menus and other user interface elements.

Significant Problems, Issues and Potential Impact on Progress

None

Work Planned Next Quarter

Continue the work on the database and the dynamic web site. Start inputting data into the beta-version of the database.

Work element TT1e: Development of Research Database (Duration: Year 2 through Year 5)

Work Done This Quarter

Uploaded the ARC year 3 work plans and the ARC quarterly technical progress report to the ARC website.

Work Planned Next Quarter

Upload the ARC quarterly technical progress report to the ARC website.

Work Element TT1f: Workshops and Training

Work Done This Quarter

No activity this quarter.

Work Planned Next Quarter

No activities are planned for the next quarter.

Technology Transfer	Year 2 (4/2008-3/2009)												Team	
	4	5	6	7	8	9	10	11	12	1	2	3		
(1) Outreach and Databases														
TT1a: Development and Maintenance of Consortium Website														UNR
TT1b: Communications														UNR
TT1c: Prepare presentations and publications														UNR
TT1d: Development of Materials Database														UNR
TT1d-1: Identify the overall Features of the Web Application														
TT1d-2: Identify Materials Properties to Include in the Materials Database														
TT1d-3: Define the Structure of the Database														
TT1d-4: Create and Populate the Database														
TT1e: Development of Research Database														UNR
TT1e-1: Identify the Information to Include in the Research Database														
TT1e-2: Define the Structure of the Database														
TT1e-3: Create and Populate the Database														
TT1f: Workshops and Training														UNR

Deliverable codes

D: Draft Report
 F: Final Report
 M&A: Model and algorithm
 SW: Software
 JP: Journal paper
 P: Presentation
 DP: Decision Point

Deliverable Description

Report delivered to FHWA for 3 week review period.
 Final report delivered in compliance with FHWA publication standards
 Mathematical model and sample code
 Executable software, code and user manual
 Paper submitted to conference or journal
 Presentation for symposium, conference or other
 Time to make a decision on two parallel paths as to which is most promising to follow through

 Work planned
 Work completed
 Parallel topic

Technology Transfer	Year 2 (4/08-3/09)				Year 3 (4/09-3/10)				Year 4 (04/10-03/11)				Year 5 (04/11-03/12)				Team
	Q1	Q2	Q3	Q4	Q1	Q2	Q3	Q4	Q1	Q2	Q3	Q4	Q1	Q2	Q3	Q4	
(1) Outreach and Databases																	
TT1a: Development and Maintenance of Consortium Website																	UNR
TT1b: Communications																	UNR
TT1c: Prepare presentations and publications																	ALL
TT1d: Development of Materials Database																	UNR
TT1d-1: Identify the overall Features of the Web Application																	
TT1d-2: Identify Materials Properties to Include in the Materials Database																	
TT1d-3: Define the Structure of the Database																	
TT1d-4: Create and Populate the Database																	
TT1e: Development of Research Database																	UNR
TT1e-1: Identify the Information to Include in the Research Database																	
TT1e-2: Define the Structure of the Database																	
TT1e-3: Create and Populate the Database																	
TT1f: Workshops and Training																	UNR

Deliverable codes

D: Draft Report
 F: Final Report
 M&A: Model and algorithm
 SW: Software
 JP: Journal paper
 P: Presentation
 DP: Decision Point

Deliverable Description

Report delivered to FHWA for 3 week review period.
 Final report delivered in compliance with FHWA publication standards
 Mathematical model and sample code
 Executable software, code and user manual
 Paper submitted to conference or journal
 Presentation for symposium, conference or other
 Time to make a decision on two parallel paths as to which is most promising to follow through

 Work planned
 Work completed
 Parallel topic